

REINFORCED CONCRETE INFILLED SHEAR WALLS  
FOR ASEISMIC STRENGTHENING

by

Lawrence F. Kahn

Robert D. Hanson

Report on Research Conducted under Grant  
No. GI-39123 from the National Science Foundation

Report UMEE 76S1  
Department of Civil Engineering  
The University of Michigan  
Ann Arbor, MI 48109

January 1976

## ABSTRACT

Five half-size reinforced concrete frames were constructed and tested to determine experimentally the effectiveness of infilled walls in strengthening existing framed structures against earthquake loads. The one-story, one-bay frames which measured 66 in. by 108 in. were tested under static, reversed cycle loads. One specimen was the unstrengthened open frame; the second used a wall cast monolithically with the frame; the third used a wall cast-in-place after the frame was constructed; the fourth used a single precast panel fitted within the frame and mechanically connected to top and bottom beams; and the fifth used a wall made of six small precast panels which were mechanically connected within the frame and then joined together.

Response of the open frame and the frame with monolithically cast wall provided reference limits for the remaining specimens. The cast-in-place wall behaved like the monolithic wall until the wall-frame connection failed just below the beam. The precast infilled walls behaved in a combined frame and shear wall action. The maximum strength of the multiple precast wall was about half of that of the other walls, although it maintained its load capability over larger deflection levels. Energy dissipation capacities of the two precast and one cast-in-place structures were similar - about half the capacity of the monolithic wall structure.

Three general conclusions were: (1) that cast-in-place walls can provide the same maximum strength as an equivalent, new monolithic wall but with less ductility, (2) that multiple precast

panels can provide a strong, ductile and easy-to-construct strengthening technique, and (3) that the cyclically degraded load capacity of shear walls should be used in structural design rather than the virgin, monotonic capacity.

#### ACKNOWLEDGMENTS

This report was submitted by Dr. Kahn to The University of Michigan in partial fulfillment of the requirements for the degree Doctor of Philosophy (Civil Engineering). Professor Hanson provided continuing guidance and support throughout the research as chairman of the doctoral committee. Professor Darvas gave many valuable suggestions regarding practical aspects of reinforced concrete design and construction. Professors Berg and Richart carefully reviewed the research and gave valuable suggestions.

The National Science Foundation provided the financial support for the experimental program through Grant GI-39123 to the University of Michigan. Sika Chemical Company provided epoxy materials. However, any opinions, findings, conclusions or recommendations expressed herein are those of the authors and do not necessarily reflect the views of NSF.

Fellow graduate student, Dr. Duane Lee, helped in both the construction and testing of the experimental specimens. Messrs. Mark Butterfield, Dean Rutila, Gerry Giza and Greg Ptucha aided in construction and testing of the specimens.

Mrs. Patricia Kahn carefully typed and reviewed the manuscript.

## TABLE OF CONTENTS

	Page
ABSTRACT	i
ACKNOWLEDGMENTS	ii
LIST OF TABLES	v
LIST OF FIGURES	vi
NOTATION	xix
Chapter	
I. INTRODUCTION	1
Purpose and Scope of Research	1
Philosophy of Strengthening	2
Review of Related Research	5
II. EXPERIMENTAL PROGRAM	7
Design of Experimental Program	7
Test Specimen Design	12
Representation of Seismic Loading	26
Materials	28
Fabrication of Specimens	33
Instrumentation	43
Test Set-Up	45
Test Procedure	48
III. TEST RESULTS	51
Specimen 1, Monolithic Wall	51
Specimen 2, Moment Frame	59
Specimen 3, Cast-in-Place Wall	63
Specimen 4, Single Precast Panel Wall	66
Specimen 5, Multiple Precast Panel Wall	71
Comparison of Results	74
IV. ANALYSIS	86
Introduction	86
Hysteresis Model	86
Concrete Modulus	90
Analytical Results, Stiffness	90

## TABLE OF CONTENTS (Continued)

	Page
Analytical Results, Load Capacity	96
Stress Coefficients	103
Recommendations	106
V. EVALUATION AND DISCUSSION	108
Introduction	108
Specimen 1	108
Specimen 2	110
Specimen 3	111
Specimen 4	115
Specimen 5	121
Shear Slip Response	124
Comparison	125
VI. SUMMARY AND CONCLUSIONS	128
VII. RECOMMENDATIONS	134
APPENDIX A: REVIEW OF RELATED RESEARCH	137
APPENDIX B: SPECIMEN DESIGN	148
APPENDIX C: MATERIALS	184
APPENDIX D: FABRICATION OF SPECIMENS	200
APPENDIX E: PULLOUT TESTS	230
APPENDIX F: TEST PROCEDURES AND RESULTS	248
REFERENCES	367

## LIST OF TABLES

Table	Page
1. Concrete Compressive Strength	29
2. Concrete Mix Design	30
3. Reinforcing Steel Properties	31
4. Stiffness of Infilled Walls	95
5. Calculated and Experimental Load Capacity	100
B-1. Summary of Design Analysis for Monolithically Cast Wall	173
C-1. Heat Treatment and Physical Properties of Eleven Gage Steel Rod	191
C-2. Physical Properties of Deformed Steel Reinforcing Bars	192
C-3. Mix 1 for Specimens 1 and 2	193
C-4. Mix 2 for Specimens 3, 4 and 5	193
C-5. Drypack Mortar Mix	193
C-6. Tests of 5/8-in. Wedge Anchors by Pittsburgh Testing Laboratory (38)	194
E-1. Pullout Tests by Strand (60)	243
E-2. Computed Loaded End Displacement for Pullout Specimens at Bar Stress of 32,000 psi	243

## LIST OF FIGURES

Figure		Page
1.	Specimen 2 after Completed Test.	10
2.	Reinforcement Diagram for Frame.	13
3.	Monolithic Shear Wall Reinforcing Detail.	16
4.	Cast-in-Place Shear Wall Reinforcing Detail.	19
5.	Single Precast Wall Panel Reinforcing and Connecting Detail.	21
6.	Detail 4a Panel-to-Frame Connector Detail.	22
7.	Multiple Precast Panel Reinforcing and Connecting Detail.	25
8.	Reversed Cycle Deflection Sequence.	27
9.	Column and Base Reinforcement in Plywood Forms.	34
10.	Beam and Slab Reinforcement in Plywood Forms.	34
11.	Placing Reinforcement for Specimen 1.	35
12.	Roughening Frame of Specimen 3 after Epoxy Bonding #3 Dowels.	37
13.	Reinforcing and Back Form in Place for Specimen 3.	37
14.	Tying Reinforcement for Single Panel of Specimen 4.	39
15.	Vertical Reinforcement and Rectangular Shear Plates Were Welded to Embedded Connector Plate, Specimen 4.	39
16.	Ear Plate, Panel-to-Frame Connector, Specimens 4 and 5.	40
17.	Erection of Single Panel with Fork Lift Truck.	40
18.	Tying Reinforcing Bars of Six Panels for Specimen 5.	42
19.	Erection of Multiple Panel Wall, Specimen 5.	43
20.	Instrumentation Set-Up.	44

LIST OF FIGURES (Continued)

Figure		Page
21.	Test Set-Up for Specimen 5.	47
22.	Two Jack Load System. Specimen 3 Shown Deflected to -1.3 in.	47
23.	Specimen 1, Load-Deflection Response.	52
24.	Specimen 2, Load-Deflection Response.	53
25.	Specimen 3, Load-Deflection Response.	54
26.	Specimen 4, Load-Deflection Response.	55
27.	Specimen 5, Load-Deflection Response.	56
28.	Specimen 1, Summary of Maximum Load and Energy Dissipation Data.	57
29.	Specimen 1, After Three Cycles to $\pm 0.8$ in.	58
30.	Specimen 1, Base of Positive Column After Cycles to $\pm 1.3$ in.	60
31.	Specimen 1 After Completed Test.	60
32.	Specimen 2, Summary of Maximum Load and Energy Dissipation Data.	61
33.	Specimen 2, Left Column After Completed Test.	62
34.	Specimen 3, Summary of Maximum Load and Energy Dissipation Data.	64
35.	Specimen 3 After Three Cycles to $\pm 0.8$ in.	65
36.	Specimen 3, Shear Failure of Negative Column During Cycle to -2.6 in.	65
37.	Specimen 4, Summary of Maximum Load and Energy Dissipation Data.	67
38.	Specimen 4, Shear Failure of Top Beam.	68
39.	Specimen 4, Anchor Bolts Pulled Out at Positive End of Base Beam at -1.68 in.	70

LIST OF FIGURES (Continued)

Figure		Page
40.	Specimen 4, Crushing at Top of Panel at Deflection of +2.58 in.	70
41.	Specimen 5, Summary of Maximum Load and Energy Dissipation Data.	72
42.	Specimen 5 After Three Cycles to $\pm 0.8$ in.	73
43.	Specimen 5 After Three Cycles to $\pm 1.3$ in.	73
44.	Specimen 5 After Completed Test.	74
45.	Maximum Load-Deflection Envelope for the Five Specimens.	75
46.	Maximum Stress Coefficient Envelope for the Four Infilled Specimens.	77
47.	First, Second and Third Cycle Coefficient Envelope for Specimens 1, 3, 4 and 5 from Top to Bottom, Respectively.	78
48.	Load Degradation as a Function of Deflection Amplitude.	81
49.	Decrease in Energy Dissipated Per Cycle.	83
50.	Cumulative Energy Dissipation of the Five Specimens.	84
51.	Load-Deflection Hysteresis Model for Infilled Shear Walls.	87
52.	Modified Stress Coefficient Envelopes for Specimens 1 and 3.	104
53.	Modified Stress Coefficient Envelopes for Specimens 4 and 5.	105
B-1.	Design of Model Frame, Specimen 2.	174
B-2.	Design of Footings for all Specimens.	175
B-3.	Design of Monolithic Shear Wall, Specimen 1.	176
B-4.	Design of Cast-in-Place Shear Wall, Specimen 3.	177

## LIST OF FIGURES (Continued)

Figure		Page
B-5.	Design of Single Precast Panel Wall, Specimen 4.	178
B-6.	Detail 4a of Panel-to-Frame Connector.	179
B-7.	Detail 4b of Connection of Single Panel to Frame.	180
B-8.	Design of Multiple Precast Panel Wall, Specimen 5.	181
B-9.	Detail Design of a Multiple Precast Panel Unit.	182
B-10.	Detail of Panel-to-Panel Connection.	183
C-1.	Average Stress-Strain Behavior of "as delivered" 11 Gage Plain Steel Bar.	195
C-2.	Average Stress-Strain Behavior Annealed 11 Gage Plain Steel Bar.	196
C-3.	Average Stress-Strain Behavior of #3 Deformed Steel Reinforcing Bar.	197
C-4.	Average Stress-Strain Behavior of #4 Deformed Steel Reinforcing Bar.	198
C-5.	Average Stress-Strain Behavior of #5 Deformed Steel Reinforcing Bar.	199
D-1.	Plywood Forms for Base of Specimens.	216
D-2.	Footing Reinforcement and Cardboard Tubes for Forming Holes for Hold-Down Bolts.	216
D-3.	Erection of #5 Column Bars.	217
D-4.	Reinforcement Layout for Top Beam and Slab.	217
D-5.	Detail of Reinforcement Near Edge Beam.	218
D-6.	Casting of the Top Beam.	218
D-7.	Removing Segmented Beam Form.	219
D-8.	Placement of Reinforcing for Specimen 1.	219
D-9.	Forms for the Columns and Wall of Specimen 1.	220

LIST OF FIGURES (Continued)

Figure	Page
D-10. Dowel Bars Epoxied into Frame, Specimen 3.	220
D-11. Spreading Epoxy on Dowel Bar.	221
D-12. Tape Used as Dam Over Hole in Columns.	221
D-13. Twisting Dowel into Epoxy Filled Hole in Column.	221
D-14. Taping Hole Closed to Retain Epoxy.	222
D-15. Slitted Duct Tape was Placed Over Holes in the Top Beam.	222
D-16. Placing Dowel in Epoxy Filled Hole in the Top Beam and Then Packing With Clay.	222
D-17. Chiseling Frame for Better Bond.	223
D-18. Wall Reinforcement for Specimen 3.	223
D-19. Detail of Top Beam-Column Joint Showing 90° Hooks, Strain Gaged Dowel Bars, and Roughened Frame Concrete.	224
D-20. Forming Infilled Wall, Specimen 3.	224
D-21. Hand Placing Drypack Concrete in 3-in. Gap at Top of Infilled Wall.	225
D-22. Packing and Smoothing Drypack.	225
D-23. Formwork and Reinforcement for Single Precast Panel, Specimen 4.	226
D-24. Vertical Bars and Shear Plate Connectors Were Welded to Embedded Panel Plates.	226
D-25. Panel-to-Frame Connector Bolted to Base Beam, Specimen 4.	226
D-26. Erection of Single Precast Panel Using Fork-Lift Truck.	227
D-27. Ear Plates Welded to Panel Plate Near Center of Panel.	227

LIST OF FIGURES (Continued)

Figure		Page
D-28.	Formwork and Reinforcement Layout for the Six Precast Panels of Specimen 5.	228
D-29.	Backside and Top of Panels #6, left and #5, Right.	228
D-30.	Positioning of Panels in Specimen 5.	229
D-31.	C-Clamps Used to Hold Panels Prior to Welding.	229
E-1.	Schematic Diagram of Pullout Tests.	244
E-2.	Load-Deflection Response for Pullout Specimens of Different Embedment Lengths Epoxied into 5/8 in. Diameter Holes.	245
E-3.	Load-Deflection Response for Pullout Specimens Epoxied into Holes of Various Diameters with Embedment Lengths of 2-5/8 in.	246
F-1.	Specimen 1 in Test Frame.	295
F-2.	Specimen 1, Tie Down Bolts in End-Block Foundation.	295
F-3.	Specimen 1 Under First Load, Strain and Load Recording Equipment in Foreground.	295
F-4.	Specimen 1, Four Jack Load System.	295
F-5.	Specimen 1, Two Jack Load System.	296
F-6.	Specimen 1, Diagram Illustrating Deflection-Time Reversed Cycle Procedure.	296
F-7.	Specimen 1, Cracking at +53.4 kips Load Level.	297
F-8.	Specimen 1, Strain Pattern at Bottom of Wall During First Load Cycle to +107 kips.	297
F-9.	Specimen 1, Strain Pattern at Top of Wall During First Load Cycle to +107 kips.	298
F-10.	Specimen 1, Strain Pattern at Bottom of Wall During First Load Cycle to -107 kips.	298
F-11.	Specimen 1, Strain Pattern at Top of Wall During First Load Cycle to -107 kips.	299

LIST OF FIGURES (Continued)

Figure		Page
F-12.	Specimen 1, Crack Pattern After Cycles to <u>+107</u> kips.	299
F-13.	Specimen 1, Cracking of Foundation.	300
F-14.	Specimen 1, Edge Beam Failure at -150 kips.	300
F-15.	Specimen 1, Repair of Edge Beam.	300
F-16.	Specimen 1, Compression Column at Load of +125.7 kips.	300
F-17.	Specimen 1, Tension Column at Load of +125.7 kips.	301
F-18.	Specimen 1, Load Deflection Response for Three Cycles to <u>+0.8</u> in.	301
F-19.	Specimen 1, Bottom Strain Gage at First Half Cycle to -0.8 in.	302
F-20.	Specimen 1, Top Strain Gage at First Half Cycle to -0.8 in.	302
F-21.	Specimen 1, Load-Deflection Curve to <u>+1.3</u> and -2.6 and +2.1 in.	303
F-22.	Specimen 1, Compression Side at Second Half Cycle to +1.3 in.	303
F-23.	Specimen 1, Tension Side at Second Half Cycle to +1.3 in.	304
F-24.	Specimen 1, South Column After Three Cycles to <u>+1.3</u> in.	304
F-25.	Specimen 1, North Column After Three Cycles to <u>+1.3</u> in.	304
F-26.	Specimen 1, Southwest Portion Collapse.	304
F-27.	Specimen 1, North Portion After Test.	305
F-28.	Specimen 1, South Portion After Test.	305

LIST OF FIGURES (Continued)

Figure		Page
F-29.	Specimen 1, Entire Specimen Three Cycles After Test.	305
F-30.	Specimen 2, After Three Cycles to $\pm 0.5$ in.	305
F-31.	Specimen 2, Deflection Sequence.	306
F-32.	Specimen 2, Load-Deflection Curve for Three Cycles to $\pm 0.5$ in.	306
F-33.	Specimen 2, Load-Deflection Curve for Three Cycles to $\pm 0.8$ in.	307
F-34.	Specimen 2, Load-Deflection Curve for Three Cycles to $\pm 1.3$ in.	307
F-35.	Specimen 2, Beam-Column Cracking at $+1.3$ in. Deflection.	308
F-36.	Specimen 2, Load-Deflection Curve for Two Cycles to $\pm 2.6$ in.	308
F-37.	Specimen 2, Crushing at Beam-Column Intersection.	309
F-38.	Specimen 2, Diagonal Cracking in North Column.	309
F-39.	Specimen 3, Load-Deflection Curve for $+0.1$ in. Cycles.	310
F-40.	Specimen 3, Second Half Cycle to $0.2$ in., $74.4$ kips.	311
F-41.	Specimen 3, Load Deflection Curve of $\pm 0.5$ in. Cycles.	311
F-42.	Specimen 3, Diagonal Crack Through North Column and Base Beam During Second Half Cycle to $+0.56$ in.	311
F-43.	Specimen 3, Strain Pattern, Bottom Gages First Half Cycle to $-0.5$ in.	312
F-44.	Specimen 3, Strain Pattern, Top Gages First Half Cycle to $-0.5$ in.	312

LIST OF FIGURES (Continued)

Figure		Page
F-45.	Specimen 3, Strain Pattern, Bottom Gages Second Half Cycle to +0.5 in.	313
F-46.	Specimen 3, Strain Pattern, Top Gages Second Half Cycle to +0.5 in.	313
F-47.	Specimen 3, Extensive Diagonal Cracking After <u>+0.5</u> in. Cycle.	314
F-48.	Specimen 3, Load-Deflection Curve <u>+0.8</u> in. Deflection.	314
F-49.	Specimen 3, Beginning of Corner Curshing, -0.72 in. Deflection.	315
F-50.	Specimen 3, Diagonal Crack in North Column, -0.72 in. Deflection.	315
F-51.	Specimen 3, Joint Slip and Drypack Crack, -0.72 in. Deflection.	315
F-52.	Specimen 3, Crushing in CIP Wall and South Column Diagonal Crack, +0.83 in.	315
F-53.	Specimen 3, Crushing in Drypack and CIP Top North Corner, +0.83 in.	316
F-54.	Specimen 3, Third Half-Cycle to -0.72 in. Deflection.	316
F-55.	Specimen 3, North Column and Wall at Third Cycle to +0.83 in.	316
F-56.	Specimen 3, South Column and Wall After Third Cycle to +0.83 in.	316
F-57.	Specimen 3, Load-Deflection Curve for Three Cycles to <u>+1.3</u> in. and One Cycle to <u>+2.6</u> in.	317
F-58.	Specimen 3, North Side at Deflection of +1.3 in.	317
F-59.	Specimen 3, South Side at Deflection of +1.3 in.	318
F-60.	Specimen 3, North Side After 2-1/2 Cycles to -1.3 in.	318

LIST OF FIGURES (Continued)

Figure		Page
F-61.	Specimen 3, North Column at +2.63 in.	318
F-62.	Specimen 3, South Column at +2.63 in.	318
F-63.	Specimen 3 at Completion of Test.	319
F-64.	Specimen 3, Bottom Surface of Beam After Test Completed.	319
F-65.	Specimen 3, Close-Up of Vertical Dowel Bar After Test Completed.	319
F-66.	Specimen 4, Dial Gage Used for Slip Measurement.	320
F-67.	Specimen 4, After Three Cycles to $\pm 0.20$ in.	320
F-68.	Specimen 4, Load-Deflection Curve for $\pm 0.2$ in. Cycles.	321
F-69.	Specimen 4, Load-Deflection Curve for $\pm 0.5$ in. Cycles.	321
F-70.	Specimen 4, North Column at +0.5 in., Second Half Cycle.	322
F-71.	Specimen 4, Base of North Column at +0.5 in., Second Half Cycle.	322
F-72.	Specimen 4, Bottom Strain for First Half Cycle to -0.45 in.	323
F-73.	Specimen 4, Top Strain for First Half Cycle to -0.45 in.	324
F-74.	Specimen 4, South Side of Base Beam After Fifth Cycle to -0.5 in.	325
F-75.	Specimen 4, Load-Deflection Curve for Three Cycles to $\pm 0.9$ in.	325
F-76.	Specimen 4, Diagonal Shear Failure of Top Beam, -95.5 kips.	326
F-77.	Specimen 4, Pullout of Anchors After First Half Cycle to -0.98 in.	326

LIST OF FIGURES (Continued)

Figure	Page
F-78. Specimen 4, Bottom Strain Pattern for First Half Cycle to -0.89 in.	327
F-79. Specimen 4, Top Strain Pattern for First Half Cycle to -0.89 in.	328
F-80. Specimen 4, Top Beam Showing Repair Using Steel Angles	329
F-81. Specimen 4, Load-Deflection Curve for Three Cycles $\pm 1.3$ in. and One Cycle -1.7 in, +2.6 in.	329
F-82. Specimen 4, Top Beam at First Half Cycle to -1.32 in.	330
F-83. Specimen 4, Ear Plate Connector at South End of Base Beam, Deflection of -1.32 in.	330
F-84. Specimen 4, Diagonal Shear Crack in Column Resulting from Wall Bearing on Column.	330
F-85. Specimen 4, Maximum Negative Deflection -1.68 in.	330
F-86. Specimen 4, Pullout of Anchors at -1.68 in.	331
F-87. Specimen 4, Maximum Positive Deflection +2.58 in.	331
F-88. Strain Gage Location in Specimen 5.	332
F-89. Specimen 5, Load-Deflection Curve for Three Cycles to $\pm 0.22$ in.	332
F-90. Specimen 5, Panels #1 Through #5, Left to Right, After Three Cycles $\pm 0.22$ in.	333
F-91. Specimen 5, Load-Deflection Curve for Three Cycles $\pm 0.5$ in.	333
F-92. Specimen 5, Panels After First Cycle $\pm 0.5$ in. Showing Diagonal Shear Cracks.	334
F-93. Specimen 5, Bottom Strain Pattern for First Half Cycle to -0.52 in.	334
F-94. Specimen 5, Top Strain Pattern for First Half Cycle to -0.52 in.	335

LIST OF FIGURES (Continued)

Figure		Page
F-95.	Specimen 5, Bottom Strain Pattern For Second Half to +0.50 in.	336
F-96.	Specimen 5, Top Strain Pattern for Second Half Cycle to +0.50 in.	337
F-97.	Specimen 5, Load-Deflection Curve for Three Cycles <u>+0.8</u> in.	338
F-98.	Specimen 5, Bottom Strain Pattern for First Half Cycle to -0.84 in.	339
F-99.	Specimen 5, Top Strain Pattern for Second Half Cycle to -0.84 in.	340
F-100.	Specimen 5, Top Connector Between #1 and #2 at +0.74 in.	341
F-101.	Specimen 5, Top of Panel #3 at +0.84 in., Second Half Cycle.	341
F-102.	Specimen 5, Second Half Cycle to +0.74 in.	342
F-103.	Specimen 5, Load Deflection for Three Cycles <u>+1.3</u> in. and One Cycle <u>+2.6</u> in.	342
F-104.	Specimen 5, First Cycle at +1.32 in.	343
F-105.	Specimen 5, Fifth Cycle at -1.26 in.	343
F-106.	Specimen 5, During Sixth Half Cycle at +1.32 in., Top Panel-to-Panel Connector Between #3 and #4.	343
F-107.	Specimen 5, Sixth Half Cycle at +1.32 in.	343
F-108.	Specimen 5, Shear Failure of South Column at -2.59 in.	344
F-109.	Specimen 5, Shear Failure at Base of North Column at -2.59 in.	344
F-110.	Specimen 5, From Left to Right, Panels #2 Through #5 at -2.59 in.	344

LIST OF FIGURES (Concluded)

Figure		Page
F-111.	Specimen 5, Shear Failure at Top of North Column at +2.68 in.	345
F-112.	Specimen 5, Shear Deflection at Top of Panels at +2.68 in.	345
F-113.	Specimen 5, Top Panel-to-Panel Connector Between #2 and #3 at +2.68 in.	346
F-114.	Specimen 5, Test Completed, Zero Deflection	346

## LIST OF APPENDICES

Appendix	Page
A. REVIEW OF RELATED RESEARCH	137
B. SPECIMEN DESIGN	148
C. MATERIALS	184
D. FABRICATION OF SPECIMENS	200
E. PULLOUT TESTS	230
F. TEST PROCEDURES AND RESULTS	248

## NOTATION

$A_v$	Area of shear reinforcement within a distance $s$ (in. <sup>2</sup> )
$A_{vh}$	Area of shear reinforcement parallel to tension reinforcement (in. <sup>2</sup> )
$A_{wh}$	Total area of horizontal wall reinforcement (in. <sup>2</sup> )
$A_{wn}$	Total area of vertical wall reinforcement (in. <sup>2</sup> )
$C$	hd for Specimen 1 (in. <sup>2</sup> )
$d$	Distance from extreme compression fiber to centroid of vertical tension reinforcement (in.)
$E_c$	Concrete modulus (psi)
$f'_c$	Laboratory compressive strength of concrete (psi)
$f'_{cf}$	Field compressive strength of concrete (psi)
$G$	Shear modulus of concrete (psi)
$h$	Wall thickness (in.)
$h_s$	Story height
$h_w$	Height of wall from top of base beam to bottom of top beam (in.)
$I$	Moment of inertia of a section (in. <sup>4</sup> )
$I_{cr}$	Moment of inertia of a cracked section transformed to concrete (in. <sup>4</sup> )
$K_d$	Degrading stiffness of hysteresis model (kips/in.)
$K_f$	Lateral stiffness of a frame without an infilled wall (kips/in.)
$K_i$	Lateral stiffness of Specimen $i$ (kips/in.)
$K_y$	Yield stiffness of hysteresis model (kips/in.)
$l_n$	Effective span length of precast panels (in.)

$l_w$	Length of wall, clear distance between columns (in.)
$s$	Spacing in stirrups (in.)
$s_1$	Spacing of vertical reinforcement in a wall (in.)
$s_2$	Spacing of horizontal reinforcement in a wall (in.)
$V$	Maximum observed lateral load occurring in a half cycle (kips)
$V_j$	Calculated joint shear capacity (kips)
$V_{pi}$	Calculated shear capacity of panel $i$ (kips)
$V_{sf}$	Calculated shear load based on shear friction hypothesis (kips)
$V_u$	Calculated total design shear force (kips)
$v_c$	Nominal permissible shear stress carried by concrete
$v_u$	Nominal total design shear stress
$\Delta$	Lateral story deflection (in.)
$\mu$	Coefficient of friction
$\rho_h$	Ratio of horizontal wall reinforcement area to the gross area
$\rho_n$	Ratio of vertical wall reinforcement area to the gross area of a horizontal section of the wall
$\phi$	Capacity reduction factor

CHAPTER I  
INTRODUCTION

Purpose and Scope of Research

The purpose of the research was to investigate experimentally the cyclic strength of infilled, reinforced concrete shear walls and to determine whether the suggested infilling techniques may be used satisfactorily for aseismic strengthening. Aseismic strengthening of existing structures in order to improve their earthquake resistance may be accomplished before an earthquake occurs or along with the repair of a previously damaged structure.

The investigation was designed to indicate the cyclic strength and strength deterioration of various reinforced concrete frames with cast-in-place and precast reinforced concrete shear walls. Investigation of the frame-to-wall connection was emphasized.

The scope of the investigation was limited. Four half-scale, one-story, one-bay reinforced concrete frames with infilled shear walls were tested. A fifth frame without an infilled wall was tested for reference. The five frames and the loading conditions were identical for all tests; the variables studied were the type of infilled wall and its connection to the surrounding frame. All infills were made of reinforced concrete, some cast-in-place and others precast.

### Philosophy of Strengthening

The current standard philosophy for the design of earthquake resistant structures is that minor damage is permitted for moderate earthquakes and that damage is accepted for severe earthquakes so long as complete collapse is prevented. While this design philosophy is adequate for most structures, it is inappropriate for the design of emergency facilities which must remain in service after a major earthquake. These facilities include hospitals, fire and police stations, National Guard armories, communication centers, and power stations.

Medical care centers must remain in service for the treatment of those injured in the earthquake. In the Managua, Nicaragua, Earthquake of 1972, two principal hospitals were severely damaged and could not be used. Four major hospitals in San Fernando, California were rendered useless by the San Fernando Earthquake of 1971. In each case, the community's existing facilities could not be used to aid in disaster relief.

The San Francisco Earthquake of 1906 and the 1972 Managua Earthquake illustrated that fires occurring after the main shock cause considerable damage and potential loss of life. In Managua the firefighting equipment was trapped beneath collapsed structures.

Police and National Guard centers must remain viable after a disaster to facilitate the maintenance of order, to provide emergency shelter and transportation, and to act as centers for the restoration of the damaged community.

Telephone and radio communications are desirable after a disaster so that the community can be organized and helped. Electric power should be maintained for cooking, heating and lighting purposes and for restoration operations.

The design philosophy required for such emergency facilities is that the facility must remain in operable condition after a severe earthquake. The State of California has recently enacted a law which does require newly constructed hospitals to meet this condition. Similar construction requirements are under legislative consideration for other emergency facilities.

Existing facilities must survive, also. Replacing existing structure with ones constructed to new, more stringent requirements would be uneconomical. To maintain the use of existing facilities after the earthquake, those facilities must be strengthened to improve their earthquake resistance.

For this new construction philosophy, improved earthquake resistance includes the limitation of structural deflections. Design by the standard philosophy prevents collapse; the details of the design often permit large, inelastic deformations by assuring member and connection ductility. While this ductility prevents collapse, large deflections of the structure may render the structure unsafe for occupancy until repairs are completed and almost certainly may lead to major damage of architectural and mechanical elements such as wall panels, ceilings, lights and other fixtures, elevators, plumbing and ventilation systems. It is damage to these non-structural elements which may reduce the facilities effectiveness.

To reduce the damage to these elements, two paths should be followed. First, the elements should be "uncoupled" from the structural system as much as possible so that they are not forced to undergo as much deformation as the structure. Second, the structural deflections should be reduced in order to minimize deformation of architectural and mechanical elements.

In new construction, the architect can specify connections of non-structural elements so that minimum damage occurs due to deflections, and the engineer can design stiffer structures in order to reduce deflections.

The restoration of existing facilities is more complex. Some architectural modifications may be made easily, but reduction of structural deformation implies major structural revisions. For each facility the structural restoration scheme will be unique and will depend upon the original structural form and material and upon the anticipated ground motion.

One common structural system which has been used for hospitals and communication facilities is the moment resisting frame made of cast-in-place reinforced concrete. The strengthening of such a structural system may include the following: (1) enlargement of both beams and columns by casting reinforced concrete around existing elements, (2) enlargement of beams only, (3) enlargement of columns only, (4) strengthening of beams and columns by attaching steel members to those elements, (5) including bracing members in some or all bays of the structure, thus forming a K-braced or cross-braced system, (6) casting a monolithic, reinforced concrete

shear wall around part of the building's perimeter and attaching the exterior frame elements to the wall, and (7) infilling some or all of the bays with cast-in-place or precast reinforced concrete shear walls.

It appears to the author that the latter system, infilling, may be the most promising technique: it can add great lateral stiffness and be economically competitive with the other techniques while interrupting the building architecture only slightly. Such structural infilled walls may replace existing interior or exterior architectural walls. Precast construction would eliminate the need for messy and difficult construction activities at the existing facility. Cast-in-place reinforced concrete walls have been used to strengthen some existing structures.

Yet, little data is available on the seismic response of infilled shear walls which were constructed within an existing frame. The results of the research described herein will aid the engineer in designing shear walls for aseismic strengthening of existing concrete framed structures.

#### Review of Related Research

The majority of past research on infilled reinforced concrete structures concentrated on the cracking and ultimate strength behavior under monotonic loading conditions. A variety of parameters were studied including various reinforcement schemes, steel percentage, aspect ratios (wall length divided by wall height), column reinforcement and column size, wall openings, and vertical loads.

Information gained from this work has been incorporated in the current standards of the American Concrete Institute, ACI 318-71 (5). A few recent studies have examined shear wall behavior under reversed cycle lateral loads (2, 12, 13, 18, 22, 23, 30, 35, 41, 61). In general, these test results have shown that monolithically cast walls exhibit cyclic, ultimate lateral load capacities somewhat lower than the monotonic load capacities; but the cyclic capacities are as great as those predicted using design provision in ACI 318-71 (5).

After the San Fernando Earthquake of 1971, some structures were repaired and strengthened with cast-in-place reinforced concrete or reinforced masonry shear walls (34, 59, 60). Typically a reinforced gunite face was applied to an existing concrete or masonry wall. Reinforcing bars were doveled into the existing wall and into the surrounding reinforced concrete frame for shear connection. No lateral load tests were performed on these structures or any prototype to determine their adequacy for aseismic strengthening.

A more detailed literature review is given in Appendix A.

CHAPTER II  
EXPERIMENTAL PROGRAM

Design of Experimental Program

Representative Structure. In order to study aseismic strengthening, a representative reinforced concrete framed structure was chosen. It was desired that the structure be of relatively modern construction but that it be built before the advent of current earthquake engineering standards. Structures built during the 1950's and early 1960's seemed to fit this criteria. Reinforced concrete construction standards were high and buildings were analyzed considering seismic forces (62). Yet, the idea of "ductile" concrete was not widespread; few engineers were concerned with the modern concepts of concrete confinement, inelastic behavior and energy absorption capabilities. Until Blume, Newmark and Corning authored "Design of Multistory Reinforced Concrete Buildings for Earthquake Motions" (20) the standards of the American Concrete Institute were little concerned with the ultimate behavior and ductility of concrete structures. In 1973 the Uniform Building Code (63) adopted more stringent requirements for the seismic resistance of reinforced concrete structures.

It was desired that the structure represent a building which may require strengthening. Further, the structural dimensions

should be similar to the scaled dimensions of model shear wall specimens tested by previous researchers. The aspect ratio (ratio of bay length to story height) should be between 1.5 and 2.0 which is consistent with previous tests and with those used in actual practice.

The representative structure chosen was three stories high without a basement and was one bay wide and several bays long. Story height was 11 ft. and the clear bay width was 16 ft. The design was based on a nominal concrete strength ( $f'_c$ ) of 4000 psi, Grade 50 deformed steel bars for principal reinforcement and Grade 40 plain steel bars for beam stirrup and column hoop reinforcement. Design followed the standards presented in References 3, 14, and 62: the Building Code Requirements for Reinforced Concrete (ACI 318-56), the BOCA Basic Building Code, 1960 Edition, and the Uniform Building Code, 1946 Edition. There were no conflicts between design criteria presented in these three volumes. The CRSI Design Handbook, 1952 Edition (27) by the Concrete Reinforcing Steel Institute was used to design all bends, hooks and extensions of the reinforcing bars.

Experimental Model. The experimental specimen chosen was a one-half scale model of one story of the representative, prototype structure. Use of a single story limited the number of variables, permitted comparison with previous research, and allowed construction and testing of a large scale model. Because of the variety of unknown factors connected with strengthening, it was

decided that a single story structure should be studied before multistory ones were investigated. A large scale specimen was required so that such variables as bond, bond deterioration with cyclic loads, roughness of construction joints, and joint details could be accurately modeled. The half-scale was selected so that readily available #3 deformed bars could be used as the primary wall reinforcement and so that standard reinforcing bars could be used to model those of the representative structure. Figure 1 is a photograph of the half-scale model of the frame (Specimen 2). Because of restraints imposed by the testing apparatus, the model was designed to most represent the base story of the three-story frame structure; although the model could represent any single story of which the frame below was infilled with a wall or was otherwise stiffened. The large concrete blocks beneath the columns and the deep base beam resemble spread footings with a grade beam.

---

Experimental Variables. The experiments were designed to study the differences in lateral load response between the reinforced concrete frame and identical frames with reinforced concrete infilled walls. The two principal variables were the type of strengthening, that is, the construction of the infilled wall, and the frame-to-wall connection. A moment frame (Specimen 2) and a frame built monolithically with an infilled wall (Specimen 1) were used as the standards by which the other tests were judged.

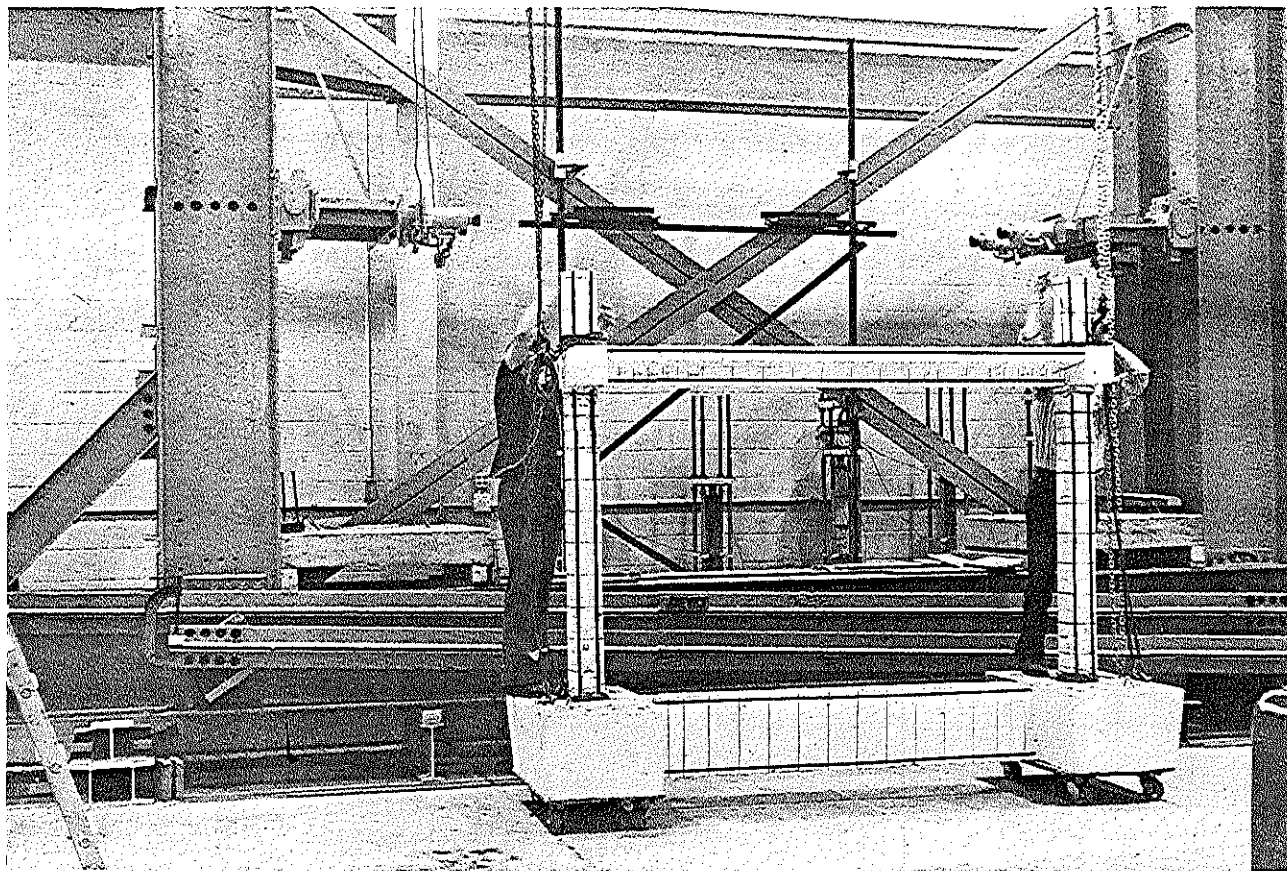


Figure 1. One-half scale model frame (Specimen 2)  
after reversed cycle test.

One infilled wall was cast within an existing frame; a single precast panel wall was fitted into a frame and mechanically connected to top and bottom beams; and a third wall was made of six small precast panels which were mechanically connected within a frame and then joined together.

The frames of the five specimens were identical except for variations in concrete strength. The steel reinforcement pattern was similar in the four walls. The percent of vertical steel reinforcement ( $\rho_n$ )<sup>\*</sup> was the same for all walls; the percent of horizontal reinforcement ( $\rho_h$ ) was varied because of the wall-to-frame connections. The mechanical properties of the steel reinforcement were the same for all specimens. The concrete compressive strength ( $f'_c$ ) varied between 3300 psi and 5600 psi, although a strength between 3600 psi and 4400 psi was typical.

Tests were conducted with no vertical load applied to the specimens. Others (2, 23, 31) have determined vertical load effects, and their findings may be used in interpreting the tests described herein. As vertical load is increased to about 40 percent of the ultimate vertical load capacity of a wall, the ultimate lateral load capacity is increased.

---

\* Where possible, all notation used in this thesis agrees with standard notation used by the American Concrete Institute (5).

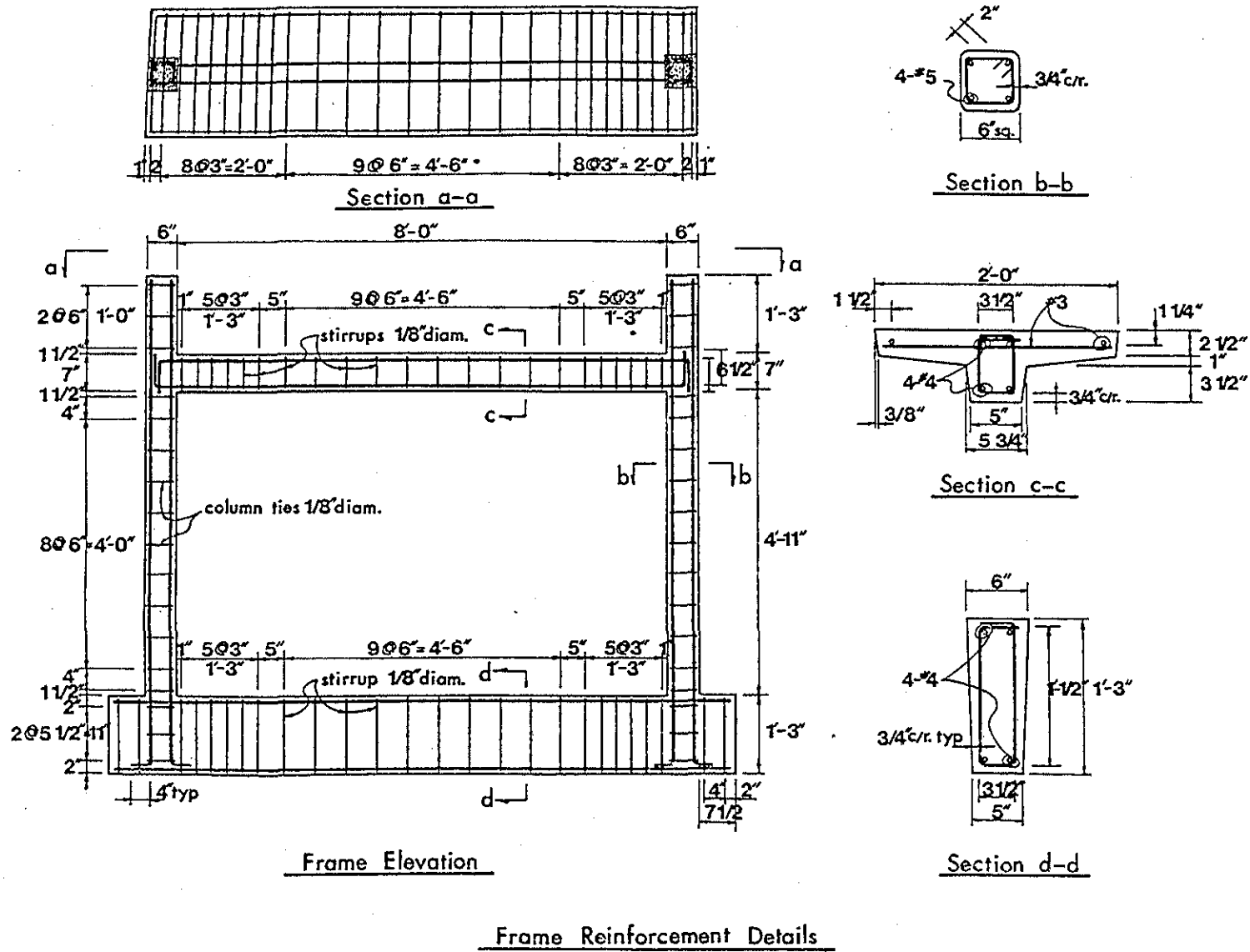
### Test Specimen Design

Frame. The reinforced concrete frame design was identical for the five specimens; it was a geometrical one-half scale model of one story of the representative frame except for the base beam and foundation blocks as described above and as detailed in Appendix B. Concrete and reinforcing steel were ordered to match the properties used for the design of the representative frame. Because of changes in criteria by the CRSI (28), the steel supplier (Bethlehem Steel Corporation) bent the bars to slightly larger radii than designed. Figure 2 presents the frame specimen design.

The base of the structural steel testing frame used to load the many specimens was constructed of two parallel bents made with W24 x 110 wide flange sections and separated a distance of 2-ft. 3-in. The foundation blocks of the test specimens had to span this spacing and to act as a beam rather than as a flat slab as is typical of footings. Therefore, the foundation blocks were designed and reinforced as deep beams according to ACI 318-71 (5).

The base beam was designed to be much stiffer than a typical story beam of the prototype frame so that the footings would have greater rotational resistance and so that the base could be considered a typical story beam with an infilled wall below it. The 15-in. depth of the beam was chosen so that the concrete could resist the design shear stresses without vertical steel reinforcement. It was desired that the base undergo minimum damage

Figure 2. Reinforcement diagram for frame.



during the tests and that the major deformations be concentrated in the upper portions of the test specimen.

The top beam which was cast with the slab was designed as a T-beam. The requirements of ACI 318-56, Section 8.7.2 (3), for the design and analysis of T-beams states, "The effective flange width to be used in the design of symmetrical T-beams shall not exceed one-fourth of the span length of the beam..." Because the span length of the model was 96 in., the effective T-width was 24 in. The slab width used in constructing the model was chosen as 24 in. in order to minimize variance between design analysis and test results.

The slab of the T-beam was designed to carry the concentrated lateral loads which were applied to the ends of the slab during the tests. A design objective was that the slab distribute lateral forces evenly to the infilled wall. In previous tests with no slab (16), forces were concentrated at the loaded corner of the wall and caused localized failure.

The columns were designed as simple tied columns with the minimum number of hoops; no additional hoops were required for shear stresses. No hoops were required nor were used in the core of the beam-column connection; current standards, ACI 318-71, do require such reinforcement. In the model frame all column hoops and beam stirrups were made of plain 11-gage wire with material properties as described in Appendix C. This wire modeled plain #2 bars of the representative frame. Therefore, the use of plain

bars was not considered to have diminished the accuracy of concrete modeling.

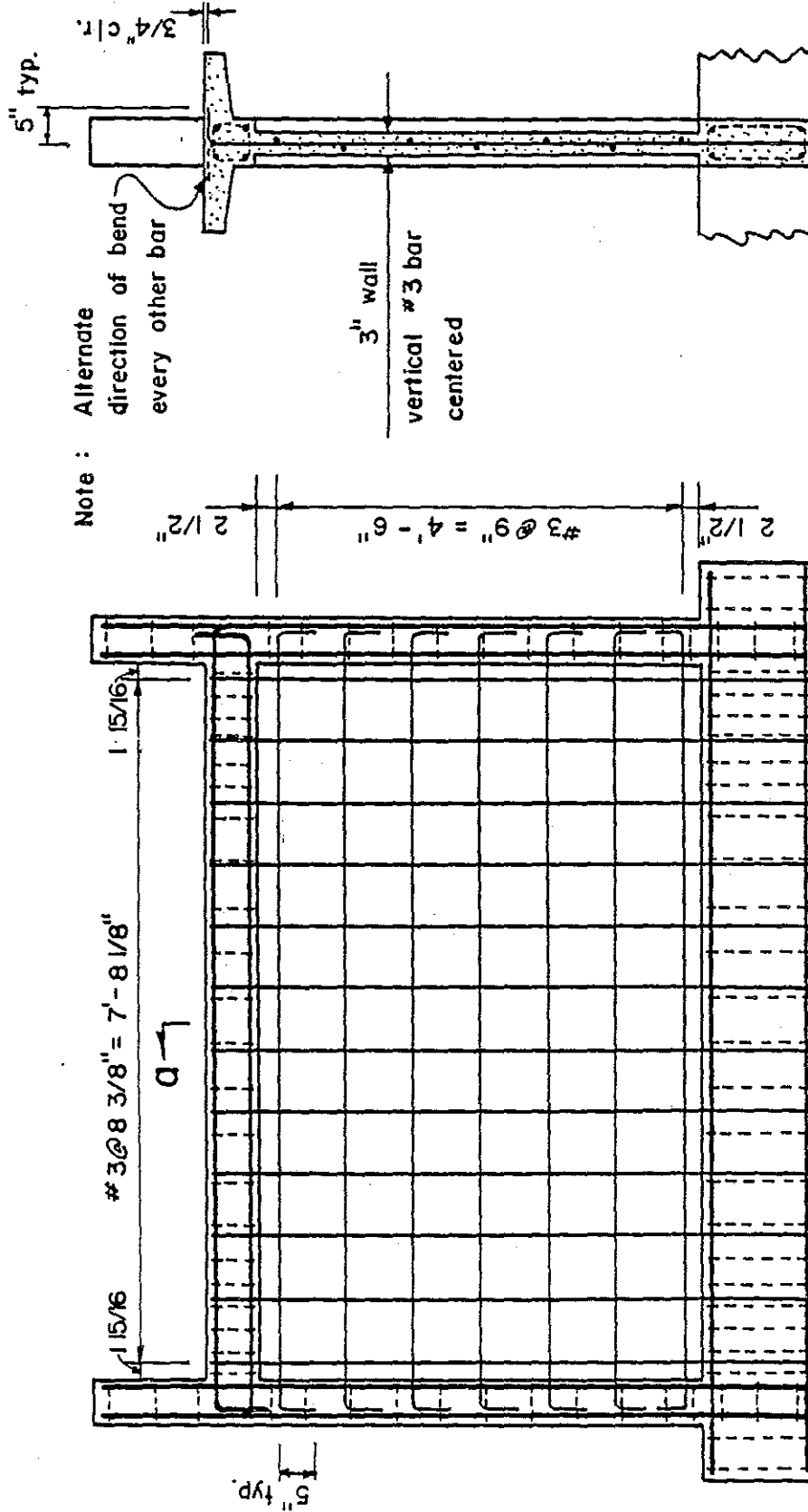
The stub column represented the continuation of the column to the story above; its main purpose in the model was as an anchorage for the column steel.

Monolithic Wall. Specimen 1 was constructed with the infilled wall reinforced and cast monolithically with the surrounding frame. The design of the wall was based on the standards for "special shear walls" of the Building Code Requirements for Reinforced Concrete, ACI 318-71, (5), and of the Uniform Building Code, 1973 Edition. Minimum bar spacing and other detail criteria were applied to dimensions on the prototype structure and then modeled for the test specimen.

Figure 3 shows the reinforcing pattern for the monolithic shear wall. The horizontal steel reinforcement ( $\rho_h$ ) was 0.435 percent, and the vertical steel reinforcement ( $\rho_n$ ) was 0.458 percent. These percentages were determined using the following:

$$\rho_h = \frac{A_{wh}}{l_w h}$$

$$\rho_n = \frac{A_{wn}}{h h_w}$$



Note : Alternate direction of bend every other bar

3" wall  
vertical #3 bar centered

Section a-a

Elevation - Monolithic Shear Wall

Figure 3. Monolithic shear wall reinforcing detail.

where

$A_{wh}$  = total cross sectional area of horizontal reinforcement (in.<sup>2</sup>)

$A_{wn}$  = total cross sectional area of vertical reinforcement (in.<sup>2</sup>)

$l_w$  = horizontal length of wall between interior faces of columns (in.)

$h_w$  = vertical height of wall between top surface of base beam and bottom surface of T-beam (in.)

$h$  = wall thickness (in.)

This amount of wall reinforcement was selected for several reasons:

(1) it satisfied the minimums specified in ACI 318-71 Section A.8.2, which were that  $\rho_h \geq 0.0025$  and that  $\rho_n \geq 0.0015$ ; (2) the amount was within the range of steel percentages tested by several researchers (12, 16, 23); and (3) easily obtainable deformed, Grade 40, #3 reinforcing bars could be used in the models at spacings which satisfied the maximum spacing permitted by the standards (5, 63).

Horizontal wall reinforcement was continued and hooked into the columns; vertical wall reinforcement was extended straight into the base beam and hooked into the top beam.

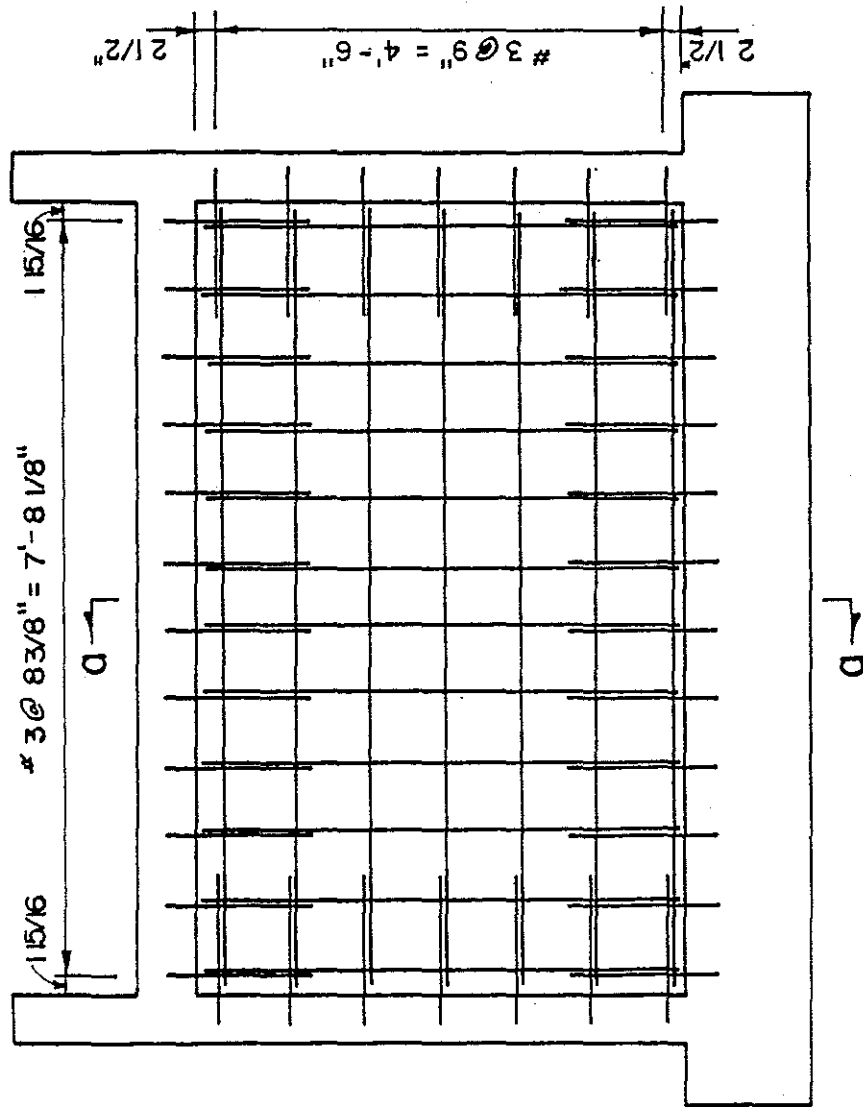
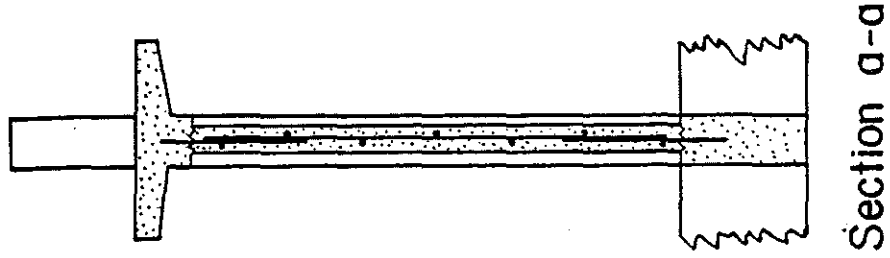
Cast-in-Place Wall. Specimen 3 was constructed with in infilled wall cast within a frame about eight months after construction of the frame. The wall was designed to have the same strength as the monolithic wall, and it utilized the same vertical and horizontal reinforcing steel percentages. The difference in design between

Specimen 1 and 3 was the connection detail of the frame to the wall. The cast-in-place wall was connected by using #3 bars doweled into the frame and by the concrete-to-concrete bond.

Figure 4 shows the reinforcing bar pattern of the cast-in place shear wall. As illustrated, a 19 in. long #3 bar was anchored into the existing frame at each location of the wall reinforcement; the lap splice of the dowels and #3 wall reinforcing bars was the principal means of assuring wall-to-frame connection and continuity. Wall reinforcing bars had a standard 90° hook at each end to assure complete bar anchorage; although the lap splice was considered adequate.

The #3 dowel bars were epoxied into holes drilled in the surrounding frame. The hole depth and diameter and the grouting technique satisfied the epoxy manufacturer's recommendations; the anchorage was designed to develop the bars' ultimate capacities. As discussed in Appendix E, the author performed pullout tests to determine the adequacy of the epoxy anchorage. It was found that the designed anchorage did develop the ultimate strength of the bar.

As specified by the Uniform Building Code, 1973, (63) the frame concrete was roughened prior to casting the wall. The concrete was chiseled so that the roughness amplitude was greater than 1/4 in. and so that aggregate was exposed all around the frame. With such roughness, full bond strength of the cold joints could be assumed; that is, the structure was designed and analyzed



Elevation Cast-in-Place Shear Wall

Figure 4. Cast-in-place shear wall reinforcing detail.

using the ultimate concrete shear stress,  $v_c$ , as specified by the Code (63).

Precast Panel Wall. The frame of Specimen 4 was infilled with a single precast panel which was cast separately from the frame. The panel was designed to resist the same lateral loads as the monolithic shear wall specimen. The vertical reinforcement layout and  $\rho_n$  in the precast panel were the same as those in the monolithic wall; the horizontal reinforcement layout was the same as Specimen 1 in the center of the panel but was altered at the top and bottom edges because of an embedded plate required for panel-to-frame connection;  $\rho_h$  was over five times larger than that of Specimen 1 due to the connector.

As shown in Figure 5, the panel was connected to the surrounding frame at the top and bottom only; no connection was made between the panel and the columns. Connection to the columns was avoided in order to prevent high concentrated shear loading of the column. An increased lateral shear load on the column might cause column failure which could result in structure collapse.

The panel-to-frame connector was designed in two parts. One was a plate which was welded to vertical reinforcing bars and embedded within the panel. The other was called the ear plate connector which was T-shaped with 1/2 in. x 1-1/2 in. x 3 in. ear plates welded to a 1/2 in. x 3 in. x 47-1/2 in. base plate (Figure 6). The base plates were attached to the top and bottom beams using Phillips 5/8 in. x 5 in. wedge anchors, which were installed in

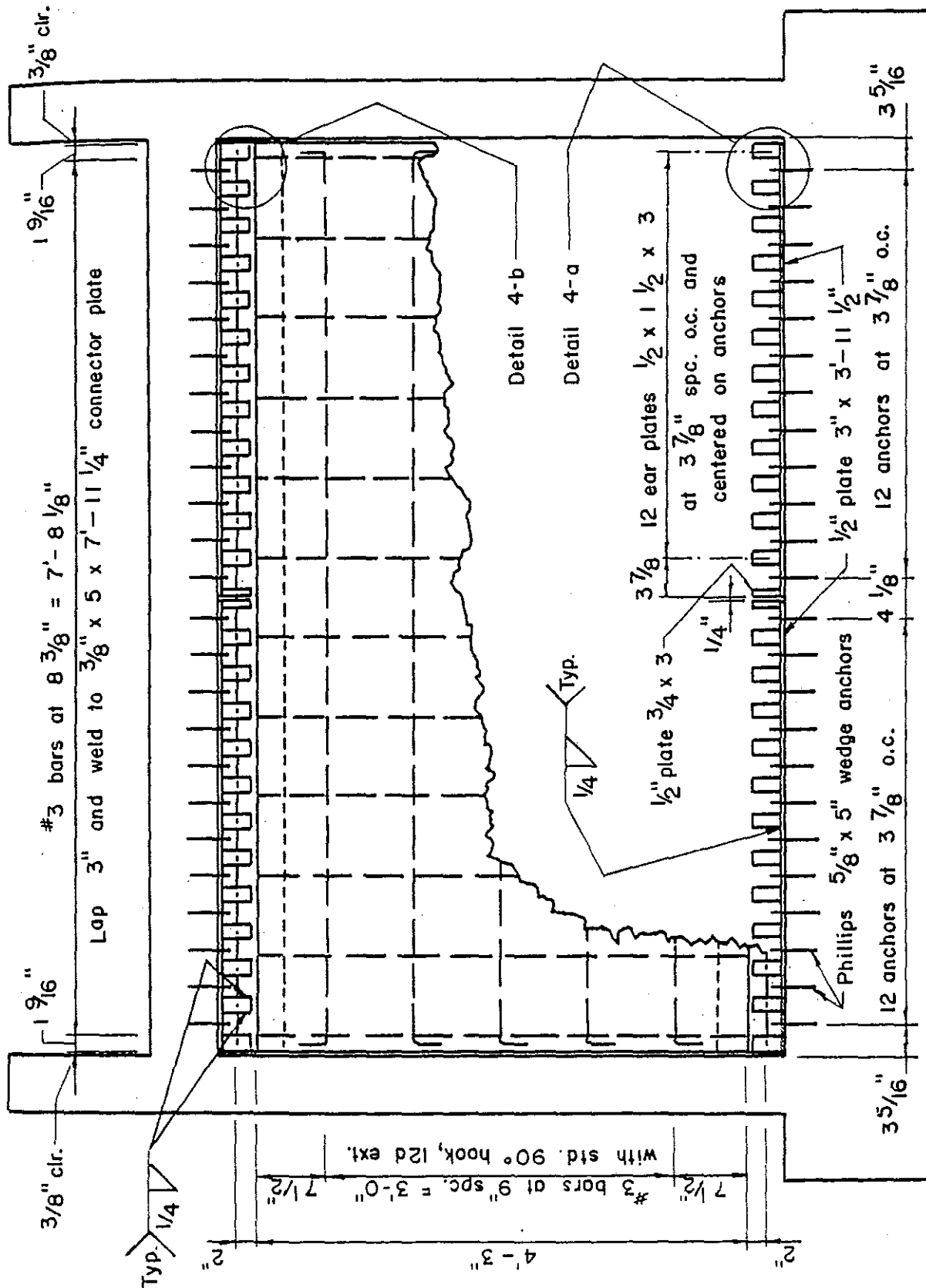
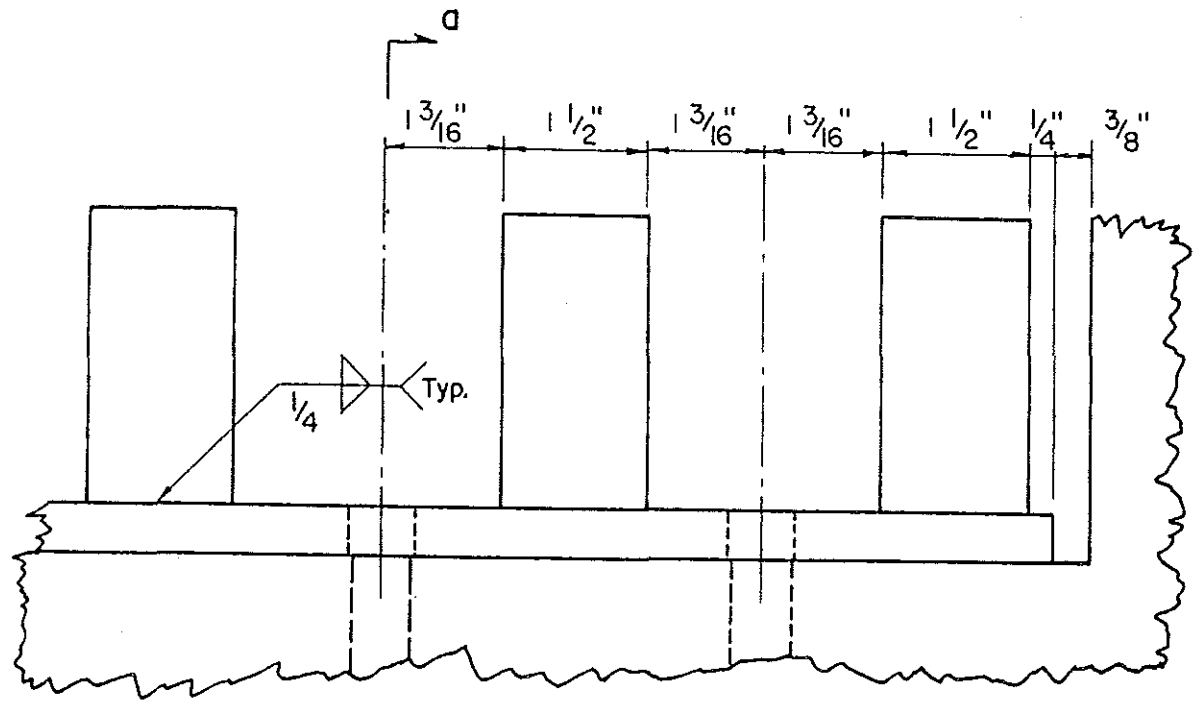
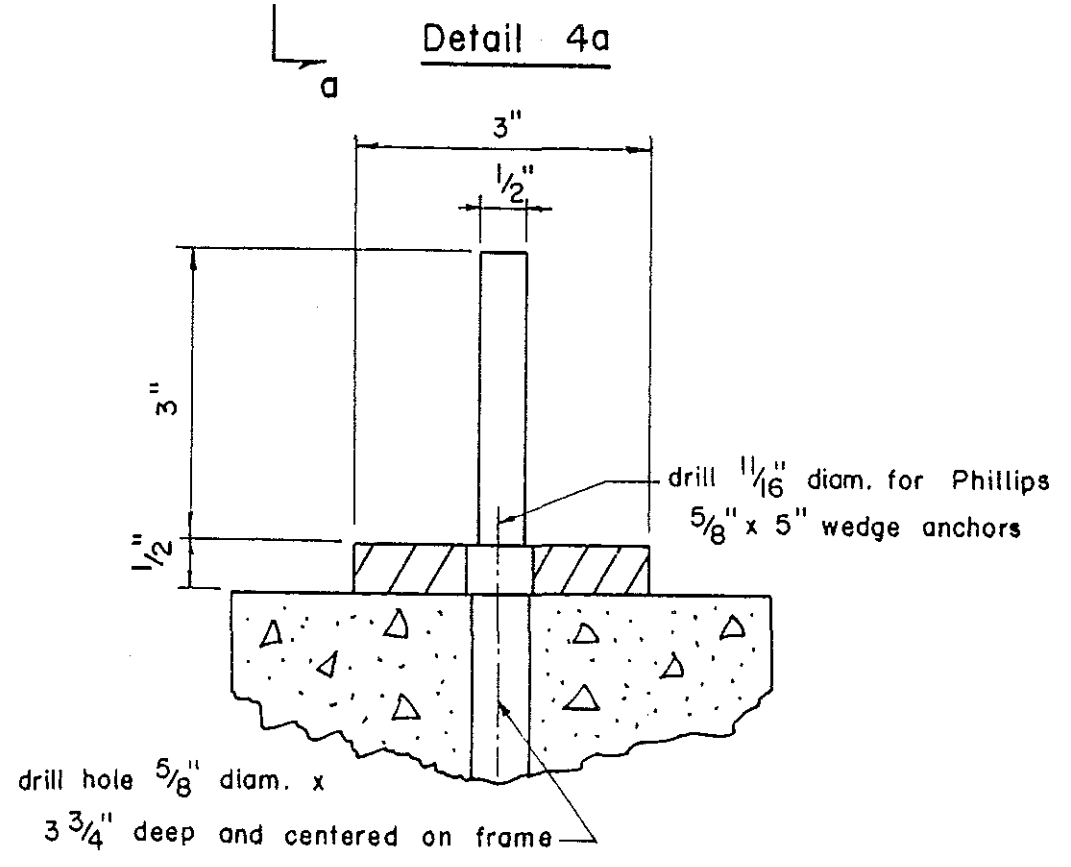


Figure 5. Single precast wall panel reinforcing and connecting detail.



Detail 4a



Section a-a

Figure 6. Detail 4a panel-to-frame connector detail.

5/8 in. diameter holes drilled in the beams. The panel was connected within the frame by field welding the embedded panel plate to the ear plate connector. A welded connection rather than a bolted connection was selected so that very accurate panel alignment was not required. It would have been difficult to align the many bolt holes which would have been required. Clearance dimensions between frame and panel were large (3/8 in. in the model, 3/4 in. in the prototype) so that the eccentricities of field construction could be accommodated and so that the panel would not contact the columns as the panel-to-frame connector slipped due to oversized bolt holes.

The panel and connection design was based on current precast design techniques as illustrated in the Prestressed Concrete Institute Design Handbook (49) and in Connection Details for Precast, Prestressed Concrete Buildings, (47) and as discussed by Diamant (32).

Grout was not placed between the panel and the frame so that the behavior of the panel and connector could be more easily determined and so that panel-to-column shear loading would be avoided.

Multiple Precast Panel Wall. Specimen 5 was constructed with an infilled wall made of six independent precast panels. The objective of this design was to make construction of the infilled wall easier and neater. For strengthening interior bays of a building, erection of small panels might be more practical because

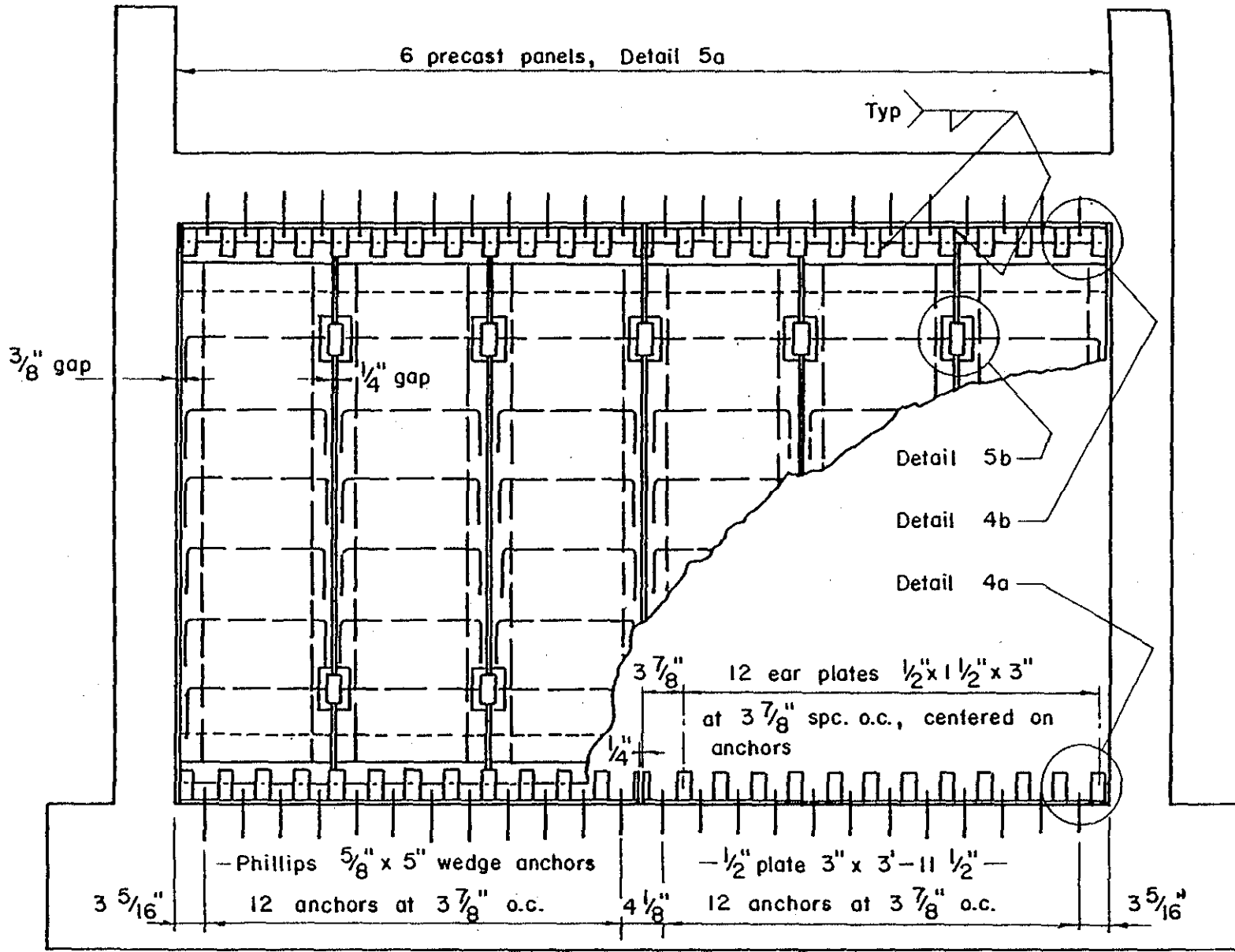
it would permit rapid, clean construction and continued building occupation.

No attempt was made to design the multiple panel wall to resist the same total lateral load as carried by the solid panel or monolithic wall. Preliminary calculations showed that the vertical reinforcement ratio would have to be increased as much as 500 percent if the multiple panel wall were to carry the same lateral load as the monolithic wall. The design of the multiple panel wall was based on facilitating construction and on copying as closely as possible the reinforcement ratios of the other shear walls.

The multiple panel reinforcement layout was altered somewhat as compared to the solid panel. As illustrated in Figure 7, the two #3 vertical bars in each panel were located toward the edge of each panel rather than evenly spaced along the wall's length; although  $\rho_n$  was the same as in other walls. The amount of horizontal reinforcement was increased to satisfy minimum shear reinforcement requirements.

Each panel was expected to behave as and was analyzed as a fixed-end deep beam which was loaded in shear along the embedded panel plates. The fixed-end condition was supplied by the panel-to-frame connectors and by horizontal panel-to-panel connectors. As shown in Figure 7, the panels were connected to the base and top beam using the same connector plate detail as for the single precast panel wall, Specimen 4. Again, no connection was made between panel and column. The six panels were

Figure 7. Multiple precast panel reinforcing and connecting detail.



joined together by lap welding steel plates which were embedded in each panel and attached to horizontal and auxiliary reinforcement. These horizontal connections were designed to transmit shear forces from one panel to another and to restrain end rotation of the panel. The design of the panel and the connections were based on current design techniques (47, 48, 49).

The gaps between different panels and between the panels and frame were not filled with grout so that the behavior of the panels could be more easily determined and because grout would have failed early in the test sequence and would have become useless.

The design philosophy of Specimen 5 was similar to that used by Muto (41) in designing cast-in-place slitted shear walls. The beam-like behavior of the individual wall segments would show greater ductility than a solid wall, even though the total lateral load resistance would be less.

#### Representation of Seismic Loading

The five specimens were subjected to similar sequences of reversed cycle deflections as illustrated in Figure 8. The deflection sequence was designed to study the structural characteristics of the various infilled walls rather than to correspond to an actual earthquake condition; although such increasing deflection cycles would represent a "worst case" seismic condition (18). Specimens were deflected three times to each deflection level. The levels were based on the calculated and

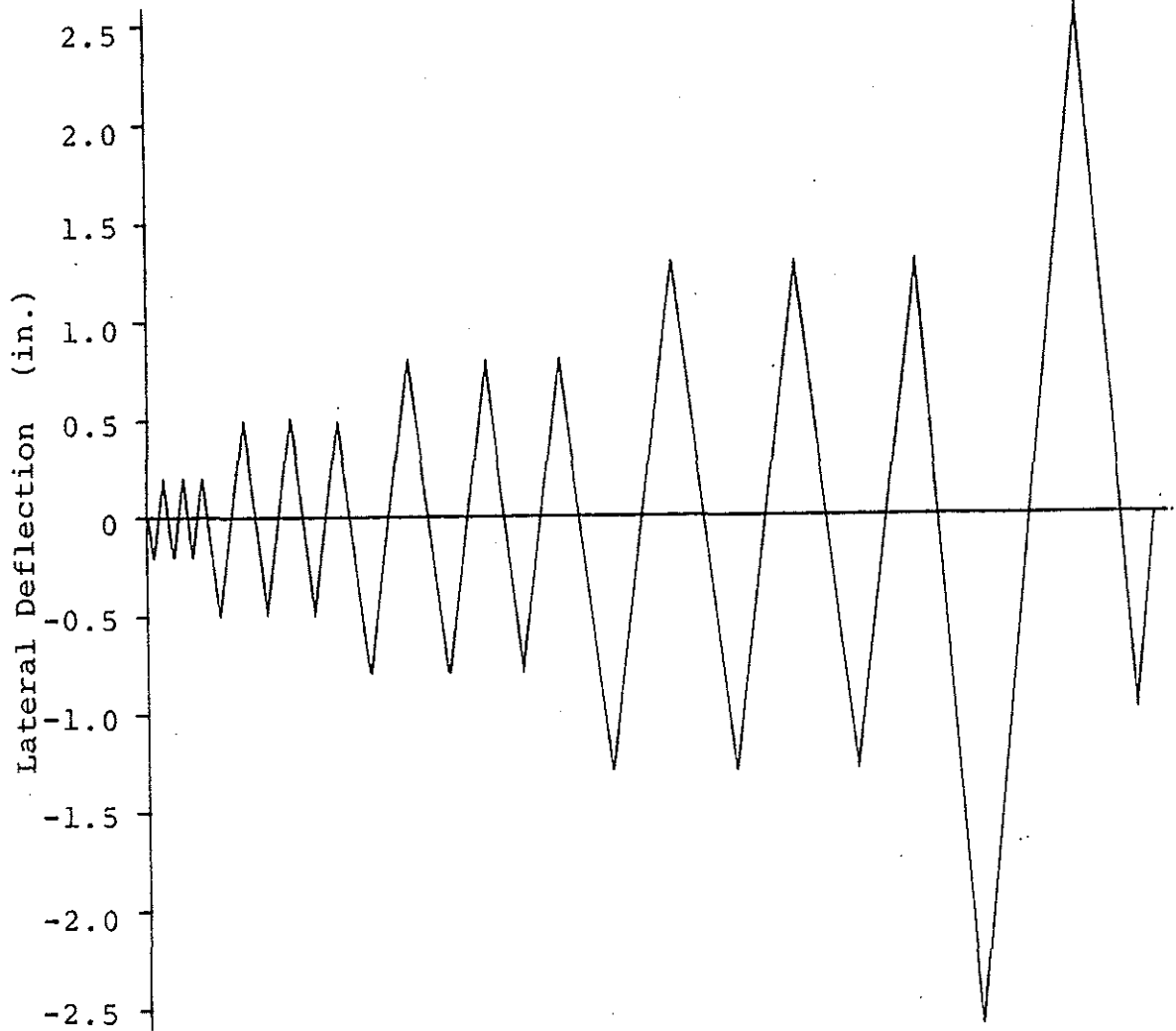


Figure 8. Reversed cycle deflection sequence.

observed response of the monolithic shear wall and were related to the deflection and loading at which column reinforcing steel first began to yield in tension. The deflection levels approximately equaled the following multiples of the first yield level: 1/2, 1, 1-1/2, 2-1/2 and 5.

### Materials

A detailed description of the materials used to construct the specimens is given in Appendix C.

Concrete. Concrete mixes were designed to have a nominal compressive strength ( $f'_c$ ) of 4000 psi. As shown in Table 1,  $f'_c$  varied between 3350 psi to 5650 psi. Two mix designs were used, the first for Specimens 1 and 2 and the second for Specimens 3, 4 and 5. A maximum size aggregate of 3/8 in. was used in both mixes in order to model a 3/4 in. aggregate of a prototype structure and to satisfy clearance requirements between reinforcing bars and forms (5). Mix designs are given in Table 2.

A special drypack concrete was used in Specimen 3. It was hand mixed in the laboratory and had a sand:cement:water ratio of 2:1:0.6 by weight.

Except for the drypack, all concrete was delivered to the laboratory in a transit mix truck. Slump tests were taken to determine if the concrete was of the desired workability, about a 4 in. slump; water was added to the mix if necessary. The mix

TABLE 1  
Concrete Compressive Strength

Element	Slump (in.)	$f'_c$ (psi)	$f'_{cf}$ (psi)	Age at Testing (days)	Strength Difference (%)
Specimen 1					
Base	3-1/4	4650	3890	355	16.3
Column	5	5650	4990	337	11.7
Beam	3	3890	3360	333	13.6
Stub	7	3670	2930	300	20.2
Wall	5	5650	4990	337	11.7
Specimen 2					
Base	3-1/4	4650	3590	475	22.8
Column	5	5650	4510	459	20.2
Beam	3	3890	2940	455	24.4
Stub	7	3670	2950	420	19.6
Specimen 3					
Base	7	3670	2880	429	21.5
Column	5-3/4	4390	3580	411	18.4
Beam	7-1/4	5100	4100	408	19.6
Stub	7	4030	2950	313	26.8
Wall	3-1/2	3470	2820	181	18.7
Drypack	0	6850	7500	180	- 9.5
Specimen 4					
Base	7	3670	2900	352	21.0
Column	5-3/4	4390	3030	341	31.0
Beam	7-1/4	5100	3090	338	39.4
Stub	7	4030	2910	221	27.8
Wall	5	4520	2940	84	35.0
Specimen 5					
Base	7	4030	2720	479	32.5
Column	6-1/2	3350	3520	461	- 5.1
Beam	6	3730	3620	458	2.9
Stub	3-1/2	3470	2820	362	18.7
Wall	5	4520	2910	94	35.6

ordered from the transit mix company was varied slightly from the design mix to account for the water content of the sand and aggregate.

TABLE 2  
Concrete Mix Designs  
Weight in Pounds Per Cubic Yard of Concrete

Material	Mix 1 for Specimens 1 and 2 (lbs)	Mix 2 for Specimens 3, 4 and 5 (lbs)
3/8 in. aggregate (dry)	1200	1205
Sand (dry)	1750	1755
Type I Portland cement	485	470
Water	315	315

Concrete strength was determined as the average strength of three 4 in. diameter x 8 in. concrete cylinders tested in compression. A minimum of six cylinders was cast with each pour of concrete. Three were cured in a lime saturated water bath at room temperature; they were tested 28 days after casting to determine a "laboratory concrete strength",  $f'_c$ . The remaining cylinders were cured adjacent to the specimens; they were tested on the first day on which the corresponding specimen test began. Their strength was

termed the "field concrete strength",  $f'_{cf}$ . The field concrete strength averaged 21 percent less than the laboratory concrete strength.

Steel. Table 3 presents the average tensile yield and ultimate stresses for the steel reinforcing bars used in the specimens. A minimum of three bars on each size were tension tested in a universal testing machine to determine their average stress-strain behavior, as detailed in Appendix C. The ultimate strain of all bars was greater than 20 percent.

TABLE 3  
Reinforcing Steel Properties

Bar Type	Yield Stress (psi)	Ultimate Stress (psi)
11-gage plain wire	37,000	46,100
#3 deformed bar	63,900	96,000
#4 deformed bar	61,200	95,500
#5 deformed bar	51,000	89,500

The 11 gage wire, as delivered, had a yield stress of 69,300 psi and an ultimate strain of less than 10 percent. This stress was too high and ductility too low to represent Grade 40 reinforcement, so the 11-gage wire was annealed at 1300°F for 30 minutes and then air cooled in order to reduce its yield stress to that given in Table 3. Ultimate strain was increased to over 25 percent.

Reinforcing Bar Welds. In Specimens 4 and 5, #3 reinforcing bars were to be welded to embedded steel plates. Three replicas of these bar-to-plate welded connections were made and were tension tested in a Universal testing machine. In each test the reinforcing bar broke at a location several inches from the weld and at a stress which averaged 7 percent less than the ultimate stress listed in Table 3. The welded connections were satisfactory.

Panel-to-Frame Connectors. Hot rolled steel plate with an estimated yield stress of 36,000 psi was used to fabricate the panel-to-frame connectors of Specimens 4 and 5. Ear plate welds were judged satisfactory because they resisted strong blows with a 16 ounce hammer.

The 5/8-in. wedge anchors used for Specimens 4 and 5 were manufactured by Phillips Drill Company. Data supplied by the company indicated that the ultimate tensile pullout resistance of the anchor was about 7,800 pounds and that the direct shear capacity was about 10,800 pounds.

Dowel Bar Anchorage. The #3 dowel bars used in Specimen 3 were anchored into holes drilled in the frame using Colma-Dur-Gel epoxy manufactured by Sika Chemical Corporation. Pullout tests were made of #3 bars epoxy bonded in drilled holes in order to determine the adequacy of the anchorage (Appendix E). The tests

showed that bars embedded in the same way as those in Specimen 3 developed the ultimate stress of the bars.

#### Fabrication of Specimens

A detailed description of specimen fabrication is given in Appendix D. Specimens 1 and 2 were constructed simultaneously as were frames of Specimens 3 and 4.

Frames. Frames for Specimens 2 through 5 were constructed identically. Concrete was cast in four lifts: the base beam and foundation blocks, the columns, the top beam and slab, and the stub columns. In each lift concrete from the transit mix truck was hand shoveled into the plywood forms and was vibrated internally with a spud vibrator and externally by holding the spud vibrator against the forms. Typically three to five days elapsed between successive pours. Cold joints were roughened and cleaned before new concrete was cast.

Reinforcement was placed and tied as designed (Figure 2). Figure 9 shows #5 column bars being tied into the foundation block; as shown, cardboard tubes were used to form holes for the hold-down bolts. After the base and columns had been cast, beam and slab reinforcement was placed as shown in Figure 10; beam steel was squeezed together about 1/4 in. to 1/2 in. to fit within the column bars.

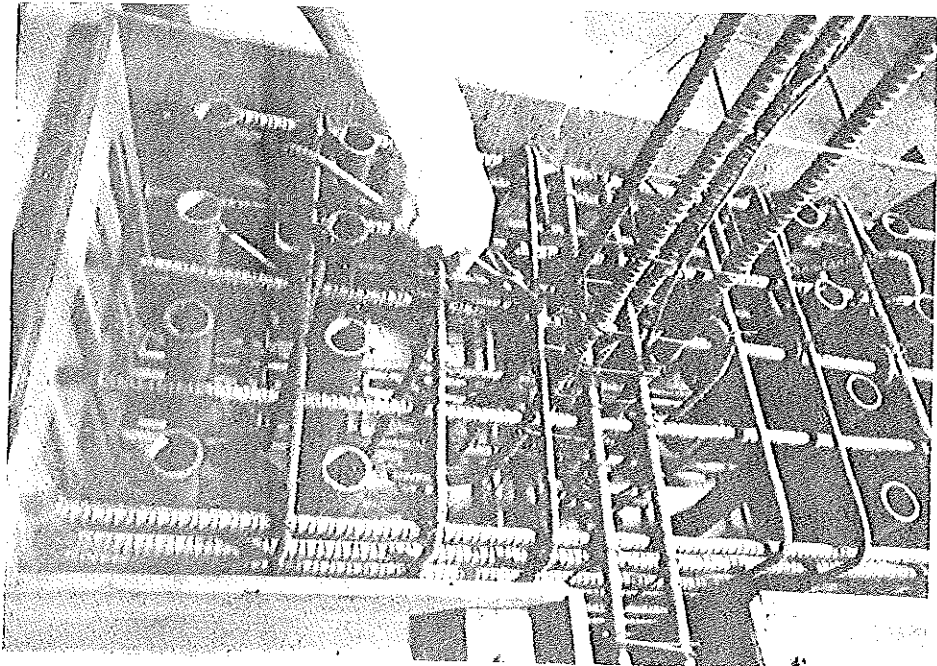


Figure 9. Column and base reinforcement in plywood forms.

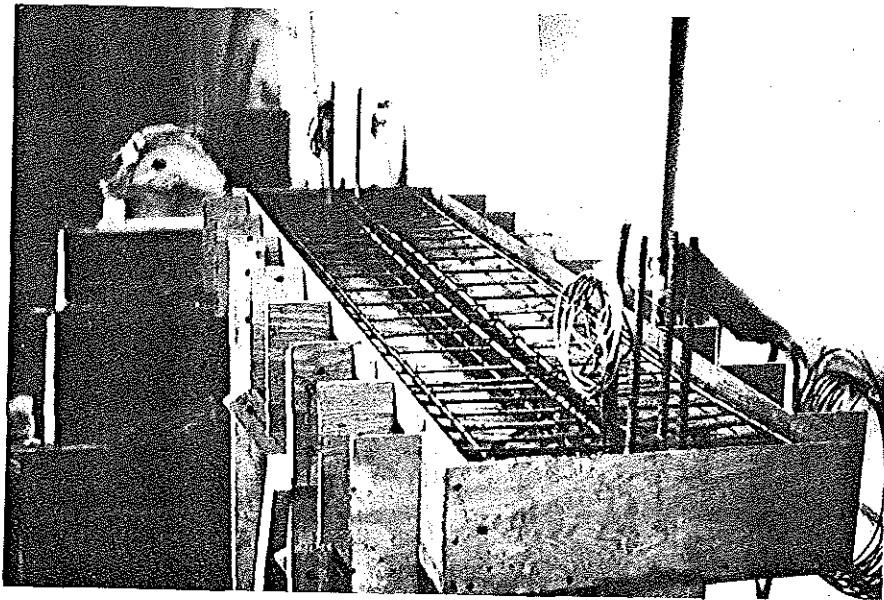


Figure 10. Beam and slab reinforcement in plywood forms.

Specimen 1. The reinforcing for the base, columns, and beam of the monolithic wall specimen was placed the same as for the other specimens. Wall reinforcement, as shown in Figure 11, was tied within the columns and base beam before the base was poured. Vertical wall bars were placed in the center of the wall while horizontal bars were placed on alternate sides of the vertical steel.

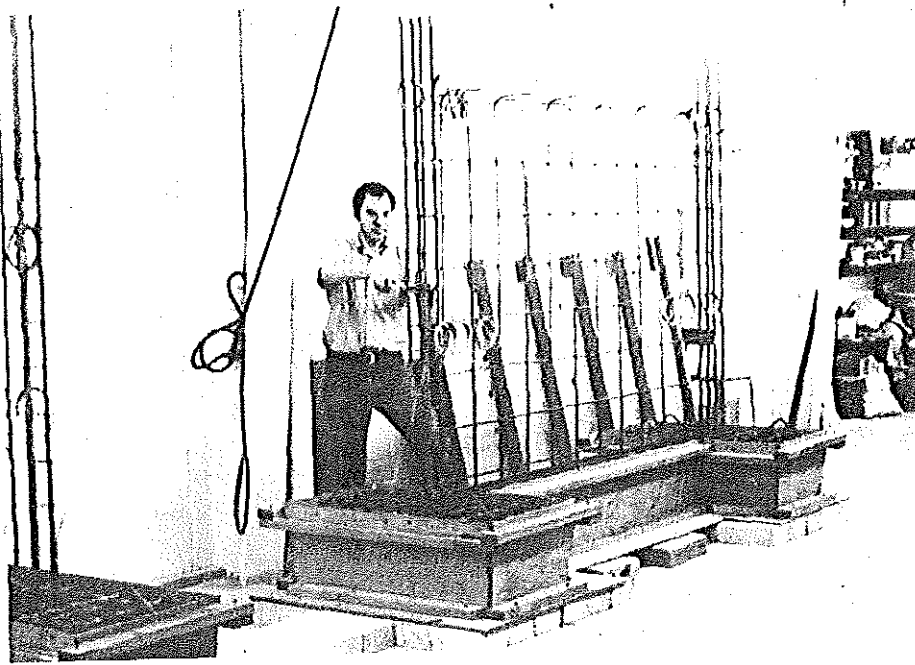


Figure 11. Placing reinforcement for Specimen 1.

After the base was cast and cured, the top surface was chiseled and cleaned in order to provide a rough connection. Columns and wall were poured up to the level of the top beam.

The plywood wall forms bulged in the middle during casting so the center dimensions were wider than the specified 3 in. while all edge dimensions remained the desired 3 in. thickness. The top surface of the wall was left rough after pouring, so it was not chiseled before the beam was cast.

Specimen 2. Specimen 2 was a plain frame with no infilled wall.

Specimen 3. Construction of the cast-in-place wall for Specimen 3 began by drilling  $5/8$  in. diameter and  $3-3/4$  in. deep holes all around the frame interior at wall reinforcement positions (Figure 4). The holes were cleaned by blowing with dry air then filled with a neat epoxy grout; #3 dowel bars were "screwed" into holes and secured in position; excess epoxy was removed. After the grout had cured the interior of the frame was chiseled and cleaned as shown in Figure 12. Depth of roughness was about  $1/4$  in.

After the vertical and horizontal reinforcement was tied to the dowel bars, a plywood form was fitted into one side of the open frame as shown in Figure 13. A second form was secured into the other side of the frame; spacers assured a 3 in. dimension between forms. The second form left a gap, whose dimension could be varied between the top of the form and the bottom of the top beam.



Figure 12. Roughening frame of Specimen 3 after epoxy bonding #3 dowels.

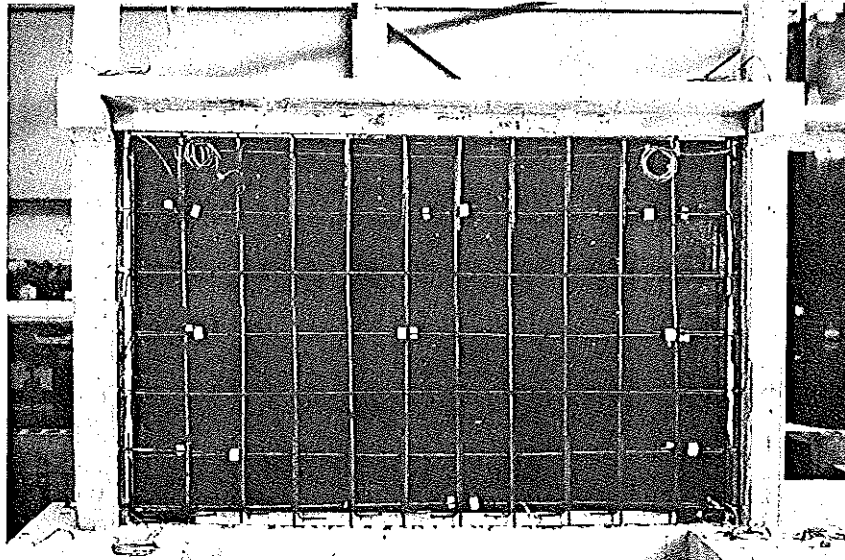


Figure 13. Reinforcing and back form in place for Specimen 3.

The wall was cast by shoveling wet concrete through this gap up to within 3 in. of the beam. One day after casting the wall, a drypack mortar was packed hard into this 3 in. space; beam and wall surfaces were setted prior to placing the drypack. No special care was taken to roughen the top surface of the cast-in-place section of the wall because it was inaccessible. Forms were stripped one week after casting.

Specimen 4. The single precast panel for infilling the frame of Specimen 4 was cast flat in a plywood form as shown in Figure 14. The wood blocks in the top, center of the panel formed holes needed for erecting the panel. Figure 15 shows the vertical reinforcing bars and rectangular shear plates welded to the embedded connector plate. As concrete was shoveled into the panel form, special care was taken to pack concrete under and around the embedded plate.

Figure 16 shows the ear plate connector bolted to the base beam. The connector was fabricated by welding the 1/2 in. x 1-1/2 in. x 3 in. ear plates to the 1/2 in. x 3 in. x 47-1/2 in. base plate. Holes, 3/4 in. diameter then were drilled in the base plate; they were centered between the ear plates. Holes 5/8 in. diameter and 3-3/4 in. to 4 in. deep were drilled into the top and base beams. The connectors were used as templates for correct hole spacing. Red Head brand 5/8 in. diameter wedge anchors were sledge hammered into the holes, and the ear plate connectors were secured.

The single panel was positioned into the frame using a fork lift truck (Figure 17). There was a 3/8 in. clearance between each

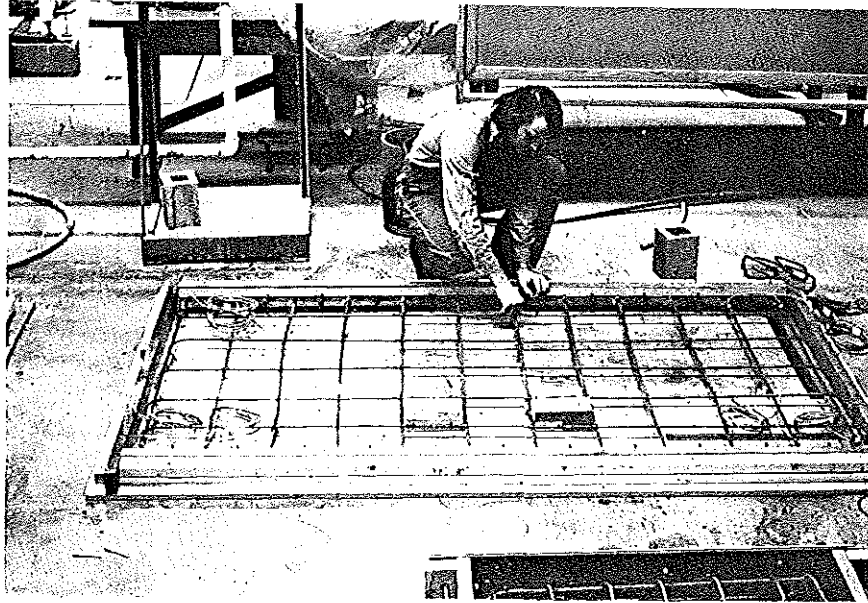


Figure 14. Tying reinforcement for single panel of Specimen 4.

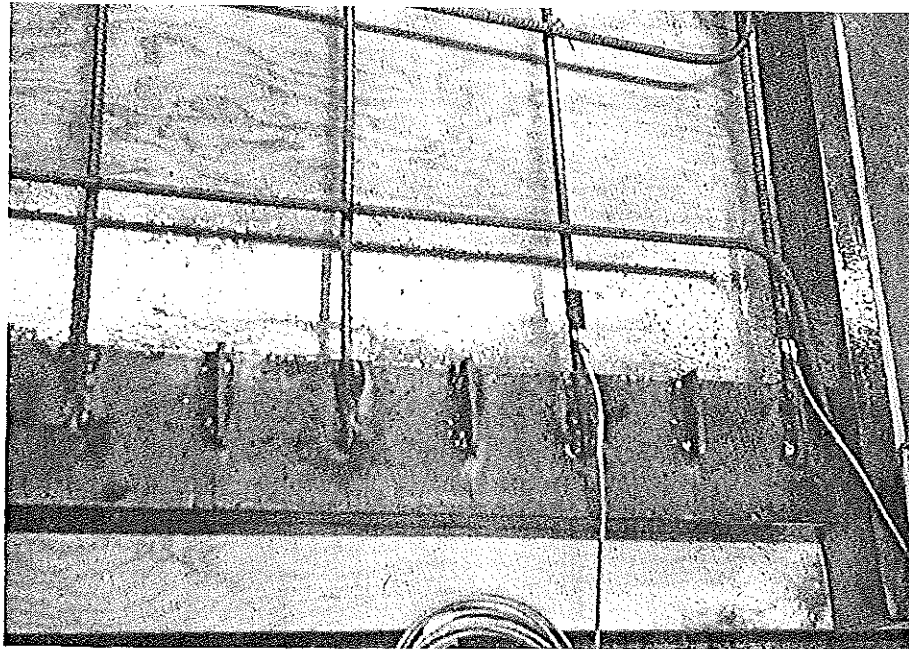


Figure 15. Vertical reinforcement and rectangular shear plates were welded to embedded connector plates, Specimen 4.

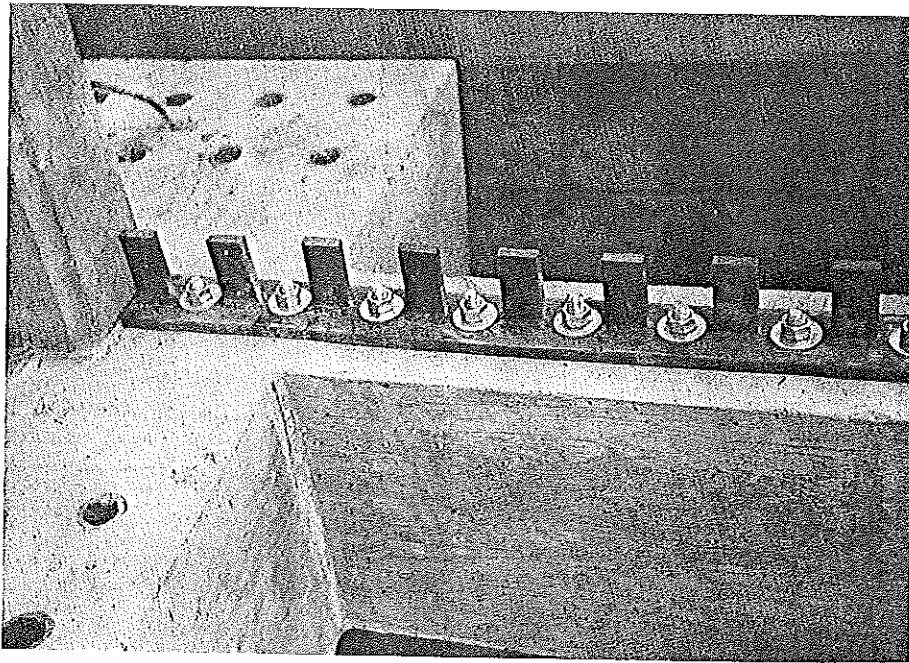


Figure 16. Ear plate, panel-to-frame connector, Specimens 4 and 5.

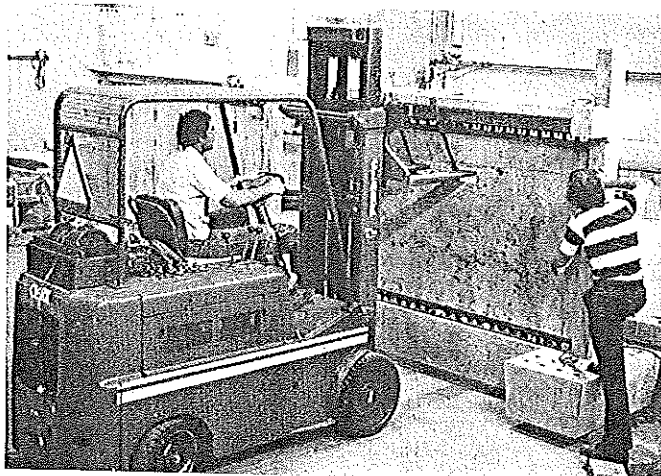


Figure 17. Erection of single panel with fork lift truck.

column and the panel. The embedded plate and ear plates were held tightly together with C-clamps. Then the plates were welded together.

Specimen 5. The six independent, panels were formed and cast next to each other in positions which corresponded to their final erected positions. Figure 18 shows the wood form with the tied reinforcement in place. The vertical bars and shear plate connectors are shown welded to the embedded panel plates whose lengths were equal to the length of each panel. The 45° auxiliary reinforcement was welded to the backside of the panel-to-panel connector plates, while #4 horizontal bars were welded to the front face; vertical #3 bars were not welded to those plates.

As concrete was shoveled into the form, special care was taken to pack concrete under and around embedded plates.

The ear plate connector was identical to that used for Specimen 4 (Figure 16). Workers erected the individual panels by lifting them into position and clamping the embedded panel plate to the ear plates as shown in Figure 19. Wood blocks and shims were used to space the panels evenly between top and bottom beams and to create gaps of 3/8 in. between the columns and end panels and gaps of 1/4 in. between panels.

The ear plates were welded to the embedded panel plates. Steel plates 1/2 in. x 1 in. x 3 in. were lapped over the embedded panel-to-panel connector plates and were welded. These lap splices joined the six panels together.

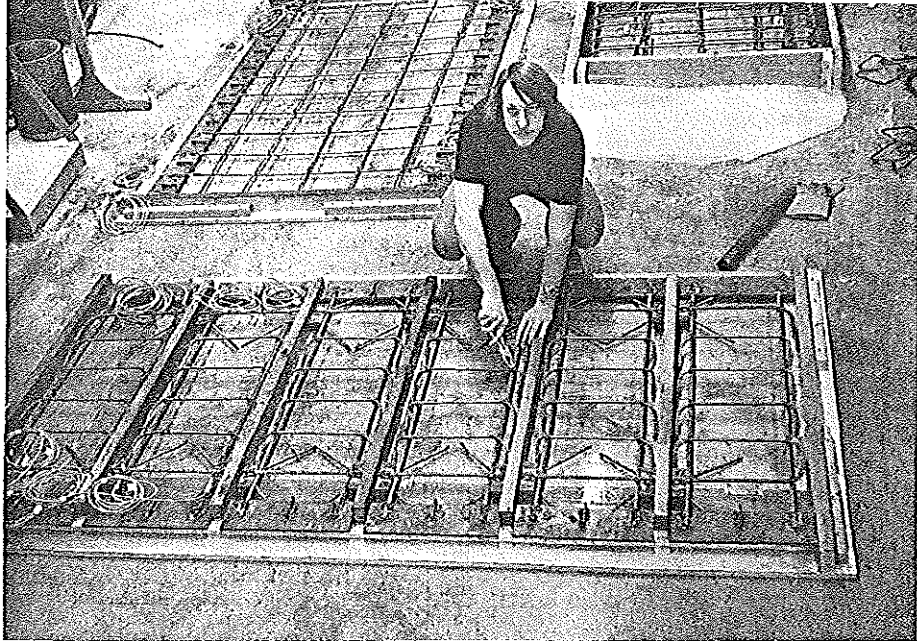


Figure 18. Tying reinforcing bars of six panels for Specimen 5.

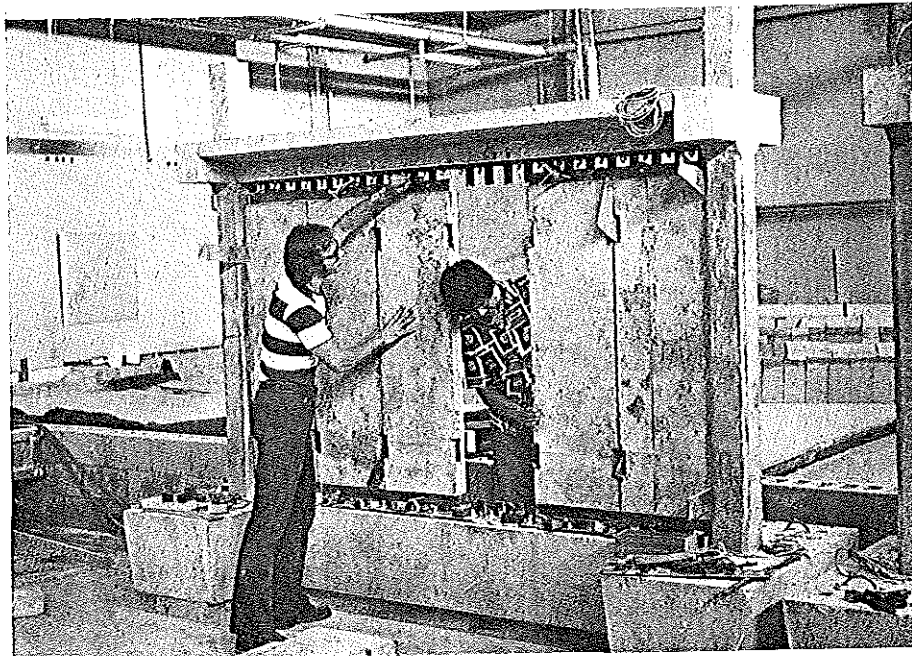


Figure 19. Erection of multiple panel wall, Specimen 5.

#### Instrumentation

Figure 20 is a drawing of the experimental set-up which shows where and what type of measurements were taken. Strain-gage load cells were attached to each hydraulic loading ram and were accurate to about  $\pm 0.2$  kips. Lateral deflection measurements were made at the level of the foundation blocks and at a position

one inch above the slab using LVDTs (Linearly Variable Displacement Transducers) and dial gages, all accurate to 0.001 in.

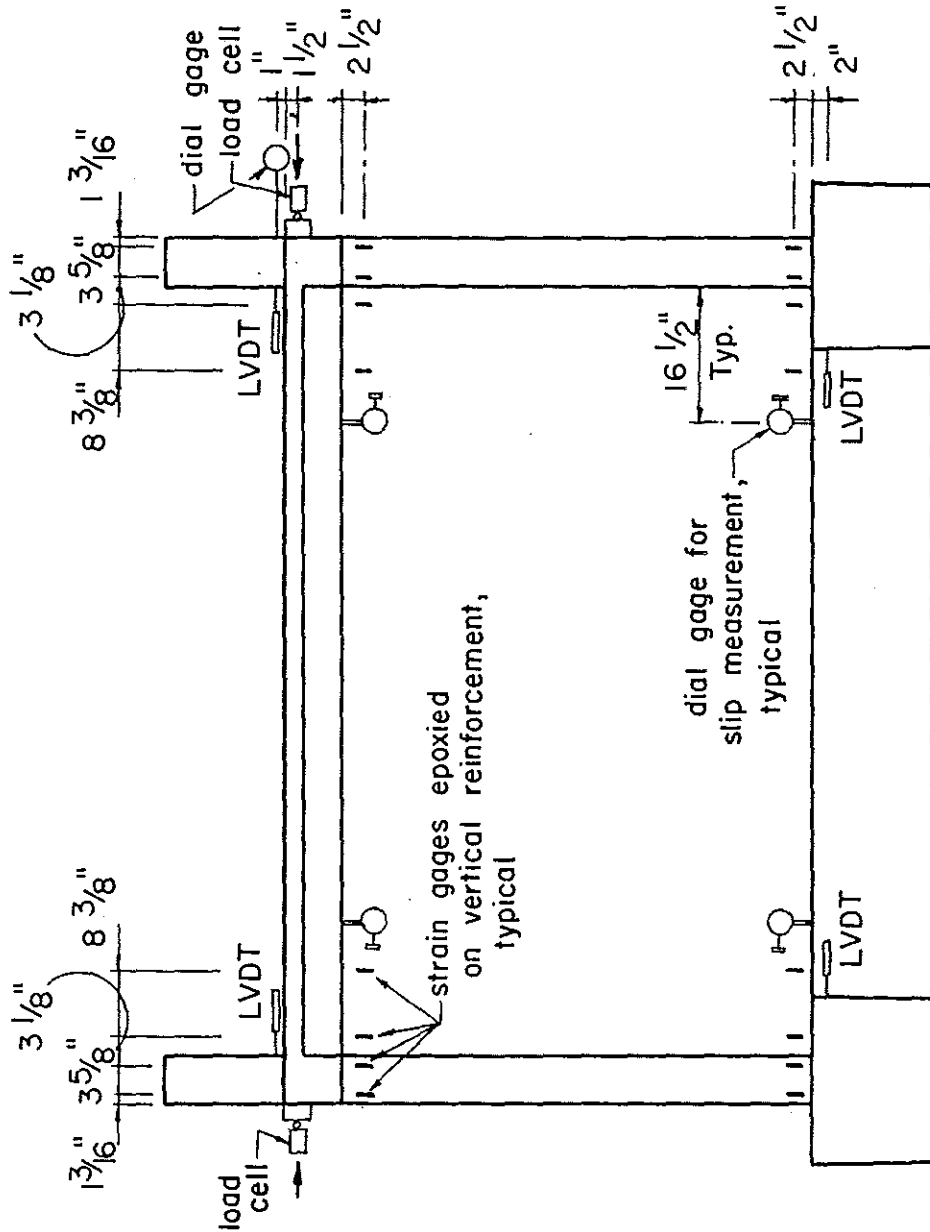


Figure 20. Instrumentation set-up.

Reinforcing bar strain was measured at locations 2-1/2 in. beneath the top beam and at similar positions 2-1/2 in. above the base beam (Figure 20). Standard 1/4 in., foil backed, electrical resistance strain gages were used. Each gage was mounted with an epoxy cement on a flat machined surface of the bar and then was covered with a waterproof and shockproof coating. The one-quarter bridge strain gage circuits were connected to a VIDAR automatic strain balancing and recording unit or to a Strain Sert manual balancing unit. Strain gage location for Specimen 5 was altered slightly so that the response of neighboring panels could be observed as discussed in Appendix F. The objective of the strain measurements was to determine the continuity between column and wall and to find whether the frame behaved in a flexural mode or as part of the shear wall system.

On Specimens 4 and 5, dial gages were mounted horizontally on the top and base beams and measured the relative movement between the infilled wall and the frame.

#### Test Set-Up

Figure 1 shows Specimen 2 after removal from the loading frame, and Figure 21 shows the complete test set-up with Specimen 5 under load. Both figures illustrate the steel loading frame, the hydraulic jack loading system and the concrete slab end restraints which fit between the specimen's foundation blocks and the vertical

steel members. The steel cross-bracing was always in place during tests (Figure 21), but it was removed for each mounting and dismounting of specimens (Figure 1).

The specimens were loaded laterally in each direction using two 50-ton hydraulic jacks as shown in Figure 22. A 1/4 in. thick strip of plywood and a 2 in. thick iron bearing plate were mounted on each end of a specimen at the level of the slab; the plywood eliminated stress concentrations resulting from small surface irregularities. Steel balls attached to the load cells fit into sockets machined into the bearing plate; the sockets were spaced 1-1/2 in. below the top of the slab and 16 in. apart. Each load cell was mounted on the ram of a hydraulic jack, and the two jacks were bolted to the horizontal, 18-in. deep I-beam (Figures 1 and 21). The ball and socket arrangement allowed angular deflections between the specimens and jacks which occurred as the specimens moved laterally. The vertical deflections of each specimen were accounted for by the large hinges between the horizontal I-beam and the vertical steel frame (Figures 1 and 21). Relative to the horizontal, the angular movements of the hinges and I-beam were typically within  $\pm 5$  degrees. As a specimen deflected, the large hinge and ball-and-socket rotated so that the position of load application on the specimen remained the same.

The specimens were held in position by thirty-two 1-1/4 in. diameter hold down bolts; 16 fit vertically down through holes in each foundation block and fastened to the bottom steel beams.

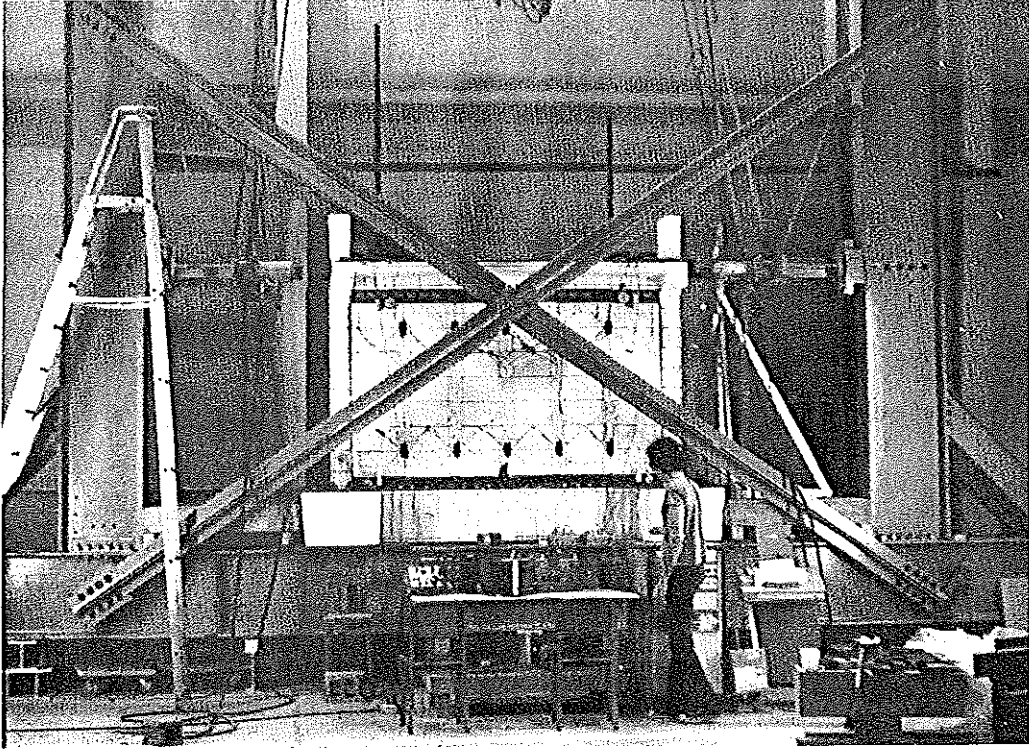


Figure 21. Test set-up for Specimen 5.

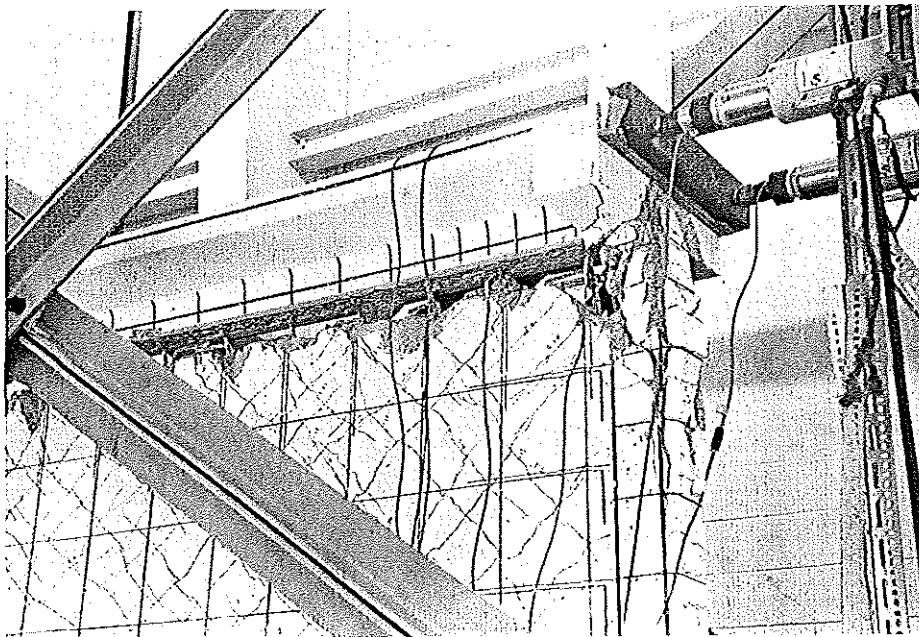


Figure 22. Two jack load system. Specimen 3 shown deflected to -1.3 in.

Sliding of the specimens on the bottom steel beams was restrained by concrete end slabs placed between the specimen and the vertical steel members. Wood and steel shims were hammered between each end slab and foundation block to create a snug fit.

#### Test Procedure

All specimens were painted white and were striped with black ink to picture the reinforcement pattern.

After a specimen was bolted and shimmed in position, the lateral deflection instrumentation was placed; and all data recording equipment was connected.

Concrete control cylinders which were field cured with the specimens were compression tested to determine  $f'_{cf}$ .

The specimen was loaded cyclically according to the deflection sequence as previously discussed in Representation of Seismic Loading and illustrated in Figure 8. As described in Appendix F, the deflection sequence given in Figure 8 was varied slightly for each specimen because of events which occurred during testing.

As the reader views Figure 21, the loads and deflections toward the right side of the figure and specimen are taken as positive, while those toward the left side are negative. The first deflection and increases in deflection magnitude always occurred in the negative direction. The column on the left, north side of the structure, is termed the negative column while the column on the right, south side is termed the positive column.

Lateral deflection measurements were taken at the top of the slab and at the top of the foundation blocks. The latter was a measure of the slip of the specimen along the test frame, and the magnitude of this slip was generally less than 0.05 in. The two LVDT deflection measurements at the slab level were averaged to give the top level deflection, while the two at the foundation were averaged to give the slip deflection. The story deflection, hereafter termed the lateral deflection or deflection, was calculated by subtracting the slip deflection from the top deflection. The dial gage mounted at the slab level permitted a quick, approximate reading of the lateral deflection during the test.

Data were recorded at discrete deflection increments. During the first six cycles data were taken at increments of 0.05 in.; during the next six cycles, at increments between 0.10 and 0.15 in.; and during the final cycle, at increments between 0.15 in. and 0.25 in. Data acquisition took about five minutes; load and deflection measurements were taken in about the first 30 seconds of that period. During the five minutes the load decreased varying amounts depending upon the load magnitude and deflection level, a greater decrease for higher loads and deflections. Deflections increased less than 0.01 in. during the 5-minute acquisition period.

As the specimens fractured, cracks were marked with wide, felt tip pens so the crack patterns could be photographed. Spalled pieces of concrete were removed to prevent them from falling on

the experimenters. In a real earthquake, spalled fragments would be displaced from the structure by the vibrations.

When the deflection sequence was completed, the specimen was given a final inspection before removal from the test frame.

## CHAPTER III

### TEST RESULTS

The load-deflection responses for the complete loading histories of the five specimens are shown in Figures 23 through 27 for Specimens 1 through 5, respectively. A cursory inspection indicates many similarities between responses of the frames with infilled walls: elastic behavior at low deflections; load degradation with increased cycles at deflections over 0.5 in.; and shear-slip type hysteresis curves in which load and stiffness increased with increased deflection.

A review of the more significant observations made during each test will show the relation between reinforcement yielding, flexural and shear cracking and the load-deflection response. Detailed cycle-by-cycle descriptions of test observations are given in Appendix F.

#### Specimen 1, Monolithic Wall

Figure 28 summarizes important data values obtained from the load-deflection curve, the maximum load and energy dissipated during each half cycle and the cumulative dissipated energy. During both the first three cycles to  $\pm 0.1$  in. deflection and the fourth through sixth cycles to  $\pm 0.5$  in., neither the load

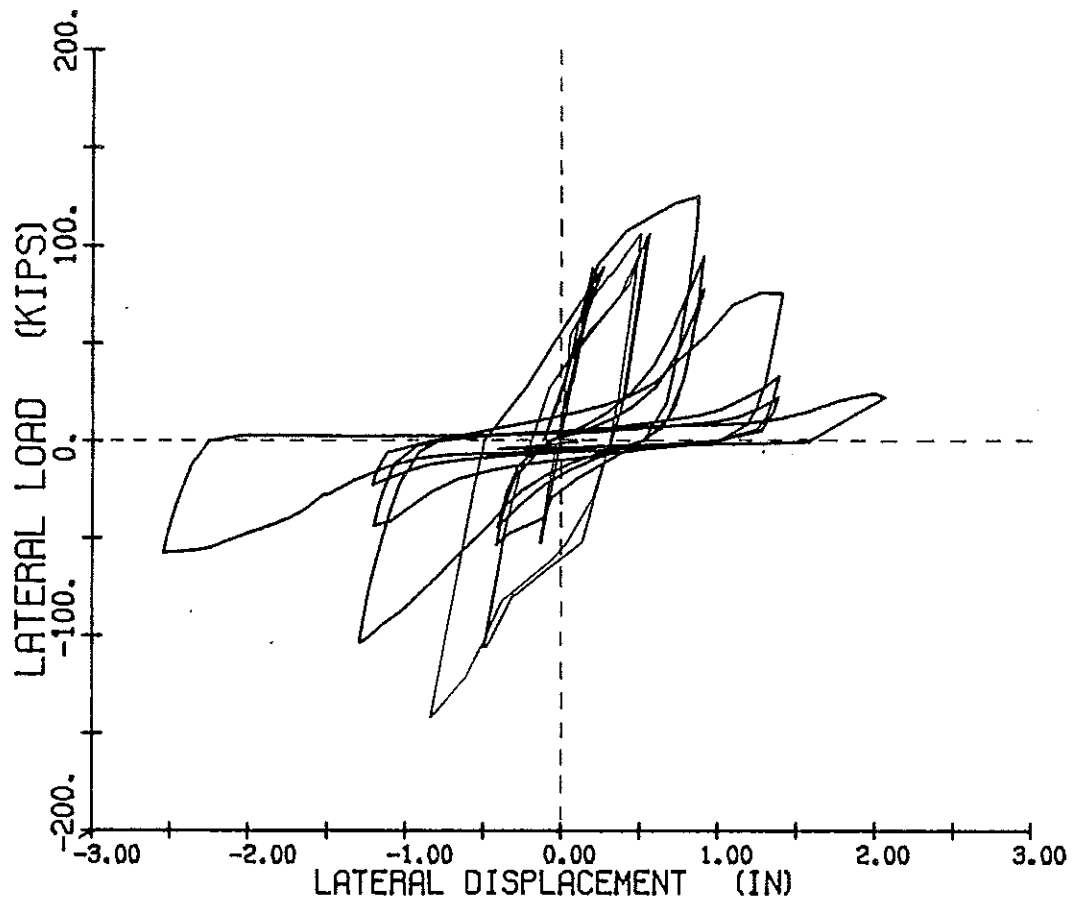


Figure 23. Specimen 1, load-deflection response.

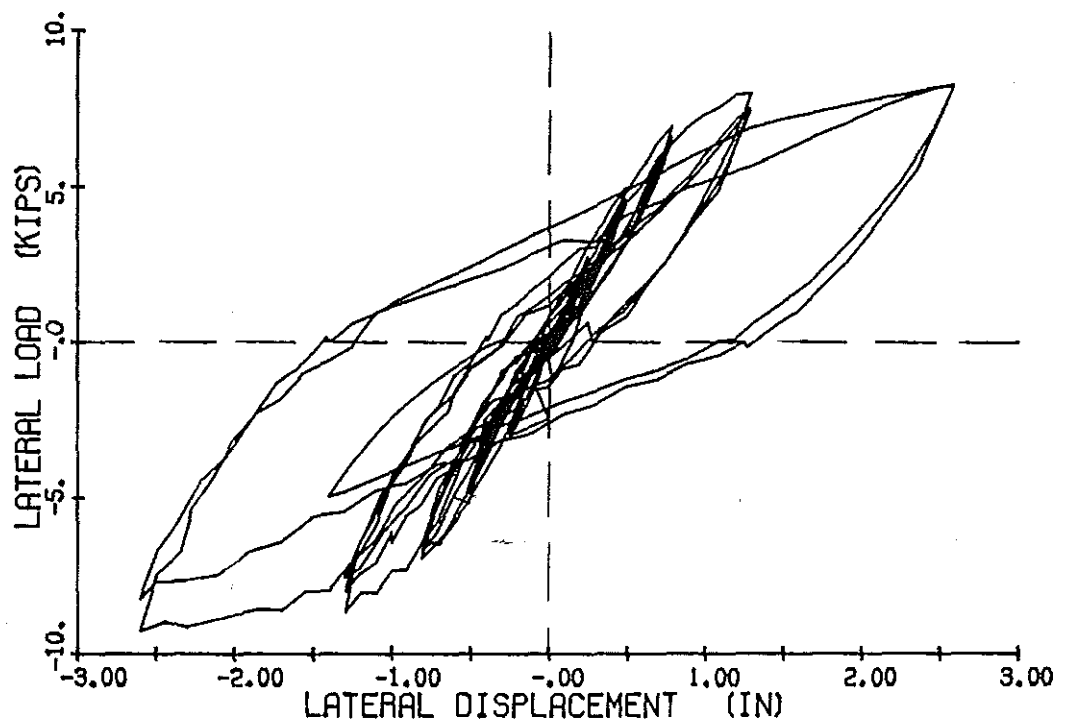


Figure 24. Specimen 2, load-deflection response.

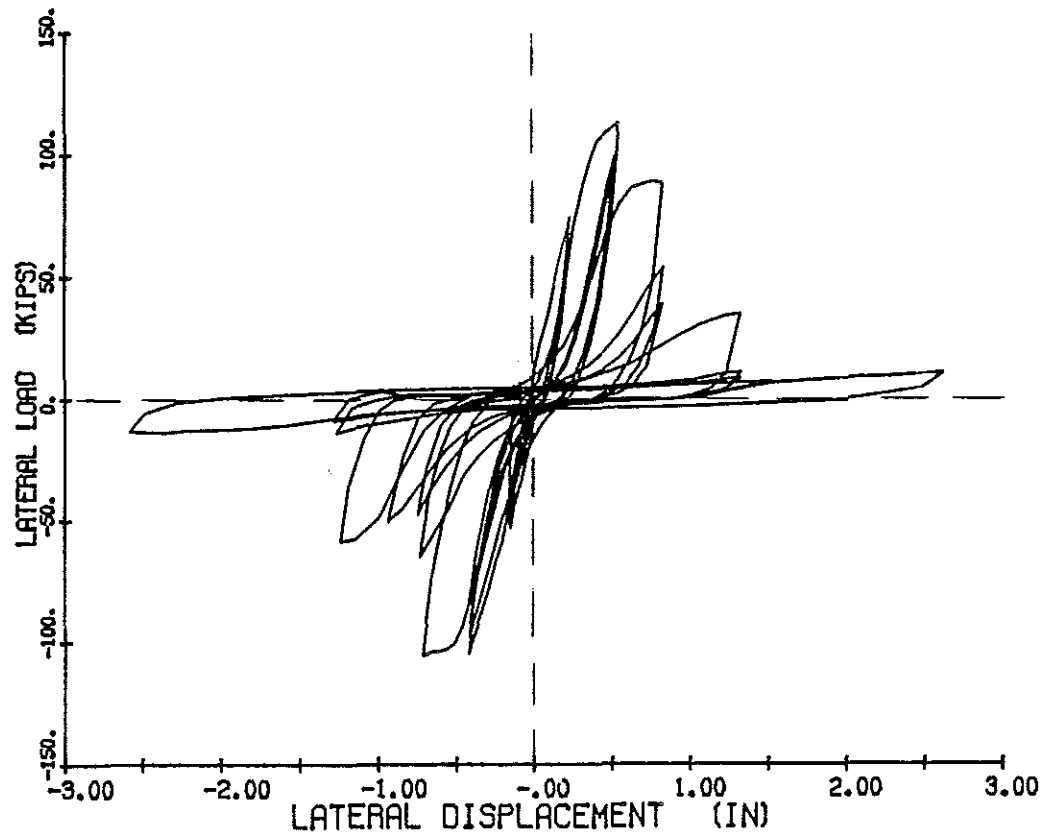


Figure 25. Specimen 3, load-deflection response.

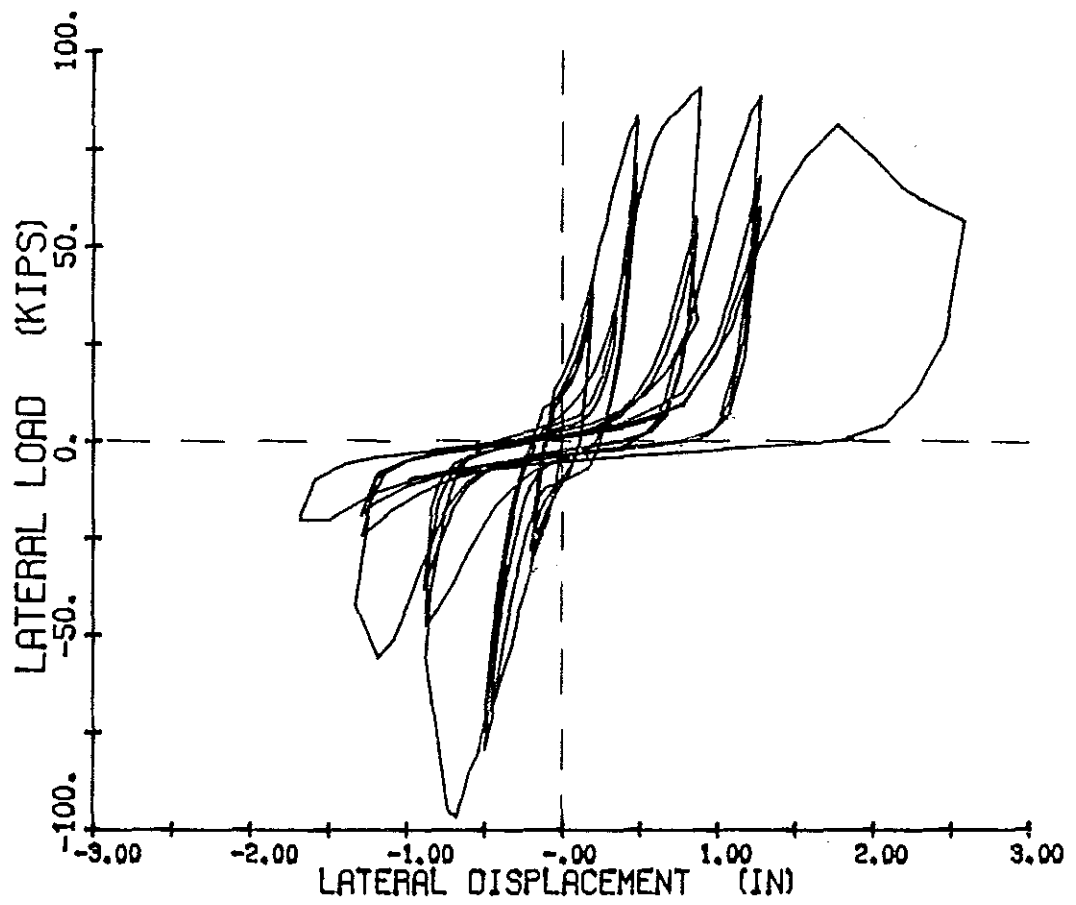


Figure 26. Specimen 4, load-deflection response.

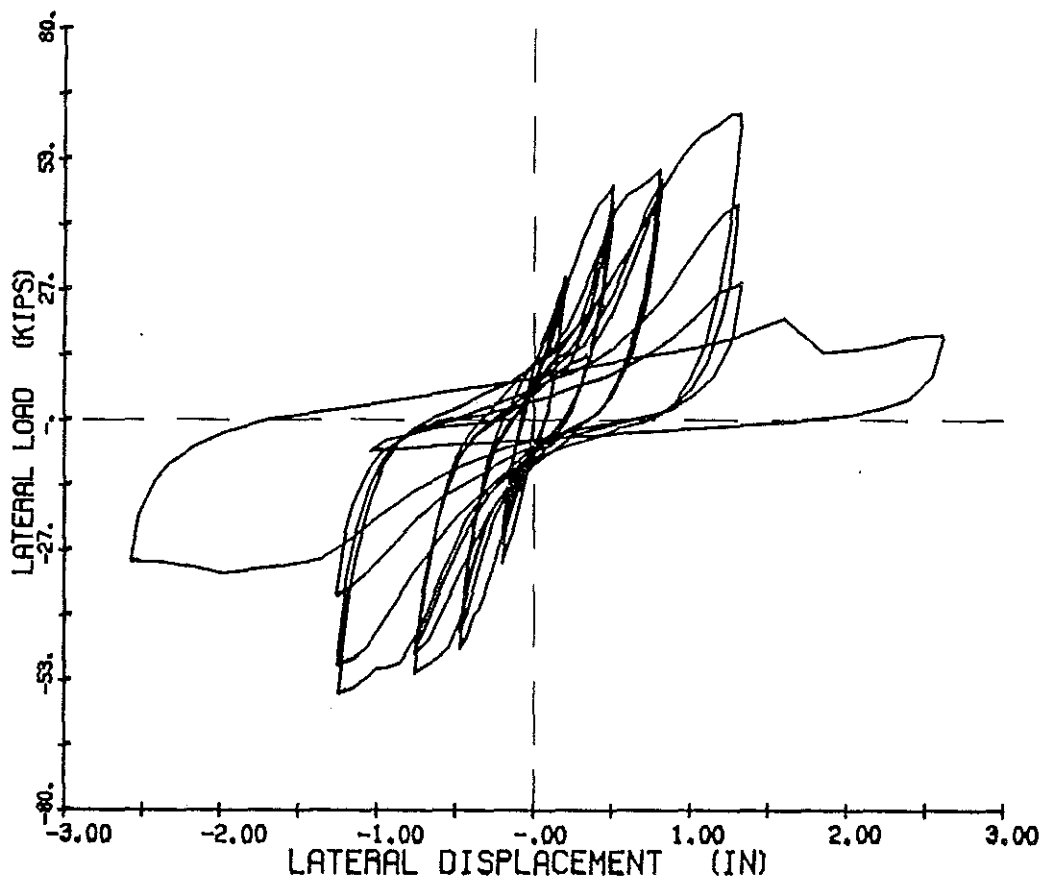


Figure 27. Specimen 5, load-deflection response.

nor the energy dissipated decreased with succeeding cycles. First yield of the column reinforcement occurred in the base of the negative column at cycle 3-1/2 with a load of 106.9 kips and +0.51 in. deflection. The first six cycles were at or below the yield load.

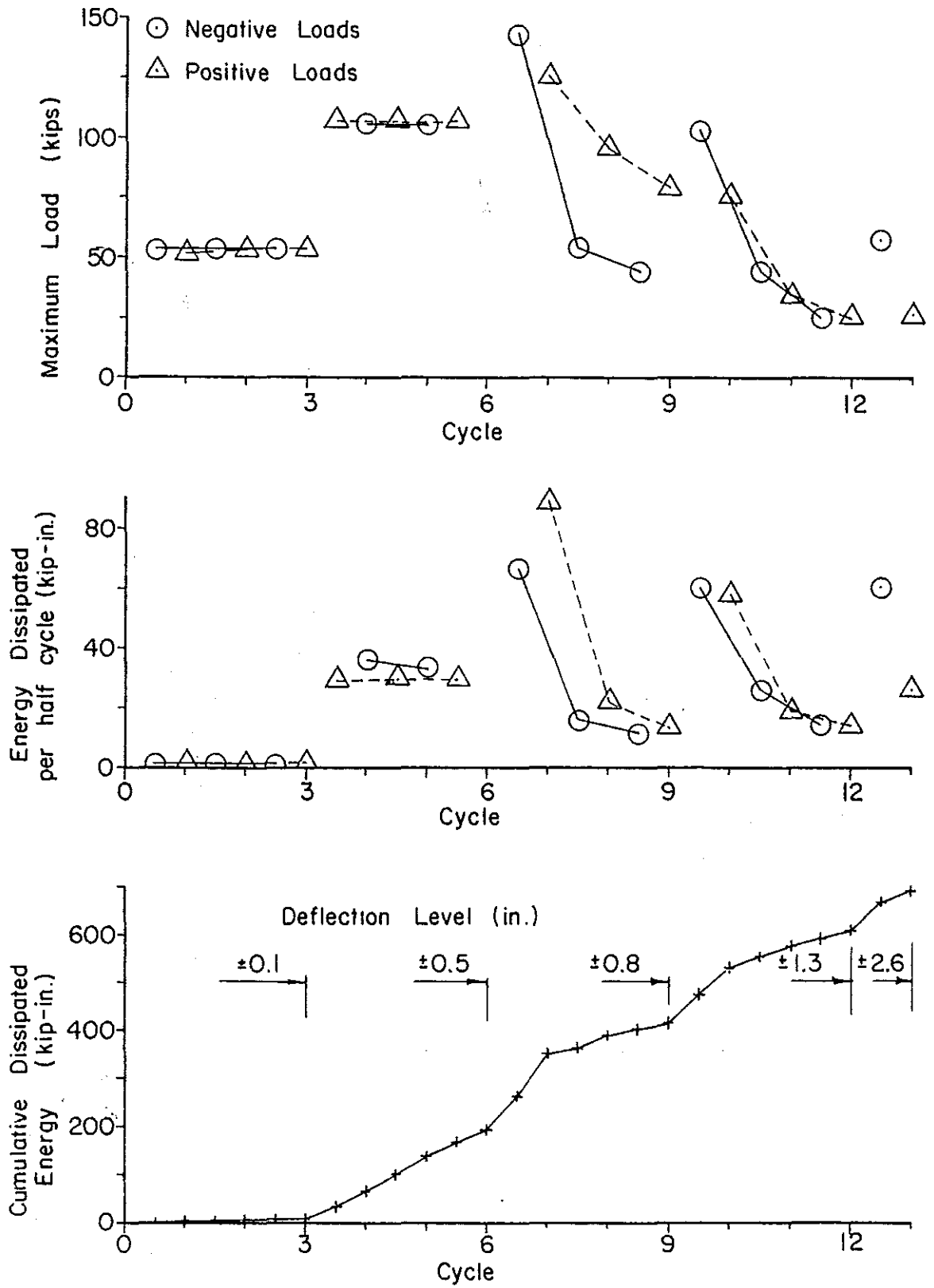


Figure 28. Specimen 1, summary of maximum load and energy dissipation data.

As the specimen was deflected to  $-0.8$  in. ( $\sim 150$  kips, cycle 6), the south edge beam failed in shear at a point of load application. The edge beam was repaired with portland cement mortar and with additional shear reinforcement; the load system was altered slightly; and the reversed cycle test was continued. The edge beam rupture did not affect the rest of the frame and wall structure.

With continued cycles to  $+0.8$  in. the base of the wall cracked extensively, and a compression-diagonal shear failure developed at the base of the positive column (Figure 29). Maximum load in each half cycle degraded greatly.

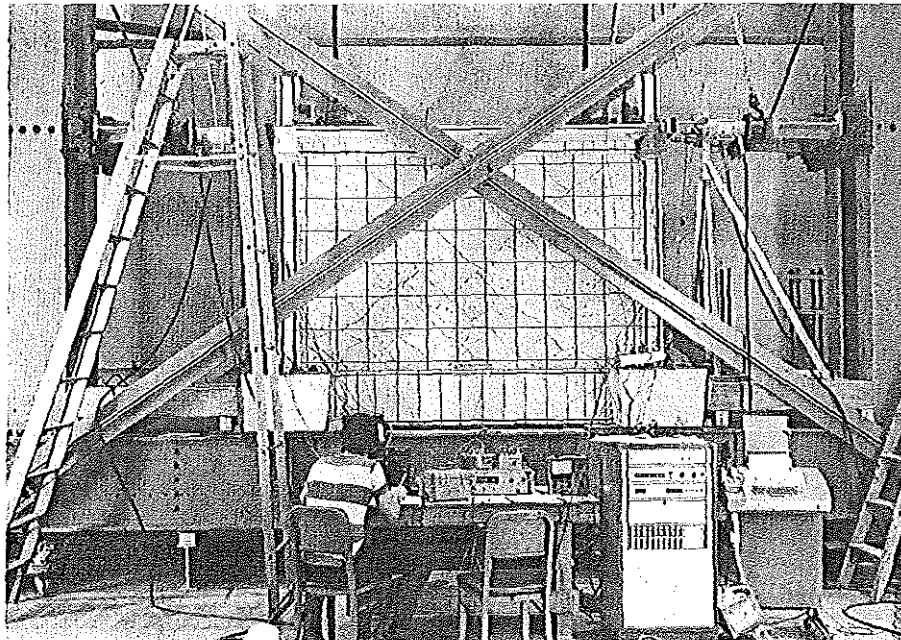


Figure 29. Specimen 1, after three cycles to  $+0.8$  in.

Deflections to  $\pm 1.3$  in. caused concrete compression failure and spalling at the base of both columns and in the wall near each column as shown in Figure 30. Deterioration at the base of the wall permitted much of the lateral deflection to occur within the lower 6 in. of the wall.

The single cycle to  $\pm 2.6$  in. produced direct compression failure at the base of the wall. Although lateral load capacity had been reduced to one-fourth the yield load capacity, the wall appeared capable of carrying vertical loads. Figure 31 shows Specimen 1 after the test.

The strain data indicated that the wall and frame had behaved as a single unit. While the strain distributions was not perfectly linear between compression and tension sides of the structure, it did approximate a linear distribution. During the cycles to the first yield load the neutral axis was located in the wall about 12 in. from the compression face. With deflections to  $\pm 0.8$  in. the neutral axis moved to 14 in. from the compression face because the concrete at the extreme compression fibers crushed.

#### Specimen 2, Frame

Figure 32 presents the data summary for Specimen 2. Column reinforcement first yielded in tension at a deflection of  $-0.80$  in. and  $-6.4$  kips during cycle 6-1/2. The data show that before and after yielding the maximum load degraded little, only 12 percent at the  $\pm 1.3$  in. deflection level. The load-deflection hysteresis



Figure 30. Specimen 1, base of positive column after cycles to  $\pm 1.3$  in.

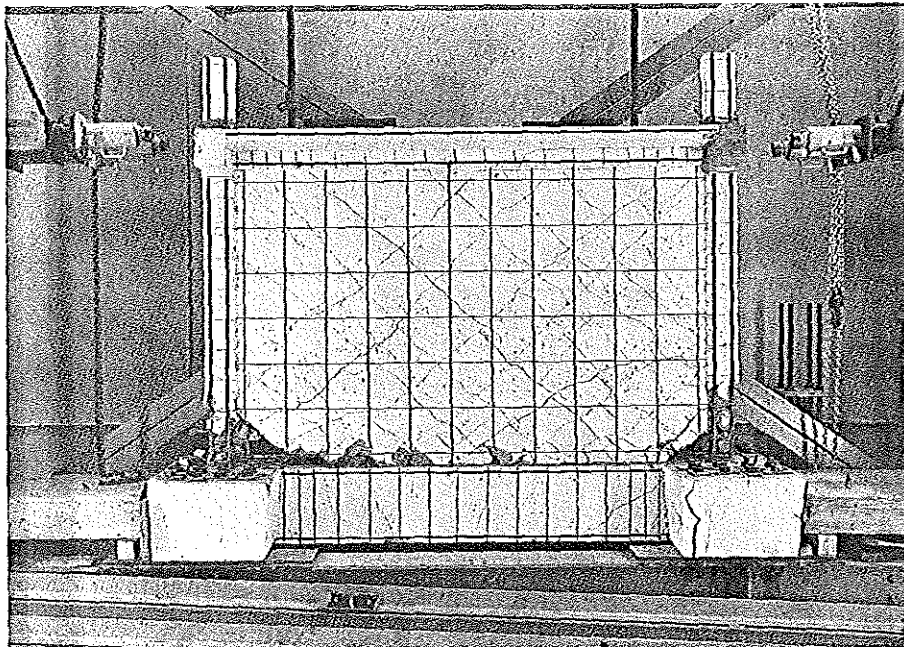


Figure 31. Specimen 1 after completed test.

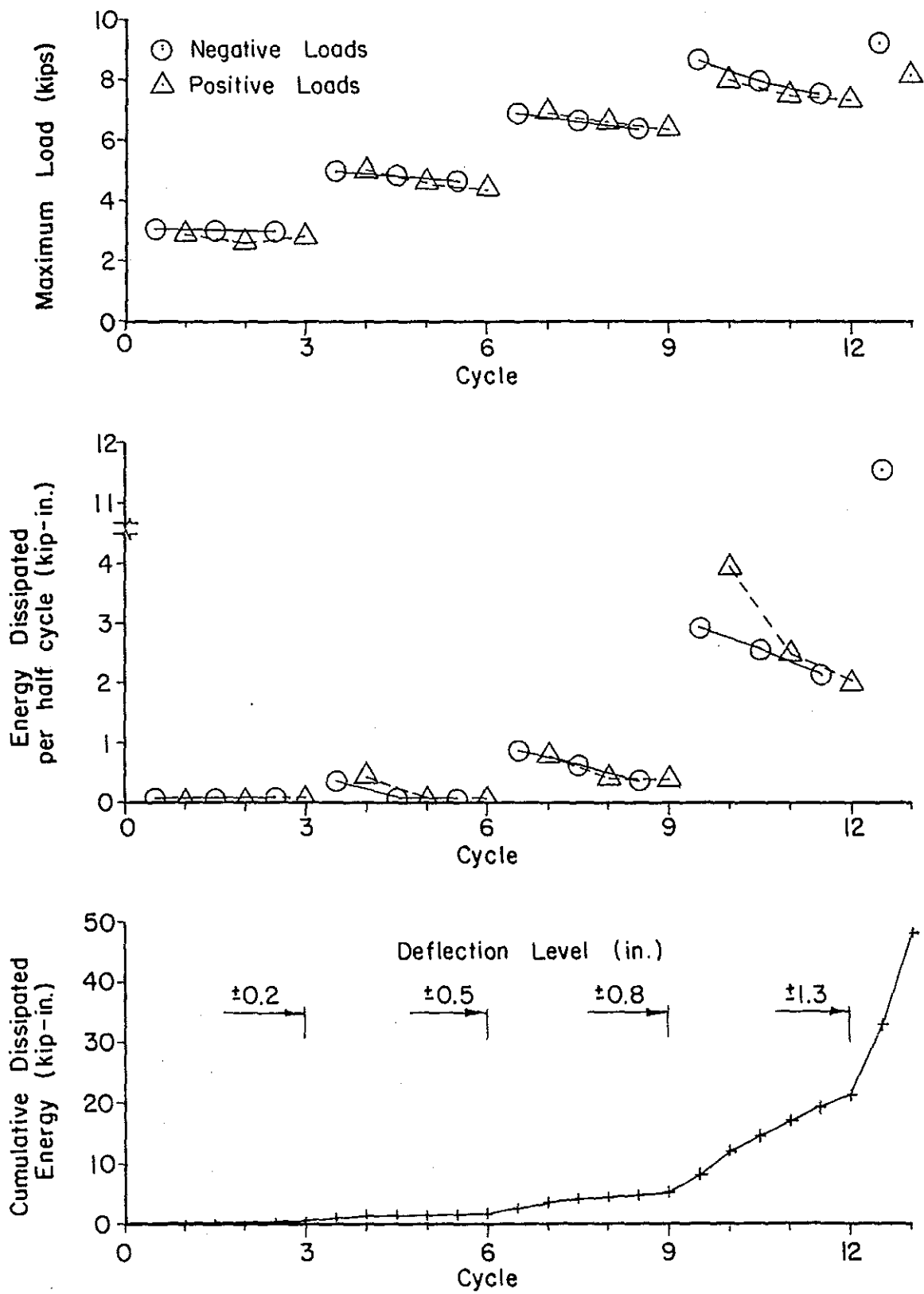


Figure 32. Specimen 2, summary of maximum load and energy dissipation data.

curves did degenerate to a shear-slip type with increased cycles as each column elongated at its base (an average strain of 0.003 in./in. over a 10 in. gage length after twelve cycles).

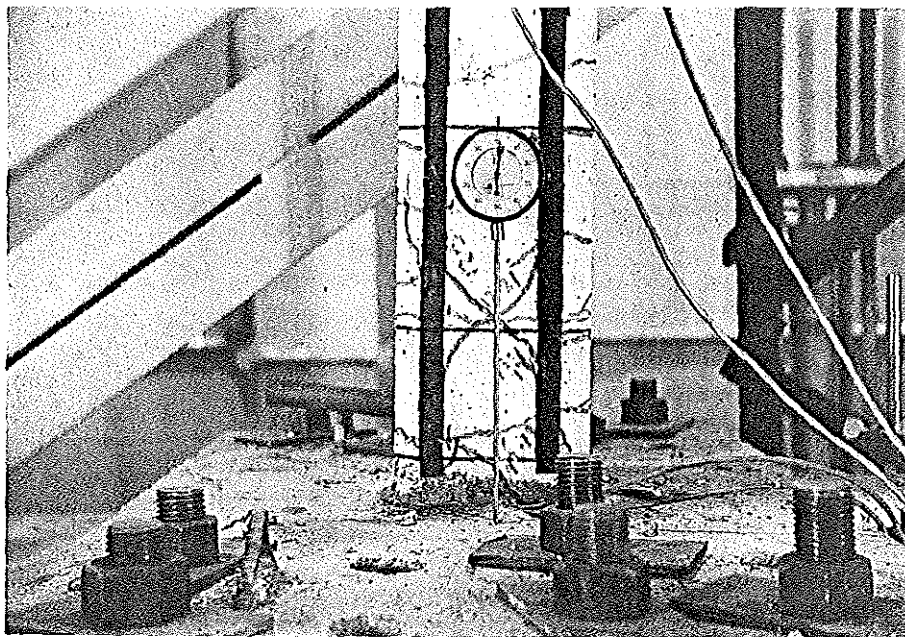


Figure 33. Specimen 2, negative column after completed test.

Cracking was well distributed in the columns and top beam as shown in Figure 33. Maximum damage occurred during the first cycle to -2.6 in., cycle 12-1/2; the negative column crushed at the inside corner of its joint with the top beam. Yet, the frame carried increased loads and dissipated its maximum energy during the +2.6 in. deflection cycle. Altogether, the moment frame

was damaged little by the test; its vertical and horizontal load capacities were judged to be the same after the test as before.

#### Specimen 3, Cast-in-Place Wall

Figure 34 presents the data summary for Specimen 3. Reinforcement first yielded in tension in the base of the positive column at  $-0.36$  in. deflection and  $-95.7$  kips during the first cycle to  $-0.5$  in. (cycle 3-1/2). Maximum load and energy dissipation in each half cycle decreased with succeeding cycles after yielding occurred.

Loss of stiffness and strength principally resulted from deterioration of the 3 in. drypack concrete joint between the cast-in-place wall and the top beam. A crack developed between the drypack and both the cast-in-place section and the beam during the first cycle to  $+0.2$  in. Slipping at the top joint caused shear forces to be transferred to the columns; diagonal shear cracks developed at the top of the columns during cycles to  $+0.8$  in. (Figure 35). Some crushing at the top of the cast-in-place wall began near the vertical bar locations as the drypack cracked. The drypack had over twice the compressive strength as the wall concrete, yet the drypack deteriorated more rapidly. During cycles to  $+1.3$  in. the drypack spalled out of the joint (Figure 22). With the deflections to  $+2.6$  in. the top of both columns failed in shear (Figure 36).

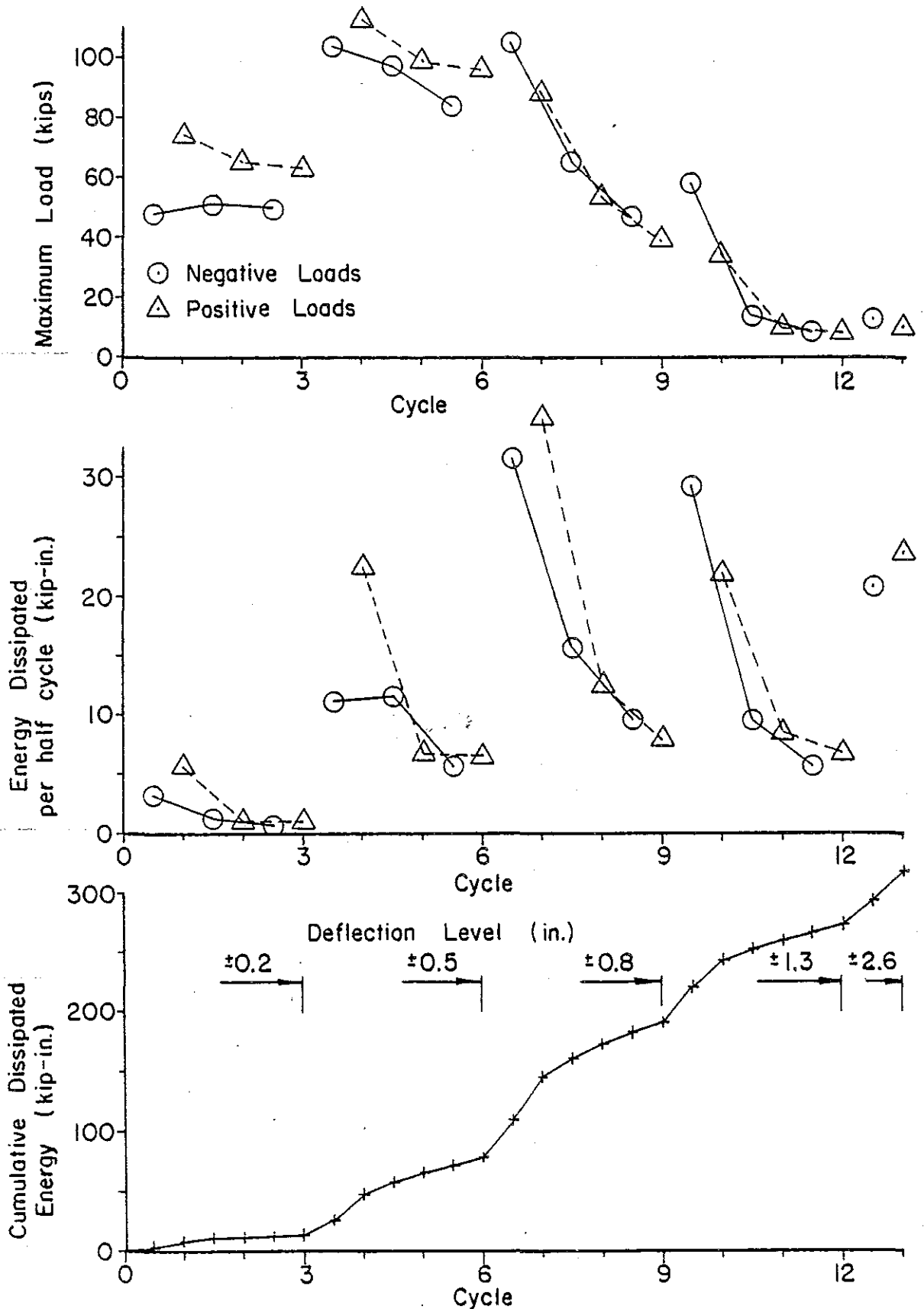


Figure 34. Specimen 3, summary of maximum load and energy dissipation data.

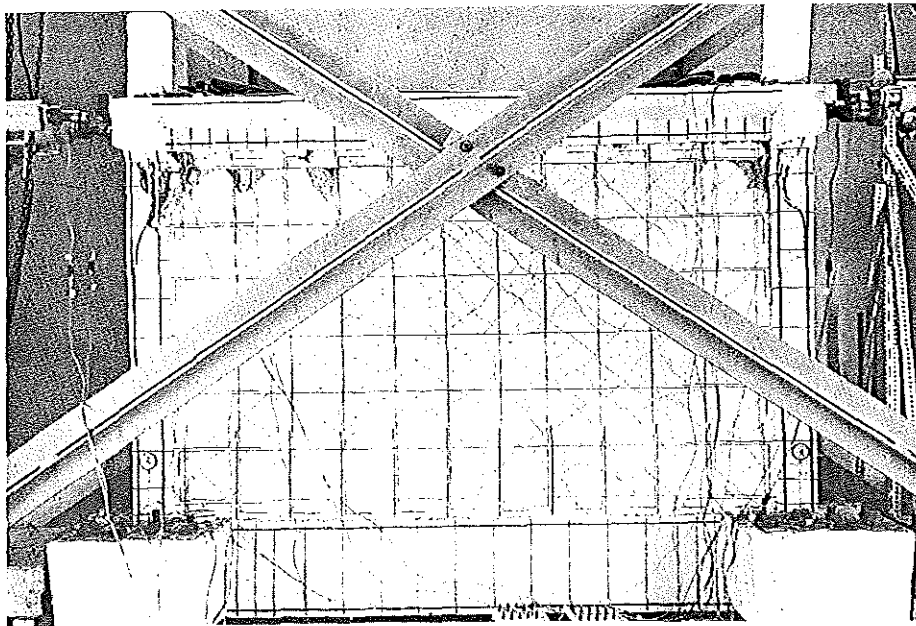


Figure 35. Specimen 3 after three cycles to  $\pm 0.8$  in.

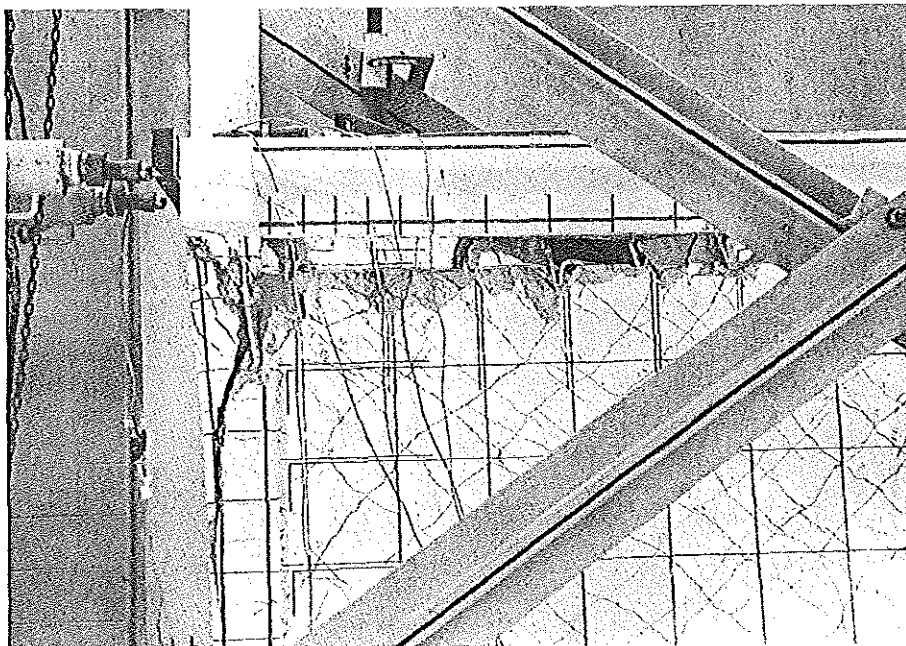


Figure 36. Specimen 3, shear failure of negative column during cycle to  $-2.6$  in.

Cracking and strain data indicated that the wall and frame separated during cycles to  $\pm 0.5$  in. Columns demonstrated flexure together with either net tension or compression, and vertical cracks developed between the lower portions of columns and wall. The strain distribution was not linear but was a combination between that of a frame in flexure like Specimen 2 and that of a shear wall like Specimen 1.

After the test the vertical load capacity of Specimen 3 was judged not capable of carrying normal working loads.

#### Specimen 4, Single Precast Panel Wall

Figure 37 presents the data summary for Specimen 4. During the fourth cycle, reinforcement first yielded in tension in the top of the positive column at  $-0.43$  in. deflection and  $-69.5$  kips (cycle 3-1/2). With loading direction reversed, yielding occurred in the top of the negative column at  $+0.55$  in. deflection and  $+83.3$  kips. Beyond the  $\pm 0.5$  in. deflection level, load capacity degraded with succeeding cycles to less than half the maximum capacity.

Cracking and strain data indicated that the structure responded with a combined frame and shear wall behavior. Columns were subjected to flexure plus net tension or compression. The wall strains showed a compression zone from the top loaded corner diagonally down to the opposite base corner. Relative slip movement between the panel and the frame equaled about one-half the total lateral deflection.

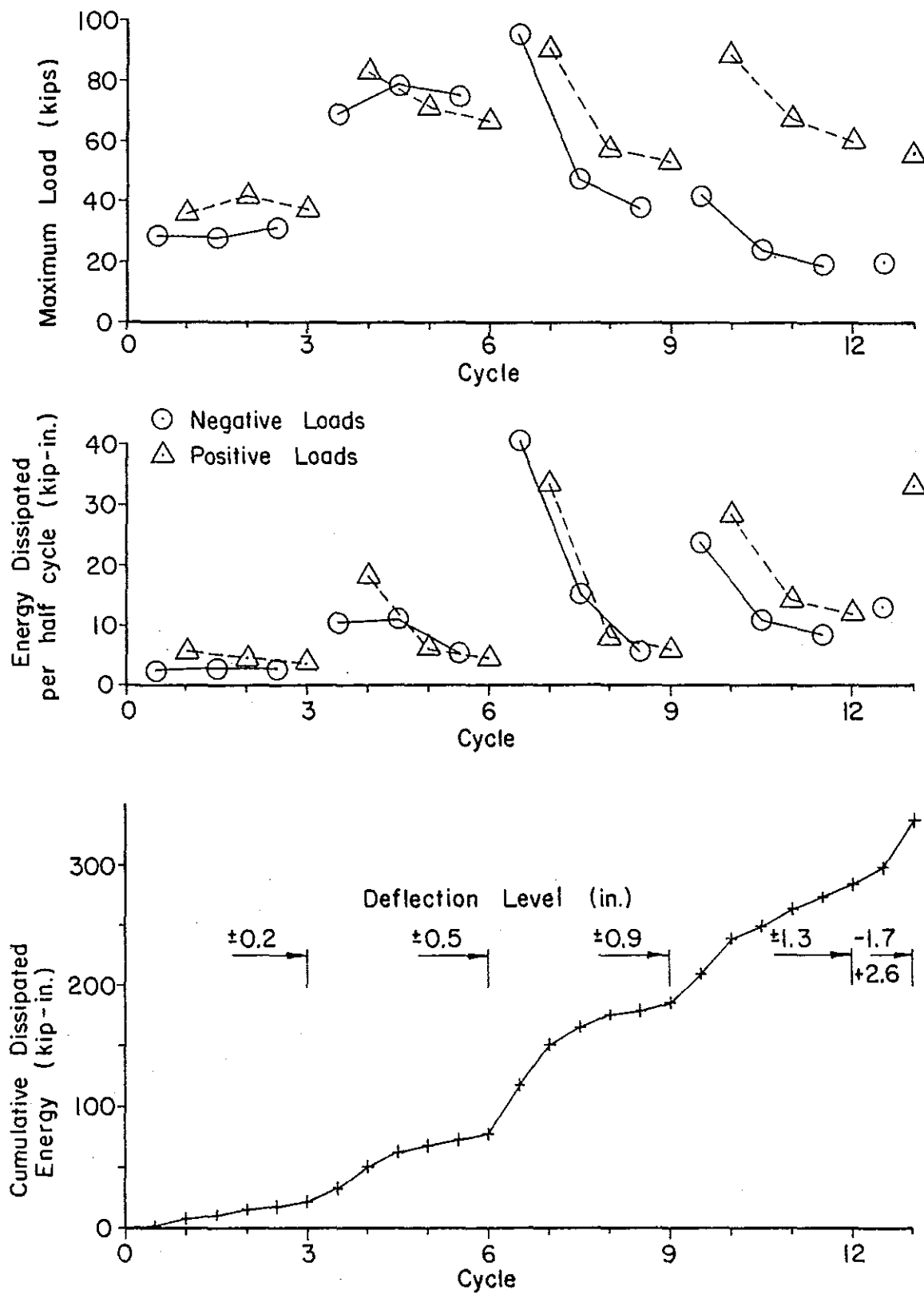


Figure 37. Specimen 4, summary of maximum load and energy dissipation data.

During cycle 6-1/2 at -0.78 in. deflection and -95.5 kips, the top beam failed in diagonal tension-shear as shown in Figure 38. The failure was precipitated by failure of welds connecting the ear plates to the embedded panel plate in the upper positive corner and by the pullout of the anchor bolts in the lower positive corner. With failure of the connection between the wall and top beam, the beam's shear span increased from about 1 in. to 1 ft.; and diagonal tension-shear failure resulted. Reversed loading did not cause similar weld failure, anchor pullout, or beam failure at the negative side of the specimen.

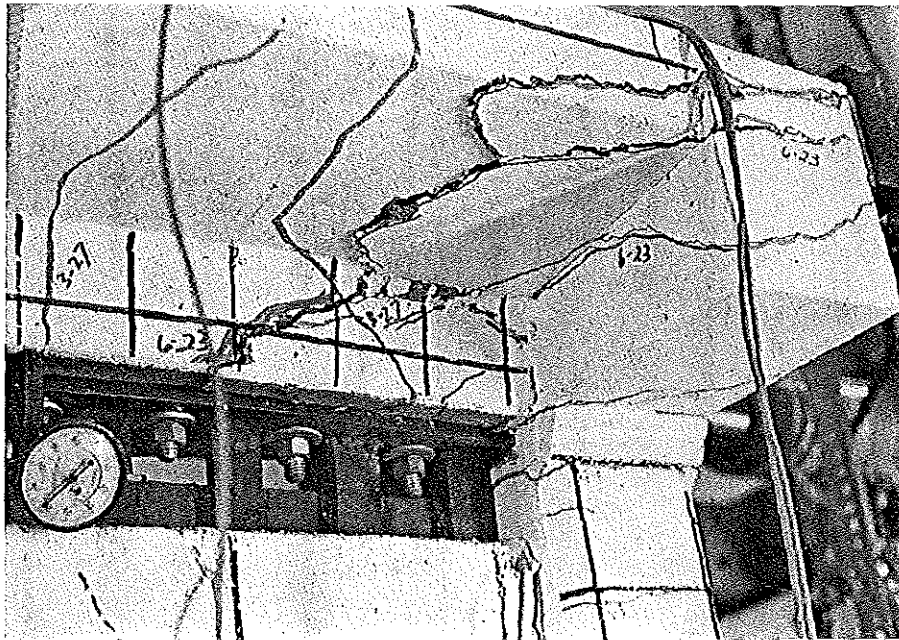


Figure 38. Specimen 4, shear failure of top beam.

The loading system was modified so that the structure could be deflected negatively again while minimizing further beam deterioration. Steel angles epoxied to the slab carried the force from the loading jacks around the damaged area and into the center portions of the top slab.

During negative deflection cycles to -1.3 in. the failure zone in the top beam deteriorated and the anchor bolts at the positive end of the base beam pulled out farther. Positive deflections to +1.3 in. caused the panel to bear against the lower portion of the positive column; this bearing resulted in a diagonal shear failure at the base of the positive column at a load of 73.2 kips.

During the final cycle the maximum negative deflection was limited to -1.68 in. because of the severe tilting of the wall which resulted from anchor bolt pullout (Figure 39). As the specimen was deflected to +2.58 in. the base of the positive column spalled, and the upper negative corner of the wall crushed under the embedded panel plate. Figure 40 shows Specimen 4 at +2.58 in. during the last cycle.

Two distinct failure modes were observed: (1) shear failure of the top beam caused by connector failure, and (2) wall crushing resulting from concentrated compression loads, and column shear failure resulting from bearing of the panel on the column.

The structure appeared able to support vertical loads after the test was completed.

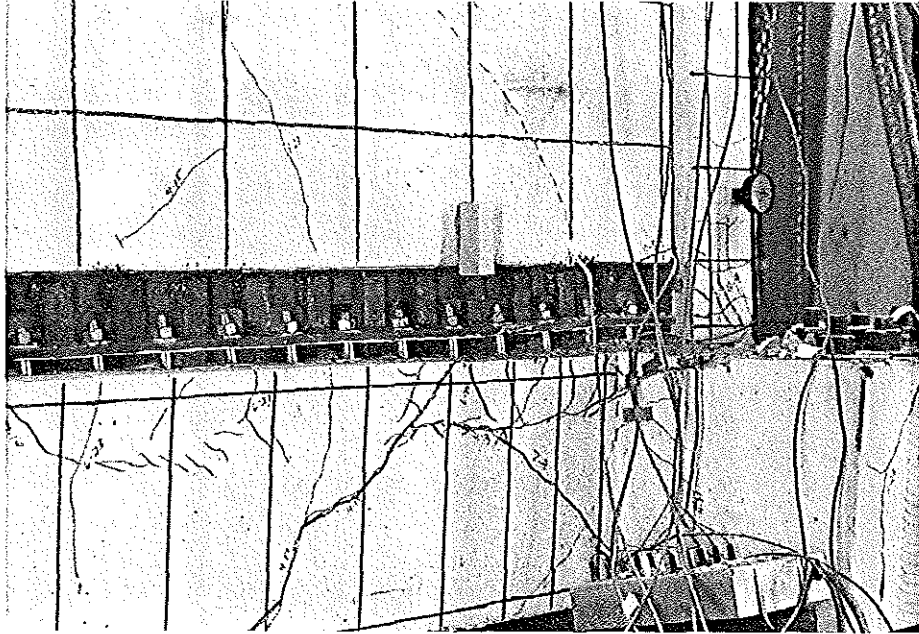


Figure 39. Specimen 4, anchor bolts pulled out at positive end of base beam at  $-1.68$  in.

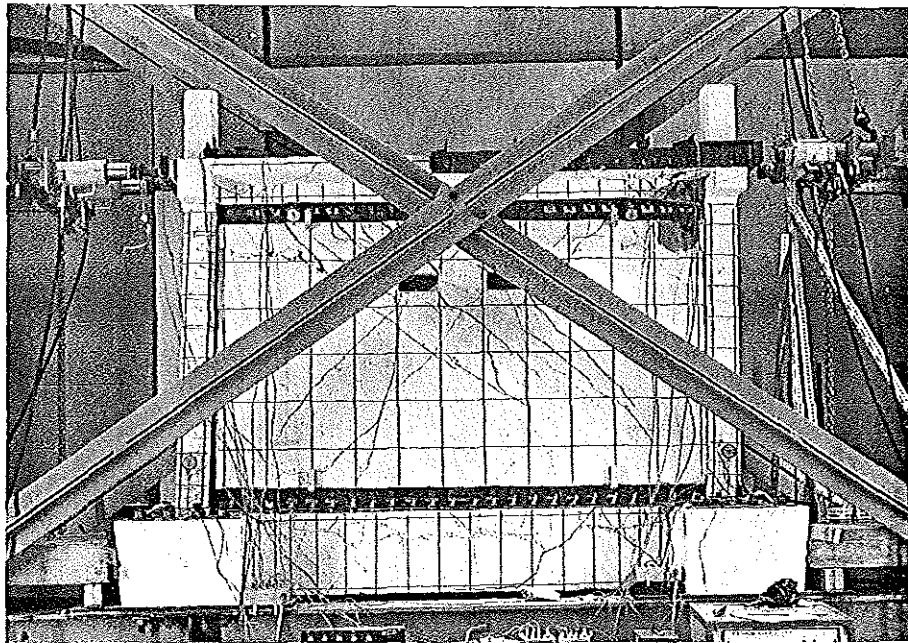


Figure 40. Specimen 4, crushing at top of panel at deflection of  $+2.58$  in.

/ 1

## Specimen 5, Multiple Precast Panel Wall

Figure 41 presents the data summary for Specimen 5. The load degraded less than for the previous infilled specimens even though the vertical reinforcement began tension yielding in an interior panel at +0.41 in. deflection and +44.1 kips during cycle 4.

Cracking and strain data indicated that the frame responded in a flexural model while the panels behaved as fixed-end deep beams. Figure 42 shows the diagonal shear cracking in the panels after deflections to  $\pm 0.8$  in. Cycles 6-1/2 through 12 to  $\pm 0.8$  in. and to  $\pm 1.3$  in. caused shear deformations within each panel which brought neighboring panels into contact at locations near the panel-to-panel connectors. With increased cycles the area of the contact points began to crush while the region between the panel-to-panel connectors and the first #3 horizontal "stirrup" began to spall (Figure 43). During cycle 12-1/2 to -2.6 in. and at deflections greater than -1.6 in., the columns bore against the panels. Diagonal shear failure resulted at the top of both columns and at the base of the negative column. With reversed loading, concrete spalled from the failed areas.

With the test completed the vertical and lateral load capacities appeared completely deteriorated because of the shear failures of columns and panels (Figure 44).

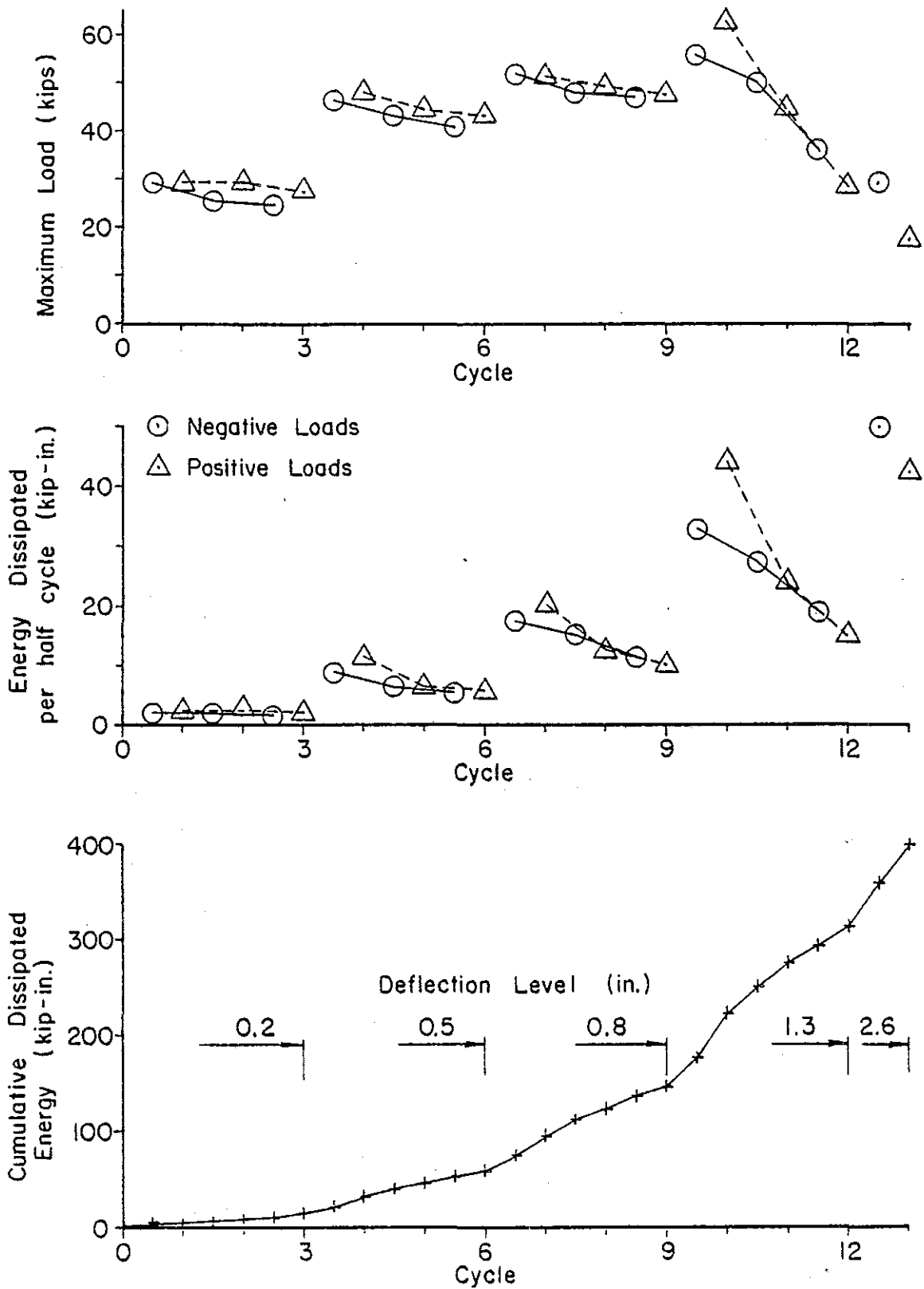


Figure 41. Specimen 5, summary of maximum load and energy dissipation data.

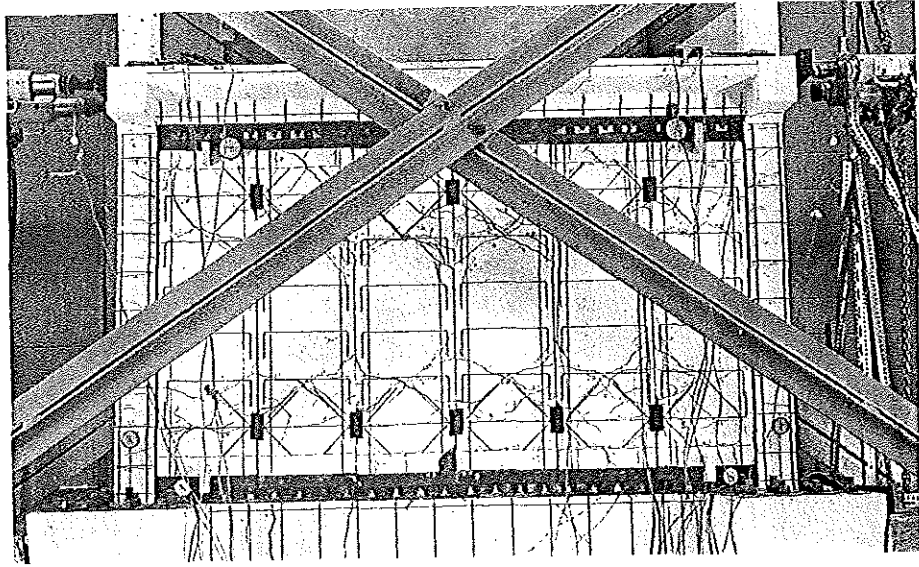


Figure 42. Specimen 5 after three cycles to  $\pm 0.8$  in.

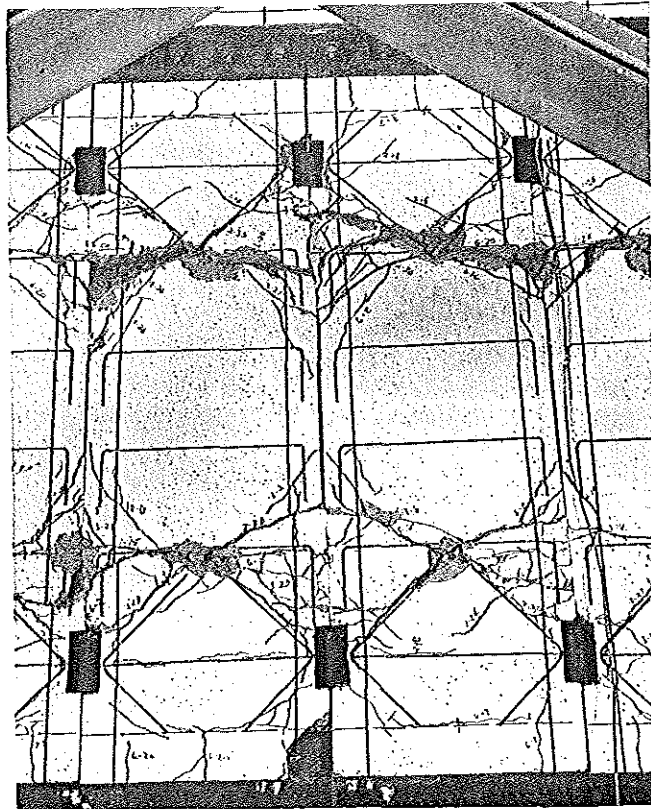


Figure 43. Specimen 5 after three cycles to  $\pm 1.3$  in.

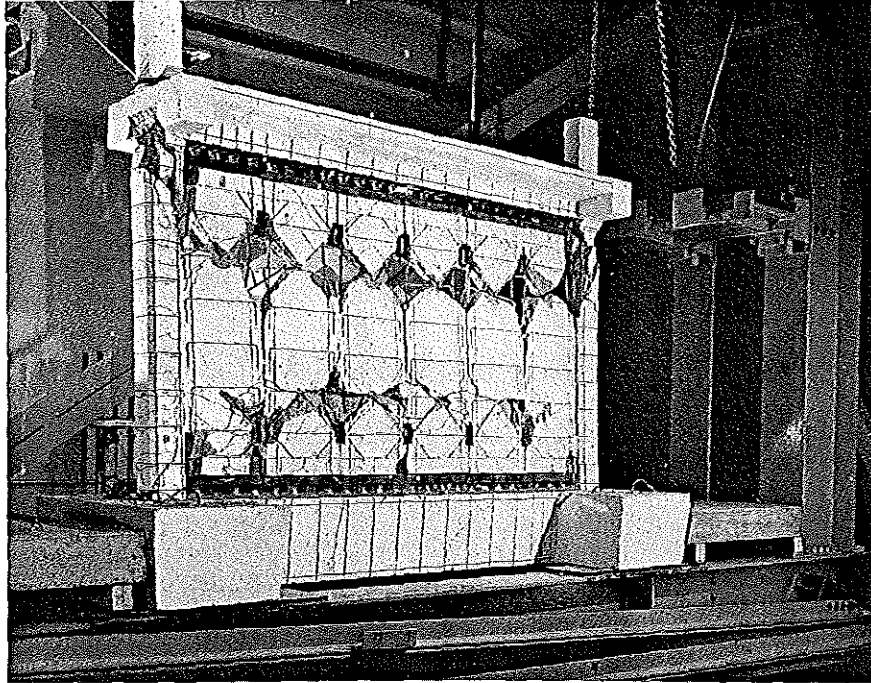


Figure 44. Specimen 5, after completed test.

#### Comparison of Results

Maximum load-deflection envelopes were formed by connecting the maximum load points which occurred during the first cycle of each deflection level. Envelopes for the five specimens are given in Figure 45. In general the envelopes of the monolithic shear wall specimen and the plain frame specimen formed the upper and lower boundaries of load capacity.

Stress Coefficient. In order to minimize the effect of concrete strength on the compared results, the maximum lateral loads during each half cycle,  $V$ , were divided by  $C\sqrt{F'_c}$  where

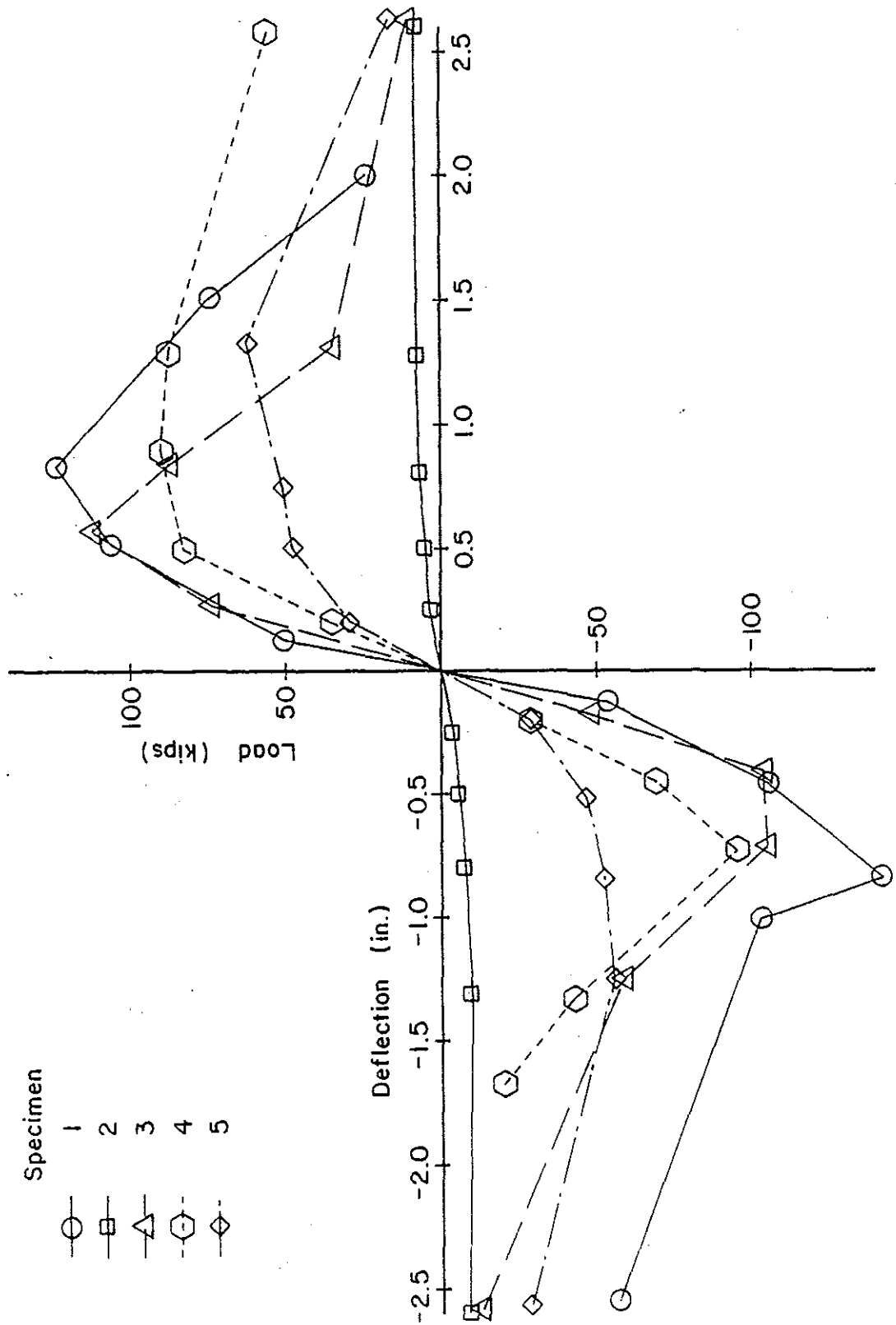


Figure 45. Maximum load-deflection envelope for the five specimens.

$C = hd$ , equal to 225 in.<sup>2</sup> for Specimen 1

$d$  = distance from extreme compression fiber to centroid of vertical tension reinforcement (in.)

The  $\sqrt{f'_c}$  was used because others (6) have found it more closely related to the shear resistance of members than  $f'_c$ . The resulting dimensionless stress coefficient,  $V/C\sqrt{f'_c}$ , for the first cycle of each deflection level was plotted against lateral deflections to form the stress coefficient envelopes given in Figure 46. The envelopes for the monolithic wall and for the cast-in-place wall were quite similar.

A dimensionless rotation deflection scale along with the lateral deflection scale are given in Figure 46. The lateral deflection was divided by the specimen story height (66 in.) to give the dimensionless rotation deflection measure which had been used by other researchers (35, 41, 52). While the envelopes for Specimens 1, 3 and 4 were different, the maximum load occurred at a rotational deflection between 0.009 radian to 0.011 radian. Maximum load for the multiple panel wall occurred at about 0.02 radian.

Stress coefficient envelopes were formed for the first, second and third cycles for each specimen as shown in Figure 47. Second and third cycle envelopes were formed in a manner like first cycle envelopes by connecting the maximum stress coefficient and deflection points which occurred during the cycle. The absolute value of the stress coefficient was used for Figure 47 so that positive and negative deflection cycles could be compared more clearly.

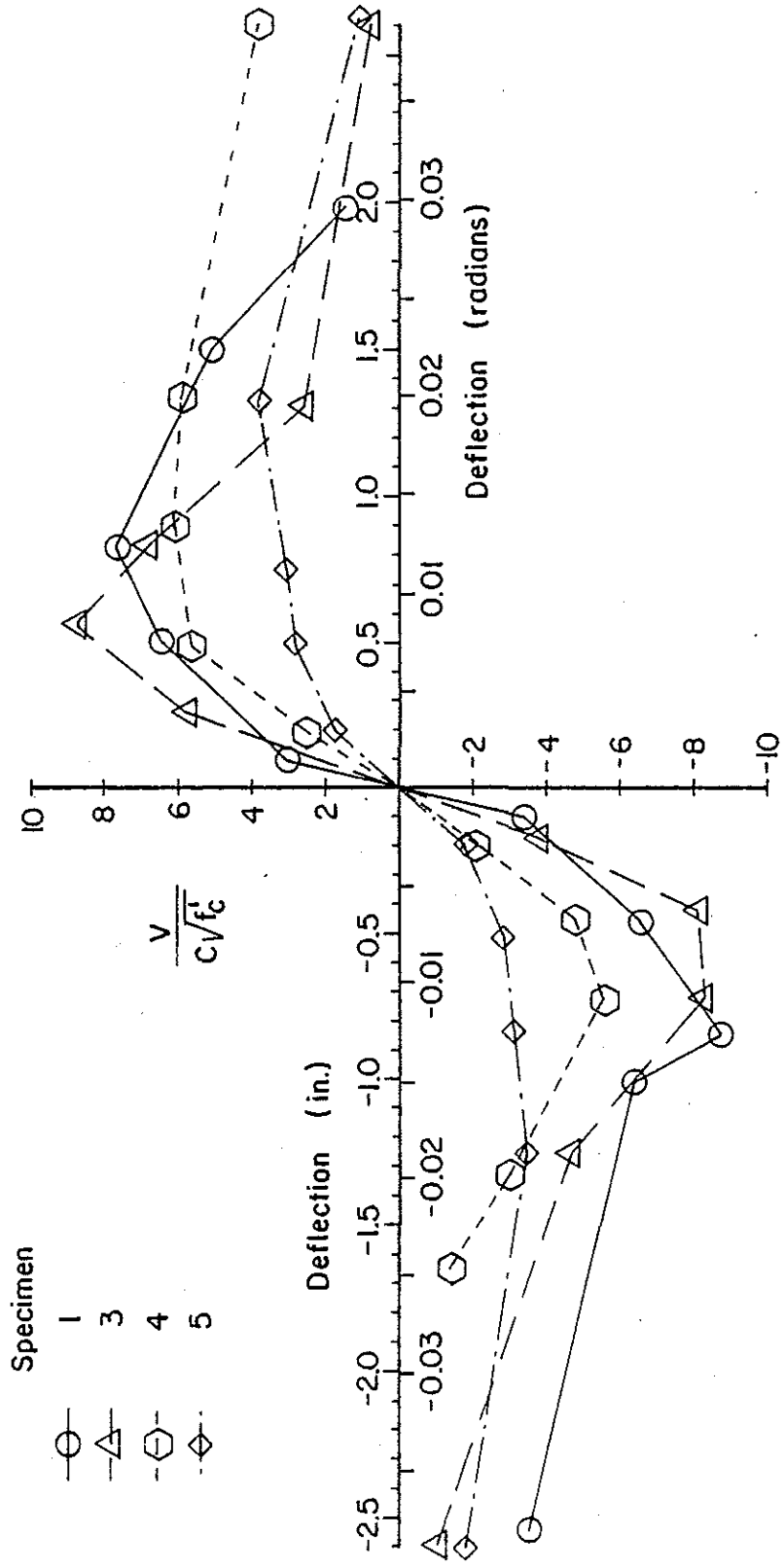


Figure 46. Maximum stress coefficient envelope for the four infilled specimens.

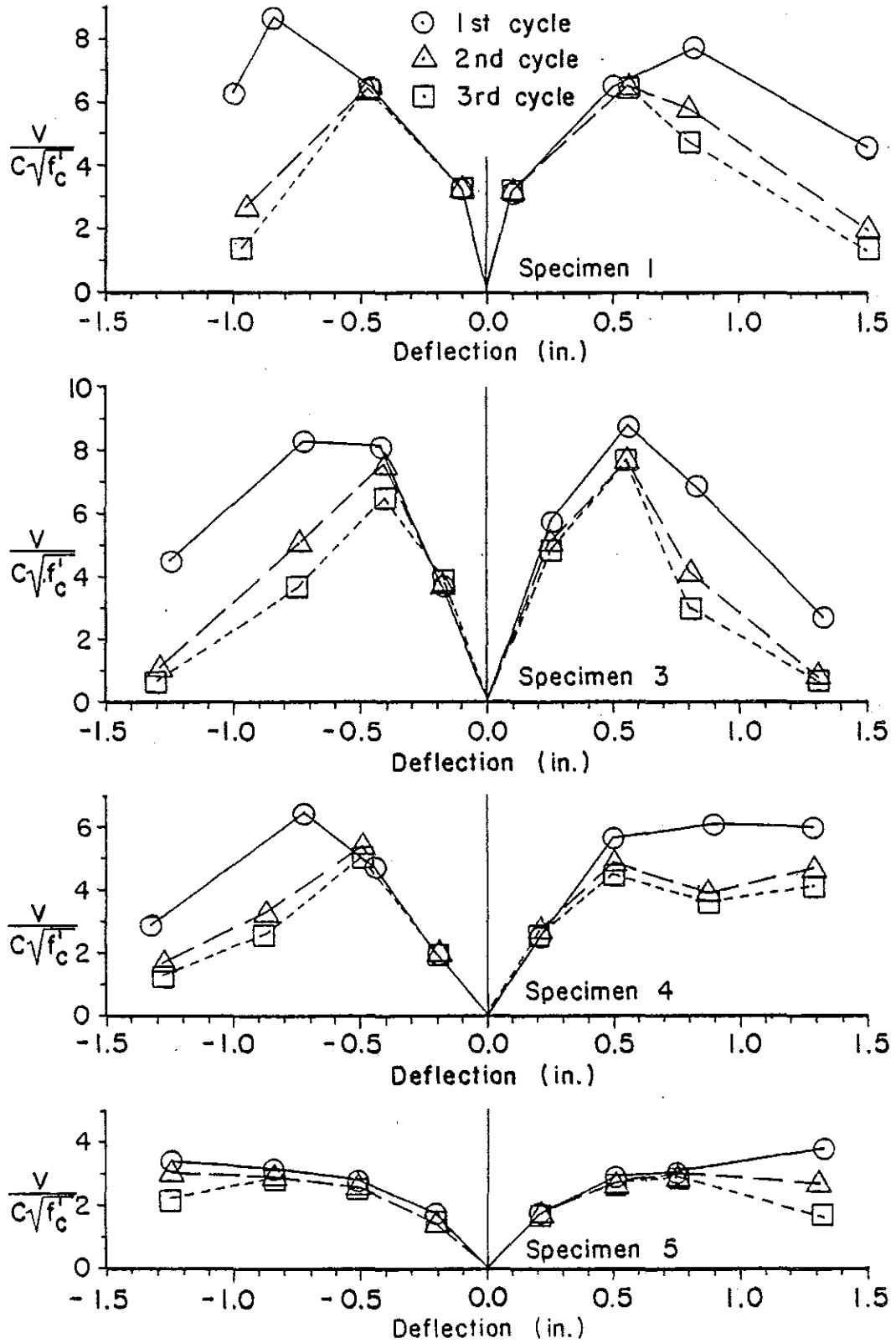


Figure 47. First, second and third cycle coefficient envelopes for Specimens 1, 3, 4 and 5 from top to bottom, respectively.

Several findings are illustrated:

(1) The positive and negative envelopes for each specimen are approximately symmetric, although the positive side shows somewhat greater load capacities.

(2) For Specimens 1, 3 and 4, the second cycle envelope was similar to the third, while both deviated substantially from the first cycle envelope at deflections greater than 0.5 in. Specimen 5 envelopes diverged at deflections greater than 0.8 in.

(3) At deflections greater than that at which the ultimate load occurred, the envelopes of Specimens 1, 3 and 4 show rapid loss of load capacity. The second and third cycle envelopes of Specimen 5 show gradual decrease in load capacity.

(4) For each specimen the maximum stress coefficients which occurred in the positive and negative third cycle envelopes were averaged. The resulting values were termed cyclic strength factors, and their comparison gave a measure of relative cyclic load capability. The cyclic strength factors were as follows: Specimen 1, 6.5; Specimen 3, 6.9; Specimen 4, 4.8; and Specimen 5, 2.8. The cast-in-place wall had a cyclic load capacity 6 percent greater than that of the monolithic wall, while the single panel and multiple panel walls respectively had cyclic load capacities 26 percent and 57 percent less than that of the monolithic wall.

Load Degradation. The stress coefficient envelopes in Figure 46 clearly show the decrease in load capability with

succeeding cycles. Load degradation of the five specimens is compared further in Figure 48. The following formula was used to calculate the percent load degradation for each specimen at each deflection level:

$$\text{Percent degradation} = \frac{\text{Maximum 1st Cycle load} - \text{Maximum 2nd or 3rd cycle load}}{\text{Maximum 1st cycle load}} \times 100$$

Figure 48 illustrates that as the deflection level increased the percent load degradation increased. That the load capacity decreased more with either the positive or negative deflections resulted from different failure modes in each direction; such a difference was particularly evident for Specimen 4. As stated before, the moment frame showed little loss in load capacity (a maximum 12 percent load degradation). At or below their yield levels, about 0.5 in. deflection, the infilled wall specimens had average load degradations of about 10 percent over the three cycles. Beyond yield the monolithic and cast-in-place wall specimens showed the greater percent loss in load capacity.

Energy Dissipation. The energy dissipated in each half cycle for the five specimens has been shown in Figures 28, 32, 34, 37 and 41. Within the three cycles of any deflection level the energy dissipated per half cycle decreased with succeeding cycles at a rate greater than that at which maximum load capacity decreased. Decreased energy dissipation primarily resulted because the load-deflection hysteresis curves degenerated to the shear-slip type; the loops became more narrow (Figures 23 through 27).

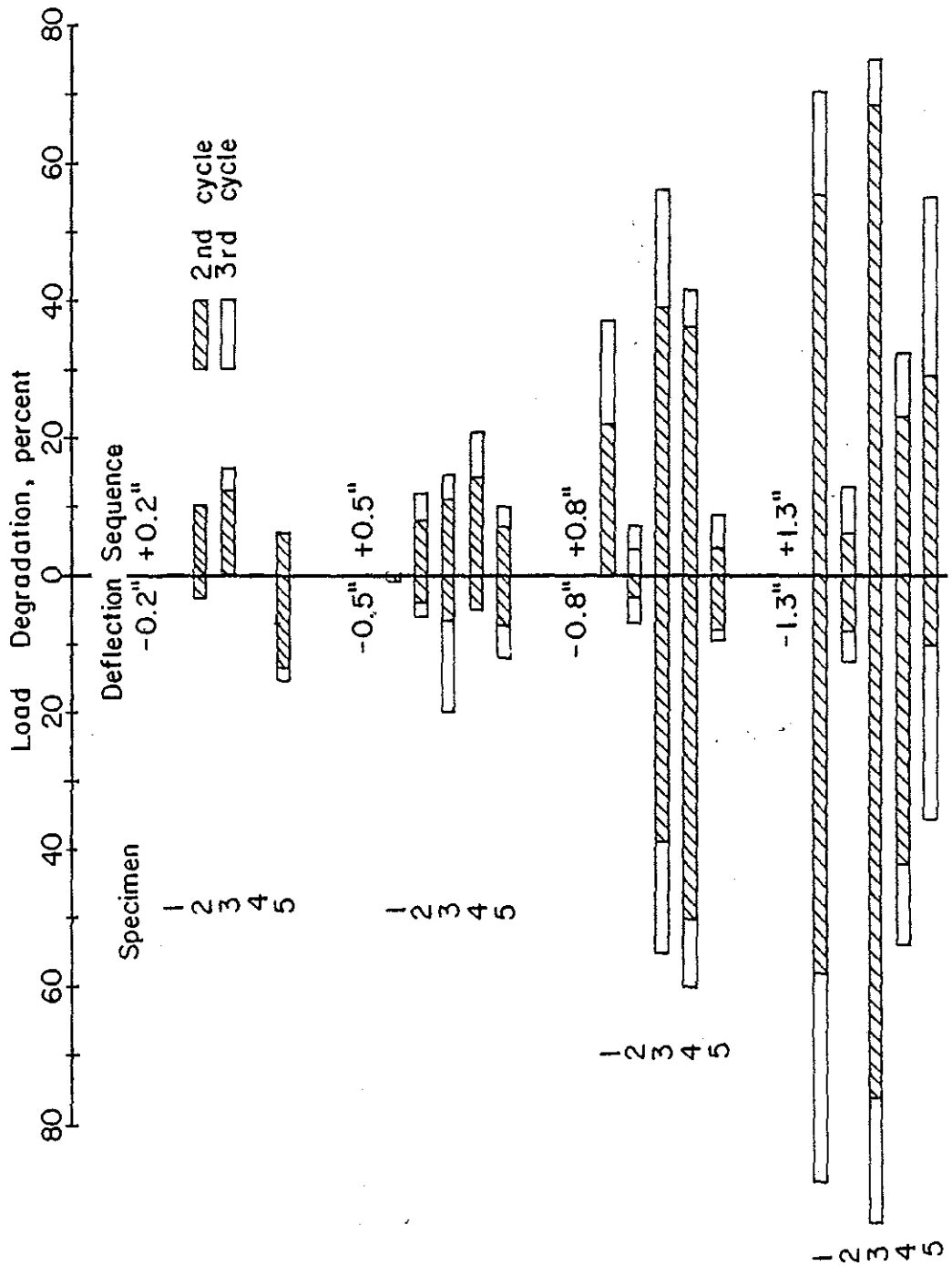


Figure 48. Load degradation as a function of deflection amplitude.

The percent decrease in energy dissipated at each deflection level is shown in Figure 49; values were calculated using the following formula:

$$\text{Percent degradation} = 100 \times \frac{\text{energy dissipated in 1st cycle} - \text{energy dissipated in 2nd or 3rd cycle}}{\text{energy dissipated in 1st cycle}}$$

Figure 49 indicates that in each specimen the decrease in energy dissipation was not proportional to deflection level as was load degradation. The trend indicated in Figure 49 is that in deflection cycles beyond the yield deflection, the energy dissipated decreased to roughly one-third the energy dissipated in the first cycle to that deflection level.

Figure 50 shows the cumulative energy dissipated with increasing number of cycles for the five specimens. Results for Specimen 1 and 2 form the respective maximum and minimum boundaries of the dissipated energy curves. Specimens 3, 4 and 5 dissipated a total of about one-half as much energy as the monolithic wall. During the first three cycles Specimens 3, 4 and 5 dissipated over twice the energy of Specimen 1; the monolithic wall responded in a manner closer to an elastic behavior than the other infilled specimens at low deflection cycles. The close similarity between curves for Specimens 3 and 4 resulted because both structures behaved similarly in combined flexure and shear modes. Because of substantial steel yielding in the panels, Specimen 5 exhibited increased energy dissipation in the later cycles. The monolithically cast wall dissipated twice the energy as the other infilled specimens because

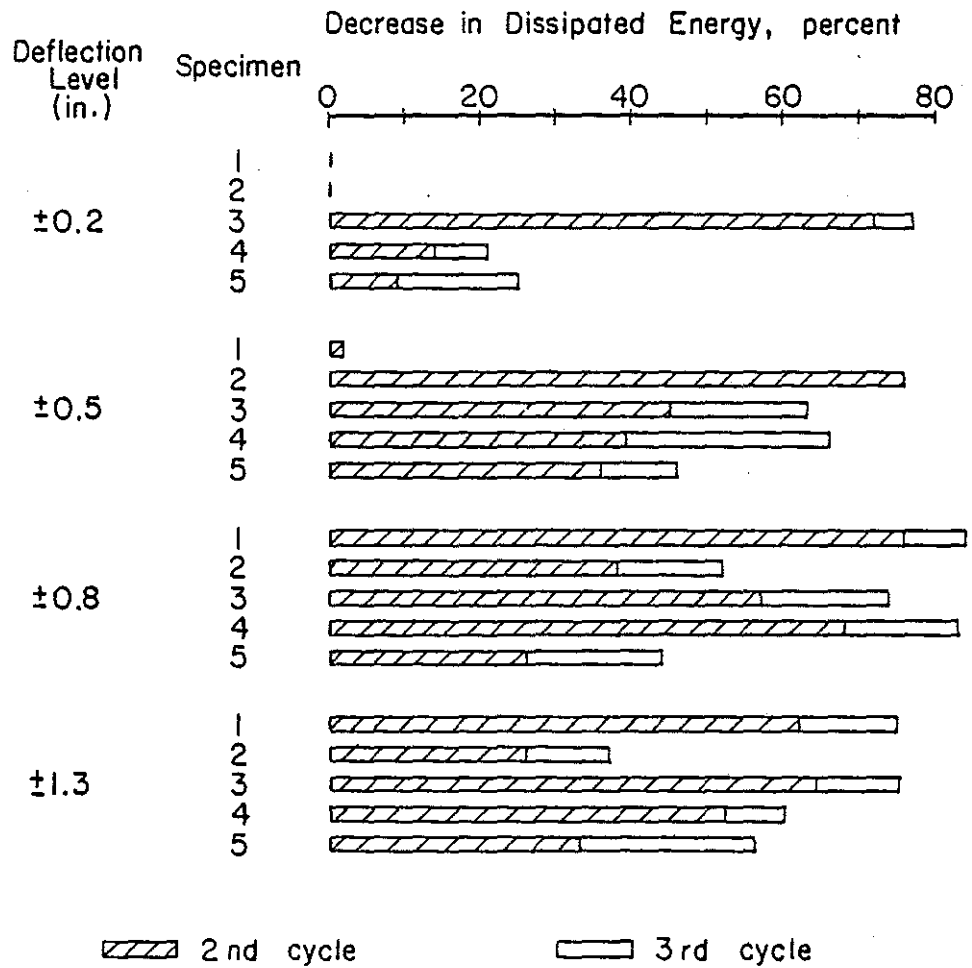


Figure 49. Decrease in energy dissipated per cycle.

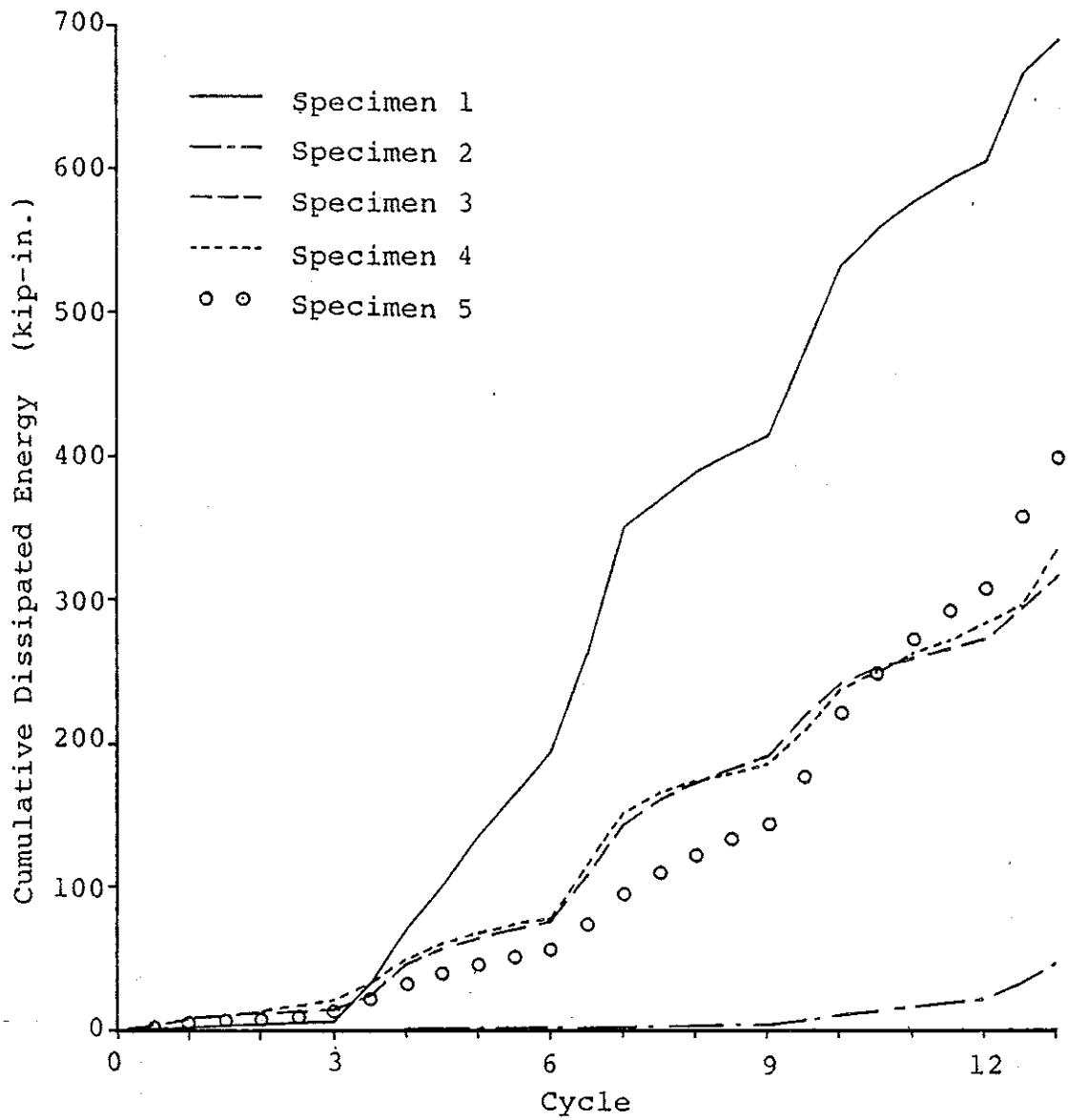


Figure 50. Cumulative energy dissipation of the five specimens.

of the greater tension yielding deflections in all four of the column reinforcing bars. In the combined flexure and shear wall behavior (Specimens 3, 4 and 5), only two of the column bars yielded in any half cycle.

## CHAPTER IV

### ANALYSIS

#### Introduction

In this chapter the experimental results are compared with loads and stiffnesses calculated using simple and currently available design techniques. A load-deflection hysteresis model is presented in which slope and load parameters are determined using calculated results; the model is proposed as an aid in further analytical research and not as a design recommendation. Finally, a simple change in current shear wall design equations is suggested.

#### Hysteresis Model

Calculated stiffnesses, as presented below, were compared with the experimental load-deflection hysteresis curves. A simple hysteresis model was developed based on this comparison, and it is shown in Figure 51. The model was developed so that the experimental findings could be utilized in future analytical research of infilled shear wall structures.

Lateral deflection is given in terms of relative story deflection,  $\Delta/h_s$ , where  $\Delta$  is the lateral deflection and  $h_s$  is

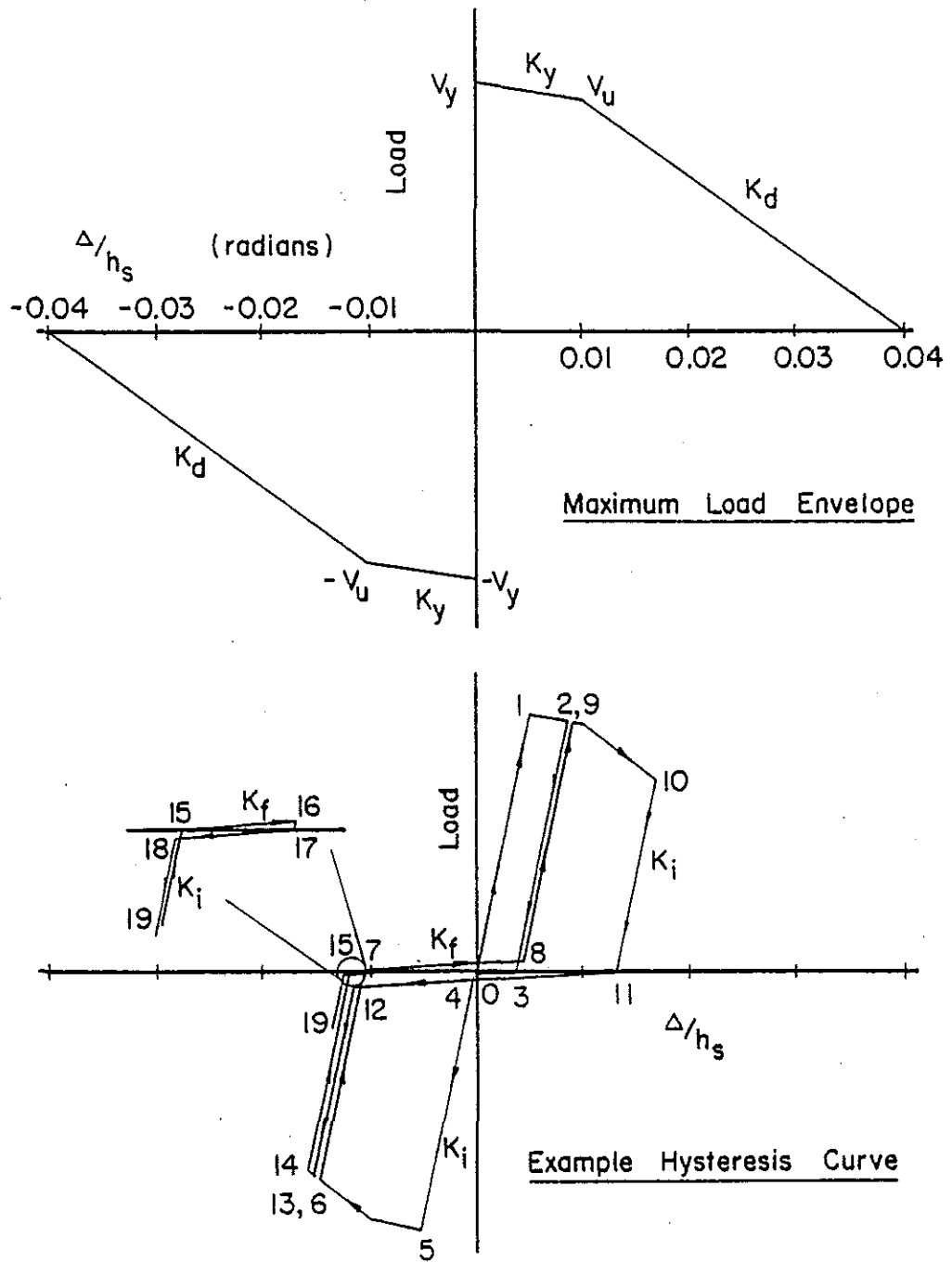


Figure 51. Load-deflection hysteresis model for infilled shear walls.

the story height, which was 66 in. for the five specimens. A maximum load envelope shows a deteriorating load capacity, where  $V_y$  is the calculated flexural yield load of the infilled structure, and  $V_u$  is the calculated ultimate shear capacity. For solid infilled walls, the ultimate load point " $V_u$ " is at a relative deflection of 0.01 radian. For multiple panel infills the deflection at  $V_u$  is 0.02 radian because of the wall's greater ductility. The load capacity becomes zero at 0.04 radians. These deflection values were selected from observation of the test data. It is suspected that variation of moment to shear ratio and differences in confinement of the concrete in the columns would change these deflections turning points.

The slope of the various straight line segments are as follows:

$$K_y = (V_u - V_y) / 0.01 h_s$$

$$K_d = -V_u / 0.03 h_s \text{ for solid infilled walls}$$

$$K_d = -V_u / 0.02 h_s \text{ for multiple panel infilled walls}$$

$$K_i = \text{Stiffness determined for each infilled specimen } i, \\ \text{where } i \text{ is the specimen number}$$

$$K_f = \text{Stiffness of frame without an infilled wall}$$

The hysteresis model in Figure 51 shows successive load points 0 through 19 where points 2 and 9, and points 6 and 13 are at the same location.

Following are the hysteresis model rules:

- (1) Prior to yield the loading and unloading occurs along line 1-5.
- (2) Maximum loads and yielding loads occur along the maximum load envelope, such as between points 1-2 and 9-10.
- (3) Beyond yield deflections, the unloading line is parallel to the loading line with slope  $K_i$  such as between points 0-1 and 2-3.
- (4) With reversal of load after yield has first occurred, the reversed loading line has slope  $K_f$ , such as between points 7-8, 11-12 and 17-18.
- (5) When the new loading line of slope  $K_f$  intersects the last unloading line in a quadrant, the slope of the loading line becomes  $K_i$  such as loading between points 7-8-9 and between 11-12-13.
- (6) Unloading from a loading line of slope  $K_f$  occurs along a line of slope  $K_i$ , such as between points 16 and 17 of 15-16-17 and 18.

The slope  $K_d$  of the maximum load envelope accounts for the lack of ductility in the infilled shear walls. Rule 5 accounts for the deterioration of maximum load and energy dissipation capacities with successive cycles. Rule 4 accounts for the shear-slip phenomena.

Because no loading or unloading line is horizontal (zero stiffness), this hysteresis model may be used in the method of characteristics structural analysis technique (42).

While further analysis using this hysteresis model was not conducted for this thesis, it is suggested that this model be used in continuing research on the strengthening of framed structures.

### Concrete Modulus

In calculating stiffness of the frame and infilled wall specimens, it was found that use of the method in ACI 318-71 for estimating the concrete modulus,  $E_c$ , was unsatisfactory because its use gave stiffnesses greater than observed. A satisfactory estimate of the concrete modulus was calculated using the following relation:

$$E_c = 500 f'_{cf} \text{ in psi} \quad (1)$$

This relation was developed by assuming that the concrete strain at a stress of  $f'_{cf}$  was approximately 0.002 in./in. Therefore, the  $E_c$  is a secant modulus to the ultimate stress point of a concrete stress-strain curve.

The  $E_c$  based on an ultimate strain was about one-half the value of  $E_c$  found using the formula given in ACI 318-71. In the following calculations of specimen stiffness, this  $E_c$  based on ultimate strain was used.

Apparently, the reversed cycle loading caused a decrease in the concrete modulus found by monotonic loading.

### Analytical Results, Stiffness

Calculated stiffness of the five specimens is discussed before calculated load capacity because structure rigidity was used to determine the yield load capacity for Specimens 4 and 5.

The lateral stiffness of the frame without an infilled wall is considered first. The frame stiffness at first yielding of column reinforcement was calculated assuming an infinitely stiff beam-column joint but including the flexibility of both beams and columns and including the overturning, axial load effects in the columns. The moment of inertia of the sections was calculated assuming a fully cracked section and using transformed areas of the steel reinforcement based on the reduced  $E_c$  given by equation (1). The calculated value of yield load stiffness,  $K_2$ , was 8.3 kips/in. which is less than that determined experimentally. This  $K_2$  may be considered  $K_f$  for the hysteresis model presented above.

A hysteresis model for the frame without an infilled wall would be different than the model proposed above. From cursory observation the author believes that Takeda's Simplified Hysteresis Rules described by Otani and Sozen (43) would be applicable to the plain frame Specimen 2, taking the elastic stiffness as  $K_2$ .

Two methods were used to calculate the lateral stiffness of the four infilled specimens. The calculated results of these methods are presented in Table 4 and are compared with the experimental stiffness values. The experimental stiffness was taken as the slope of the line joining the maximum load point in cycle 4 (+0.5 in. deflection) to the following zero load point; this unloading stiffness was chosen because it best estimated the elastic response of the structure with regard to the proposed hysteresis model. For each specimen the experimentally determined unloading stiffness at deflections greater

than the yield deflection was similar for one cycle compared to another.

Method 1 used to calculate lateral stiffness was the standard technique given by Blume, Newmark and Corning (20) which used the following equation to find the lateral deflection:

$$\Delta = \frac{V h_s^3}{3 E_c I_{cr}} + \frac{6 V h_s}{5 h l_w G} \quad (2)$$

where

$$G = 0.4 E_c$$

$I_{cr}$  = Moment of inertia of cracked wall and column structure.

Equation (2) combines elastic cantilever bending plus shear deformation to determine the deflection. The ratio of  $V/\Delta$  was the lateral stiffness. This elastic technique was not expected to yield the same  $K_1$  values as those observed in cycles beyond the yield deflection level.

The second method used to determine lateral stiffness was an equivalent diagonal strut technique proposed by Smith and Carter (58). With this method the relative stiffnesses of the surrounding frame and infilled wall were first determined. Based on this relative stiffness a bearing area between the frame and infill was determined for diagonally opposite top and bottom corners. They proposed that the lateral force was carried between these corners by a segment of the wall with a width determined by the bearing area; that is, the lateral force was carried by an

equivalent diagonal strut. Graphs given by Smith and Carter (58) were used to determine the effective bearing area and the modulus of the strut was taken to be that of the wall material. Lateral deflection was calculated using simple truss equations.

Specimen 1. The  $K_1$  calculated using Method 2 (diagonal strut technique) was closer to the experimentally observed stiffness than that found using Method 1 as illustrated in Table 4.

Specimen 3. As found for Specimen 1,  $K_3$  calculated using Method 2 was closer to the observed stiffness.

Specimen 4. The lateral stiffness of Specimen 4 was calculated first using Method 1. The calculation was based on the resistance of the panel alone with the assumption that the panel did not slip within the frame. The resulting stiffness was 870 kips/in.

Hole size in the panel-to-frame connectors were 1/8 in. larger in diameter than the anchor bolt diameter. It was assumed that a relative slip of 1/4 in. would develop at the panel's calculated flexural yield load. The calculated yield load was divided by the sum of the calculated yield deflection plus slip deflection to give a slip-stiffness. The sum of the panel's slip-stiffness and that of the separate frame was a total lateral stiffness

with a value of 170 kips/in. This value closely matched the slope of the loading lines of the actual hysteresis curve.

The diagonal strut method was modified for a third stiffness calculation. Because the panel was connected to the top and bottom beams only, the assumed bearing of the frame against the infilled wall could occur only between beam and panel. This limited bearing reduced the effective width of the diagonal strut by only one-half, and it increased the slope of the diagonal strut slightly. With these two modifications, the calculated diagonal strut stiffness was 170 kips/in.

The close agreement between the calculated slip-stiffness and diagonal strut stiffness was coincidental.

Specimen 5. Method 1 was modified to calculate the stiffness of Specimen 5 because the multiple panel wall behaved as a series of fixed-end beams. The four center panels were assumed fixed at the panel-to-panel connectors, giving a span length,  $l_n$ , of 36-1/4 in. The two end panels were assumed fixed at the edge of the embedded plate,  $l_n = 51$  in., and the columns were fixed at the beam faces,  $l_n = 59$  in. The total stiffness of the specimen was calculated by summing the individual stiffnesses of the panels and columns. The individual stiffnesses were determined using Equation (3):

$$\frac{V_{pi}}{\Delta} = \frac{12 E_c I_{cr}}{l_n^3} \quad (3)$$

where

$$V_{pi} = \text{Shear load carried by a single panel}$$

Equation (3) is a modification of Equation (2); fixed-end bending has been substituted for cantilever bending, and shear deformations are neglected. The total calculated stiffness was 630 kips/in.

The calculated stiffness was reduced to 260 kips/in. by substituting an  $I$  determined using only the transformed area of the vertical steel for  $I_{cr}$ . This lower value of stiffness is recommended for use in the hysteresis model because it was closer to the experimentally observed stiffness.

TABLE 4.

STIFFNESS OF INFILLED WALLS (kips/in.)

	Specimens			
	1	3	4	5
Method 1 <sup>a</sup>	2090	1730	870 (170) <sup>c</sup>	260 <sup>d</sup>
Method 2 <sup>b</sup>	440	250	170	---
Experimental	520	300	290	170

a = elastic bending plus shear technique (20)

b = equivalent diagonal strut technique (58)

c = adjusted to account for connection slippage

d = modified for  $I$  based on steel area only

### Analytical Results, Load Capacity

The load capacities of the five specimens were determined using both flexural and shear calculations. The calculated results are listed in Table 5 and are compared with the experimentally observed yield and ultimate loads.

For the frame, Specimen 2, the load at first yield,  $V_y$ , was calculated using a working stress analysis, while the ultimate load,  $V_u$ , was calculated using a Whitney stress block analysis. In both flexural analyses the stresses due to overturning moments were considered.

Five methods were used to calculate the capacities for the infilled structures. The yield load,  $V_y$ , was calculated using a working stress, flexural analysis; these results are given in Table 5. For Specimens 1 and 3 the overturning moment causing yield at the base of the tension columns were calculated based on cantilever bending of the entire column-wall structure. As discussed below, the yield load of Specimen 4 and 5 were calculated based on a combined frame and wall response; the stiffnesses determined for each specimen were used to find the frame and wall interaction.

Of the four methods used to calculate the ultimate load capacity,  $V_u$ , only the calculations based on shear stress requirements of ACI 318-71 gave results which estimated, without exceeding, the experimentally observed ultimate loads. These  $V_u$  results are listed in Table 5. The three unsatisfactory methods are discussed first.

One method used to calculate  $V_u$  was a Whitney stress block, flexural analysis. For Specimens 1 and 3 a linear strain distribution was assumed from the extreme fiber of one column to the other, and for Specimens 4 and 5 the distribution was assumed linear across each panel or column element. In each case the calculated ultimate flexural load was greater than calculated shear capacity and the experimentally observed ultimate load.

Barda (12) recommended the following equation for calculating the shear capacity of low rise infilled walls:

$$V_u = hd (8.4 \sqrt{f'_c} + 0.95 \rho_n f_y) \quad (4)$$

The  $V_u$  calculated using Equation (4) was over 30 percent greater than the experimentally observed ultimate loads for both Specimens 1 and 3. Barda's recommended analysis was not considered satisfactory for predicting reversed cycle load capacity.

Benjamin and Williams (16) recommended Equation (5) for predicting the monotonic capacity of infilled walls:

$$V_u = \frac{0.1}{P/C + 0.1} C + 2.2P \quad (5)$$

where

$$C = A_s f'_c (15 + 1.9 (L/H)^2)$$

$$P = f_y \rho_n hL$$

$$A_s = \text{area of steel in compression column (in.}^2\text{)}$$

L = center-to-center distance of columns (in.)

H = distance from base of wall to center of beam (in.)

This bending plus shear equation gave calculated capacities over 40 percent greater than the experimentally observed ultimate loads for Specimens 1 and 3.

The calculations giving the best predictor of ultimate, cyclic load capacity were those based on ultimate shear stress requirements given in Section 11 of ACI 318-71. The nominal permissible shear stress carried by concrete,  $v_c$ , was taken as  $3.3 \sqrt{f'_{cf}}$  for walls and  $2 \sqrt{f'_{cf}}$  for beams (multiple precast panels). For solid walls (Specimens 1, 3 and 4), the nominal total design shear stress,  $v_u$ , was taken in accordance with ACI 318-71 recommendations as

$$v_u = \frac{A_{wn} f_y}{h s_1} + v_c \quad (6)$$

where

$s_1$  = spacing between vertical reinforcement (in.)

The vertical wall reinforcement was considered the principal shear reinforcement for the solid walls in the manner consistent with past research results (6, 12, 16). For the panels of Specimen 5, the beam requirements of ACI 318-71 were used to determine the ultimate shear stress:

$$v_u = \frac{A_v f_y}{h s} + v_c \quad (7)$$

where

$A_v$  = area of horizontal, shear reinforcement (in.<sup>2</sup>)

$s$  = spacing of horizontal reinforcement (in.)

The ultimate shear capacity was determined by

$$V_u = \phi v_u hd$$

where

$\phi$  = capacity reduction factor which was selected as 0.85 according to requirements of ACI 318-71

$d$  = distance from extreme compression fiber to centroid of tension reinforcement (in.)

The  $d$  distance was calculated to be the distance from the extreme compression fiber to the centroid of the tension steel for ultimate moment conditions with all tension steel at the yield stress.

The calculated  $V_u$  results based upon Equations (6) or (7) and (8) are listed in Table 5 for Specimens 1, 3, 4 and 5. In each case the calculated capacity was less than the experimental ultimate capacity. Yet, the calculated loads were greater than the maximum loads recorded in cycles subsequent to the ultimate load.

The application of Equations (6) or (7), and (8) required different analyses for each specimen because of the different construction techniques. Furthermore, the method of determining the yield load for the two precast infilled structures necessitated the use of stiffness calculations not detailed above. Therefore, a brief specimen-by-specimen discussion follows.

TABLE 5  
CALCULATED AND EXPERIMENTAL  
LOAD CAPACITY (kips)

<u>Parameter</u>	<u>Specimen</u>				
	1	2	3	4	5
Experimental $V_y$	106.5	6.4	90.4	76.4	45.3
Calculated $V_y$	125.6	6.7	117.0	77.5	52.7
Experimental $V_u$	150.0	9.3	113.0	95.5	62.7
Calculated $V_u$	98.5	8.6	87.0	65.5	60.0

Specimen 1. The  $d$  was calculated as 75 in. by assuming continuous column and wall flexure. Equations (6) and (8) were applied directly to find  $V_u$  given in Table 5.

Specimen 3. The  $d$  was calculated as 75 in. which was the same as for Specimen 1 because of identical vertical reinforcement. Again, Equations (6) and (8) were applied directly to calculate  $V_u$  given in Table 5.

Additional calculations were made to determine the strength of the wall-to-top beam joint because the failure of Specimen 3 resulted from joint deterioration rather than base shear.

As the drypack-to-beam joint failed, the dowel bars resisted the shear forces. The resistances of these dowels may be calculated in terms of the shear-friction hypothesis (5). Tensile forces in the reinforcement were resisted by compressive forces between the

cracked concrete sections. The shear loads may be considered to be resisted by friction between these concrete sections; and the friction force is equal to the compression times the coefficient of friction,  $\mu$ . For concrete cast against concrete,  $\mu = 1.0$  has been suggested (5, 19). The following equation gives the shear friction load,  $V_{sf}$ , of the wall:

$$V_{sf} = \mu(\rho_n f_y h l_w) \quad (9)$$

$V_{sf}$  equaled 84.3 kips, which was slightly less than the calculated  $V_u$  listed in Table 5. This difference was considered insignificant. Where the calculated joint capacity is significantly less than that given by Equations (6) and (8), the lower value should be used to estimate the ultimate capacity.

Specimen 4. Flexure calculations which assumed separate frame and panel response were made to determine the load at first yield of the column steel. Because of the stiffening influence of the infilled panel on the beams, the columns were assumed fixed at the beam-to-column connections. The fixed-end columns were calculated to yield under a lateral load of 8.1 kips at a deflection of 0.41 in. Multiplying the panel stiffness calculated above times the column yield deflection gave a separate panel load of 69.4 kips. The sum of these loads equaled the yield load capacity, 77.5 kips. This calculated yield load was slightly greater than that observed.

The ultimate capacity of Specimen 4 was calculated as the shear strength of the infilled panel alone by using Equations (6) and (8). The  $d$  was determined by the ultimate moment of the panel without contribution from the columns, and it equaled 56 in.

Specimen 5. The load causing first yield in a single interior panel was calculated using a flexure, transformed section analysis. The stiffness for columns and panels were found using Method 1 with  $I_{cr}$  based on a fully cracked concrete section.

The individual stiffnesses were summed to give a cracked section stiffness of 630 kips/in. for the entire structure. Multiplying this stiffness by the interior panel deflection at first yield gave a calculated yield load of 52.7 kips for the structure.

The ultimate shear capacity of each panel was calculated using  $d = 13.7$  in. with Equations (7) and (8) to give a  $V_{pi} = 15.0$  kips for each panel. The four interior panels would develop their ultimate shear capacities at smaller deflections than for the exterior panels or columns because of higher stiffness of the interior panels. Therefore, the total shear capacity of the structure was calculated as the sum of the capacities of the four interior panels alone. The resulting  $V_u$  equaled 60.0 kips.

The test of Specimen 5 showed that the shear capacity of the four interior panels did develop simultaneously and that the exterior panels and columns did not begin failing, exhibit their ultimate capacities, until after the interior panels were deteriorated

significantly. This failure sequence substantiates the method of calculating the ultimate shear capacity.

#### Modified Stress Coefficients

The stress coefficients which were calculated and discussed in Chapter III were modified based upon calculated  $d$  and  $f'_{cf}$  values in order to reflect the results of the above analysis. Previously the stress coefficient was calculated by dividing the maximum load in a particular half cycle by  $C \sqrt{f'_c}$  where  $C$  was  $hd$  for Specimen 1, and  $f'_c$  was the laboratory concrete strength. The modified stress coefficients have been calculated by dividing the maximum load in a particular half cycle by  $hd \sqrt{f'_{cf}}$  where the  $d$  value is that for the specimen under consideration and  $f'_{cf}$  is the field concrete strength of the infilled wall. The  $d$  values were as follows:

Specimen	$d$ (in.)
1	75.3
3	75.0
4	56.0
5	54.8

The  $d$  for Specimen 4 was that found for the panel alone, and for Specimen 5 it was the sum of the individual  $d$  values for the four interior panels,

First, second and third cycle envelopes of the modified stress coefficients are given in Figure 52 for Specimens 1 and 3 and in

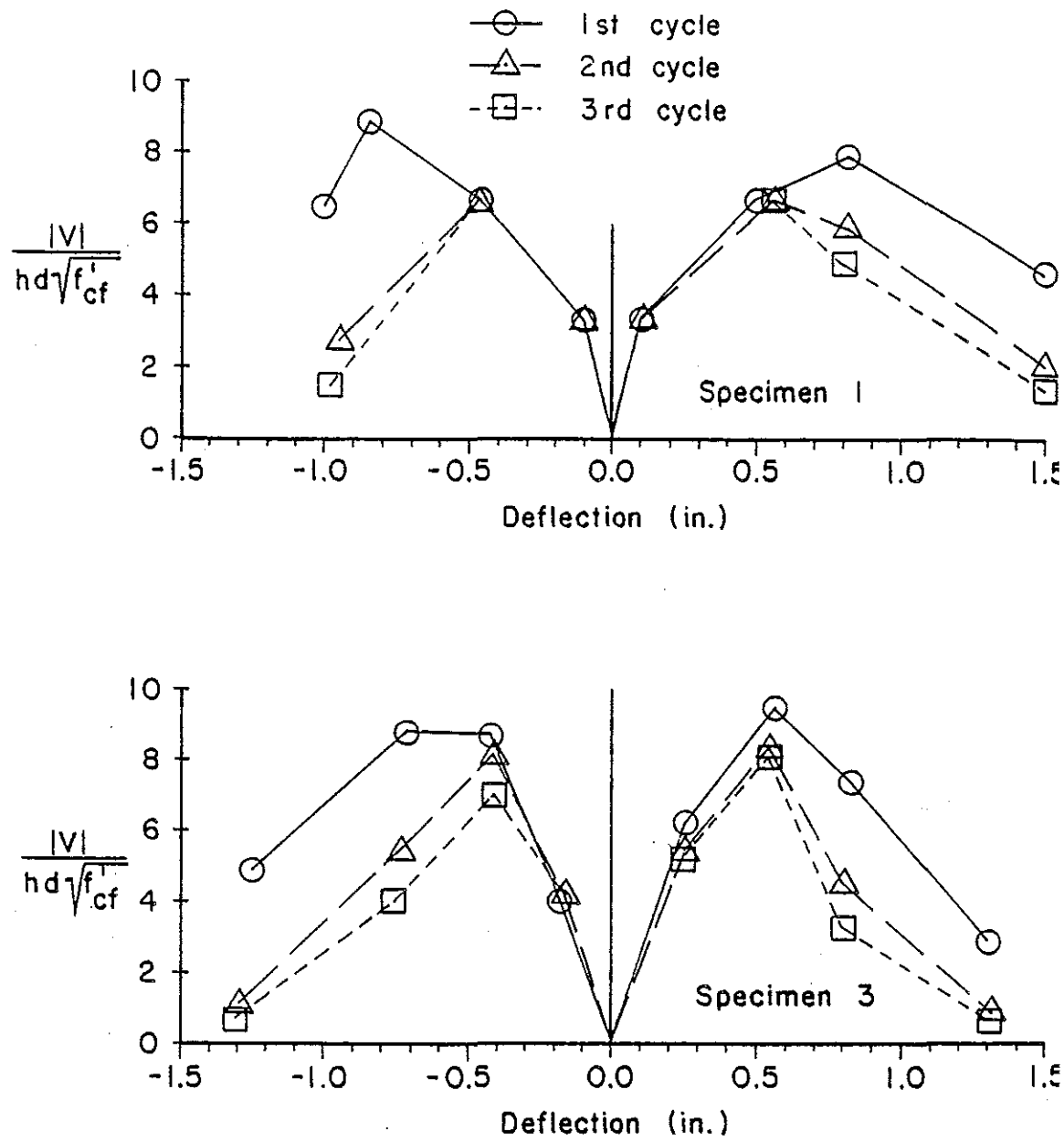


Figure 52. Modified stress coefficient envelopes for Specimens 1 and 3.

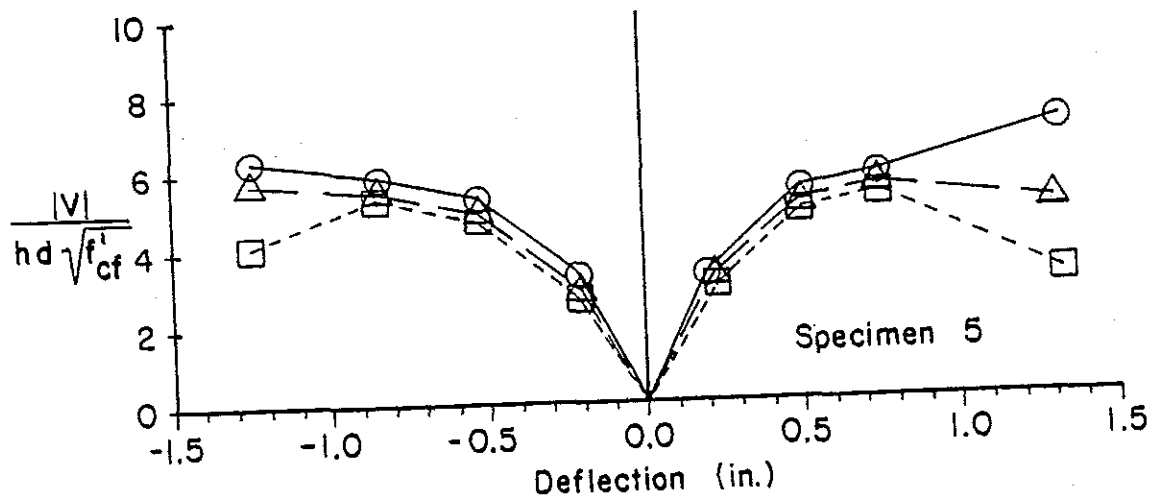
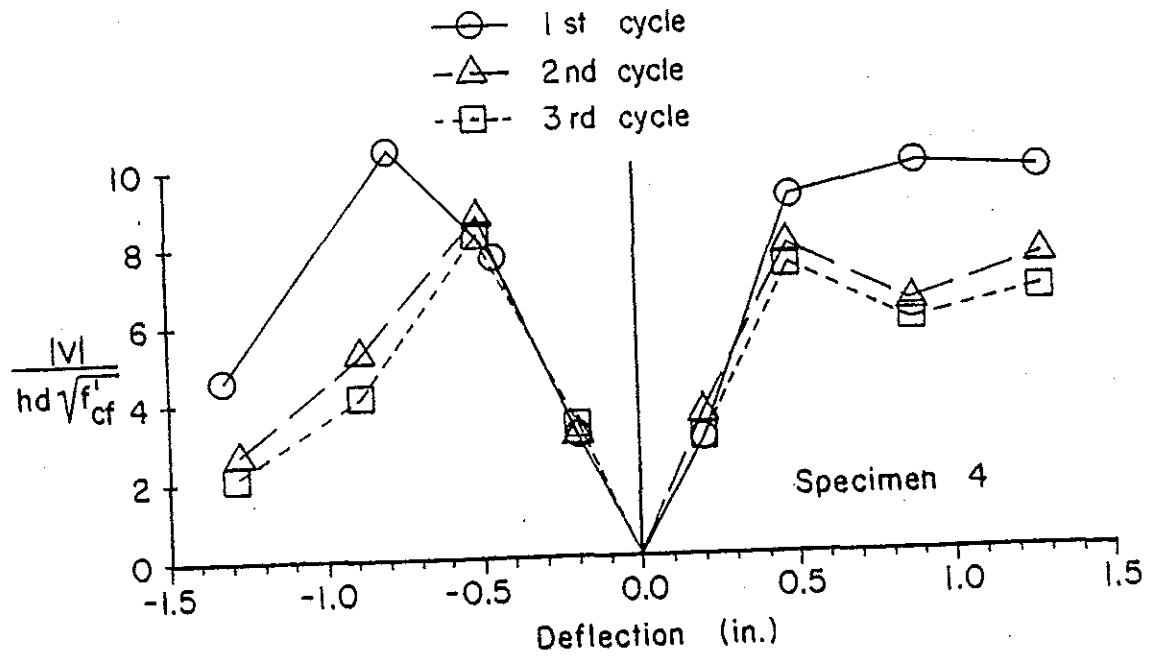


Figure 53. Modified stress coefficient envelopes for Specimens 4 and 5.

Figure 53 for Specimens 4 and 5. The envelopes for Specimens 1 and 3 were changed little from those given previously in Figure 47. The envelopes for Specimens 4 and 5 were quite different; the modified stress coefficients were 61 percent greater for Specimen 4 than the previous coefficients, and they were 87 percent greater for Specimen 5. The increase for Specimen 4 made the envelopes appear similar to those of Specimens 1 and 3.

Though the modification increased the stress coefficients for Specimen 5, the maximum modified stress coefficient remained less than the maximums of the other specimens. At deflections of 0.8 in. and greater, the third cycle modified stress coefficients of Specimen 5 were greater than the third cycle coefficients of the other specimens. This quantitative result emphasizes that the multiple panel wall demonstrated better ductility and cyclic resistance than the other infilled walls.

#### Recommendations

The principal recommendation is that the design should consider not only the ultimate capacity of the infilled structure but also the cyclic capacity beyond the yield deflection. This cyclic capacity is related to the amount of reinforcement;  $v_c$  seemed to be reduced after the occurrence of the ultimate load as evidenced in Figures 52 and 53. Therefore, the author recommends that the design  $v_u$  for cyclic loading be reduced to that calculated without the addition of  $v_c$ . This would reduce the maximum  $v_u$  from  $10 \sqrt{f'_c}$  to  $7 \sqrt{f'_c}$ .

For the multiple panel wall, designed as a series of deep beams, the standards for deep beams in ACI 318-71 seem adequate.

Best estimates of the ultimate capacities of the monolithic and cast-in-place walls were calculated using equations (6) and (8) based on shear stress requirements of ACI 318-71. The ultimate capacity of the specimen made with the single precast panel was estimated best by calculating the shear capacity of the panel alone. And the ultimate capacity of the multiple panel wall was estimated best by summing the shear capacities of the four interior panels which had the same lateral stiffness. For infilled walls built similarly to the specimens, similar methods for calculating ultimate capacities are recommended.

Stiffness calculated using the equivalent diagonal strut method more closely predicted the experimentally observed stiffness than the cantilever bending plus shear method for the structures with the monolithic, cast-in-place and single panel walls. The equivalent diagonal strut method is suggested for calculating  $K_1$  for frames with solid infills.

For the multiple precast panel wall the stiffness was calculated by summing the lateral stiffness of each fixed-end panel and column. When the moment of inertia was that of the transformed steel only, the calculated stiffness approximated the observed stiffness.

CHAPTER V  
EVALUATION AND DISCUSSION

Introduction

In evaluating the response of the test specimens, the behavior of each will be discussed first individually and then a general comparison will be made. The three strengthening construction techniques are compared to the response of the shear wall cast monolithically with the frame.

The discussion of the test results for each specimen concentrates in the following areas: load capacity, ductility, comparison with previous research, response of wall-to-frame connection, possible effects of alternate methods of construction, and the general adequacy of the strengthening technique. Herein the term ductility relates to the structure's ability to maintain the yield load or maximum load at deflections beyond the yield load deflection.

Specimen 1, Monolithic Wall

Reversed cycle loading appeared to decrease the ultimate load capacity and the ductility of the monolithically cast shear wall. Benjamin and Williams (16) conducted monotonic tests on infilled shear walls similar to Specimen 1. Their results showed ultimate capacities about 30 percent greater than for Specimen 1 and a ductility about twice that for Specimen 1.

Others (12, 18, 23 and 52) have also found a reduction in load capacity and ductility of shear walls when the walls were subjected to reversed deflection cycles. The decrease in energy dissipation and stiffness of Specimen 1 with increasing cycles agreed with similar findings by Shiga, Shibata and Takahashi (52). As found by others, the reversed cycle loading appeared to alter significantly the response of the monolithically cast wall compared to response under monotonic loading.

Yet the ultimate failure mode was like that described for monotonic tests (16): cracking and yielding at the base of the wall followed by shear failure of the compression column. Deterioration of load capacity of Specimen 1 rapidly proceeded after this column failure because the crushed concrete spalled from the columns with reversed deflections. In other tests (18), where the crushed concrete had been confined in the column core by closely spaced ties, the load capacity was maintained and did not rapidly deteriorate with further cycles. Current standards in ACI 318-71 for closely spaced ties or spirals assure confinement of broken concrete; thus, ductility in new construction would be better than demonstrated in this test. Nevertheless, shear walls constructed according to pre-1963 standards as was Specimen 1 would probably exhibit the same brittle type behavior.

The column-to-wall connection remained intact throughout the test; the monolithic construction provided an excellent joint. Further, no deterioration occurred at the wall-to-top beam

connection. The rough joint apparently provided satisfactory shear transfer. The failure between the wall and the base beam was not a connection failure. No chiseled beam concrete was evident as the wall spalled away; the failure plane was ground smooth. The roughened beam provided small keys which were sheared. Separation between wall and beam resulted from tension yielding of the vertical reinforcement.

Based on the experimental and calculated results, it appeared that the vertical reinforcement in tension resisted the cyclic shear forces. As concluded by others (12, 16), increasing the amount of reinforcement would increase the cyclic capacity. But increasing the width of the concrete wall would not increase the cyclic capacity.

#### Specimen 2, Frame

The moment frame responded in a ductile manner with its load capacity predicted from flexural considerations.

No ties were included around the core at the beam-to-column connection. Such core confinement was not required in older codes (3, 4) although it is now required (5). The connection did not exhibit significant degradation during the deflection cycles. The edge beams with their reinforcement provided sufficient confinement to prevent connection failure.

Strengthening of frames designed similarly to Specimen 2 probably would be necessary only for the purpose of reducing

displacement and thereby reducing architectural damage. The ductile, inelastic response of the frame seemed adequate to provide safety against collapse.

#### Specimen 3, Cast-in-Place Wall

Failure of the wall-to-top beam connection was the most significant feature of the test on Specimen 3. The maximum capacity of the structure was controlled by the strength of the drypack joint. Upon failure of the connection the lateral load capacity was reduced to half its maximum value. There was little ductility. The deflection at joint failure was about 1-1/2 times the deflection at first yield. Furthermore, failure of the connection led to shear failure of the columns. Such column failures reduced the vertical load capacity.

The joint failed prematurely because of the type of construction. The drypack was not securely bonded to the top beam or to the cast-in-place wall, as evidenced by the cracking under the first load applications and by the rough condition of the bottom of the top beam after the test. It is hypothesized that (1) the top surface of the cast-in-place section was smoother than was thought at the time of construction so that little mechanical bond occurred, and (2) after the dry concrete was packed into the three inch space, sufficient shrinkage occurred so that a gap formed between the drypack and the roughened top beam. Because of this shrinkage gap, the shear load was transferred from the top beam to the wall by bearing at the loaded-end corner and by dowel action

of the epoxied dowel bars. The dowel action initiated longitudinal cracking in the drypack and eventually caused the joint to split. Further, as the dowels bent due to relative displacement of the beam and wall, the drypack near the top of the joint crushed around the bar. This localized crushing resulted in an annulus being created around the dowel which permitted greater relative displacement. The cyclic loads caused the progressive failure of the shear transfer by dowel action and resulted in the splitting and spalling of the drypack. Lack of bond of the drypack to the CIP wall weakened the entire joint by not restraining the splitting drypack.

If the shear could have been transferred by concrete-to-concrete mechanical and chemical bond, the connection would not have deteriorated as rapidly. One construction method which might provide such direct shear transfer is the use of an epoxy mortar rather than a portland cement mortar to fill the construction space between the CIP segment and the top beam. Excellent chemical bond develops between concrete and epoxy, and epoxy mortar demonstrates little shrinkage. A low slump epoxy mortar made to manufacturer recommendations (54, 55, 57) could be placed in a manner similar to that of the drypack. With an epoxy connection the structure probably would respond more like Specimen 1 with shear failure occurring at the base of the wall.

An expansive portland cement mortar would not be as effective as an epoxy mortar because the cement has a poorer chemical bond.

Gunite has been used to construct shear walls within existing frames (34, 59, 60). The same shrinkage gap would result with the

gunite as occurred with the drypack construction. Even if an expansive cement were used in the gunite, settlement of the concrete after placement would create the space between the top beam and the wall. Dowels joining the beam to the gunite wall would be required to carry the seismic forces. As for Specimen 3, progressive failure of the dowel-wall joint would result; and it would initiate shear failure of the columns. The author concludes that shear walls built using a gunite technique would fail in a manner similar to that exhibited by Specimen 3; their load capacity and ductility would be similar.

Strain gage results evidenced lack of continuity between the CIP wall and the columns. Besides the failure at the top beam joint, the connection between the wall and columns was less rigid than the wall-to-frame joint of the monolithically cast wall. In Specimen 3 the columns bent in a flexural mode, and cracks developed between the wall and columns.

Shrinkage of the cast-in-place concrete probably caused the reduced continuity between the wall and columns. The roughened frame and dowels were designed to provide the best joint; yet separation occurred. Shrinkage in the wall might have produced tensile stresses sufficient to break the chemical bond between the columns and wall which would have resulted in an initial separation of the segments. The wall's mechanical interlock with the roughened frame transferred shear stresses; yet the separation allowed some degree of separate frame and wall response. With increasing cycles the mechanical interlock wore, thus reducing the stiffness of the

shear transfer mechanism. Such a wear reduction would account for the trend toward more separate frame and wall response with increasing cycles. The author concludes that while this vertical cold joint was a good connection, it did not provide a connection which forced rigid continuity between frame and wall or which induced pure shear wall behavior like Specimen 1.

An alternate construction which might have assured better continuity would have been the use of an expansive cement concrete rather than the normal mix used. Tensile, shrinkage stresses would have been eliminated which would have improved the chemical bond.

Application of an epoxy coating on the frame surface before casting would not have been satisfactory. The time needed to place the formwork before casting would be longer than the pot life of the epoxy.

Specimen 3 demonstrated a maximum load factor and a ductility similar to that of Specimen 1, even though the specimens failed in different modes. After completion of the deflection sequence the vertical load capacity of Specimen 3 was nil, while Specimen 1 appeared capable of carrying a vertical floor load. Although the cast-in-place wall provided the shear resistance of a "new" structure, it was not satisfactory for a strengthening scheme because the failure mode reduced the vertical load capacity of the original framed structure.

A modified cast-in-place technique could be used for satisfactory strengthening. One scheme would employ an expansive cement concrete for the wall plus an epoxy mortar for the beam-to-wall joint as discussed above. This first method would respond similarly to Specimen 1.

A second scheme would use the first method for constructing the infilled wall plus exterior hoop reinforcement for the columns. Higashi and Kokusho (35) found that steel bands bolted around existing columns increased the columns' shear resistance and ductility. Similar steel bands could be placed along the top one-quarter of the column length and along the bottom one-quarter. These hoops would act as exterior shear reinforcement and would confine the column concrete at the areas where shear failures occurred in Specimens 1 and 3. After the bands had been placed, the infilled wall could be cast. Dowels similar to those used in Specimen 3 would be epoxied between the band locations. The failure mode of a structure strengthened using this second scheme would be more ductile than that demonstrated by Specimen 1 or 3. Models tested by others (18) with confined column concrete have shown better ductility than that of Specimen 1.

#### Specimen 4, Single Precast Panel

The response of Specimen 4 was most influenced by the connection of the single infilled panel to the frame and by the construction gap between the panel and the columns.

The flexibility of the mechanical connectors permitted nearly independent frame and wall behavior. The lack of wall-frame continuity yielded a structure with lateral stiffness at the first yield level equal to about half the yield stiffness of Specimen 1 and with a maximum lateral capacity equal to about three-fourths that of the monolithic structure.

In Specimen 4 the maximum positive and negative loads were about the same, although the failure modes were different in the two directions. The pullout of the positive-end base anchor bolts and weld rupture at the top positive corner resulted in the shear failure of the top beam. That failure occurred at the maximum negative load. Repeated cycles in the negative direction achieved loads less than half the maximum value.

The maximum positive load was achieved and was maintained over a deflection range of 0.5 in. to 1.8 in. In the positive direction, failure resulted by crushing in the wall and not by a failure of the connection.

That the maximum loads in both directions were nearly the same implied that even if the anchors and welds had not failed in the negative direction the maximum negative load would not have been significantly greater. Yet, the connection failure did reduce greatly the ductility in the negative direction compared with that in the positive direction.

Negative direction ductility was similar to that exhibited by Specimen 1: rapid decrease in load capacity upon attainment of the

maximum load which occurred at a deflection about 1-1/2 times greater than the yield level. Positive direction ductility was much greater than that of Specimens 1 and 3 but not as great as that of Specimen 2. Maximum load was maintained to a deflection of 3.6 times the yield deflection.

Prevention of weld and anchor bolt pullout would have increased the ductility of the specimen. The weld was weak because it was in a corner location which made placement of a good weld difficult. An improved connection design would locate the weld farther from the corner to permit welding in a more convenient position, thus assuring a stronger weld. Anchor bolt pullout resulted because of the prying action of the wall on the line of bolts and because of the repeated, cyclic loads which caused a progressive pullout. The prying action was a function of the use of a single panel and cannot be altered by different bolt placement. The forces could be reduced if the bolts yielded in tension before any pullout occurred. By yielding the bolts could distribute the tension load before the pullout of any one anchor. Smaller diameter bolts made of a low yield stress steel would assure bolt yielding. The bolts were originally designed for a shear resistance about twice that observed; therefore, bolt size could be reduced according to the design technique originally presented (Appendix B). The pullout of the anchors might be prevented by epoxy grouting the bolts into the drilled holes. First the grout would bond the bolt in the hole as it secured the

dowels of Specimen 3; no dowels pulled out. Second, the epoxy would fill the annulus around the bolt. The progressive, "walking" type of pullout resulted because the bolt rotated in the hole causing higher pullout stresses first on one side of the hole, and then with a reversed cycle on the other side. By eliminating the rotation the pullout stresses would be more evenly distributed around the circumference. With the bolt anchorage and welding improved, connection failure like that observed would be prevented.

Further, with the anchor bolts grouted, the lateral stiffness of the structure would be increased. Slip between the frame and wall would be reduced; bearing of the bolts in the connector holes would occur at smaller lateral deflections.

If the anchor bolts were to be epoxy grouted into the existing frame, use of mechanical wedge anchors would be superfluous. The epoxy could provide adequate pullout resistance. Connection cost would be reduced, as an example, by use of a threaded steel rod rather than wedge anchors. The threads on the embedded portion of the rod would provide a good interlock with the epoxy grout.

Failure in the positive direction resulted from crushing in the wall at the location beneath the top panel-to-frame connector. The failure appeared to be initiated by bending of the embedded panel plate. Inspection of the failure zone after the test showed that the embedded plate was bent laterally with the top beam displaced relative to the wall and base. The bending may have been caused by the 3/8 in. eccentricity in load resulting because of the lap

weld of the ear plates to panel plate and because the vertical reinforcing bars were welded to one side of the panel plate.

Because such a minor eccentricity possibly initiated the wall failure, larger eccentricities may cause wall failure at reduced lateral loads. Simpler connection details involving structural steel angles as described by others (35) would have larger eccentricities which would cause out-of-plane bending in the connector and wall. The author believes that such out-of-plane designs should be avoided. The ear plate connector used in this study was designed to transfer the shear stresses from the frame to the wall in a line as close to the center plane of the structure as possible. Eccentricity was minimized. A similar goal is recommended for the design of precast panel connectors.

The construction gap between the panel and the frame was highlighted above as a major influence on the behavior of Specimen 4. Once the gap was closed between the panel and the column, the panel began bearing on the column. The bearing caused the column to fail in shear.

The failure of the columns once the panel came into bearing illustrated the design objective discussed in Chapter 2 and Appendix B. This objective was to disconnect the panel and columns. If there would have been a connection between the columns and the panel, the author estimates that the columns would have failed in shear at a deflection of less than  $3/4$  in. rather than at a deflection of more than 2 in. as occurred in Specimen 4. The construction gap permitted greater

ductility than would have occurred without the gap. Slip between the panel and frame permitted the gap to be closed. The slip resulted from the rotation of the anchor bolts in the drilled holes and from the sliding of the connector plate until the holes bore against the anchor bolts. Only after the anchors had been sufficiently extracted was the bolt rotation large enough to permit the panel to bear on the column.

The 3/8-in. gaps used in Specimen 4 were larger than the 1/4 in. slip permitted by the holes in the connector plates but were not sufficiently large enough to account for bolt rotation. By epoxy grouting the anchor bolts, the rotation would be reduced and the gap would not have been closed.

In future designs of precast panel walls, the gap should be sized so that they are larger than calculated slip plus anchor bolt displacement. The panel should not be positively connected to the columns. If the spaces between the panel and surrounding frame must be filled for architectural reasons, the author suggests that a weak, crushable material like foam concrete be used.

Altogether, the use of the single precast panel seemed to be a satisfactory method of strengthening an existing frame. Although the panel did not provide as great a lateral resistance as a "new" shear wall, it demonstrated greater ductility than Specimen 1. In seismically loaded structures good ductile capacity has been shown to be beneficial. The panel-to-beam connection could be modified to improve the anchoring of the bolts and to assure good

welds. The separation of the panel and columns provided the improved ductility and eliminated the occurrence of column shear failure.

#### Specimen 5, Multiple Precast Panel

The maximum load capacity of Specimen 5 was less than half that of Specimen 1. The outstanding characteristics of the multiple panel structure were its ductility and its cyclic load capacity.

That the maximum load was about half that of a solid wall agreed with the experimental results of Muto, Ohmori, and Takahashi (41) who tested slitted, cast-in-place walls. The failure mode of the multiple panel wall was like that of the slitted wall, both types behaved as a series of fixed-end beams which failed by shear at the fixed-end locations. The slitted walls demonstrated better ductility and lower elastic stiffness than solid walls; and, for these reasons, Muto, et.al., recommended their use for aseismic construction.

Specimen 5 achieved its maximum load at a deflection about 3.2 times the deflection at first yield. The load resisted by Specimen 5 increased with deflections beyond the yield deflection, and the maximum load in succeeding cycles degraded little. The ductility exhibited by these findings showed that the multiple panel wall was more ductile than the monolithically cast model. That the cumulative energy dissipated by Specimen 5 equaled only about half that dissipated by Specimen 1 resulted because Specimen 5 carried less than half the load at most deflection levels.

The interior panels failed in shear at the fixed-end locations near the panel-to-panel connections. The concrete spalled as it cracked and slid with the cyclic motion. The spalling reduced the potential ductility of the panels.

The shear strength of the individual panels could have been increased by closer spacing of horizontal reinforcing bars. The same percentage of horizontal reinforcement may have been used, but close spacing of smaller diameter bars would have better distributed the cracks. Distribution would have decreased the sliding motion of the large chunks of cracked concrete, forced more aggregate interlock, and resulted in higher shear strength. As discussed in Chapter III, closer horizontal bar spacing was required by ACI 318-71, Section 11.9 for deep beams; but the required spacing was not used in the design so that the reinforcement layout resembled that of Specimen 1.

Increasing the percentage of horizontal reinforcement would increase the shear strength of the panels. Flexural strength and lateral stiffness of the panels could be increased by increasing the area of the vertical reinforcement.

The ductility of the panels could be improved by confining the concrete in the locations near the panel-to-panel connectors. Actual closed stirrups like those used in beams could be used to replace the single layer of horizontal bars. Small diameter vertical bars could be located on each side of the panel to form a grid, and transverse hooks could join vertical bars on opposite sides of the panel. The resulting three dimensional reinforcing

cage would basket broken concrete so that the concrete could transfer load even after rupture. This maintenance of load would enhance the already good ductility of the multiple panel wall.

Forming such three dimensional cages would not be unusually difficult or uneconomical because the panels would be constructed in a precast concrete factory. Industrialized techniques could be incorporated.

The panel-to-frame connection was satisfactory. The connector's design and construction was identical to that used for Specimen 4. The superior behavior of the connector for Specimen 5 resulted because the multiple panel wall did not subject the anchor bolts to as great a prying force as did the single panel and because the load resistance of Specimen 5 was less so the connection was subjected to less total shear force.

Nevertheless, the slip of the connector was sufficient to allow the panels to bear against the columns. This bearing caused shear failure of the columns of Specimen 5. As discussed above for Specimen 4, the slip could be reduced by epoxy grouting the anchor bolts; the reduction of slip and enlargement of the construction gap would prevent column failure. For a full size structure the author estimates that the gap should be about one inch wide.

Shear failure of the columns of Specimen 5 destroyed the structure vertical load capability. But because this failure was only a function of gap width, minor modification in the design

of the system would eliminate future possibility of shear failure.

Altogether, the multiple panel infilled wall provided a good method for aseismic strengthening. Construction was simple and clean, the maximum lateral strength of wall-frame system was over seven times that of the plane frame, the calculated stiffness was over thirty times that of the frame and the ductility was superior to that of the monolithic shear wall.

#### Shear Slip Response

The load-deformation response of all four infilled specimens was of the shear-slip, deflection hardening type. After each structure deflected beyond its yield deflection level, the lateral stiffness at lower deflection levels was greatly reduced. Such stiffness degradation has structural advantages and disadvantages for the seismic behavior of a building.

The principal advantage is that the reduced stiffness causes the natural period of the building to increase; this increase likely would decrease the seismic accelerations of the structure compared to its originally stiff response. The reduction in stiffness may aid in the prevention of structural collapse due to large overturning moments provided the vertical load capacity remains intact.

The principal disadvantage is that the reduced stiffness may permit large deflections which would result in greater architectural

damage. The inelastic shear-slip and load degrading type response dissipates little energy compared to an inelastic flexural type response; therefore, increasingly larger deflections may be required to dissipate the seismic energy.

The prime objective of aseismic strengthening is the reduction of deflection. At loads below their yield loads all infilling techniques demonstrated that they would stiffen a frame and thereby reduce deflections. Even as the stiffness of the walls degraded at deflections beyond their yield deflections, the lateral stiffnesses did not become less than that of the plain frame. It therefore appears that even as the load-deflection responses degenerated to the shear slip type the infilled walls stiffened the frame and in practice would reduce building deflections even after yielding of the wall systems.

Further analytical research using the hysteresis model proposed in Chapter IV will define better the expected reduction in deflections for various frames strengthened with infilled walls.

#### Comparison

Of the construction methods examined in this study, the multiple precast panel infilled wall showed the most promise for aseismic strengthening. It provided a ductile strengthening system with an energy dissipation capacity equal to that of the other construction techniques tested. For strengthening of a framed structure, a multiple panel system appears easier to erect

within an existing structure than the other techniques. Because of the relatively clean construction process, the on-going operations in a building would be little disturbed using the precast system.

A drawback of the multiple panel system is that its maximum lateral load capacity is only about half that of a solid, cast-in-place wall using the same percentage reinforcement. A different design than that used for Specimen 5 could incorporate more reinforcement to increase the strength of the system is desired.

But for the strengthening of a building, the restoration system must be carefully controlled. A too strong wall might cause structure failures not examined in this study, failures such as separation of foundation and superstructure due to increased overturning moments. Therefore, the strongest, most rigid construction is not necessarily the best or most appropriate strengthening system for a particular structure.

Maintenance of vertical load capacity is essential. If the precast walls are made with sufficiently wide construction gaps between the panel and columns, shear failure of the column is prevented and the frame's vertical load capacity is not affected. The failure mode of the cast-in-place wall destroyed the vertical capacity; therefore, the cast-in-place technique should not be used unless construction modifications are made as discussed above.

One of the most important properties of an earthquake resistant structure is good ductility, the ability of a structure to maintain

increasing loads over reversed cycle deflections which are several times greater than the yield deflection. Infilling systems using both the single and multiple panel precast walls showed significantly better ductility than the monolithically cast shear wall and the cast-in-place infilled wall. The multiple panel wall demonstrated the less load degradation over cycles than the single panel structure; therefore, the multiple panel system exhibited the best ductility.

Besides being applicable to the strengthening of reinforced concrete frames, the multiple panel system and the single precast panel technique could be used to strengthen steel framed structures. Instead of using anchor bolts to attach the panel-to-frame connector to the beams, the connector could be welded directly to the steel members. Such precast shear walls could be used for new construction as well as for strengthening existing buildings.

## CHAPTER VI

### SUMMARY AND CONCLUSIONS

Aseismic strengthening of an existing structure will be unique. The strengthening scheme will depend on the condition of the superstructure, the foundation and the building architecture. The research presented in this thesis provides an indication of techniques useful for strengthening one type of superstructure.

Some emergency care facilities such as hospitals demand improved seismic resistance so that they may function satisfactorily after a severe earthquake. Reduction of structural deflections is one method of improvement which limits damage to architectural and mechanical systems plus items such as medical equipment and supplies.

A technique for reducing deflections is to infill selected frames of a structure with shear walls which increase the structure's lateral load capacity and stiffness. This thesis experimentally investigated three construction techniques for infilling existing reinforced concrete frames with reinforced concrete shear walls. The increases in load capacity and stiffness were compared with analytical predictions, and the adequacy of such strengthening techniques was concluded.

The one-half scale models used for the experimental investigation represented one story and one bay of a low-rise reinforced concrete framed building designed and built in the 1950's or early

1960's. One test specimen was a reference frame which was constructed without an infilled wall. Four specimens were built with infilled walls constructed using different techniques: one wall was cast monolithically with the surrounding frame to provide a reference shear wall similar to "new" construction; a second wall was cast within an existing frame, and it resembled past restoration of actual structures (34, 59, 60); a third wall was a single precast panel which was fitted within an existing frame and anchor bolted to the top and bottom beams; and the fourth used six independent, precast panels which were anchor bolted to the top and bottom beams and then were joined together. The frames of all specimens were identical; the amount of vertical steel reinforcement equaled 0.46 percent in all walls, and the horizontal reinforcement was approximately the same.

The five models were tested statically under reversed cycle deflections of increasing magnitude. Loads were applied to the slab of the top beam while the base was fixed. Deflection, load and strain data were recorded.

The frame responded in a ductile manner with the average of maximum and negative loads equal to 8.8 kips. The yield and ultimate loads were accurately predicted using standard methods although the actual stiffness was less than calculated because of cyclic deterioration.

The monolithically cast structure showed the greatest maximum lateral load of all specimens (150 kips) because of its higher

concrete strength and because the monolithic connection between wall and frame provided better continuity than that in the other filled structures. The brittle failure mode was like that observed in previous monotonic tests of infilled shear walls; vertical steel yielded in tension which permitted separation of the wall from the base, the column under compression then split diagonally in shear. Failure occurred at a deflection 1-1/2 times the yield deflection. After failure the load capacity decreased to less than half its maximum value, and cycles to increased deflections evidenced further load and stiffness degradation.

With the effect of different concrete strengths discounted, the observed maximum load capacity of the cast-in-place wall was the same as that of the monolithically cast specimen. The failure mode was the deterioration of the joint between the cast-in-place wall and the top beam. Crushing and slipping at the joint resulted in shear failure at the top of the columns and complete loss of the structure's vertical load carrying capacity. This brittle failure occurred at a deflection about 1-1/2 times the yield deflection. As for the monolithic specimen, the load, stiffness and energy dissipation capacities degraded to less than half the maximum values with increasing cycles and deflection levels.

For the monolithic and cast-in-place models, the observed ultimate loads respectively were 52 percent and 30 percent greater than values calculated using the shear stress requirements of ACI 318-71. Yet the calculated values were significantly greater than the maximum loads observed in cycles following the cycle in which

the ultimate load occurred. For both structures the lateral stiffness calculated using an equivalent diagonal strut technique equaled approximately the observed unloading stiffness.

The specimen made with the single precast panel responded with a combined flexure and shear wall behavior. The ultimate load capacity was three-fourths that of the monolithic structure, while its ductility was double. With deflections in one direction the structure maintained its maximum load to over 3-1/2 times its yield deflection; although the load capacity degraded with cycles to constant deflection levels. In the other direction the panel-to-frame connection failed and caused a rapid loss in load capacity and ductility. The connection failure was weld fracture and anchor bolt pullout; recommended modifications have been suggested to assure satisfactory panel-to-frame connection. The maximum load was approximately predicted by calculating the shear capacity of the panel alone.

The multiple precast panels of the fifth specimen responded as a series of deep beams fixed at their panel-to-panel connections. The ultimate capacity of the wall equaled about half that of the monolithic structure. At deflections over three times that causing yielding in the panels, the four interior panels failed in shear. As the shear deflection increased, the exterior panels bore against the columns and caused their shear failure. The multiple panel wall carried increasing lateral loads beyond the yield deflection level, and prior to the ultimate shear failure the maximum loads degraded little with repeated cycles. The sum of the calculated

shear capacities of the four, stiffer interior panels approximately equaled the observed ultimate capacity.

The energy dissipation capacities of the two precast and one cast-in-place models were similar, yet they were half the capacity of the monolithically cast specimen. The latter dissipated twice the energy because of the greater tension yielding deformations in the column reinforcement; the combined flexural and shear wall response of the other specimens limited the tension yielding.

Comparison of the test results showed that only the cast-in-place wall developed the equivalent load capacity of the monolithically cast structure; yet both specimens constructed with precast infilled walls demonstrated over twice the ductility of the monolithically cast or cast-in-place specimen. In all cases except the multiple panel structure, the maximum load degraded significantly with repeated deflections to magnitudes as great or greater than the yield deflection level. The multiple precast panel infill showed little cyclic degradation until the panels failed in shear at a relative deflection of 0.02 radians.

These test results indicated the general adequacy for aseismic strengthening by the three infilling techniques. The cast-in-place wall as constructed was considered unsatisfactory, even though it increased the lateral resistance of the structure to equal that of a monolithic shear wall. The failure mode of the wall-to-frame joint caused loss of the vertical load capacity of the structure which could prove disastrous in an actual building. With

modifications, such as non-shrinking grout for the wall-to-frame joint and exterior shear reinforcement of the columns, a cast-in-place technique might be adequate. As constructed both precast infilling techniques were satisfactory. The panel-to-frame connection would be improved by epoxy grouting the anchor bolts in the frame; this modification would increase the already good ductility of the single panel and multiple panel systems.

An important consideration in both precast panel infilling techniques has been shown to be the gap between the panel and the column. With a sufficiently large gap, bearing of the panel on the column is avoided and shear failure assures that the vertical load capacity of the original structure is maintained.

The author concludes that the multiple precast panel infilling technique shows the greatest promise for successful aseismic rehabilitation. The technique provides greater ductility and cyclic load capacity than the other infilled shear wall systems, while it increases the lateral load capacity and stiffness of the frame. Because the wall may be precast in narrow units, erection of the wall within an existing building appears as though it would be easier and cleaner than construction of other types of infilled walls. Further, the multiple panel system appears applicable for strengthening both reinforced concrete and steel framed buildings.

## CHAPTER VII

### RECOMMENDATIONS

Some findings of this experimental program may be used in the design of reinforced concrete shear walls for new construction and for strengthening existing buildings. The following design guidelines are suggested.

1. The ultimate capacities of monolithic, cast-in-place and single precast panel walls should be calculated using the provisions of Section 11.16 of ACI 318-71. The quantity "d" should be calculated based on an ultimate concrete strain analysis.

2. The best estimate of the shear capacity of a structure with a single precast panel is the capacity of the panel alone.

3. The ultimate capacity of a multiple precast panel wall is equal to the sum of the shear strengths of those panels with greatest lateral stiffness.

4. For anchoring precast panel connectors to existing frames, mild steel bolts or threaded rods should be epoxy grouted into drilled holes. Standard wedge anchors used without grouting are not recommended.

5. The design of precast panel-to-frame connectors should minimize the eccentricity of shear transfer from the beam-to-panel.

6. Precast panel walls should be connected only to top and bottom beams; connection to columns should be avoided. The panel should be spaced a distance from the column greater than the maximum possible relative deflection between the panel and frame.

7. Single panel units of a multiple panel wall should be designed and detailed as fixed-end deep beams. Concrete should be confined. Horizontal reinforcement should be in the form of closely spaced stirrups. Recommendations for spacing of stirrups in beams given in Appendix A of ACI 318-71 should be followed.

8. In constructing a cast-in-place infilled wall special care should be taken in connecting the wall to the frame. Dowels should be epoxied into drill holes all around the frame and the frame roughened as was done for Specimen 3. An expansive cement concrete is recommended for casting the wall. The joint between the cast-in-place section and the top beam should be constructed using an epoxy mortar or other highly adhesive and non-shrink grout. It is recommended that steel bands be secured around the bottom and top portions of the columns of the frame before a cast-in-place wall is constructed. These bands should be designed to confine the column concrete.

9. A cast-in-place wall also may be constructed with a gap between the wall and the column in order to prevent column shear failure. Dowels should be epoxied into the top and bottom beams only. A minimum 1 in. strip of styrofoam or other crushable material could be included between the columns and cast-in-place wall to form the separation gap. The wall-to-top beam should be constructed as recommended above in 8.

10. The anticipated cyclic load capacities should be used in designing shear wall systems.

The design and construction of strengthening systems could be improved by further research in the area of aseismic strengthening. Because of the promise shown by the precast panel techniques studied in this thesis, those construction methods should be investigated. Important variables would include the amount and spacing of vertical and horizontal reinforcement plus different panel-to-frame connection systems. The strengthening of steel as well as reinforced concrete frames should be included.

Experiments with smaller scale models and analytical research is needed to determine the effects of strengthening on multistory structures.

## APPENDIX A

### REVIEW OF RELATED RESEARCH

Considerable amount of both theoretical and experimental research has been conducted on reinforced concrete frame, shear wall and infilled shear wall structure. Only that work most directly related to the current study is reviewed. Very limited research has been directed at strengthening of structures for earthquake resistance nor has much information been published on the repair and rehabilitation of earthquake damaged structures. The available information is reviewed. The many studies referenced concerning precast concrete construction and joining of precast structures has not been reviewed because they were volumous and too general in content. Information gained from the precast concrete publications was used in a broad sense to design the specimens tested.

#### Experimental Studies on Reinforced Concrete Infilled Frames

Benjamin and Williams (16) tested over 45 single-story, single-bay reinforced concrete shear walls with surrounding frames. The frames and walls were cast monolithically. The model scale varied from 1/8 to 3/8 full size. Parameter studies included the geometry of the wall panel, amount and direction of reinforcement in the wall, and the amount of reinforcement in the columns. All structures were loaded monotonically. Some differences in behavior were noted between models of different scale, but the difference in load-deflection behavior was slight. The aspect ratio of wall length to wall height ( $l_w/h_w$ ) was varied from about one to three. Walls with

greater aspect ratios had greater ultimate and first-crack loads, but the average base shear stress at ultimate load was nearly constant for the panels. Load-deflection behavior was quite different for the various walls. Different amounts of vertical and horizontal reinforcement were used as well as different schemes of orthogonal and diagonal reinforcing. The standard vertical-horizontal reinforcing pattern was found superior for the same amount of steel. Panels reinforced with vertical steel only were as strong as those with vertical plus horizontal reinforcement. Reinforced walls were much more ductile than unreinforced walls, and reinforcing increased the ultimate lateral load of walls with aspect ratios greater than one. Increasing the amount of column steel markedly increased the lateral load capacity; yet, increasing the column cross-section did not have significant effect on the strength.

A further study by Benjamin and Williams (17) on shear walls connected to end walls and roof and floor diaphragms showed that if the end walls were not cast integrally with the shear wall, the end walls did not act as flanges to form a unitary structure.

A recent study on one-story, one-bay reinforced concrete infilled structure was reported on by Barda (12) and by Barda, Hanson and Corley (13). Eight shear walls were cast monolithically with end walls, top diaphragm (roof) and foundation slab. Overall length of the 1/3 scale models was 75 in., roof and foundation width was 60 in., walls were 4 in. thick and end walls were 24 in. wide. The height of the specimens was varied so that the aspect ratio ranged from one to four. Nominal compressive strength of the

concrete was 3000 psi; steel reinforcement was grade 60 deformed bars. Test results showed that the shear strength was not affected by differences in the amount of end-wall reinforcement. Load reversals caused a 10 percent reduction in the ultimate shear strength. For walls with aspect ratios of 2 or more, vertical wall reinforcement was more effective than horizontal reinforcement. Horizontal reinforcement was most effective in the wall with  $l_w/h_w$  of one. One specimen after being severely damaged due to cyclic loading was repaired with cast-in-place concrete. Retesting showed that the strength of the repaired wall was about 23% less than the structure when new. Barda (12) compared the experimental behavior with that predicted using Cervenka's (24) inelastic finite element analysis, and he found that the analysis predicted a much stiffer and stronger behavior than actually observed. A principal conclusion was that in all cases, the equations given in the ACI Building Code Requirements (ACI 318-71), Reference 5, conservatively predicted the strength of the shear wall structures.

Shiga, Shibata and Takahashi (51) conducted reversed cycle, lateral load tests on eight single story model reinforced concrete shear walls which were cast monolithically with surrounding frames. The wall height was 23.6 in., length was 34.6 in., and thickness was 2 in. The large base slab was 19.5 in. thick, the beam measured 8 in. deep and 6 in. wide; the columns were 4.7 in. x 6 in. Walls were reinforced with 1/2-in. deformed bars with a yield stress of 57 ksi. Five specimens used 0.25 percent vertical and horizontal steel while three used 0.50 percent. The concrete mix consisted of

a maximum 3/8-in. aggregate with water-cement ratio of 0.64.

The specimens were tested under reversed-cycle, lateral loads; the load was applied directly at the beam-column joint. Vertical loads up to 20 tons were applied to each column. The cracking load was slightly higher for walls with 0.5 percent reinforcement; cracking occurred at an angle deflection of 0.0004 radians. Ultimate strength of the walls occurred at deflection of 0.004 radians.

Effective stiffness (slope of line through hysteresis peaks) and equivalent viscous damping (ratio of area within hysteresis loop to potential energy) capacity decreased with increased number of cycles. Damping was reduced to three percent. In all cases the lateral stiffness of the structures deteriorated to about one-fourth the value of the virgin stiffness after a few cycles. Stiffness degraded only slightly beyond the fifth load cycle. Load-curvature hysteresis curves were of the strain-hardening type with very low stiffness near the zero deflection region.

Capacity of many structure quickly deteriorated after the ultimate load was reached. Vertical load slightly increased the stiffness of the system. Both a fifth-order polynomial and a piecewise linear mathematical models were developed.

Some test have been performed on steel frames with infilled reinforced concrete walls (41, 61). Tamura, et. al., (61) tested a 1/3 scale model of a single-story, single-bay steel frame with a precast reinforced concrete infill panel. The panel was attached to the frame by four corner plates; the gap between the panel and the

frame was grouted with mortar. The panel was tested under a static and a forced, steady state dynamic load. The structure showed three levels of dynamic response: (1) a stiff, elastic behavior under low loads, (2) a strain hardening behavior under moderate loads as the mortar grout failed, and (3) the flexible response of the frame as the panel-frame connection deteriorated.

Muto, Ohmori, and Takahashi (41) conducted cyclic load tests on vertically slitted walls infilled into steel frames. The walls measured 85-in. long, 52-in. high and 2-in. thick. In the slitted wall reinforcement was not continuous through the slits, and the slit length was about 40 percent of the wall height. Seven slits were spaced equally along the length of the wall, and asbestos sheets were inserted in the slits. The walls were cast-in-place and connected to the top and bottom beam with 1/2-in. diameter studs spaced at 6 in. centers. Comparison with a test of a conventional, non-slitted infilled wall showed that the conventional wall demonstrated an ultimate lateral load nearly twice that of the slitted wall; the former failed in a typical mode. The slitted wall showed extensive, well distributed cracking at failure; the slitted portions appeared as fixed-end deep beams which failed at their ends in a flexural mode. Load-curvature hysteresis curves of the slitted walls were of the strain hardening type with very low stiffness near the zero deflection region. The authors stated that slitted shear walls expand vertically under lateral deformations, producing compressive forces which reduce the need for tensile reinforcement.

Further reversed cycle tests on slitted infilled walls were conducted by Delisle and Heidebrecht (31). Vertical loads producing a normal stress of about 350 psi reduced stiffness deterioration and increased energy dissipation of slitted wall specimens compared to similar models tested without such vertical loads. Lateral load tests on walls with and without slits showed that after cracking the stiffness of the slitted wall deteriorated more rapidly than that of a solid wall and that the slitted wall dissipated less energy than the solid wall. It was concluded that slitted shear walls do not show any benefits over ordinary shear walls.

Dawson and Ward (30) tested one-fifth scale, one-bay by one-bay, four story steel frames which were constructed with and without mortar infilled walls. The study concentrated on the lack-of-fit between the wall and frame; an analytical model was developed. Under static loading, an equivalent diagonal strut system was determined by placing shims between the wall and underside of the beam. The lack-of-fit produced a hardening type stiffness behavior.

Bertero, Popov and Wang (18) tested two, one-third scale models which were planar, one bay, three story high reinforced concrete frames with monolithic reinforced concrete infilled walls. The models represented the bases of a 20 and a 10 story building. The first model was tested under monotonic lateral load with superimposed vertical load; the yield shear stress  $V_y$  equaled  $9.5\sqrt{f'_c}$ , and the ultimate shear stress  $V_u$  equaled  $11.3\sqrt{f'_c}$ . These values were ten percent greater than calculated. The second model was subjected to reversed cyclic deflections of increasing magnitude. The cyclic

loading caused large degradation in initial stiffness and about a 35 percent reduction in displacement ductility. The ultimate capacity was not affected by the load reversals. In both models failure was initiated by crushing in the lower corner of a wall and then was followed by crushing of the spirally reinforced column.

#### Experimental Studies on Reinforced Concrete Shear Walls

Several studies have been conducted on monotonically loaded shear walls and deep beams which have provided the basis for the provisions in the Building Code Requirements for Reinforced Concrete (5). Some recent investigations (1, 22, 23) have given information of the cycle response of shear walls.

In tests by Alexander, Heidebrecht and Tso (2), lateral cyclic loads were applied to one-half scale, one-story reinforced concrete shear walls. Main parameters were vertical load, steel arrangement, and wall aspect ratio. The walls had heights of 54 in., thickness of 4 in. and lengths of 9 ft., 6ft., and 3ft. ( $l_w/h_w = 2.0, 1.3,$  and 0.67). The panel was loaded through a top flange beam to produce a uniform shear. Principal steel reinforcement was 1/8 in. bars at 4-1/2 in. spacing in each direction, 0.3 percent reinforcement.

Added steel at the panel edges improved ductility. Vertical load increased the ultimate horizontal capacity and caused more uniform crack distribution; improved crack distribution decreased the stiffness degradation. Panels with shorter length had greater ductility. Repetition of deflection cycles at less than peak

deflection indicated stabilization of lateral load-displacement hysteresis curves and, thus, of energy dissipation.

Cardenas and others (22, 23) reported experiments on 13 half-scale reinforced concrete shear walls. All wall cross-sections were 3 in. thick and 75 in. long. Heights ranged from 6 ft to 21 ft. Grade 60 reinforcing steel and 6000psi concrete were used. High rise walls were studied in six tests. Principal findings were that the strength of high rise walls was governed by flexure, design provisions in ACI 318-71 (5) were adequate and afforded a conservative design, and the amount and distribution of vertical reinforcement influenced load-deformation and energy absorption characteristics. Walls having vertical reinforcement lumped near each edge had higher moment and curvature capacity than walls with uniform steel distribution, and the former showed greater energy absorption. Axial compression increased the moment capacity but decreased the curvature at ultimate load. Tests on low rise walls showed that the minimum requirement for horizontal and vertical steel reinforcement developed the full load potential of the wall; but increasing amounts of reinforcement increased the ductility. One low rise wall was subjected to reversed loading cycles; the ultimate lateral load was reduced to that predicted using equations in ACI 318-71 (5), whereas monotonically loaded walls demonstrated significantly greater ultimate capacities.

#### Analytical Studies of Infilled and Shear Wall Structures

Many analytical studies have been performed on infilled frame and shear wall structures. The report by Cervenka (24) is most

closely related to the proposed research. Carvenka developed a finite element analysis for reinforced concrete shear walls which accounts for the true concrete and steel material behavior. The analysis compared well with the results of experiments performed on models loaded monotonically.

#### Repair and Strengthening for Earthquake Resistance

The most recent publications (34, 59, 60) concerning the repair and rehabilitation of structures have dealt with structures damaged by the San Fernando Earthquake of 1971. Much damage occurred to masonry bearing wall and the framed structures with masonry infill. Fratt (34) reported that repair and strengthening of masonry walls was accomplished by removing the outer wythe of brick and replacing it with 4 in. of reinforced gunite. Reinforced concrete shear walls were also reinforced with a gunite skin. Dowels were epoxied into the existing wall and top and bottom floor slabs. The joints were roughened to a depth of 1/4-in.

Strand (60) reported on the repair of Kaiser Hospital in Panorama City. Existing reinforced concrete shear walls were strengthened with reinforced gunite. Reinforcing bars epoxied into drilled holes were used as shear connections between the surrounding frame, the existing wall, and the gunite wall. Sandblasting existing walls seemed the best preparation before gunite. Some shear walls were strengthened with reinforced gunite. Pullout tests were made to determine the depth of embedment required for reinforcing bars when epoxied into the existing concrete walls; these tests are described in Appendix E.

The Holy Cross Hospital was strengthened by infilling frames. Spracklen (59) reported that to reduce lateral deformations, some windows in the Service Building were replaced with an 8-in. thick, reinforced concrete block masonry wall. To provide additional lateral load resistance to the main tower, new shear walls were added, some existing shear walls were removed and replaced and others were repaired and strengthened. Where no serious yielding of reinforcement was evident, cracks were repaired by epoxy injection. New and replacement walls were cast using gunite made with shrinkage compensating cement. Concrete strength was specified as 3000 psi, and an average strength of 4000 psi was achieved. Joints around new walls were roughed 1/4-in. using a chisel. New walls were reinforced using 0.25 percent steel reinforcement in each direction. Existing walls were reinforced with gunite "skins" applied after sandblasting the original concrete. Dowels were epoxied into holes drilled into the existing concrete. Holes were 1/2-in. diameter greater than the dowel and 10 bar diameters deep.

Higashi and Kokusho (35) used one-third scale reinforced concrete models to test four different strengthening techniques. The first technique was the casting of a wall within an existing reinforced concrete frame. Beams and columns measured 7.1 in. x 7.9 in.; wall thickness was 3 in. No reinforcement joined the frame and wall; connection was provided by shear keys spaced all around the frame. Under lateral load the structure failed at a deflection of 0.01 radian as the shear keys ruptured followed by column shear. Load capacity decreased rapidly after failure.

A second technique used four narrow precast panels to infill the center opening of an existing frame. Gaps equal to the size of one panel were left between each column and the infilled wall. Both chemical and mechanical connectors were used to join satisfactorily the panels to the frame. The minimum lateral strength of these panel structures was about one-fourth the capacity of frame with a monolithically cast infilled wall.

A third technique used wing walls cast adjacent to columns of an existing frame. The lateral capacity was increased only slightly.

The fourth technique used exterior metal bands which were clamped around the columns of the frame. The shear capacity and ductility of the frame was increased significantly by use of the exterior shear reinforcement; although the total capacity of the structure was only about one-tenth that of a frame with an infilled wall.

APPENDIX B  
SPECIMEN DESIGN

Prototype Frame

As discussed in Chapter 2, the representative, prototype frame from which the specimens were modeled was a three-story, one-bay reinforced concrete frame. The frame was designed according to standards available in the 1950's and 1960; these standards were ACI 318-56 (3), the BOCA Code (14) and the UBC/46 (62).

The frame was designed as though it were part of a hospital located in Zone 3 earthquake region (14). Anticipated dead load was 75 lb/sq ft from the structure, 20 lb/sq ft from wall partitions and 10 lb/sq ft from hanging ceilings and ventilation. Live load was taken as 40 lb/sq ft. These loads were prescribed in Sections 705 and 707 of the BOCA Code (14). Horizontal wind load was prescribed as 15 lb/sq ft on vertical surfaces and equivalent earthquake forces were applied according to the specifications given in Appendix K-11 of the BOCA Code (14).

Dimensions of the prototype structure were an 11-ft story height, a clear span single bay width of 16-ft, and continuous bays on 17-ft centers. Floor slabs were square with center-to-center spans of 17-ft.

The concrete strength ( $f'_c$ ) was assumed to be nominally 4000 psi. Principal reinforcement was assumed Grade 50 while secondary hoop and stirrup reinforcement was assumed Grade 40.

The floor slab was designed as a two-way slab using Method 2 as

presented in ACI 318-56. The design gave a 5-in. thick slab reinforced with #4 bars on 6-1/4 in. centers over the beams and on 9-1/4 in. centers at mid-span for the middle strip.

The traditional working stress method was used to design the beam. The top T-flange of the beam was taken as 48-in wide because of the requirement that the flange width be not greater than 1/4 the clear span and that it not exceed 8 times the slab thickness on either side of the beam (Section 705, ACI 318-56). Overall beam depth was 14-in. with a width of 10-in. These dimensions provided the necessary  $b$ ,  $d$  and  $d'$  for the beam and were standard dimensions. Compression reinforcement was carried throughout the length of the beam to satisfy negative moment and anchorage requirements and to limit long term deflections. Both tension and compression reinforcement each consisted of two #8 bars. Beam web reinforcement was needed to satisfy strength requirements for a distance of 28-in. from each column face; #2 stirrups spaced at 6 in. satisfied this requirement. Stirrups were continued throughout the beam at 12-in. spacing to satisfy the provision that where compression reinforcement is used, stirrups shall be spaced at no more than 48 tie diameters.

The 12-in. x 12-in. column was reinforced with four #10 bars located at the corners. The design was tension controlled; moments at the first story level dictated the design. Axial stresses were small. No shear reinforcement was required. Hoops made of #2 bars were spaced on 12 in. centers along the column length to satisfy minimum tie provisions.

The footing and base beam design had to be greatly modified so

that the model specimen could be easily tested in the available load frame. Therefore, the base of the prototype was not designed in detail. This modification achieved the desired results in that experimental failures occurred in the frame and not in the foundation structure.

In all cases the clear distance between the reinforcement and the concrete surface was 1-1/2 in.

It is interesting to note that the lateral load design was controlled by wind forces rather than by prescribed equivalent seismic forces. When wind or earthquake forces were applied in the design, the allowable concrete and steel stress were raised by 33 percent as permitted in the building codes (14, 62).

#### Model Frame

The frames of all specimens were a 1/2 scale model of one bay and one story of the prototype frame as shown in Figure B-1. All dimensions were halved to design the model frame while material strengths were kept the same. As stated above, the base beam and footing were designed specifically for the specimens, Figure B-2, and additional slab reinforcement was included near the columns. The additional slab steel was included to provide direct shear reinforcement for the concentrated lateral loads applied during the tests. Further, the slab steel used in the model was #3 bars rather than #2 bars as prescribed by direct scaling because the #3 bars had deformations which provided the necessary bond anchorage whereas the #2 bars did not. The author believes that these differences didn't affect

significantly the structural behavior of the specimens.

The concrete aggregate was scaled, also. The maximum size aggregate in the prototype concrete was  $3/4$  in., so the maximum size aggregate used in the specimens was  $3/8$  in. The nominal strength of the concrete in the specimens varied between 3000psi and 5000psi. The modeling of the aggregate was necessary to satisfy form-to-reinforcement clearance requirements. Yet, the author believes that the aggregate modeling affected only slightly the concrete shear failure behavior because of the difference in aggregate interlock between  $3/4$  in. and  $3/8$  in. concrete. Results indicated that aggregate interlock was not a factor in the observed failure modes.

The one-story model frame was reanalyzed based on the actual steel yield stress properties and a nominal concrete strength of 4000 psi. The lateral load causing first yield of the reinforcing in the columns was calculated to be 6.44 kips; this load considers axial tension and compression forces in the columns and their effect on concrete moment capacities. The interstory yield deflection was calculated to be 0.36 in. based on an elastic analysis and a fully cracked concrete section moment of inertia. The ultimate lateral load causing concrete strain of 0.003 in the columns and top beam was calculated to be 7.77 kips. The column ultimate rotation would be 0.0022 radians which approximately would yield an interstory deflection of 0.50 in.

#### Monolithic Shear Wall

The monolithic shear wall of Specimen 1 was designed as a non

load bearing wall, and the wall design satisfied provisions in ACI 318-71 (5) for earthquake resistant structures. Some design restrictions were that the minimum horizontal and vertical steel reinforcement areas could not be less than 0.0025 times the gross section; that bar spacing in the prototype could not be greater than 18 in. which meant that the spacing in the model could not be greater than 9 in. For testing purposes, the wall thickness was chosen to be 3 in. (a prototype wall thickness of 6 in.). Number 3 reinforcing bars were selected for the model so that the bond deterioration could be more accurately modeled by using deformed bars rather than plain bars; deformed bars smaller than #3 were not readily available. The resulting design of the wall was one which satisfied the minimum model and construction requirements and was not one based on a particular structural load criteria. That is, the wall was not designed to resist a chosen seismic loading but rather it was designed to represent what might be a typical infilled wall for aseismic rehabilitation.

The reinforcement scheme is shown in Figure B-3. The vertical #3 bars were spaced 8-3/8 in. on centers while the horizontal #3 bars were spaced 9 in. on centers. In the prototype, this reinforcement would be #6 bars at 16-3/4 in. and 18 in. spacing respectively. In present practice a more typical prototype reinforcement for the same steel percentage would be #5 bars at 11-5/8 in. and 12-1/2 in. or #4 bars at 7-1/2 in. and 8 in. respectively. But modeling requirement for both material yield strength and bond necessitated the use of the larger bars at maximum allowed spacing.

This reinforcement represented vertical and horizontal steel

percentages for the infill of 0.436 percent and 0.416 percent respectively. These percentages fall within the range of those used in previous tests of reinforced infill walls by Barda (13) and by Benjamin and Williams (16); those reinforcement ratios were 0.25 percent and 0.50 percent. Others (23) have presented the steel reinforcement ratio for shear walls based on the total wall area; that is, the area surrounding the "concentrated" reinforcement (columns) and the wall itself. By using the total vertical steel area divided by the total horizontal cross sectional area, the vertical steel ratio was calculated to be 1.07 percent. With this method of calculating reinforcement percentage, Benjamin and Williams (16) tested frame-wall structures with 1.67 percent reinforcement, and Cardenas and Magura (23) tested shear walls made with 2.3 percent total reinforcement.

The monolithic shear wall was designed as the standard on which the design and behavior of all infilled walls would be compared. The principal reinforcement of all other infills tested in this study were generally the same as for the monolithic infill. The prime difference in steel detailing was the connection of the monolithic wall to the frame. The monolithic wall reinforcement was continued into the beam and columns as far as possible and was bent to a 90° hook with a 5 in. extension (13 bar diameters). The anchorage thus provided was considered to be the best possible reinforcement connection. The concrete of the columns and wall were cast together; thereby creating the best concrete joint. The base beam was roughened by chiselling before the wall was poured, and the top of the wall

pour was left very rough for the beam connection. These roughened and cleaned cold joints were considered the best of typical construction joints.

After the monolithic shear wall was designed, it was reanalyzed to determine critical lateral loads by using several techniques and incorporating actual steel properties and assuming an  $f'_c$  of 4000 psi. The results of the analyses are summarized in Table B-1.

An elastic technique which assumed linear strain relations and a working stress type of concrete analysis was used to determine the lateral load at which tension yielding would first occur in the vertical column steel. The analysis treated the wall-frame structure as a cantilever beam. The calculated load at first yield ( $V_y$ ) was 119.6 kips.

The load causing an ultimate flexural failure was calculated by treating the structure as a cantilever beam and by assuming an ultimate concrete strain of 0.003. It was assumed that all steel yielded and that no work hardening occurred. A standard Whitney stress block analysis was used, similar to that recommended in ACI 318-63, Chapter 16 (3). The calculated ultimate flexural load was 162.6 kips.

The ultimate shear load ( $V_u$ ) condition of the wall was based on provisions of ACI 318-71, Section 11.16 (5).

The distance from the extreme compression fiber to the centroid of tension reinforcement,  $d$ , was calculated as 76 in., assuming all steel yielding. Using this  $d$  and a  $\phi$  factor of .85,  $V_u = 122.6$  kips; using the same  $d$  and a  $\phi$  factor of 1.0,  $V_u = 144.2$  kips. Another

provision in this Section allows  $d$  to be calculated as 80 percent of the length of the wall ( $l_w$ ), where the term "length of wall" is not defined. Assuming the total structure length, including columns, is the wall length (108 in.), then  $0.8 l_w$  is 86.4 in. With this  $d$  and a  $\phi$  of 1.0,  $V_u$  is 164 kips.

A shear strength was calculated based on a formula suggested by Barda (12):

$$V_u = bd (8.4 \sqrt{f'_c} + 0.95 \rho_n f_y).$$

This formula gives an ultimate shear of 193.7 kips. Barda's technique was used to calculate the load at first cracking. It was found as 103.4 kips based on a  $l_w$  of 96 in., and 116.3 based on a  $l_w$  of 108 in.

The empirical equations developed by Benjamin and Williams (16) were used to determine first cracking and ultimate lateral loads.  $V_u$  was found to be 115.2 kips. Using a wall length of 98 in., the  $V_u$  was calculated as 196.4 kips.

#### Cast-in-Place Wall

The wall thickness and reinforcement design were the same for the cast-in-place wall (Specimen 3) as for the monolithic wall (Specimen 1). Based on the previously assumed material properties, the design strength of this cast-in-place wall was the same as that of the monolithic wall. The only difference was accommodation of the construction difference; that is, building the wall within an existing frame rather than building frame and wall at the same time. The design problem was to provide adequate connections between the frame and the wall which was to be cast within the frame.

Rehabilitation work of several buildings after the San Fernando Earthquake served as design examples (50, 60). Continuity of wall reinforcement with the frame was achieved by anchoring short reinforcing bars into the existing frame, lapping the wall reinforcement with these anchored bars and then casting the wall within the existing frame. This work is described in Appendix D.

Requirements for anchoring reinforcing bars into existing structures was not specified by building codes except that the anchor must develop its design strength. Therefore, the technique of joining the dowel bar to the frame was a principal design parameter.

The author chose to anchor the bars by epoxy grouting the bars into holes drilled into the frame from the experiences gained using that technique in the rehabilitation of buildings damaged in San Fernando (59, 60) and subsequent discussions with Mr. Leon Stein, an engineer with the California State Department of Architecture. From observing the repair of many buildings after the San Fernando Earthquake, Mr. Stein believed that the epoxy grouting of bars set in drilled holes provided an excellent wall to frame connection and that such a connection would be regarded as satisfactory by building officials of the State of California. Other research reported in Appendix E showed that Portland cement grouts were not as strong as epoxy grouts.

Some published data was available on which to base the design of a dowel bar connection using epoxy grout (53, 54, 55, 56, 57, 59). In order to gain a better basis on which to design the dowel bar connection, the author conducted a series of pullout tests of bars

epoxy grouted into holes drilled in a concrete slab. Those tests and their results are presented in Appendix E. The epoxy used in the tests was Colma-Dur Gel produced by Sika Chemical Corporation. Although this epoxy was also used in the test specimens, Sika Corporation will stop producing this epoxy. For the reader's information, the epoxy replacing Colma-Dur Gel is Sikadur Hi-Mod which is claimed to have better bonding Characteristics (33, 56, 57).

The pullout tests showed that a #3 reinforcing bar epoxy bonded in a drilled hole with a diameter 1/4 in. greater than the nominal bar diameter and depth greater than 7 bar diameters developed the bar's ultimate tensile capacity. For design safety the embedment depth for the #3 dowel bars used in Specimen 3 was 10 bar diameters (3-3/4 in.) and the hole diameter was 5/8 in.

Number 3 dowel bars were used to correspond with the #3 wall reinforcing bars; a dowel was used at each frame-wall location where a wall bar was located as shown in Figure B-4. Therefore the lap was about  $37 d_b$  (bar diameters). In ACI 318-56 (3) the minimum required lap was  $24 d_b$ . In ACI 318-63 (24b) the minimum lap for Grade 40 steel in tension was  $24 d_b$  while that for Grade 60 steel in tension was  $36 d_b$ ; yet these criteria were required to be increased by 20% for bars located closer than 6 in. or  $6 d_b$  from an outside edge ( $28 d_b$  and  $43 d_b$  respectively). In ACI 318-71 (5) a more detailed criteria was given. The basic development length which is taken as the minimum lap length,  $l_d$ , given in Section 12.5 is

$$l_d = \frac{.04 A_b f_y}{\sqrt{f'_c}} \quad \text{but not less than } .004 d_b f_y \text{ or } 12 \text{ in.}$$

For  $f_y = 40$  ksi and  $f'_c = 4000$  psi (assumed material properties),  $l_d$  from the formula was 2.8 in. For  $f_y = 61$  ksi, and  $f'_c = 3470$  psi (the actual material strengths)  $l_d$  from the formula was 4.6 in.

Because the tension laps in the shear wall occur at a position of high moment, the minimum  $l_d$  was increased by 30 percent (Section 7.6). Even with this increase, the minimum 12 in.  $l_d$  was the lap distance requirement for the assumed and actual material properties.

In designing the dowel wall bar splice, it was decided to lap the bars  $36 d_b$  because the author did not want a weak splice to initiate failure of the wall structure.

The wall bars were terminated in a standard  $90^\circ$  hook (4-1/2 in. extension) with a clear spacing of about 1 in. between the existing frame and the hook. This hook was not required for anchorage by ACI 318-71. It was used to provide added integrity and strength at the edge of the wall and to keep the anchorage from deteriorating as the joint was cyclically loaded.

The cast-in-place wall to frame connection was designed to carry the maximum permissible shear via concrete-to-concrete bond. For this purpose, design required roughening the frame surface (ACI 318-71, Section 11.16). Roughening was achieved by chiseling the surface to a depth greater than 1/4 in.

The wall construction as described in Appendix D was accomplished by placing concrete into forms which were constructed within the frame. A gunite procedure similar to that used in the repair of other structures (Appendix A) was not used because of the high cost of gunite construction. The cast-in-place procedure chosen meant

that the entire wall could not be cast all at once; an opening had to be left at the top, under the top beam. After the majority of the wall was placed, the design specified that this opening be filled with a drypack concrete. The design assumed that this drypack joint was as strong as that between the rest of the wall and the frame. Such drypack connections are typical in precast construction (49). The lap splice of the top dowel bars and the wall bars was still 12 in. if the length within the drypack were disregarded. The actual shear capacity of the drypack, cold joint was unknown for this design.

#### Single Precast Panel Wall

The design of the single precast panel was based on the calculated yield and ultimate lateral loads of the monolithic shear wall; those loads are listed in Table B-1. For comparison purposes the reinforcing bar layout was the same in the precast panel (Specimen 4) as for the two previous walls (Specimens 1 and 3). The interior of the panel had the same horizontal and vertical steel percentages as the other walls. If the embedded steel plates (termed panel plates) used for connections were considered part of the horizontal reinforcement, then the total  $\rho_h$  was 0.0243 based on total horizontal steel area divided by the vertical cross-sectional area of the monolithic shear wall. As shown in Figure B-5, the panel plates replaced the two horizontal bars located at the top and bottom of the monolithic wall. Maximum spacing requirements (ACI 318-71) dictated the position of the remaining five bars. The horizontal bars had standard 90° hooks

at their ends to insure adequate anchorage.

Vertical reinforcing bars were welded to the steel panel plates. The size of the weld was designed so that the bar would yield before the maximum working stress level of the weld was reached. This welded joint assured continuity between the panel, the panel-to-frame connector and the frame. An unwelded lap connection between plate and bar would not have satisfied code criteria.

The principal design problem of the precast panel wall was concerned with the panel-to-frame connection. The first design decision was to connect the panel to the top and base beams only and to avoid positive connection with the columns. The decision considered the ultimate, probable failure mode of the shear wall structure.

In a seismically loaded structure the lateral forces would be transmitted uniformly through the floor diaphragm to the beam. From the beam this load could be channeled directly into the shear wall through a beam-to-wall connector, or it could be channeled into the column, then into the wall through a column-to-wall connector. This column connection could be a mechanical connector, or it could be a column-grout-panel bearing condition. In either column-wall connection, the total horizontal shear would have to be transmitted through a short column length. Existing columns in a framed structure are not likely to have been designed for such a high shear condition.

A shear failure in a column could lead to collapse of a portion of the structure. The load factors (safety factors) placed on the original design of reinforced concrete columns is much higher than

that placed on other structural members as a reflection of the consequences of column failure in relation to that of other members. Therefore the author wanted to avoid any condition which might overload the column in shear.

A combination of both beam and column connections was considered unsatisfactory. The direct connection of column to wall was estimated to be much stiffer than a mechanical or epoxy connection of beam to wall, particularly after numerous load cycles. The higher stiffness would cause most load to be transferred through the columns, possibly causing column shear failure before sufficient load could be carried by the beam-wall connection.

Muto has investigated and constructed cast-in-place, reinforced concrete walls built within structural steel frames (34). The primary wall-frame connection mechanism which he used was standard shear studs welded to the top and bottom beam; no studs or other connectors were welded to the columns. That Muto avoided positive column connections gave further substantiation that similar connection should not be incorporated in this current study.

Therefore, no column-to-panel connection was used. The 3/8 in. construction clearance gap between the panel and column was not filled with grout to assure column-wall discontinuity.

The total load was designed to be carried from the top beam, to the panel, to the base. To facilitate construction and to comply with current construction practice, a mechanical connection was selected which used standard concrete anchors as the mechanism to attach the panel plus connector to the frame. The author chose a

design ultimate lateral loads of 200 kips for the total anchor system. Even though this load was somewhat greater than the  $V_u$  loads listed in Table B-1, it was desired that the structural failure mode not be limited by connection conditions.

#### Anchors

The concrete anchor chosen was a 5/8 in. diameter wedge anchor manufactured by ITT Phillips Drill Company of Michigan City, Indiana (commonly referred to as Red Head Anchors). Phillips Company was the only company which provided detailed data sheets (38, 39) on different anchors from which a research design could be made; although other manufacturers did send standard advertising literature. Because of the available information, Phillips brand anchors were selected. Anchor bolt data is given in Appendix C.

A wedge type anchor was selected rather than a "self-drilling" anchor because the wedge type was a bolt itself and required smaller anchor spacing and edge distance for comparable pullout and shear resistance. To carry the 200 kip shear load and to meet edge distance and spacing requirements, 5/8 in. diameter anchors were selected. This selection considered combined shear and pullout using the formula recommended by Phillips (39):

$$\frac{\text{Applied tensile load}}{\text{Tensile load capacity}} + \frac{\text{Applied shear load}}{\text{Shear load capacity}} = 1$$

The maximum tensile load assumed for each of the 24 anchors was equal to one-half the ultimate load of a #3 reinforcing bar because there were two anchors for each vertical bar. The maximum shear load

assumed for each anchor was equal to  $1/24$  the design load of 200 kips. It was believed that plastic yielding of the connection system would distribute the shear load among all the anchors.

No special consideration was given to the problem of reversed cycle loading. The working load design safety factor recommended by Phillips (39) was four times greater for cyclic loads than for static loads, but no scientific data for this increase was given. At the time of original design, no research known to the author had been completed on the cyclic and dynamic capacities of concrete anchors. Therefore, only the static anchor capacities as determined by Phillips (38) were used as the ultimate design capacities.

After the panel was under construction, Bechtel Power Corporation published results of a study on concrete expansion anchors which were tested under static, alternating and earthquake loads (15). Stud and shell type expansion anchors of  $5/8$ ,  $3/4$  and 1 in. diameters, supplied by six manufacturers were tested under tension, shear and combined tension-shear loads. Principal findings were that alternating tension loads caused "walking", progressive pullout, under loads greater than one-half the static pullout capacity after 6000 cycles. Pullout capacities for the three sizes were the same under alternating loads as for static loads; although some fatigue failures did develop due to material imperfections and notches in some anchor designs. After two million cycles at 20 percent of the static capacities, the selected anchors' dynamic (earthquake) capacities were comparable to their static capacities. In general, it appeared that the load capacity of stud anchors were the same

under static and earthquake conditions. Therefore, the design of anchors used in Specimen 4 seemed to be adequate; the design was not altered as a result of this new study.

#### Ear Plate Connector

The panel connector was made of a steel base plate and steel ear plates as shown in Figures B-5, B-6, and B-7. The base plate was sized to remain elastic under a lateral load of 160 kips. The ear plates were designed to begin yielding under a lateral load on the structure of 120 kips and to be fully plastic under a load of 200 kips. The welds were designed to be at their maximum working stress levels under a lateral load of 160 kips. Depending on the actual end fixity developed by the ear plate to panel plate weldment, the ear plate was calculated to yield at a load between 100 and 130 kips and to become fully plastic between 160 and 220 kips.

It was desired that the ear plates begin yielding at a lateral load which approximated the first yielding load of the panel. Ear plate yielding was necessary so that the total shear would be distributed throughout the panel and to each concrete anchor. Too stiff an ear plate might lead to an overstress of one anchor, cause a failure of that anchor, and thereby perpetuate a progressive failure of the anchors. The designed plasticity was to resemble the behavior of bolted steel connections under ultimate conditions.

Furthermore, hot rolled steel plates were used for the connector to insure a low yield stress level around 36 ksi.

The panel connector was designed in two, 47-1/2 in. lengths

rather than one, 95-1/4 in. length in order to ease construction. First, one length would have been too heavy for two workers to install; second, with existing laboratory equipment, drilling holes in the long base plate would have been very difficult. Also, it was desired to model a connector which might be used in the field; field use might require a multiple unit connector.

The length of the ear plates in conjunction with the extension of the panel plate was designed to accommodate both sufficient lap weld length and adequate clearance above the concrete anchor as shown in Figure B-7. The weld length along the vertical edges of the ear plate was designed to carry the expected lateral shear forces; horizontal weld lengths were not included in the design because overhead field welds, in the case of the top-beam panel connector, are often unsatisfactory.

An ear plate connector as described was selected rather than a single structural angle so that the load distributed to the anchors and to the panel would be as symmetric and near the center of resistance as possible. Using a connection made of lapping angles would have simplified construction. One angle would have been anchored to the beam and the other to the panel. The resulting indirect load path from the line of vertical reinforcement in the panel to the anchors might have caused premature connection failure. The advantage of lapping angles would have been the avoidance of the many short welds necessitated by use of ear plates; such welds are often brittle and understrength. In this test ear plate welds did not fail; although welds between some ear plates and the embedded panel connector did fail.

### Panel Plate

As discussed above, the panel plate was secured within the concrete wall by welding the vertical reinforcing steel to the plate. It was desired that the concrete-to-plate bond would transmit all the panel shear force, the total lateral load. The author was skeptical of the concrete to plain steel bond capabilities.

ACI 318-63 (4) indicates plain reinforcing bars develop one-half the bond compared to deformed bars. For 4000 psi concrete, the ultimate bond stress calculated based on Section 1801 of ACI 318-63 was 250 psi. A plain plate embedded 3 in. for the full wall length would develop an ultimate shear of over 140 kips based on this ultimate bond stress. This ultimate load is less than the designed capabilities of the wall panel. A failure mode of the system caused by panel plate-to-concrete delamination was not desirable.

Utilization of a larger plate for deeper embedment and larger bond area was undesirable for several reasons. A larger plate was considered uneconomical; a minimum steel cross sectional area was desired. The 3/8-in. x 5-in. plate size was readily available where larger sizes were not. From past experience, the author did not want to rely on a concrete-to-plain steel bond even if the minimum bond area criteria was satisfied.

Shear connectors were welded on the plate to improve the wall-to-plate shear transfer. The small plates used as shear connectors were designed to transfer a 200 kip lateral force. Design of these "stiff" connectors was based on a discussion by Viest (64). Push-off tests using "stiff" rectangular plate connectors showed that steel-

to-concrete connection failure occurred when the concrete crushed in bearing; bearing pressure next to connector exceeded three times the concrete cylinder strength (64). The ultimate load design of the shear connectors used in the precast panel was based on assuming that failure would occur when the bearing stress reached  $f'_c$ . The following formula was used to select the number of connectors needed:

$$N = \frac{V_u}{H W f'_c}$$

where

$N$  = number of connectors

$V_u$  = total lateral design load (200 kips)

$H$  = height of shear connector (3/4 in.)

$W$  = length of shear connector (3 in.)

$f'_c$  = ultimate concrete stress (assumed 4000 psi)

The connectors were welded at 4 3/16 in. spacing along one side of the panel plate and alternating between welded reinforcing bars (8 3/8 in. spacing) on the other side.

Panel-Frame Connection. Field welding the panel/panel plate system to the ear plate/panel connector systems was chosen rather than bolting. While either welding or bolting could be designed to carry the anticipated forces, welding was considered an easier and, therefore, more practical and economical construction technique. Bolting would have required accurate alignment of ear plate and panel plate holes. In a rehabilitation of an existing structure, absolute squareness of the existing frame could not be assured; therefore,

precise proportioning of the panel connector would be difficult or impossible. To avoid such alignment and positioning difficulties, welded connections were selected.

Altogether, the precast panel wall and its connection system were designed to be as practical and as congruent with current design practice as possible, and they were designed to transfer the same lateral shear load as the monolithic wall and to exhibit a ductile failure mode.

#### Multiple Precast Panel Wall

The multiple precast panel wall (Specimen 5) was designed for use in interior bays of a building where clean and rapid construction methods were required.

The load resistance of the multiple panel wall would be different than that of single panel or cast-in-place walls because of the lack of continuity between panels. Even if gaps between panels were grouted after panel erection, the author believed that after high cyclic loads the grout and its bond would be destroyed and the slits would reappear.

The multiple panel wall reminded the author of slitted shear walls advocated and tested by Muto (41). Muto's slitted shear walls showed lower ultimate lateral loads and increased flexibility as compared to solid shear walls of the same dimensions and percentage reinforcement. But Muto claimed that the energy dissipation characteristics were improved (41). The area of the wall above and below the level of the ends of the vertical slits failed as a deep beam in a flexure-shear mode. The slitted wall appeared to behave

as a series of deep, fixed-end beams; the ultimate moment capabilities at the ends of these beams determined the wall's lateral load capacity.

The author believed that the multiple panel wall would behave similarly to Muto's walls. Design of the panels was based on assuming that they react as a series of deep beams. It was desired that the same vertical and horizontal steel percentages be used in Specimen 5 as in the other specimens so that the various walls could be compared easily and so that the walls might be economically similar (same amount of steel and concrete).

Six individual panels were chosen to constitute the infilled wall as shown in Figure B-8. Selection of the number of panels was based on several purposes. First, more than two panels were necessary so that the wall would behave as a multiple panel wall. Because 12 #3 bars were to be used as vertical reinforcement, the number of panels had to be such that 12 bars could be used efficiently. It was desired that full size, prototype panels be no more than 36 in. wide so that they could be trucked through large doorways without being turned sideways; therefore, the half scale model panel should be less than 18 in. wide. Finally, the weight of the model panel should be no more than what two or three erectors could carry; one model panel of a six panel wall would weigh about 210 lbs. Six panels met these conditions. More than six panels did not accommodate use of the 12 vertical reinforcing bars.

No attempt was made to design the multiple panel wall for resisting the same total lateral load as carried by the solid panel

or monolithic wall. Preliminary calculations showed that the vertical reinforcement ratio would have to be increased as much as 500 percent if the multiple panel wall were to carry the 160 kip lateral load. The design of the multiple panel wall was based on facilitating construction and on duplicating as closely as possible the reinforcement patterns of the other shear walls.

Yet, the multiple panel reinforcement layout was altered somewhat as compared to the solid panel. As illustrated in Figures B-8 and B-9, the two #3 vertical bars in each panel were located toward the edge of each panel rather than evenly spaced along the wall's length. The amount of horizontal reinforcement was increased to satisfy minimum shear reinforcement requirements as discussed below.

Each panel was expected to behave as and was analyzed as a fixed-end deep beam which was loaded in shear along the panel plates. The fixed-end condition was supplied by the panel-to-frame connectors at the top and bottom edges of each panel and by the horizontal panel-to-panel connectors. The panel-to-panel connection was designed to carry the vertical racking shear forces between panels; it served to unify the multiple panel wall and to prevent end rotation of each panel. This connector served the same purpose as the solid top and bottom portions of Muto's slitted shear wall.

As in Specimen 4 no connection was made between the wall panels and the columns. Because of the omission of panel-to-panel connectors on the column side of the end panels, the fixity of the end panels was less than that of the interior panels. A 3/8-in. gap between end panels and columns was designed to prevent column shear

failure.

The lateral load capacity of each panel was determined by the ultimate moment and shear resistance of the panel. Using a Whitney stress block analysis with  $f'_c = 4000$  psi and actual steel properties, the ultimate moment capacity of the panel was calculated to be 94 kip-in. A "fixed" condition was assumed to exist somewhere between the edge of the panel plate and the panel-to-panel connector. A shear load which would produce this ultimate moment was calculated to be in the range of 3.4 to 5.2 kips. Summing this lateral load capacity for six panels yielded a total lateral load capacity for the wall which ranged between 20.4 and 31.2 kips. This calculated wall resistance was far less than the 160 kips design load for the solid panel wall.

To assure that the ultimate moment could be developed at the top and bottom of each panel, a #4 horizontal bar was used at the level of panel-to-panel connectors. The #4 bar improved the moment capacity perpendicular to the vertical bars in the fixed-end segment of the panel. As shown in Figure B-10, this #4 bar was welded to the panel-to-panel connector plate. The plate was secured within the panel with the bent #3 auxiliary reinforcement which was also welded to the plate. In final construction of the wall, these panel-to-panel connectors were field welded together using a lap-splice plate, as shown in Figure B-10.

An extra #3 horizontal bar was located between the top and bottom panel-to-panel connectors to satisfy minimum spacing requirements for shear reinforcement in beams (ACI 318-71). The spacing between horizontal bars was about  $d/2$ ; 90° hooks were used to anchor

these horizontal "stirrups" rather than 180° hooks so that the bar extension might strengthen the vertical edges of the panels in case the panels should bear against one another. The design ultimate shear capacity of each panel was 18.4 kips based upon requirements of ACI 318-71 and an  $f'_c = 4000$  psi and actual steel properties.

The panel-to-frame connection was nearly identical to that in Specimen 4. For the multiple panels the length of each panel plate was equal to the individual panel dimension. Because of material availability, a 4-in. wide base plate was used instead of a 3-in. wide plate.

The 1/4-in. gaps between panels and 3/8-in. gaps between the wall and the column were not grouted so that the behavior of the steel connections could be observed. The mechanical connectors were designed to transmit the anticipated forces, so grout was not necessary for load carrying capacity. The author believed that the wall would be subjected to cyclic load, any typical cement grout would crumble and would not be useful at ultimate load. An example of such deteriorating grout behavior was given by Tamura, et al (61).

Altogether, the multiple panel wall was designed to provide a convenient erection procedure for the interior of existing structures and to utilize the same  $\rho_n$  as the other infilled walls. While this wall would stiffen the structure, the lateral load capacity was calculated to be about one-fourth the capacity of the other walls because the assumed behavior was that of a series of fixed-end beams rather than that of a unified shear wall.

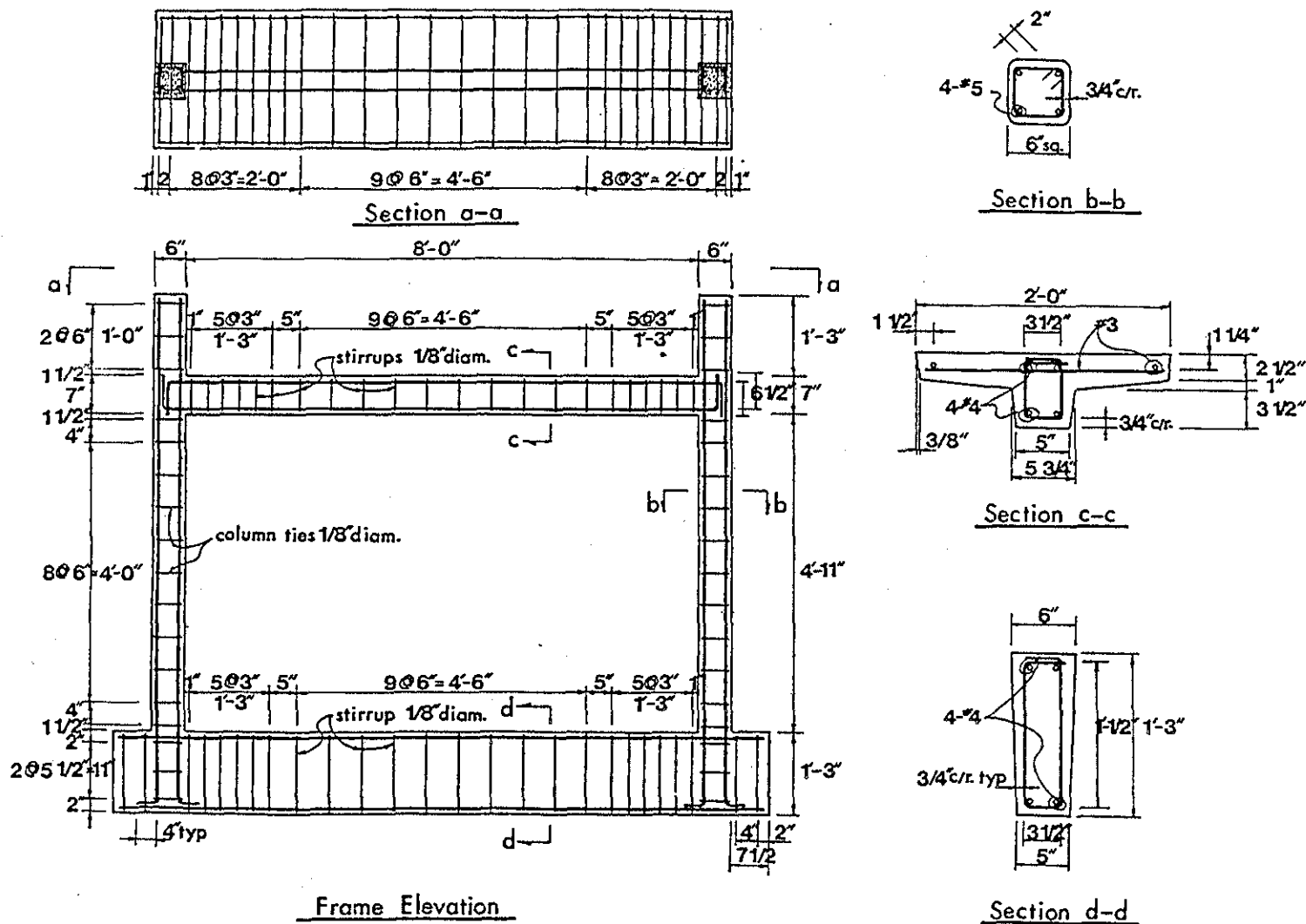
TABLE B1

Summary of Calculated Design Shear Loads  
for the Monolithic Shear Wall-Frame (kips)

	$V_y$	$V_u$ d = 76 in.	$V_u$ d = 96 in.	$V_u$ d = 86 in.
Working Stress Analysis	119.6			
Ultimate Flexural Analysis		162.6		
ACI 318-71 $\phi = .85$		122.6	154.8	139.4
ACI 318-71 $\phi = 1.0$		144.2	182.1	164.0
Barda (12)	103.4	193.7	228.6	
Benjamin and Williams (16)	115.2		196.4*	

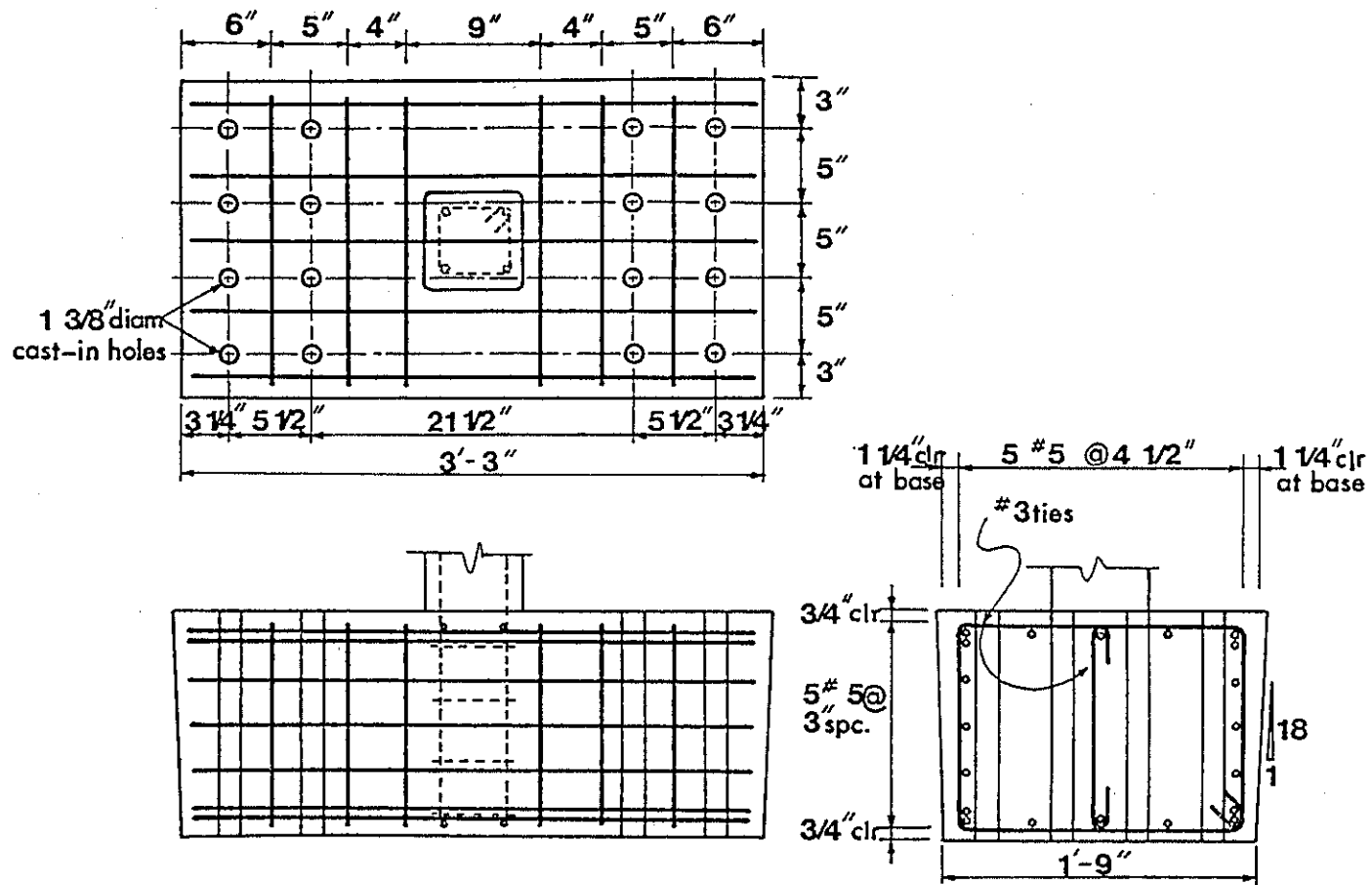
\*  
d = 98 in. by their formula.

Figure B-1. Design of model frame, Specimen 2.



Frame Reinforcement Details

Figure B-2. Design of footings for all specimens.



Footing Reinforcement Detail

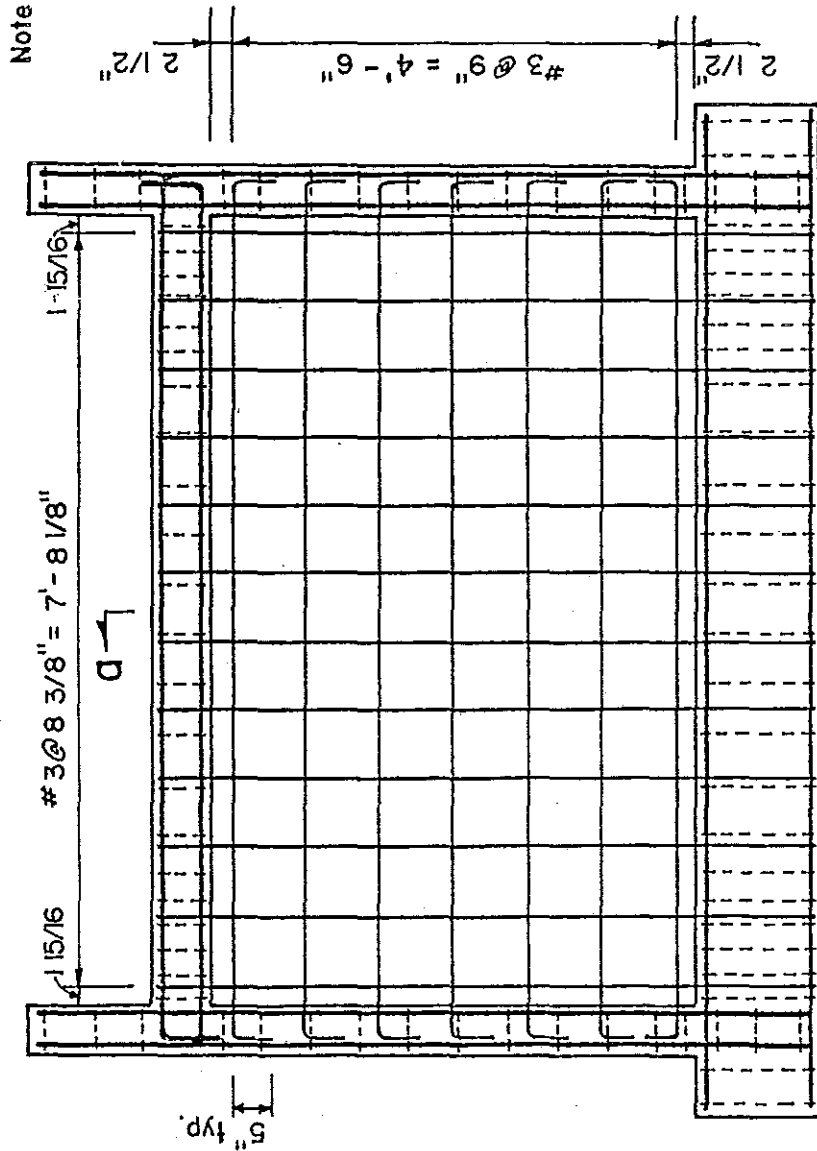
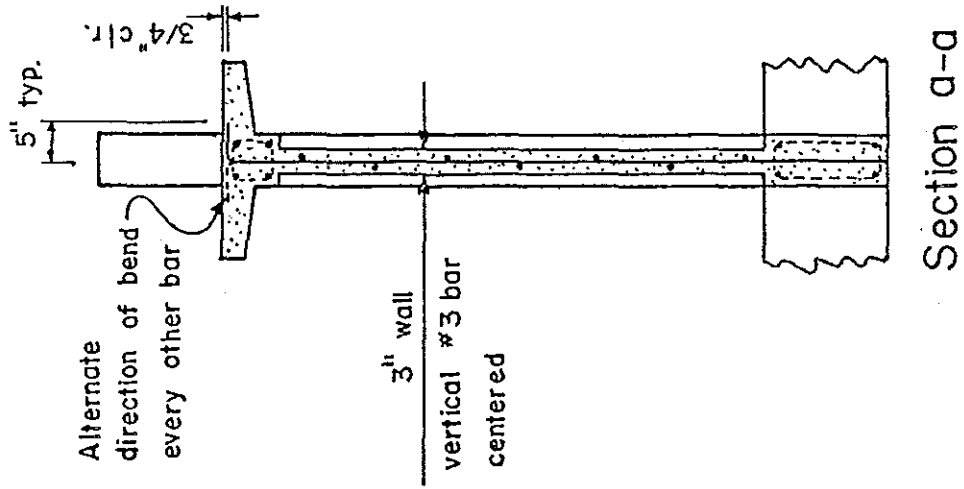


Figure B-3. Design of monolithic shear wall, Specimen 1.

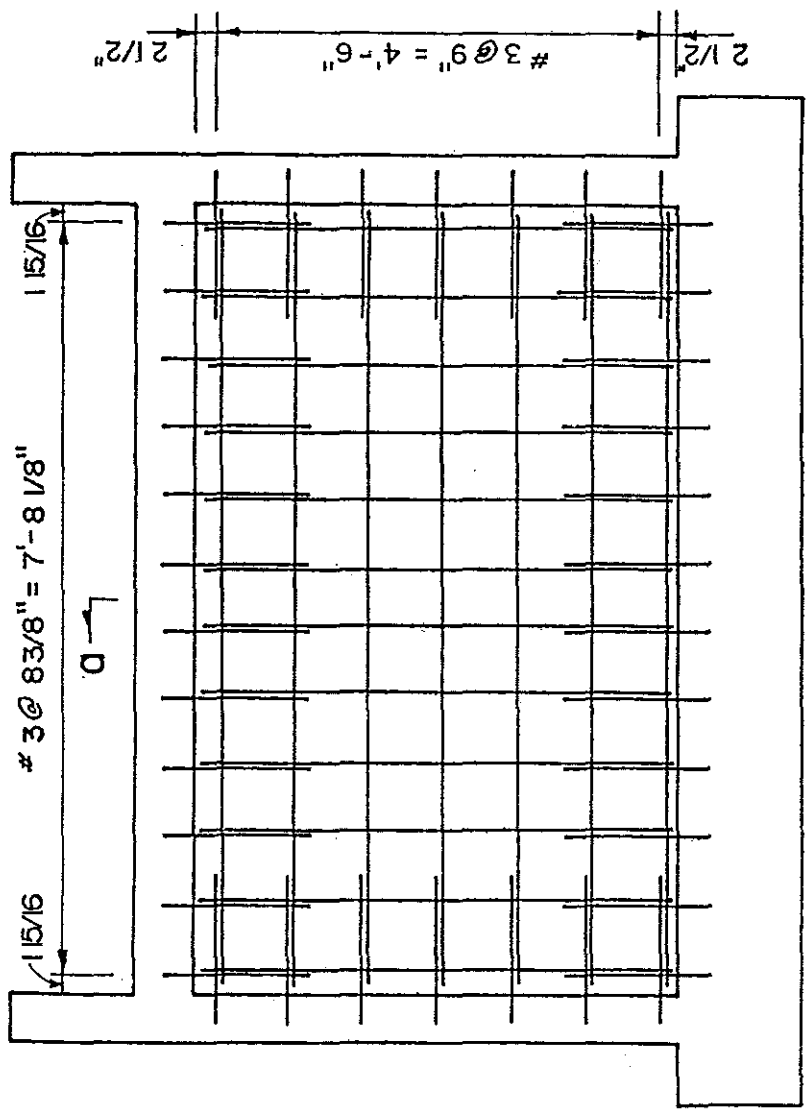
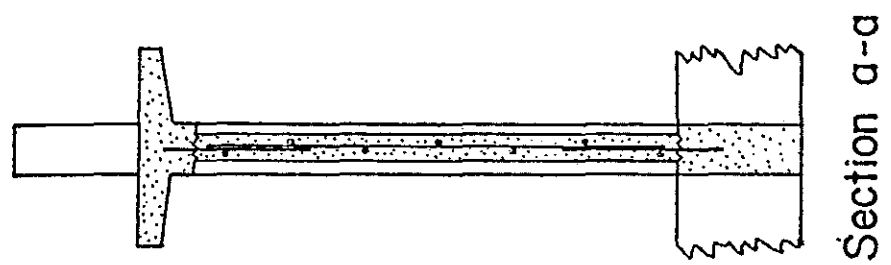
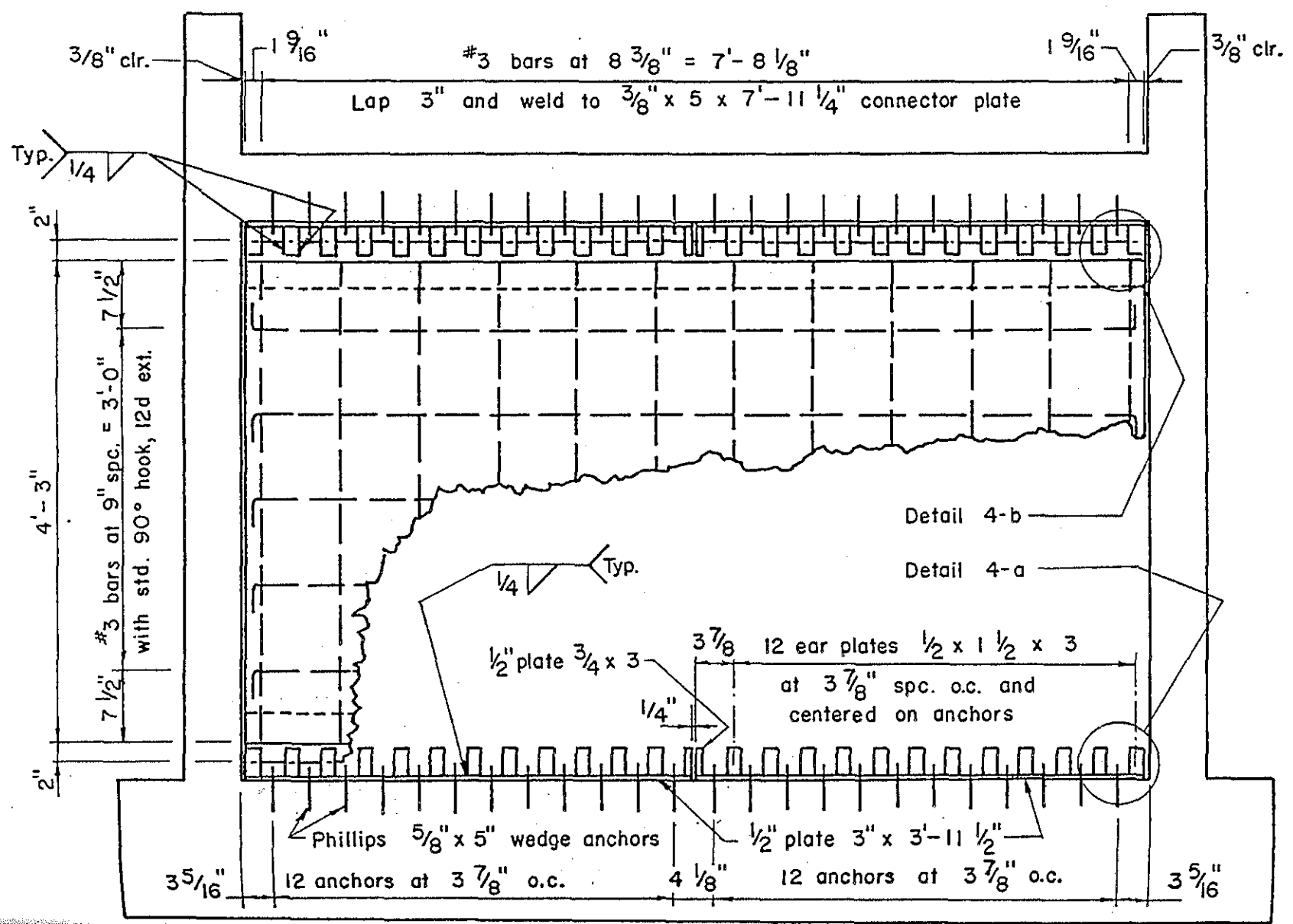
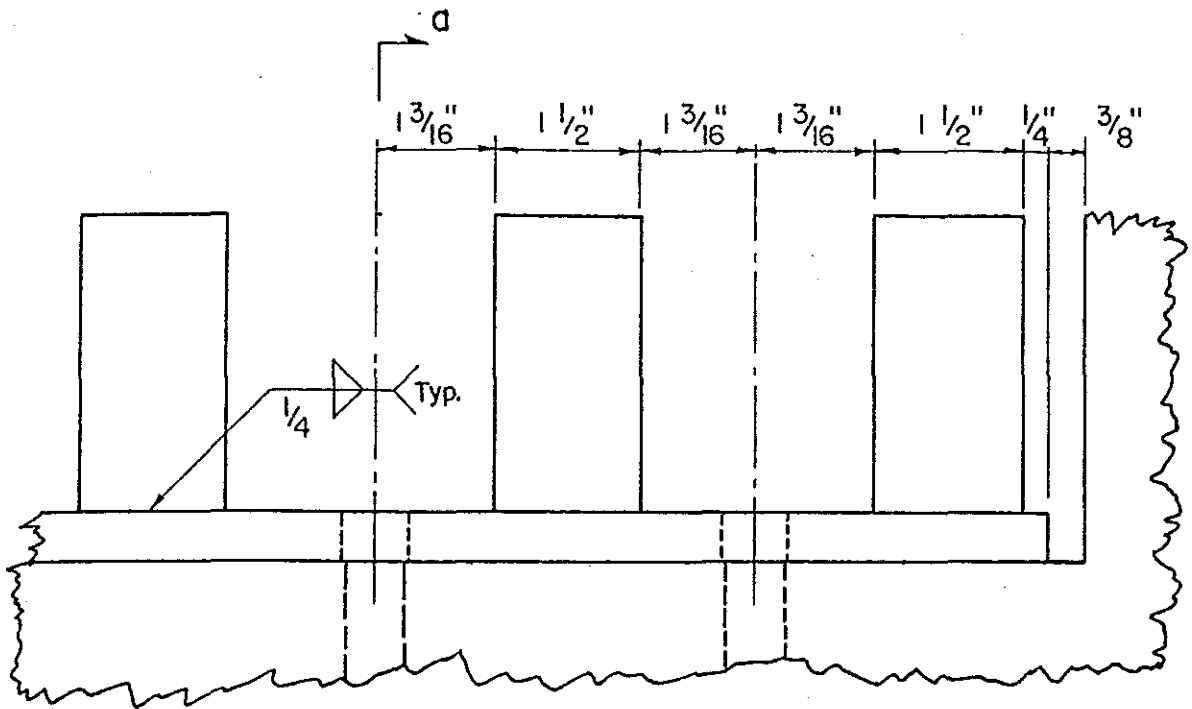


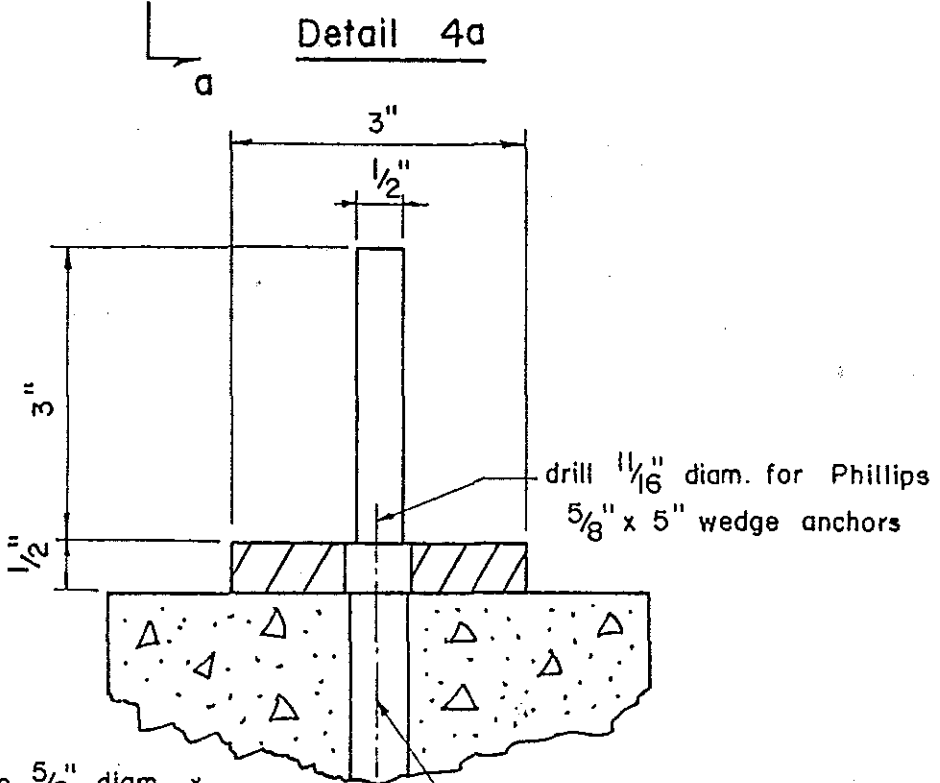
Figure B-4. Design of cast-in-place shear wall, Specimen 3.

Figure B-5. Design of single precast panel wall, Specimen 4.





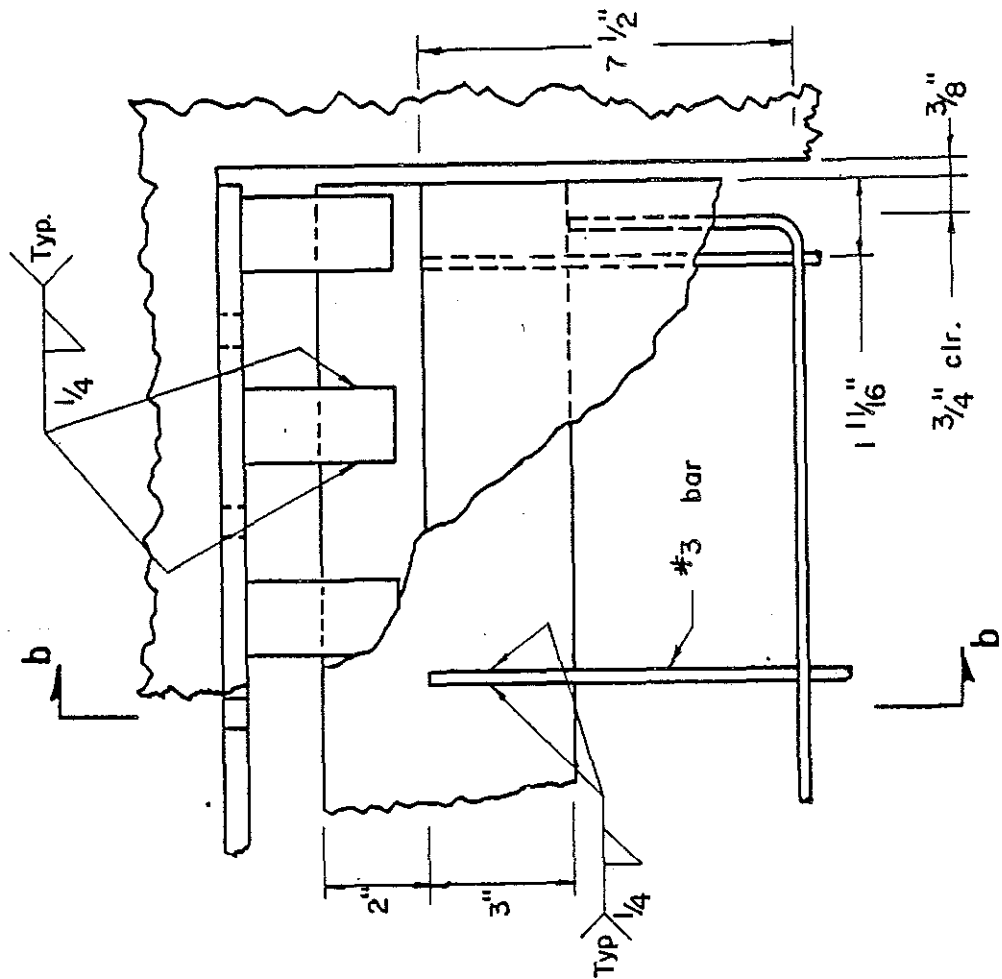
Detail 4a



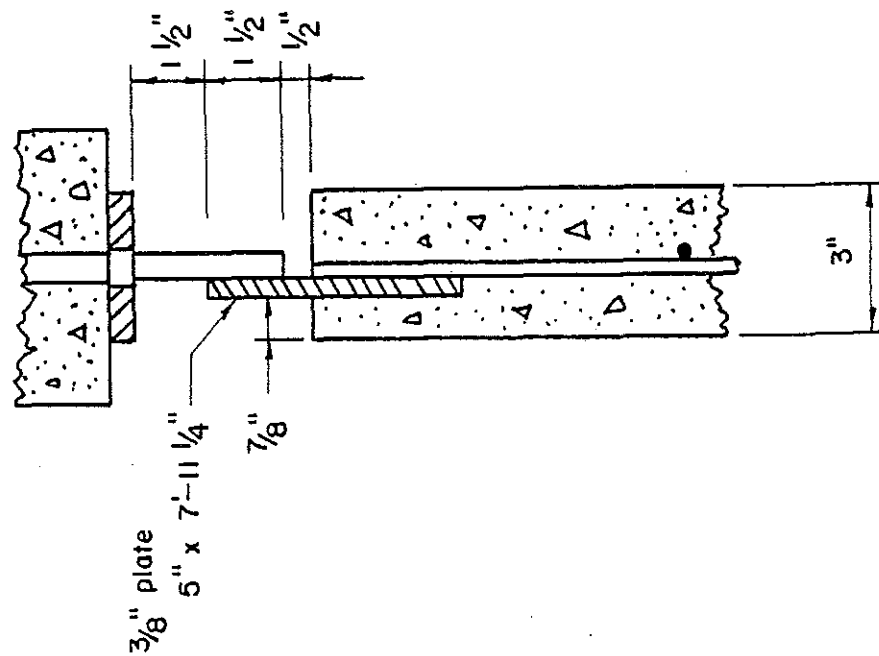
drill hole  $5\frac{5}{8}$ " diam. x  $3\frac{3}{4}$ " deep and centered on frame

Section a-a

Figure B-6. Detail 4a of panel-to-frame connector.



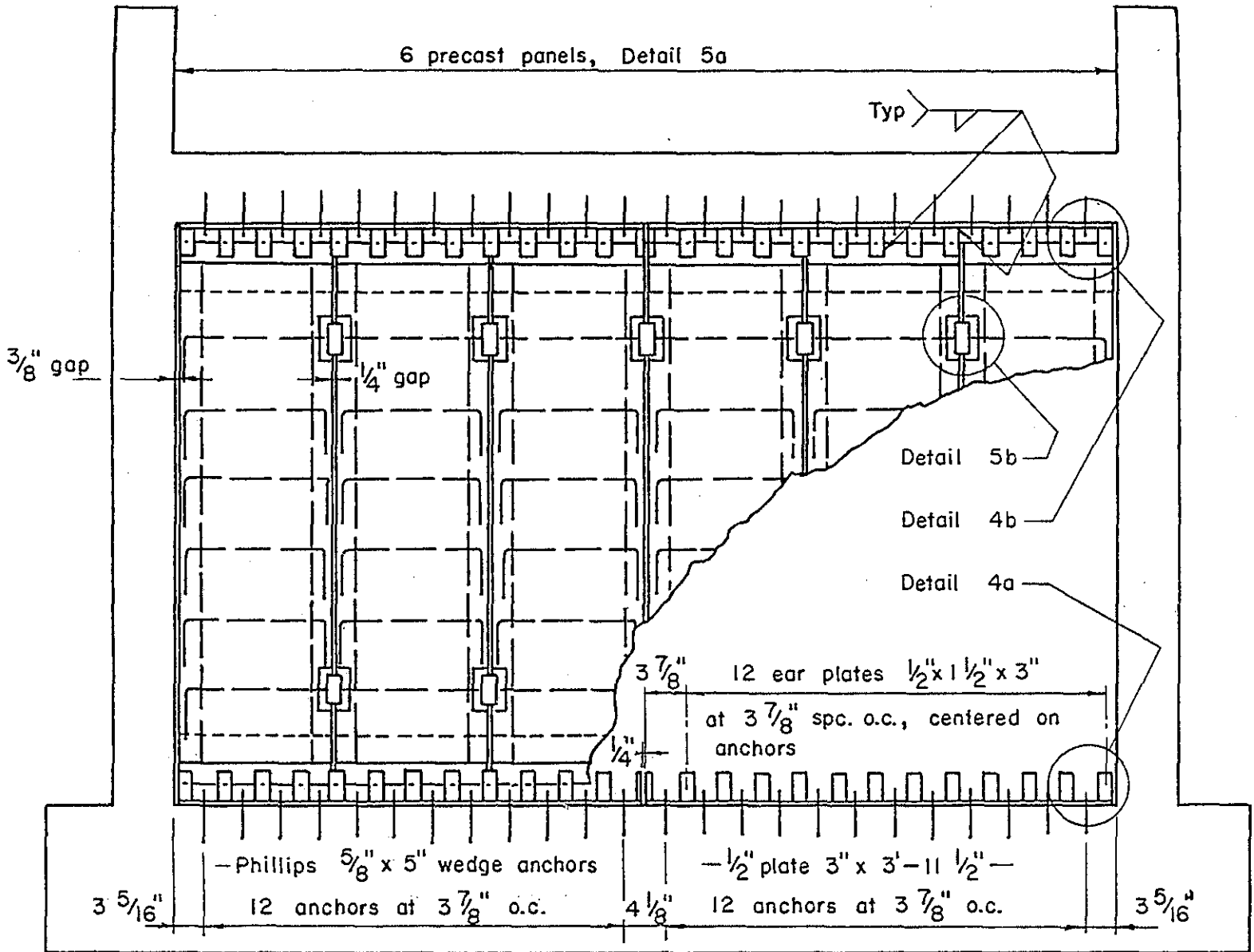
Detail 4b



Section b-b

Figure B-7. Detail 4b of connection of single panel to frame.

Figure B-8. Design of multiple precast panel wall, Specimen 5.



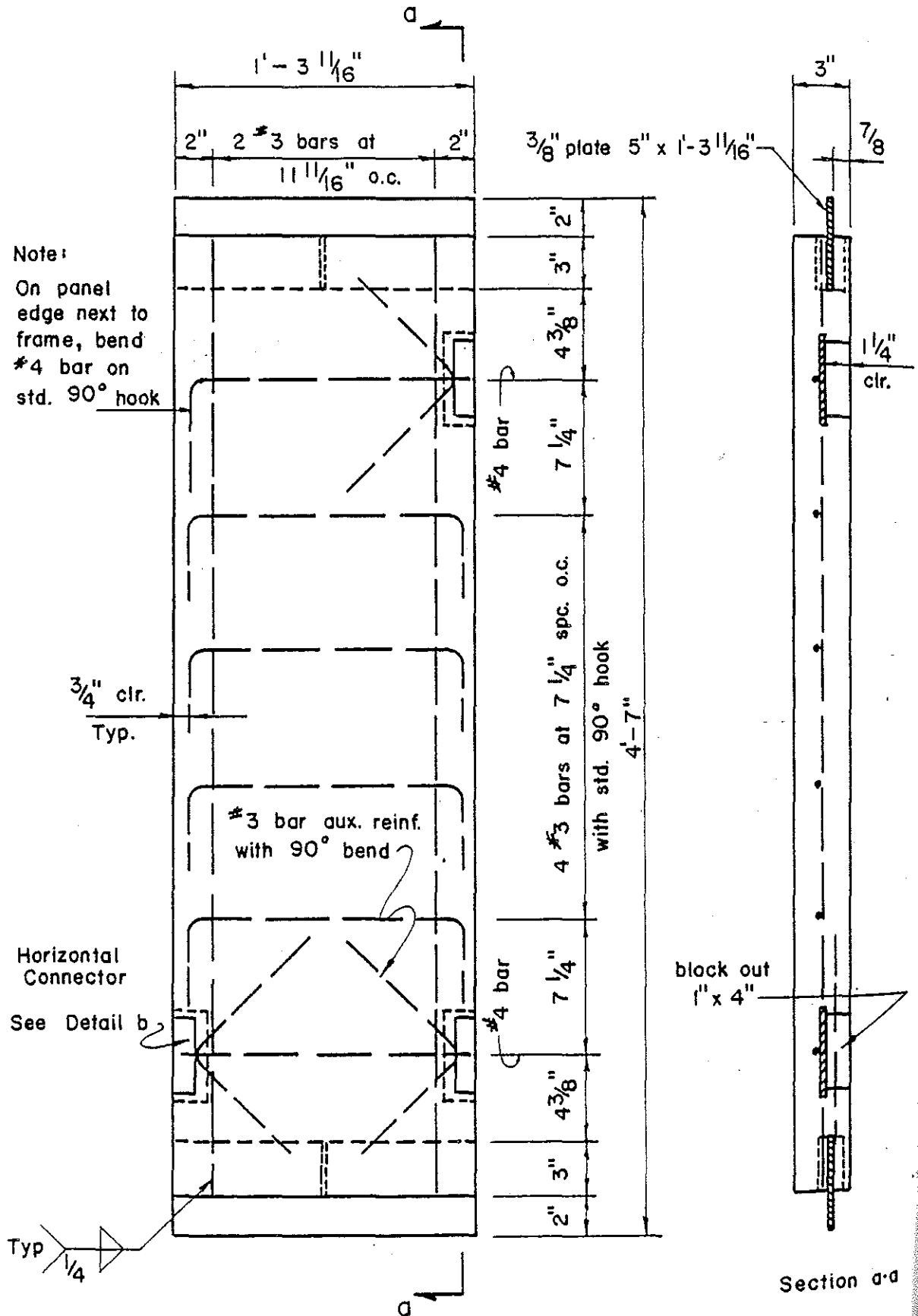


Figure B-9. Detail design of a multiple precast panel unit.

Detail 5b

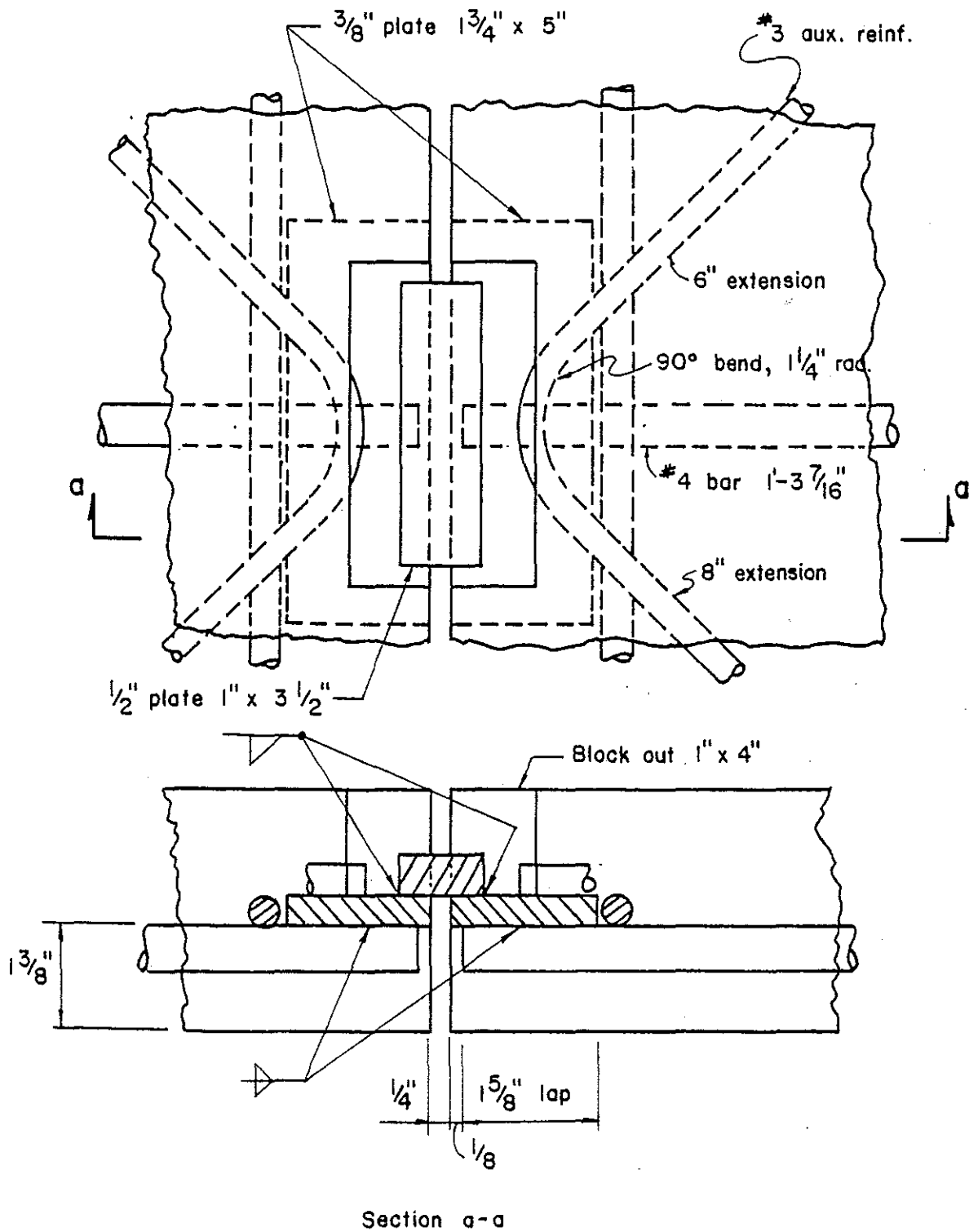


Figure B-10. Detail of panel-to-panel connection.

## APPENDIX C

### MATERIALS

#### Steel

Tensile tests of the reinforcing steel rods were used to determine the physical properties of the material. One foot lengths of the 11-gage wire used for column ties and stirrups were tested on an Instron Universal Testing Machine. Strain was measured using an Instron Strain Gage Extensometer with a 2.5 cm gage length and maximum extension of 0.25 cm. Strains greater than 10 percent were determined by measurement of head movement and specimen length between the testing grips.

The larger #3, #4 and #5 deformed steel bars were tested on a Baldwin Universal Testing Machine. Three 2-ft lengths of each size were tensioned. Strain was measured with a strain gage extensometer which had a 2-in. gage length and maximum strain capability of 4 percent. Strains greater than 4 percent were measured directly over a 10-in. gage length using large calipers. Strain measurement using the caliper method was within 0.002 in/in.

Column Ties and Stirrups. Eleven gage steel rods with an average diameter of 0.122 in. was used for all column ties and stirrups. The rod was originally cold drawn and was delivered pre-bent to the required tie and stirrup dimensions; some straight sections from the same steel batch were delivered for use in material testing. Tension tests of the cold drawn wire showed an average yield stress of 69.3 ksi as determined by the 0.2 percent offset method, and

the average ultimate strain was only 5.0 percent. The average tensile stress-strain behavior of four as-delivered rods is shown in Figure C-1.

The high yield stress, low ductility and lack of strain hardening character made direct use of the wire inappropriate for modelling grade 40 reinforcing bars. A series of rods were subjected to different heat treatments and then were tested in tension to determine their physical characteristics. Table C-1 summarizes the heat treatment and respective yield and ultimate stress capacities; four or more specimens were tested for each condition. After the rods were maintained at the desired annealing temperature for 1/4 or 1/2 hour, the rods were cooled by either removing them from the oven and allowing them to cool under room conditions or by turning off the oven and letting the rods cool in the oven as the oven cooled, a period of about one day.

A heat treatment of annealing at 1300°F for 1/2 hour and room cooling produced the desired yield stress, ductility and work hardening conditions. All pre-bent stirrups and ties were heat treated in this manner. The average tensile stress-strain behavior of eight annealed rods is shown in Figure C-2.

As indicated in Table C-1, two groups of four rods each were subjected to the 1300°F treatment on different days. Taken independently the average yield and ultimate stresses of each group were 41.1 ksi and 32.8 ksi for yield, and 50.8 ksi and 41.5 ksi for ultimate. This spread gives an indication of property variability.

A surface ash was found on all heat treated wire. That ash was

removed by brushing with steel wool before the stirrups and ties were used in the model structures.

Beam, Column and Wall Reinforcement. Grade 40, Number 3, 4 and 5 deformed steel reinforcing bars were purchased for use as beam, column and wall reinforcement from Bethlehem Steel Corporation. Most bars were delivered pre-bent according to design specification and current standards of the Concrete Reinforcing Steel Institute.

The results from tension tests of three bars of each bar size are given in Table C-2. Average tensile stress-strain behavior of three bars are shown in Figures C-3, C-4 and C-5 for #3, #4 and #5 bars respectively. As is typical, the yield stress of the Grade 40 steel was considerably greater than 40 ksi.

#### Concrete

Control Cylinders. Ultimate concrete strength was determined as the average strength of three concrete cylinders, 4-in. diameter and 8-in. long, tested in compression (ASTM C39). A minimum of six test cylinders were cast with each pour of concrete, for the base beam, column, beam, stub column, and wall element. Three of the cylinders were cured in a lime saturated water bath which was at room temperature, and these cylinders were tested 28 days after casting to determine the "laboratory concrete strength",  $f'_c$ , (ASTM C31). The remaining cylinders were cured adjacent to the model structures, and they were tested on the day on which the structures were tested to determine the "field concrete strength",  $f'_{cf}$ , (ASTM C31). Casting of the control cylinders was not standard

in that the concrete was consolidated by vibrating with a spud vibrator rather than by rodding.

Test cylinders of the drypack concrete used in Specimen 3 were cast in a manner which simulated the way the drypack was placed in the specimen. Each cylinder mold was filled in three levels. Drypack concrete was shoveled in the mold to fill it loosely one-half full. The material was packed down hard using the flat end of a one-inch diameter rod; this compressed the material so that it filled about one-third the mold. Shovelling and packing were repeated two more times until the mold was full. After setting three days the molds were stripped from the drypack cylinders. Three cylinders were cured in the water bath, and three were field cured.

Laboratory and field concrete strengths for the many pours are given in Table 1. The field strength averaged 21 percent less than the laboratory strength.

Mix Design. Reference 46, Design and Control of Concrete Mixtures, was used as a guide in selecting the proper mix design. Type I portland cement and a well graded sand (ASTM C136) were used. For half scale modeling purpose, 3/8 in. gravel was selected as the maximum size aggregate. Several trial mixes were prepared to develop a concrete with an  $f'_c$  of 4000 psi and with good workability, 4-in. to 5-in. slump. Mix I, is given in Table C-3; the water/cement ratio was 0.65. Mix 1 may be regarded as a standard, high-slump 5-1/2 bag mix.

Specimens 1 and 2 were cast using Mix I, with slight variations

in the water content because of transit mix delivery as described below. Upon conducting the 28-day compression tests on the control cylinders for Specimens 1 and 2, it was found that the concrete strength was above the 4000 psi desired. Therefore, the mix proportion was altered slightly by reducing the cement content and raising the water/cement ratio to 0.67. Table C-4 gives the mix design (Mix 2) used for the frames of the remaining Specimens 3 through 5 and for the cast-in-place and precast wall elements. Mix 2 may be regarded as a standard, high-slump 5 bag mix.

Transit Mix. All concrete used in the specimens was delivered to the University in a transit mix truck.\* The two or three cubic yard mixes were batched at the concrete company site, located about 5 miles from the University. Upon delivery of the concrete, slump tests were made to determine workability. If the slump was less than 3 in., an appropriate amount of water was added and mixed so that a slump of about 5 in. was obtained. No concrete was delivered with a slump over 5 in. Therefore, the exact water/cement ratio was unknown.

When the concrete was ordered, the mix proportions were adjusted assuming a two percent water content for the sand and 3/8-in. gravel. Further, the water content ordered per cubic yard was about 7 gal. less than required by the design mix. Tables C-3 and C-4 give the mixes ordered for Specimens 1 and 2 and for Specimens 3 through 5, respectively.

---

\* Killins Concrete Company, Ann Arbor, Michigan.

Drypack. For Specimen 3 a special drypack mortar was used to fill the three inch gap at the top of cast-in-place wall. The mix for this drypack mix is listed in Table C-5.

#### Reinforcing Bar Welding

Fabrication of reinforcing in Specimens 4 and 5 involved welding. To insure that the plate-to-reinforcing bar weld was sufficient to develop the bar's capacity, four sample specimens were constructed and tested. These specimens were made of two #3 bars lap welded to a 3/8-in. thick plate. Weld length was 2-1/2 in. on each side of a bar. The bars were pulled in tension in a Universal testing machine. The average yield stress was 62,600 psi, and the average ultimate stress was 89,000 psi; these values were based on a nominal bar area of 0.11 in<sup>2</sup>. A comparison with plain #3 bars described above shows that the welded joint reduced the yield stress by 2 percent and the ultimate stress by 7 percent. Because these reductions were small the author considered the welded joint satisfactory. The precast wall panels were designed and constructed assuming that the welded bar-plate joint would develop the yield capacity of the reinforcing bar.

#### Panel-to-Frame Connectors

The steel used for the panel-frame connectors of Specimens 4 and 5 was hot rolled steel plate. From previous experience with similar plate the author knew that the yield stress of the material was between 35 ksi and 45 ksi and that the ultimate strain was greater than 20 percent. No material tests were performed to

accurately determine the properties of the steel connector plates. Design was based on an assumed yield stress of 36 ksi.

Four sample specimens were made with welds identical to those connecting the many ear plates to the base plate. These 1/4-in. fillet welds were tested by pounding the specimens with a five pound sledge hammer. No sample welds broke. It was assumed that the ear plate welds would sustain the standard working capacity of 2.6 kips per inch of 1/4-in. weld. Arco welding rod 7014 was used for these welds.

#### Concrete Anchors

Phillips Drill Company, Red Head brand wedge anchors, 5/8-in. diameter and 5-in. long, were used to anchor the panel connectors to the frames of Specimens 4 and 5. The author did not perform any tests on the anchors to determine their material properties or their anchoring and pullout resistance.

Technical information supplied by Phillips Drill Company (38) indicated that the strength of the anchor bolt material was sufficient so that the concrete would fail before the bolt. Pullout and shear tests of the 5/8-in. wedge anchor were conducted by the Pittsburgh Testing Laboratory; that test data was given in the Phillip's Company catalogue (38) and is repeated in Table C-6 below. The Laboratory stated (38):

Procedure for tensile tests was axial loading until ultimate failure of concrete or anchors. Procedure for shear tests was loading to a steel plate bolted to the anchors in a plane perpendicular to the axis of the anchor. Concrete blocks used for tests were of a 1:3:5 mix, having a compressive strength as indicated ...

TABLE C-1  
Heat Treatment and Physical Properties  
of Eleven Gage Steel Rod

Annealing Temperature °F	Annealing Time (hours)	Cooling Method Used	$\sigma_y$ ksi	$\sigma_u$ ksi	Average $\sigma_y$ ksi	Average $\sigma_u$ ksi
None*			70.0	84.3	69.3	78.9
			71.0	84.4		
			68.0	73.5		
			68.3	73.4		
1000	1/2	Oven 24 hrs.	90.5	94.0	87.8	91.2
			91.1	94.4		
			92.3	96.1		
			77.3	80.3		
1500	1/4	Oven 24 hrs.	35.9	44.0	38.3	49.2
			39.7	54.3		
			44.4	54.7		
			33.1	43.6		
1350	1/2	Oven 24 hrs.	37.2	46.6	34.3	44.6
			37.6	46.2		
			35.9	46.2		
			26.6	39.3		
1300	1/2	Room	36.8	46.6	37.0	46.1
			36.3	44.8		
			45.7	56.0		
			45.5	56.0		
			28.9	37.8		
			36.8	45.3		
			36.8	45.5		
			27.8	37.6		

TABLE C-2

Physical Properties of Deformed Steel  
Reinforcing Bars

Bar Size	$\sigma_y$ (ksi)	$\sigma_u$ (ksi)	$\epsilon_u$ (in/in)	Average $\sigma_y$ (ksi)	Average $\sigma_u$ (ksi)	Average $\sigma_u$ (ksi)
#3	64.6	96.2	0.117	63.9	96.0	0.131
	63.8	95.4	0.154			
	63.3	96.5	0.122			
#4	61.2	95.7	0.139	61.2	95.5	0.140
	61.4	95.9	0.134			
	60.9	95.0	0.147			
#5	50.3	90.0	0.158	51.0	89.5	0.154
	50.6	89.2	0.149			
	52.2	89.2	0.155			

TABLE C-3

Mix I for Specimens 1 and 2

Item	Design Weight per Cubic Yard (lbs)	As Ordered Weight per Cubic Yard (lbs)
3/8 in gravel	1200	1225
Sand	1750	1785
Cement	485	485
Water	315	240

TABLE C-4

Mix 2 for Specimens 3, 4 and 5

Item	Design Weight per Cubic Yard (lbs.)	As Ordered Weight per Cubic Yard (lbs.)
3/8 in gravel	1205	1790
Sand	1755	1230
Cement	470	470
Water	315	240

TABLE C-5

Drypack Mortar Mix

Type I Cement	36 lbs
Sand	72 lbs
Water	12 lbs

TABLE C-6

Tests of 5/8-in. Wedge Anchors by  
Pittsburgh Testing Laboratory (38)

Pullout		Shear	
Tension Load lbs.	Failure Type	Shear Load lbs.	Location of Failure
7429	Concrete	10,400	Shear
8289	Concrete	11,100	Shear
7629	Concrete	10,900	Shear

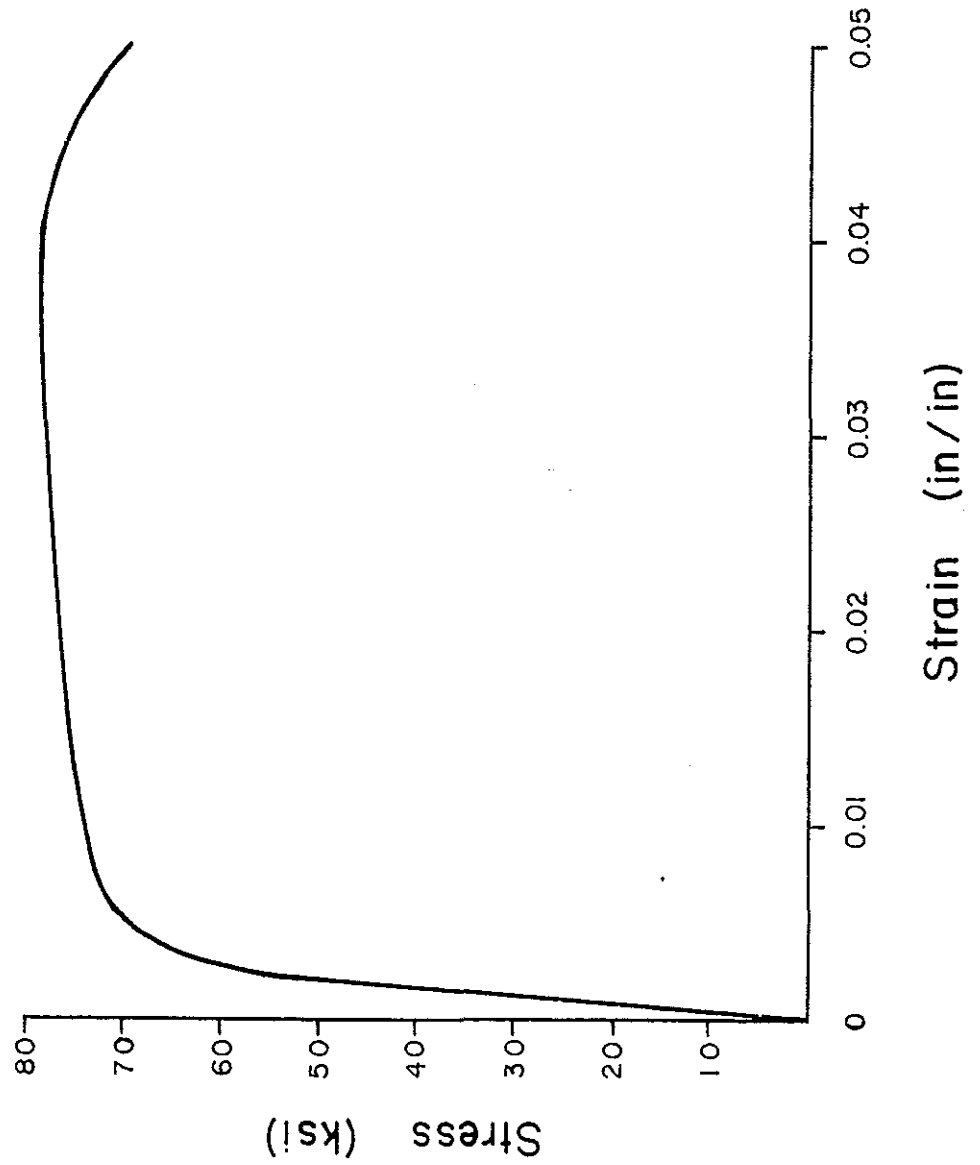


Figure C-1. Average stress-strain behavior of "as delivered" 11 gage plain steel bar.

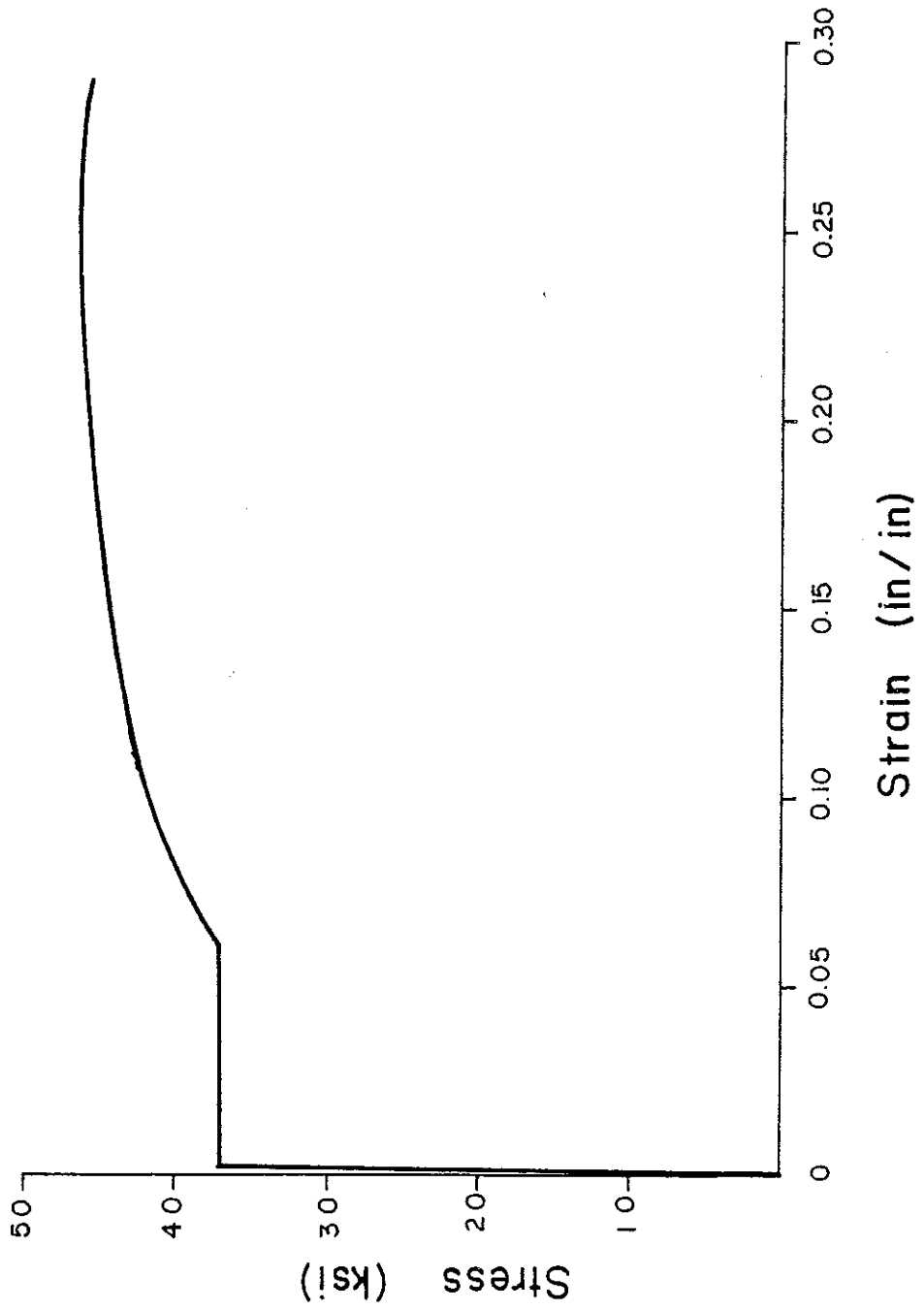


Figure C-2. Average stress-strain behavior of annealed 11 gage plain steel bar.

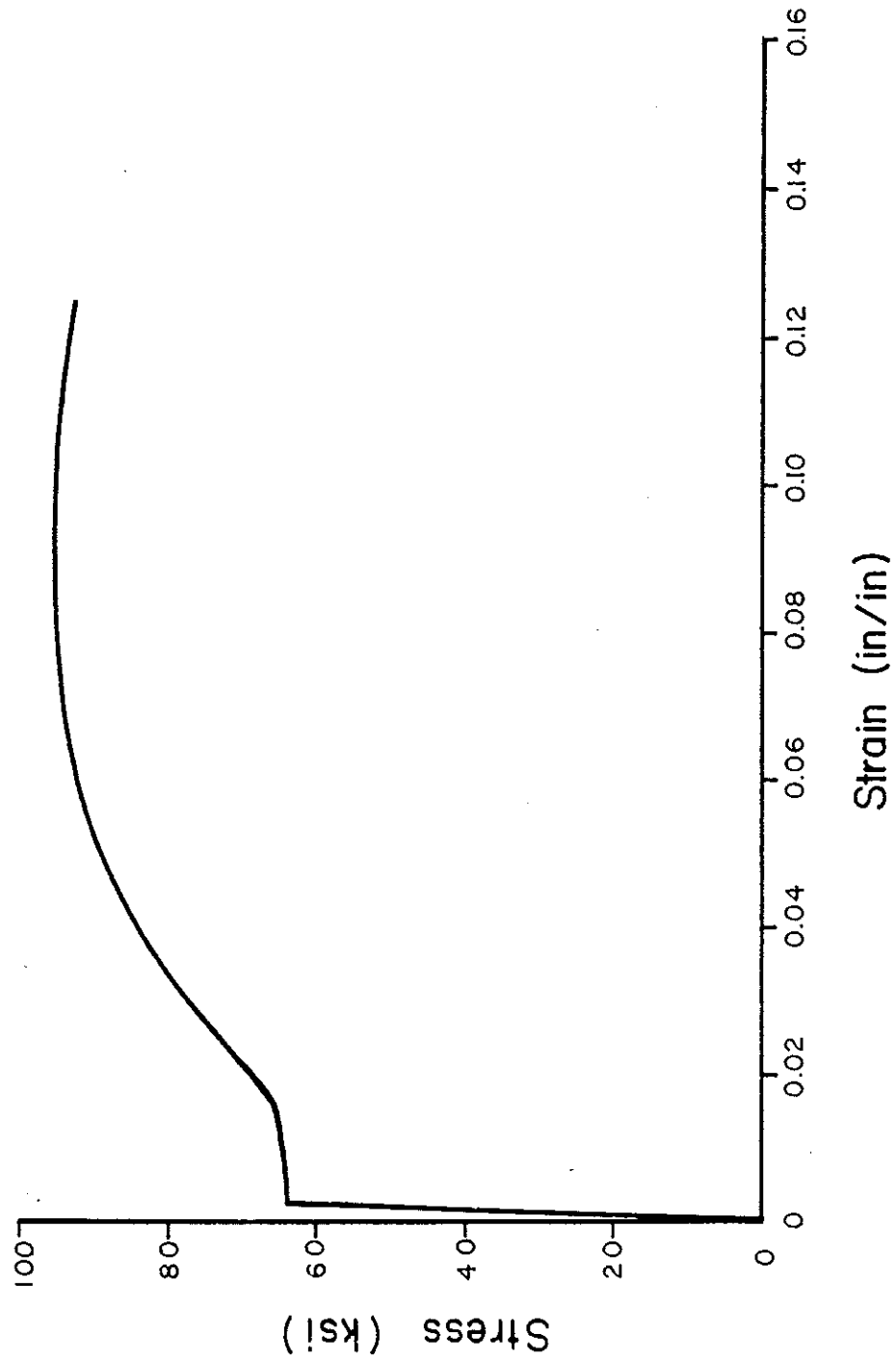


Figure C-3. Average stress-strain behavior of #3 deformed steel reinforcing bar.

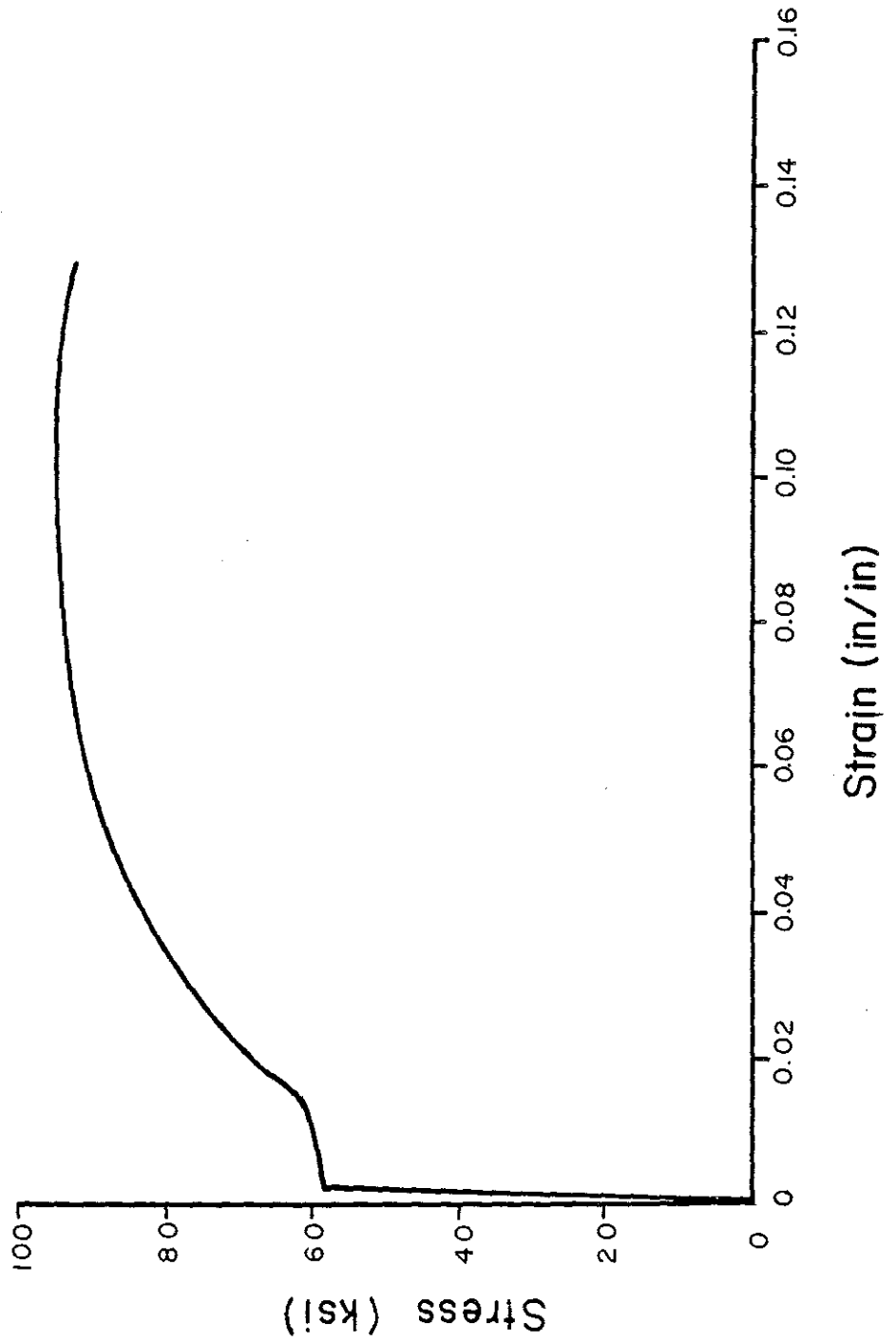


Figure C-4. Average stress-strain behavior of #4 deformed steel reinforcing bar.

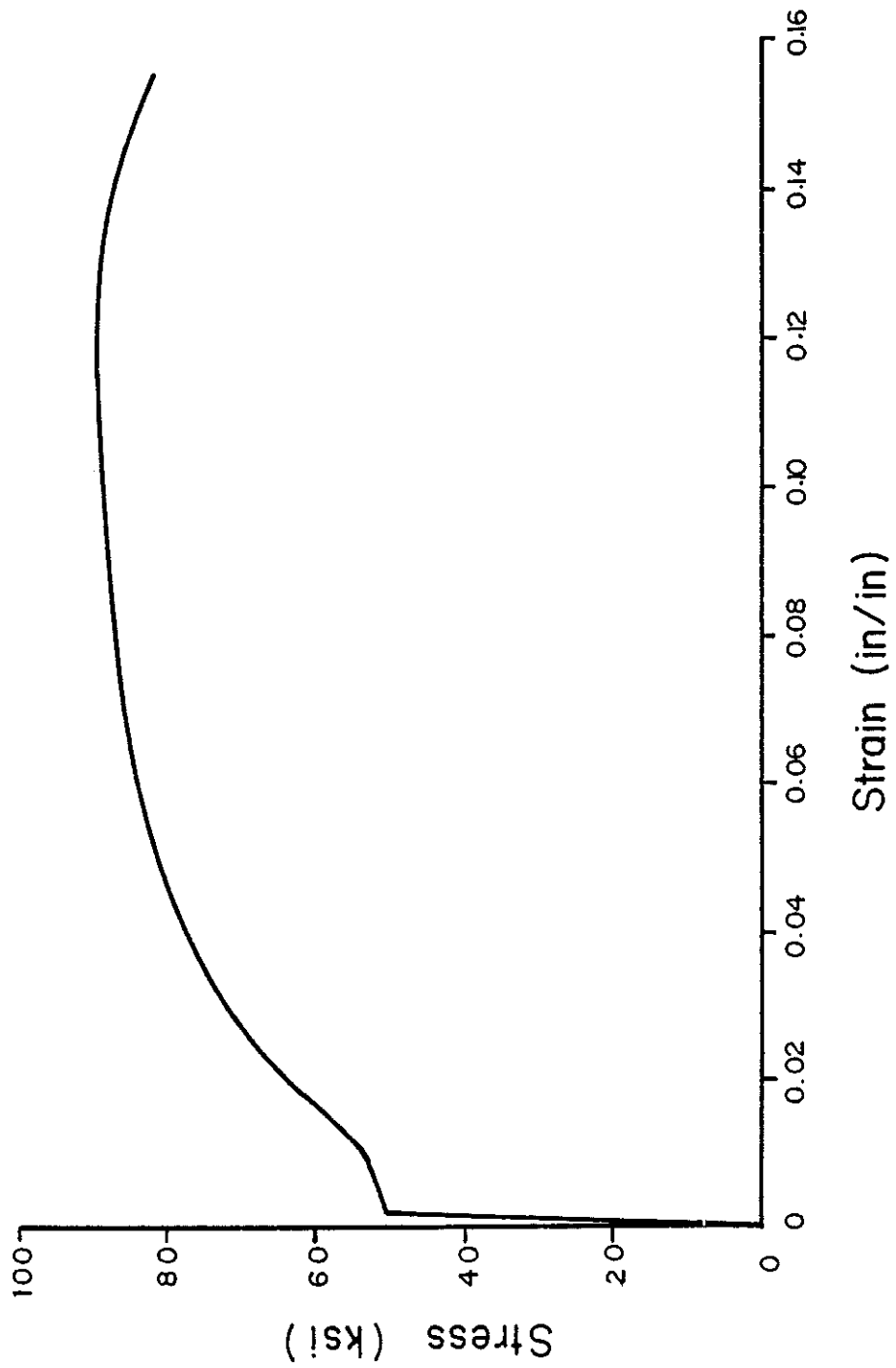


Figure C-5. Average stress-strain behavior of #5 deformed steel reinforcing bar.

APPENDIX D  
FABRICATION OF SPECIMENS

Frames

All frames for Specimens 2 through 5 were constructed in an identical manner. Two sets of plywood forms were built so that two specimens could be constructed simultaneously. The vertical side forms for the base and the beam were canted out from bottom to top at a slope of about one-in-eighteen so that removal of the forms would be simplified (Figure D-1). Furthermore, beam forms were segmented to facilitate stripping.

Holes used for the hold-down bolts were cast into the footings by placing 15-in. long, hollow cardboard cylinders in the forms as shown in Figure D-2. The cylinders were held in place by wood dowels screwed to the plywood bottom and by wood spacers clamped to the top of the form. The cardboard was coated with orange shellac to prevent the paper from becoming water soaked when the concrete was placed. These cylinders remained in the concrete when the wood forms were removed.

Reinforcement. Frame reinforcement design is detailed in Appendix B, Figure B-1, and the footing reinforcement is shown in Figure B-2. Base reinforcement was tied together outside the base

form, then it was lifted into the form. This construction allowed more accurate positioning of the base beam stirrups.

Once the base reinforcement was positioned in the form, the vertical column bars (previously strain gaged) were located. A column hoop was tied to the top of the footing to aid in placement of the #5 column bars. After the many column hoops were tied in place, the completed column "cage" was held vertical with wire guys attached to the form (Figure D-3). As shown in Figure D-2, the horizontal base beam #4 bars were included within the #5 column bars. With the base and column steel in place, the base concrete was cast.

After the beam form was in place and the column was cast; the pre-fabricated beam reinforcing cage was placed (Figures D-4 and D-5). The beam #4 bars and stirrups were tied together outside the form to permit easier and more accurate construction. The horizontal beam steel had to be squeezed together to fit within the column steel.

With the primary beam steel in place, the edge beam reinforcement was located. One of the top #3 bars was not included within the column core because the radius of the bend of the #4 beam bar was so large. Nevertheless, it is believed that the stirrups surrounding the edge beam steel sufficiently confined the concrete. Also included with the #3 bars of the edge beam was a #3 bar bent into a triangular shape. The latter was included as auxiliary reinforcement for the concentrated loads applied by the jacks; the purpose of the #3 bar was to prevent the corners of the slab from cracking.

Finally, the #3 bar slab reinforcement was tied to the beam steel as shown in Figures D-4 and D-5. The beam was cast after this reinforcement was placed.

The stub column reinforcing was merely a continuation of the column steel. The hoops were tied in place after the beam was cast.

Casting. Four separate concrete pours were required for frame construction. The base was cast first. Concrete was poured from the transit mix truck into wheelbarrows from which it was shoveled into the form. A spud vibrator was used to consolidate the concrete. The surface was leveled using a wood screed; the area within the vertical column steel was left rough, though nearly level with the surrounding concrete surface. The surface was not troweled. A few hours after casting, the base was covered with wet burlap and enclosed in plastic sheets. The burlap was kept water saturated for three days. On the third day after casting the plastic and burlap were removed, and the wood forms were stripped from the base.

Before the columns were cast, the concrete surface at the column base was cleaned by wire brushing and roughed by chiseling. All laitance was removed; the depth of surface roughness was greater than 1/4-in.

The column forms and beam form were set-up together to insure correct frame dimensions. Wire guys were used to keep

the column forms vertical. Columns were cast about seven days after the base was cast. Concrete was shoveled into the forms, which were vibrated externally by holding the end of a spud vibrator against the form. The top level of the column pour was between 1/2-in. and 1-in. below the bottom of the beam. This space was necessary for placement of the beam reinforcement bars. The top surface was kept moist with wet burlap.

The top surface of the column was chiseled and cleaned. After the beam and edge-beam reinforcement was placed, the beam concrete was cast usually two or three days after the column was cast. Concrete was poured from the transit mix truck into a wheelbarrow which was lifted to the beam level by a fork lift (Figure D-6). It was shoveled into the form and internally vibrated. The surface was leveled with a screed. A few hours after casting, the concrete was covered with wet burlap and a plastic sheet. The burlap was kept moist until the forms were removed. Column and beam forms were removed three days after the beam was cast (Figure D-7).

Between three to five weeks after the beam was cast, the stub columns were formed. This occurred on the same day that bases of other frames or precast wall units were being cast.

Mortar blocks were used for proper clearance between reinforcing bars and the form. The typical clearance was 3/4-in. Because no standard chair is manufactured for less than a 1-1/2 in. clearance, special spacers had to be made. These spacer blocks were constructed of mortar with a tie-wire cast in so that the

spacer could be easily tied to a reinforcing bar. The blocks measured about 1-1/4 in. x 1-in. x 3/4-in. The mortar mix was equal parts sand and portland cement with sufficient water to make the mix workable (approximately a 4-in. slump). From past experience the author estimates that the mortar strength was greater than 6000 psi.

#### Monolithic Wall, Specimen 1

Construction of Specimen 1 with the monolithic shear wall was similar to that of the frames. The reinforcement of the surrounding frame was identical to that of the frames described above. The reinforcing details are shown in Appendix B, Figure B-3.

Reinforcement. The wall reinforcement was placed before any concrete was poured (Figure D-8). The base and column reinforcement were erected as for a plain frame. Special spacer bars (#3 bars, 4-in. long) were tied to the top of the base beam steel at the appropriate spacing location for the vertical wall reinforcing bars. The vertical #3 bars were placed and tied at the center of these spacer bars. The bottom of the vertical bars rested on the bottom of the base form. While this detail would not be allowed in actual practice, the resting of bars on the bottom permitted much easier construction. The author considered that this deviation from practice would not alter the structural behavior. The direction of the bend at the top of the vertical bars was alternated.

Horizontal #3 bars were placed after the vertical bars were erected. While the vertical bars were located at the center of the wall, the horizontal bars alternated sides of the vertical bars as is standard practice. Each cross of vertical and horizontal bars was tied to assure proper dimensions after pouring.

It was noted that the bent portions of the horizontal bars touched the inner surfaces of the column hoops; therefore, the horizontal bars were set into the frame the maximum distance possible.

The base was poured after the wall steel was placed. Two weeks after the base was cast, the columns and wall was poured.

Beam reinforcing steel was tied in place rather than prefabricated outside the form because of the bends in the vertical wall bars. Beam and slab reinforcement were identical to that of the frame.

Formwork. Formwork for constructing the base of Specimen 1 was the same as that for the frames, but special forms were made for building the column, wall and beam. Figure D-9 shows the formwork of the column and wall. The column forms were made of nominally 2-in. thick boards screwed together, while the wall forms were of 3/4-in. plywood with 2 x 4 stiffeners. The column form was screwed to an edge stiffener of the wall form. Each side of the wall form was made of two plywood sections which were butted together. The beam form was tightly screwed and glued to the wall

form; the edge beam, beam, column and wall forms were all screwed together to assure correct dimensions.

Special spacer-ties were made to hold the interior faces of the wall form at a 3-in. spacing. Iron pipe with a 3/8-in. inside diameter was cut to 3-in. lengths. These pieces of pipe were placed at 12 locations between the wall forms in which 1/4-in. diameter holes had been drilled previously. Lengths of 1/4-in. diameter treaded steel rod were inserted through the holes in one plywood form, through the pipe, and out the hole of the opposite plywood form. With a small washer and nut on each end of the threaded rod, the forms were tightened together. The 3-in. length of pipe kept the wall forms apart while the treaded rod was designed to keep them from spreading.

Casting. The base was cast as for the frames. Before the wall and columns were placed, the surface of the base beam where the wall and column would join was cleaned and chiseled.

The column and wall were cast two weeks after the base. The top of the concrete surface was about 1/4-in. to 1/2-in. below the bottom of the beam; this surface was quite irregular, and it was not screeded.

The concrete was poured from the transit mix truck into a wheelbarrow which was raised to the level of the beam by a fork lift. The concrete was shoveled into the column-wall forms. A spud vibrator was pressed by hand against the column and wall forms to consolidate the concrete.

When the wall pour was nearly complete, it was noticed that the plywood of the wall forms had crushed beneath the washers of the spacer-ties and that the wall forms had bulged severely. On one side of the structure, the two-piece wall form had split at the butt joint; the screws of the 2 x 4 stiffeners had pulled out. Large clamps were fabricated to keep the forms from bulging farther. The concrete pour was completed.

When the forms were removed one week after the pour, the wall dimensions were measured. The center of the wall was about 5-in. thick while the edge boundaries remained 3-in. thick. The one side of the wall where the form had separated seemed to have bulged somewhat more than the other side. Because the connection boundaries were the correct dimensions, it was decided that the structure remained a useful test specimen.

The beam was cast two days after the wall pour while the wall and column forms were still in place. The top surface of the wall concrete was cleaned but not chiseled before the beam was poured. The surface was very rough with irregularities as great as 1/2-in. The top surface of the beam was screeded but not troweled.

About one month after the beam was cast, the stub columns were cast.

#### Cast-in-Place Wall - Specimen 3

Specimen 3 was constructed by setting reinforcement within an existing reinforced concrete frame and casting concrete within the

frame. The frame was constructed as discussed above. The reinforcement design is shown in Appendix B, Figure B-4.

Reinforcement. The infilled wall was connected positively to the surrounding frame by using #3 dowels grouted into the frame as shown in Figure D-10. Dowel spacing was the same as the spacing of the wall reinforcement of Specimen 1.

Installation of these dowels was an important construction procedure because it determined the capacity of the frame-wall connection. Holes, 3-3/4 in. deep were drilled into the frame beams and columns using a 5/8-in. diameter termite drill bit and rotary drill. The termite bit had a hollow core; drilling with this type bit was easier than with the standard, solid shaft masonry bit. Once drilled, the holes were cleaned by blowing them out with dry air and by scraping the sides and bottom with a small chisel.

A neat epoxy cement (Sika brand Colma-Dur-Gel) was used to grout the #3 reinforcing bars into the frame. Dowels were grouted into each separate member of the frame on a different day so that the wet epoxy bond of one set of bars would not be disturbed by further construction. So that the epoxy did not set before it was placed, a single 8 oz. cup of the epoxy was mixed and poured at a time. After mixing, the epoxy was poured in a caulking gun from which it was shot into the holes. For each dowel, epoxy was spread on the bar over the 3-3/4 in. length to be embedded; this insured

that all crevices around the bar deformations were filled and coated (Figure 11). Slightly different epoxy techniques were required for the base, column and beam because their hole orientations were vertical downward, horizontal and overhead vertical upward, respectively.

For the base beam, epoxy was squeezed from the caulking gun and allowed to dribble down in the middle of the hole until the hole was two-thirds full. The pre-coated dowel was inserted gently with an up-and-down and a rotary movement. When the bar touched bottom the extra epoxy was cleaned from around the hole, the bar was secured in a vertical position, and it was allowed to cure undisturbed.

For the columns, a short piece of masking tape was placed half-way over the hole to act as a dam before any epoxy was poured (Figure D-12). The spout of the caulking gun was inserted into the hole; as epoxy was injected into the hole, the spout was slowly withdrawn until the hole was full. The coated dowel bar was quickly twisted into the hole (Figure D-13). Excess epoxy was removed; the hole was taped closed so that the epoxy would not ooze out (Figure D-14). If a bar was not inserted quickly enough, epoxy flowed from the hole and the hole had to be refilled. Two times when bars were being inserted, large bubbles were produced which implied that the hole was not filled. In these cases, the bar was withdrawn and the hole was refilled. After satisfactory installation, the bars were secured horizontally.

Overhead installation for the top beam was more difficult. Heavy duct tape was secured over the holes; the tape was slit at the hole (Figure D-15). The spout was inserted through the slit and epoxy injected until the hole was full. A coated dowel bar was quickly twisted through the slit, excess epoxy removed, and molding clay jammed around the bar (Figures D-15, D-16). The clay prevented the epoxy from running out the hole. The dowel was secured in a vertical position.

After the epoxy had set, any tape and clay surrounding the holes were removed. The frame's interior was chiseled to provide a rough surface for bonding to the infilled wall; roughness depth was about 1/4-in. (Figure D-17).

Wall reinforcement was tied to the dowel bars (Figures D-18, D-19). Ninety degree hooks were used to insure adequate bar anchorage.

Formwork. The plywood formwork for this cast-in-place wall was essentially the same as that used for the monolithically cast wall. One side the form covered the complete frame opening (Figure D-18); sheet metal strips were nailed around the edge of the form to compensate for slight irregularities of the frame. The second side of the form was in two sections in order to facilitate concrete placement (Figure D-20). The second side extended to within three inches of the bottom of the top beam; this gap allowed

room for concrete placement. The two sides of the form were held 3-in. apart by ties made of 1/4-in. threaded rod spaced on 18-in. centers.

Casting. The standard concrete mix #2 was used to cast the wall (Appendix C). With the first section of the form in place the concrete was shoveled easily into the 12-in. space. The second piece of the form was positioned and pouring was continued through the 3-in. top gap. Concrete was cast up to the top of the second form; the 3-in. gap was left open. The concrete was vibrated externally by holding the end of a spud vibrator against the form.

The following day, the 3-in. gap at the top was filled using a drypack mortar (Figures D-21, D-22). The drypack mix is listed in Appendix C; it was mixed in a wheelbarrow at the site and placed by hand.

Two weeks after casting, the forms were removed.

#### Single Precast Panel, Specimen 4

Specimen 4 was built with a frame constructed as described above and with a single precast panel which was mechanically connected within the frame. Design drawings for the panel and panel-frame connector are given in Appendix B.

Panel. The single panel measuring 51 in. x 95-1/4 in. x 3 in. was cast flat on a level concrete floor in a plywood form as shown

in Figure D-23. Mortar chairs spaced the #3 reinforcing bars in the center of the wall. The vertical bars were lapped 3 in. on and were welded to the embedded panel plates (Figure D-24). Figure D-24 also shows the shear plate connectors welded to the panels plates. Wood dams were placed below and on top of the panel plate so that the 5 in. wide plate would be embedded 3 in. into the extended 2 in. outside of the concrete panel.

Also shown in Figure D-23 were two 3 in. thick wood blocks placed near the top and center of the panel. These formed holes in the panel which were necessary for later construction procedures.

Wet concrete was shoveled in the form, screeded and steel troweled. Wet burlap and plastic sheets were placed over the newly cast panel. Forms were removed three days after casting; the panel was kept moist for five days.

Panel-Frame Connector. The panel-frame, ear plate connector is shown in Figure D-25. The 1/2-in. x 1-1/2 in. x 3-in. ear plates were first welded to the 1/2-in. x 3-in. x 47-1/2 in. base plates. Holes of 3/4-in. diameter were then drilled in the base plate.

Positions for drilling anchor holes into the base beam and top beam were laid out by using the drilled ear plate connectors as templates. Four 47-1/2 in. connectors were used within the frame. For each connector location, two 3-7/8 in. deep holes were drilled into the beam. The 5/8 in. wedge anchor bolts were sledge hammered into those cleaned holes. The connectors were placed over the anchor

bolts and were secured with nuts. The remaining holes were drilled 3-7/8 in. deep into the frame; the in-place connectors assured that all holes would be located correctly. No steel reinforcement was encountered in the drilling. All holes were drilled using a 5/8-in. termite bit and 3/4-in. rotary drill. Holes were cleaned by blowing them out with dry air. The remaining anchor bolts were hammered into the holes, and their washer and nuts placed and secured with a torque of about 70 ft. lbs.

Panel Erection. The panel was lifted and placed within the frame using a fork-lift truck (Figure D-26); forks were placed through the holes formed in the panel. C-clamps held the panel plate tight against the ear plates; the maximum gap between any part of any ear plate and the upper or lower panel plate was about 1/16-in. Ear plates were welded to panel plates by a professional welder; the connection is shown in Figure D-27.

#### Multiple Precast Panel Wall, Specimen 5

Specimen 5 was built with a frame constructed as described above and with six precast panels which were mechanically connected within the frame. Design drawings for the panels and panel-frame connector are given in Appendix B. The panel-frame connectors including concrete anchor bolts were the same as those for Specimen 4.

Panels. The six panels were formed next to each other in positions that corresponded to their future erected positions (Figure D-28). The panels were cast flat on a level concrete floor. A single large plywood sheet was used as the form base; 1-1/2 in. x 3-in. boards separated the panels.

Figure D-29 shows the top of panels #5 and #6. The panel-to-panel connector plates were held off the bottom of the form by 1-in. x 1-1/4 in. x 4 in. wood blocks, which made the space for welding the panel-to-panel connectors together. Also shown are the vertical #3 bars which were lapped 3 in. on and welded to the panel plate, the shear connector welded on the panel plate, and #4 horizontal bar welded to the panel-to-panel connector plates, the 45° auxiliary #3 bars welded to the far side of the panel-to-panel connector plates, and the strain gages epoxied to the vertical bars.

As the concrete was shoveled into the forms, special care was taken to push concrete under the embedded panel plate. The concrete was vibrated with a spud vibrator, then screeded and steel troweled. The panels were covered with wet burlap and plastic sheets. Forms were removed three days after casting; panels were kept wet a total of five days.

Panel-Frame Connector. The ear plate connector fabrication and anchor bolt installation were identical to that of Specimen 4.

Panel Erection. The author and two assistants lifted the individual panels into position as shown in Figures D-30 and D-31. Wood blocks were used to space correctly the panels between top and bottom beams, and small plywood shims helped to gap the panels 3/8-in. between columns and 1/4-in. between panels. C-clamps held the panel plates to the ear plates. A professional welder later welded the plates together.

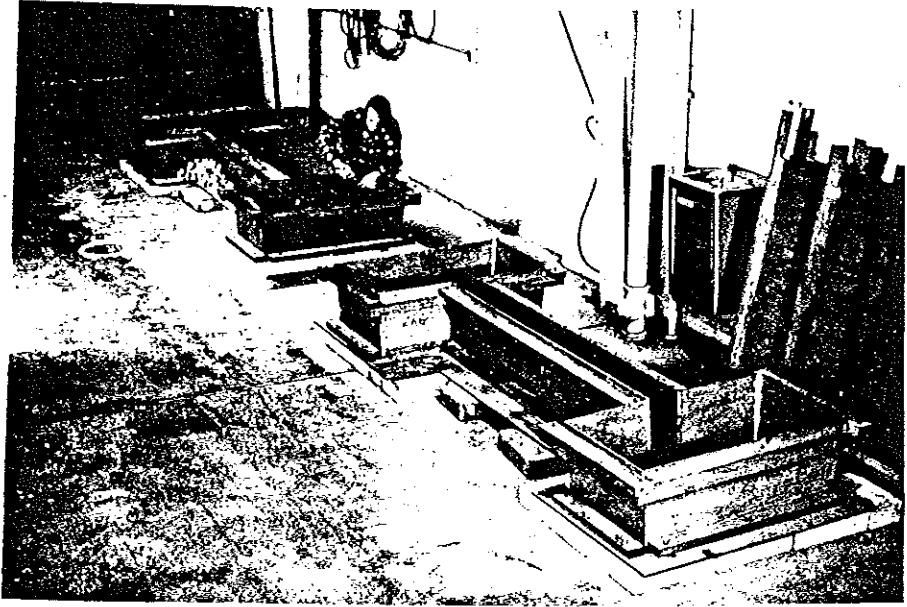


Figure D-1. Plywood forms for base of specimens.

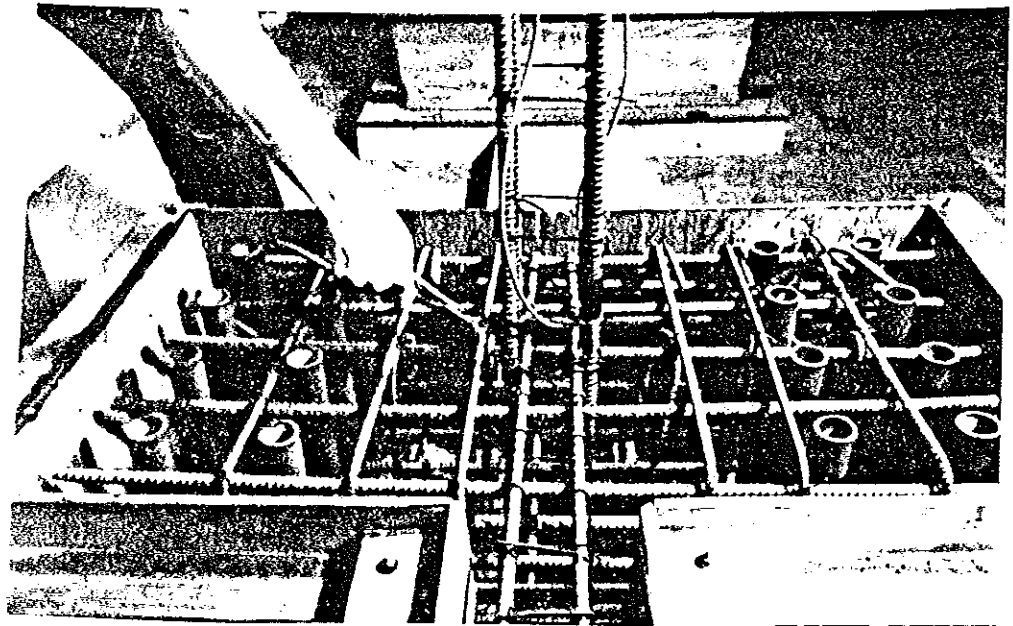


Figure D-2. Footing reinforcement and cardboard tubes for forming holes for hold-down bolts.

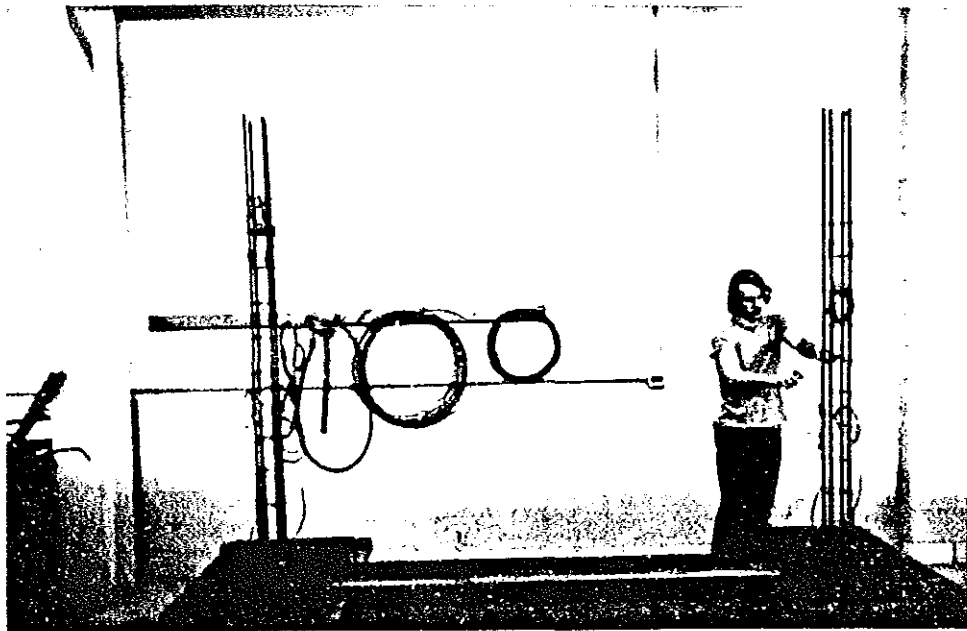


Figure D-3. Erection of #5 column bars.

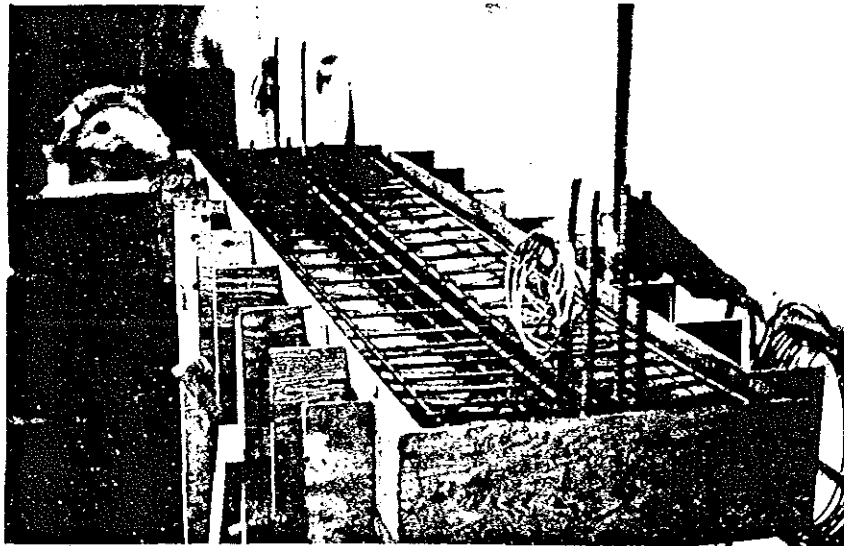


Figure D-4. Reinforcement layout for top beam and slab.

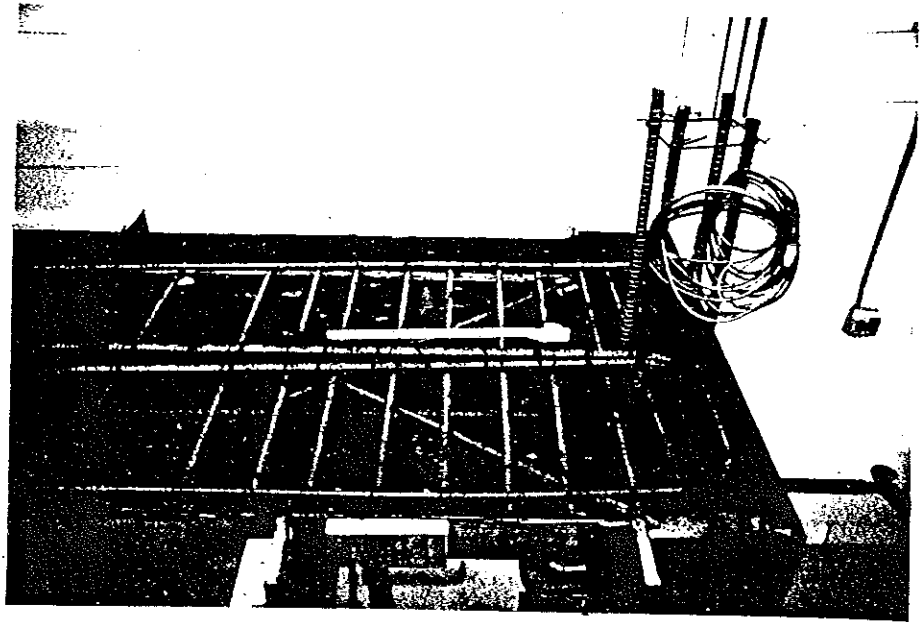


Figure D-5. Detail of reinforcement near edge beam.

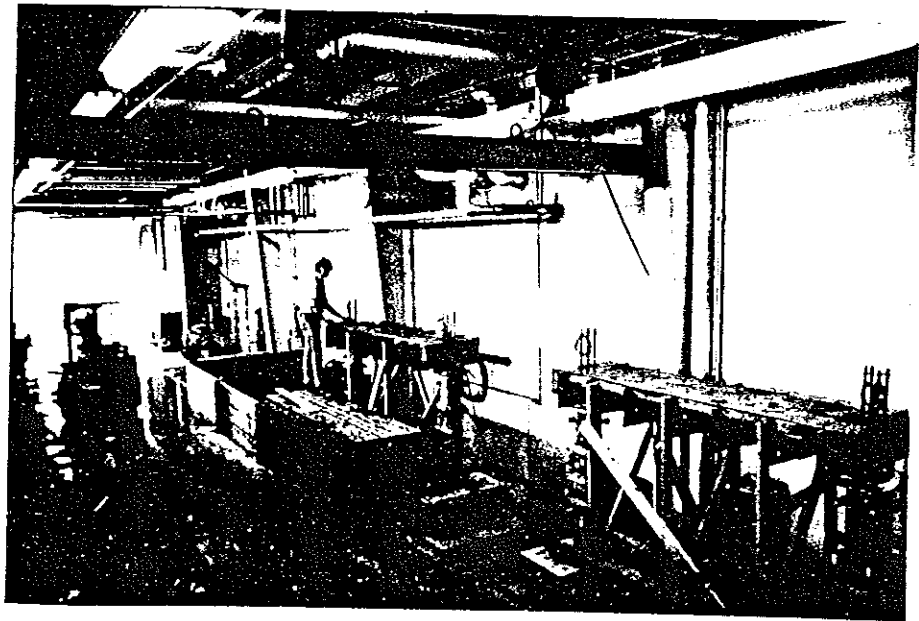


Figure D-6. Casting of the top beam.

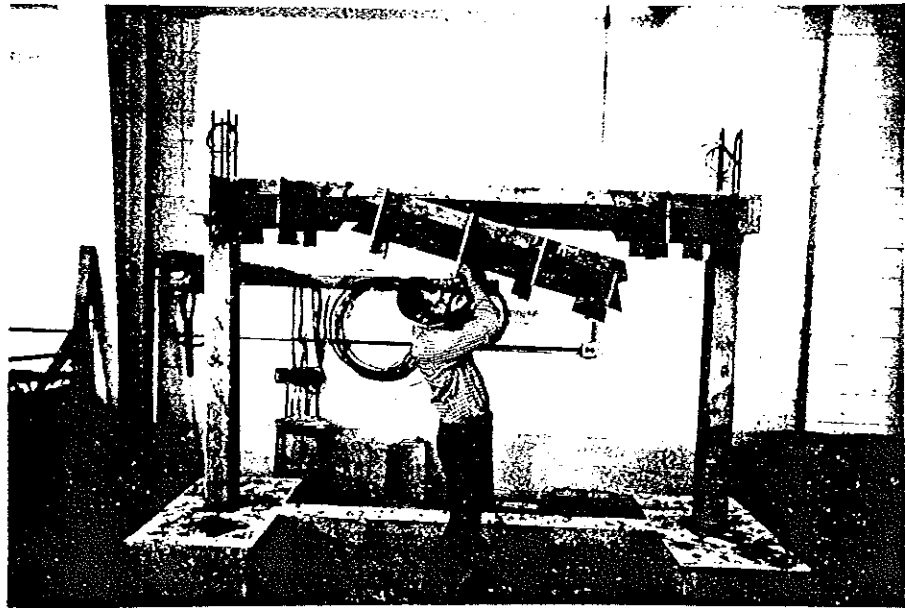


Figure D-7. Removing segmented beam form.

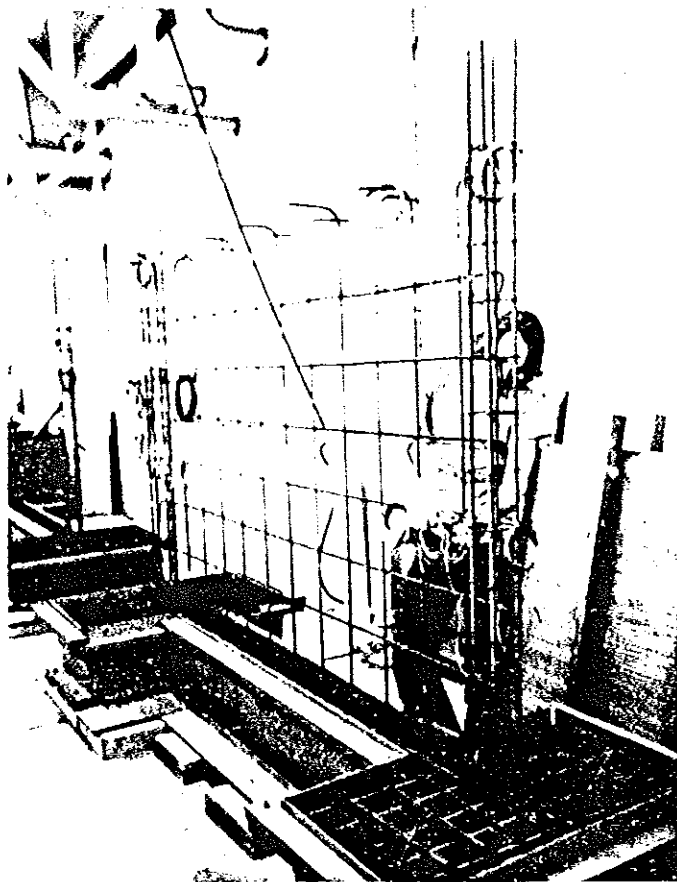


Figure D-8. Placement of reinforcing for Specimen 1.

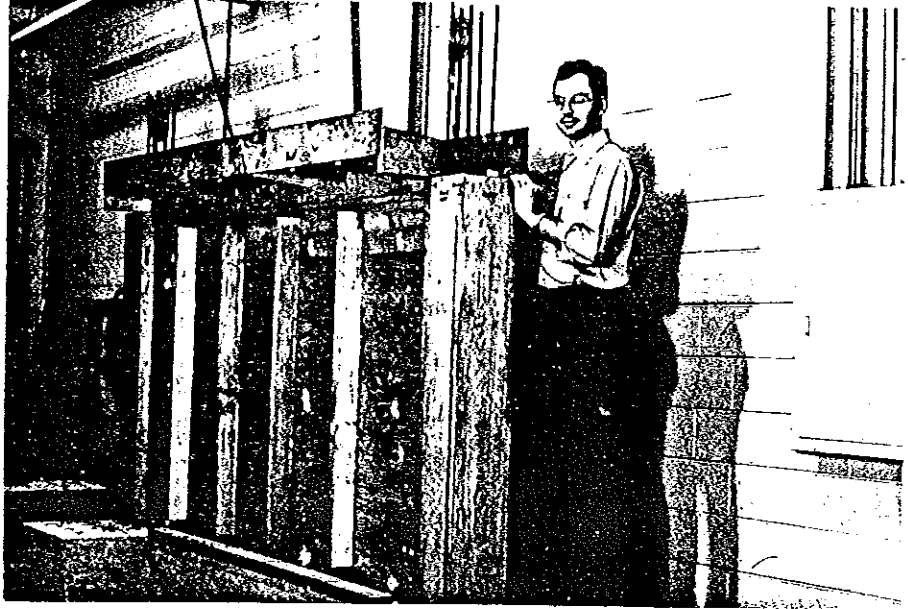


Figure D-9. Forms for the columns and wall of Specimen 1.

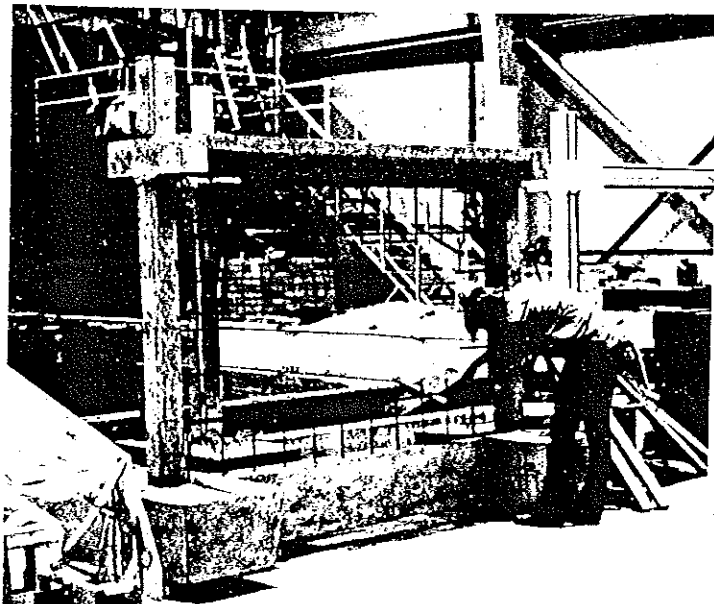


Figure D-10. Dowel bars epoxied into frame, Specimen 3.



Figure D-11. Spreading epoxy on dowel bar.



Figure D-12. Tape used as dam over hole in columns.



Figure D-13. Twisting dowel into epoxy filled hole in column.

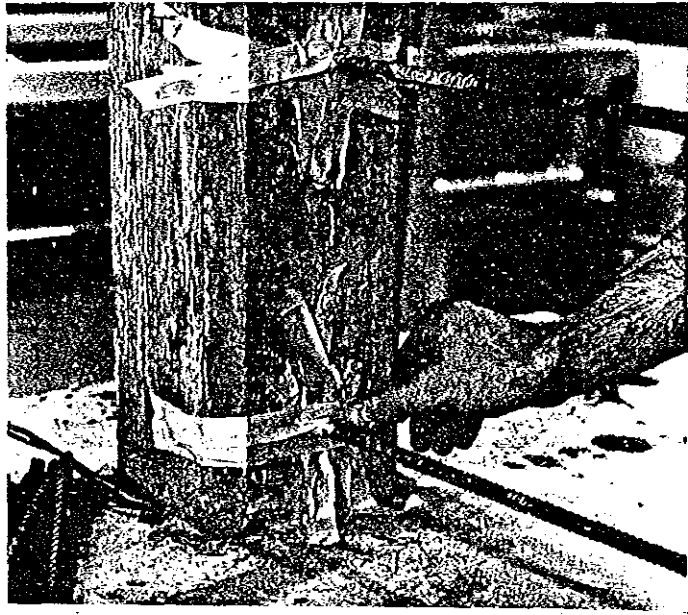


Figure D-14. Taping hole closed to retain epoxy.

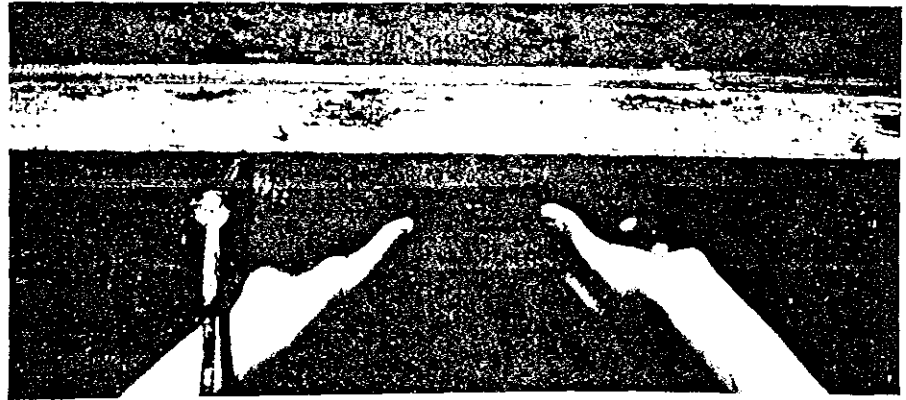


Figure D-15. Slitted duct tape was placed over hole in the top beam.

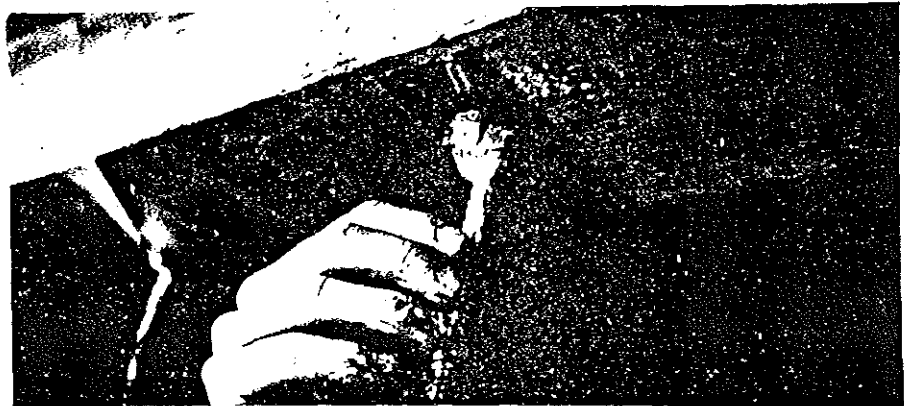


Figure D-16. Placing dowel in epoxy-filled hole in the top beam and then packing with clay.

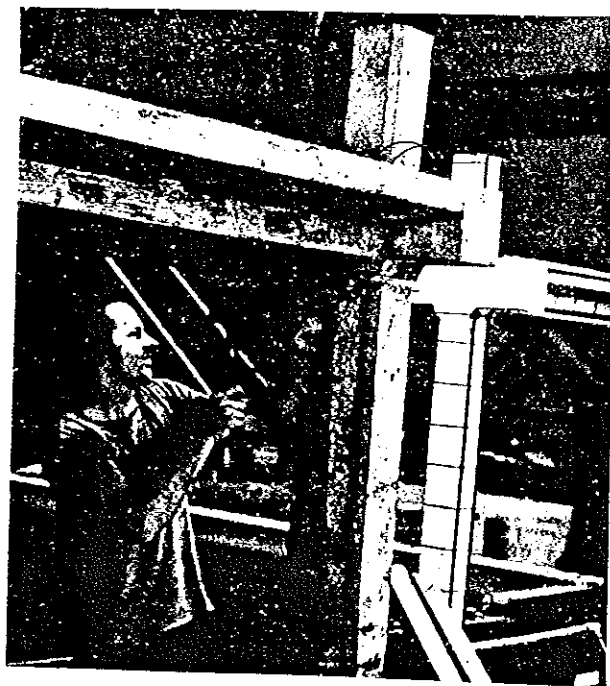


Figure D-17. Chiseling frame for better bond.

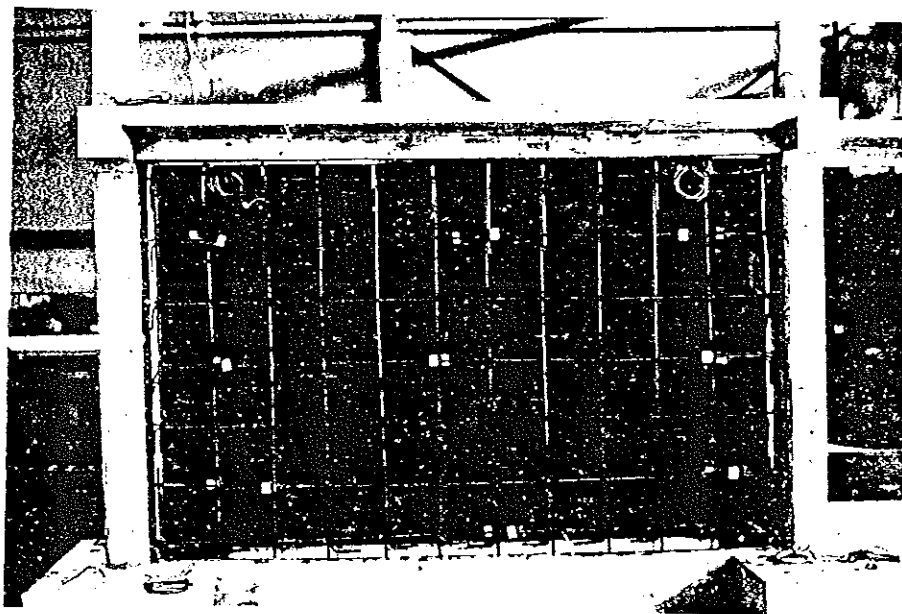


Figure D-18. Wall reinforcement for Specimen 3.

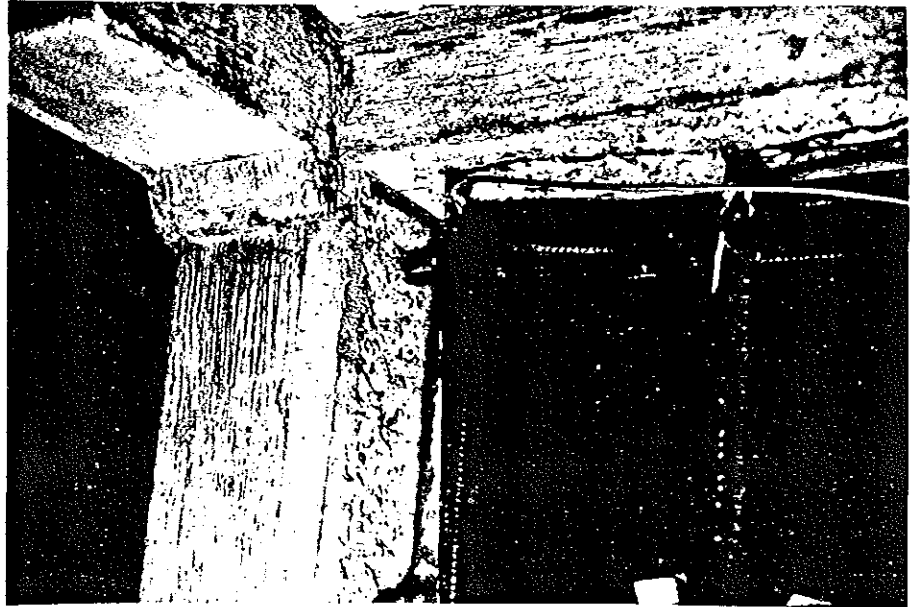


Figure D-19. Detail of top beam-column joint showing 90° hooks, strain gaged dowel bars, and roughened frame concrete.

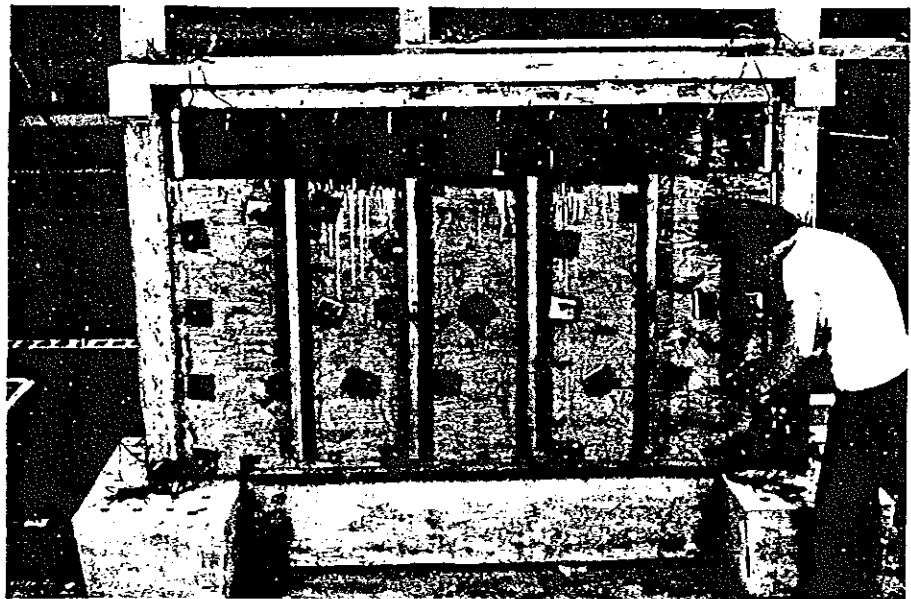


Figure D-20. Forming infilled wall, Specimen 3.

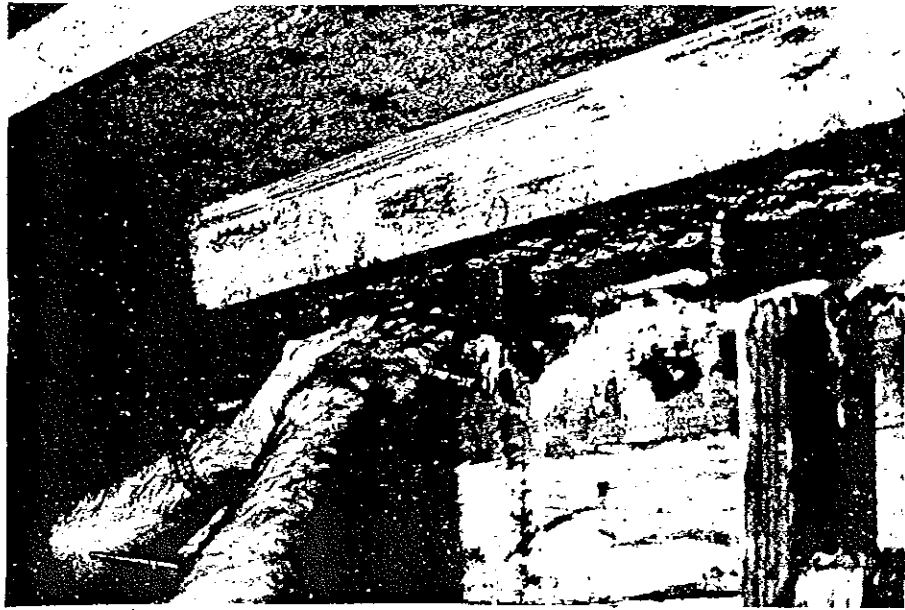


Figure D-21. Hand placing drypack concrete in 3-in. gap at top of infilled wall.



Figure D-22. Packing and smoothing drypack.

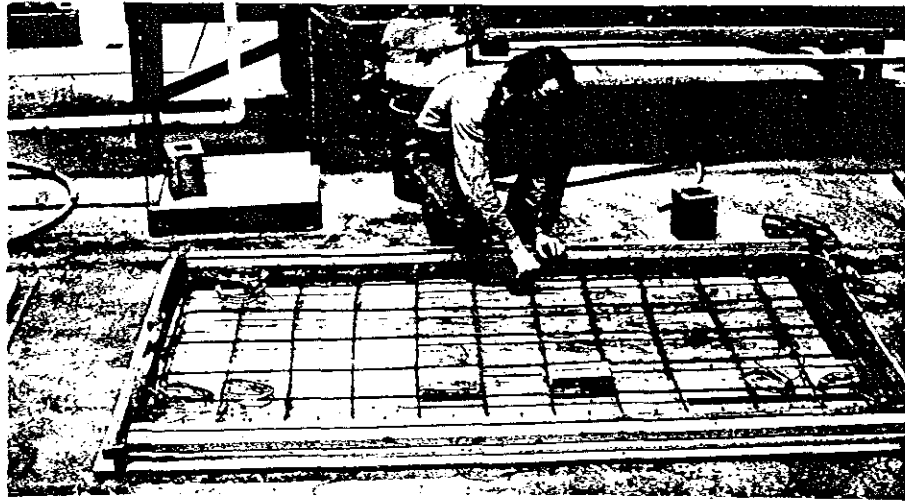


Figure D-23. Formwork and reinforcement for single precast panel, Specimen 4.

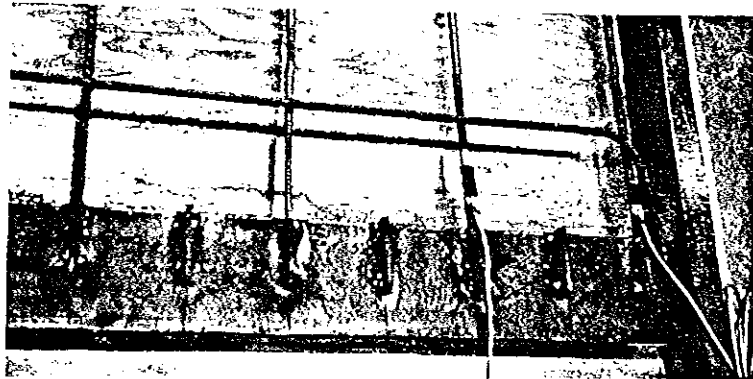


Figure D-24. Vertical bars and shear plate connectors were welded to embedded panel plates.

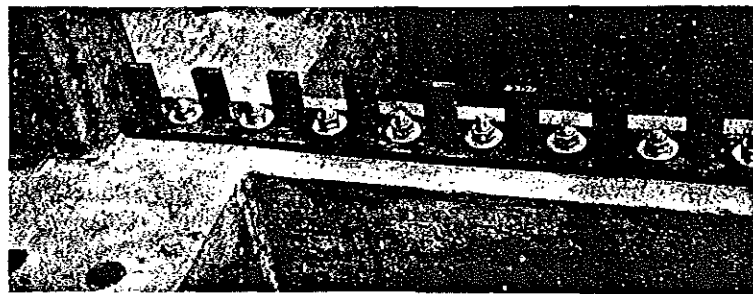


Figure D-25. Panel-to-frame connector bolted to base beam, Specimen 4.

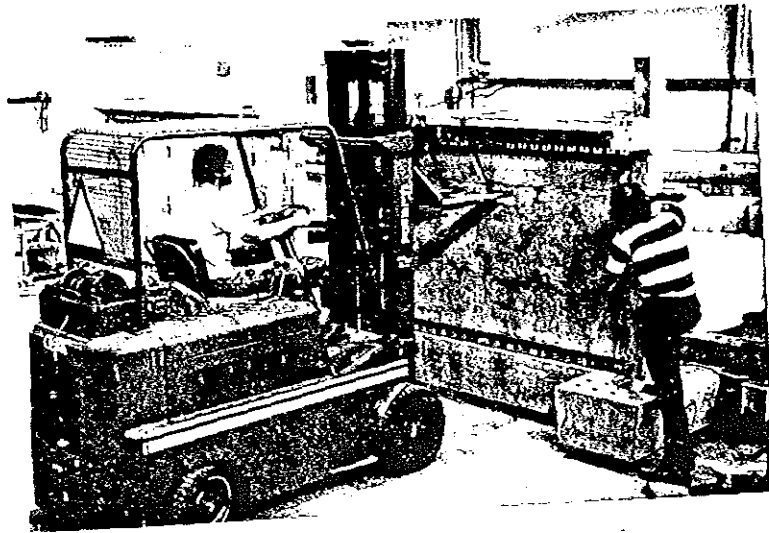


Figure D-26. Erection of single precast panel using fork-lift truck.

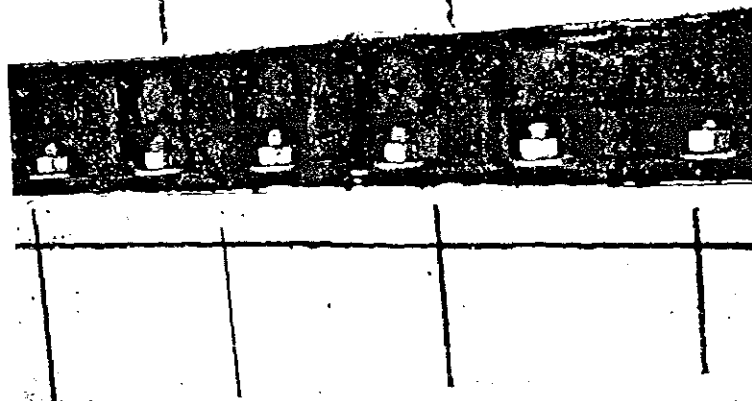


Figure D-27. Ear plates welded to panel plate near center of panel.

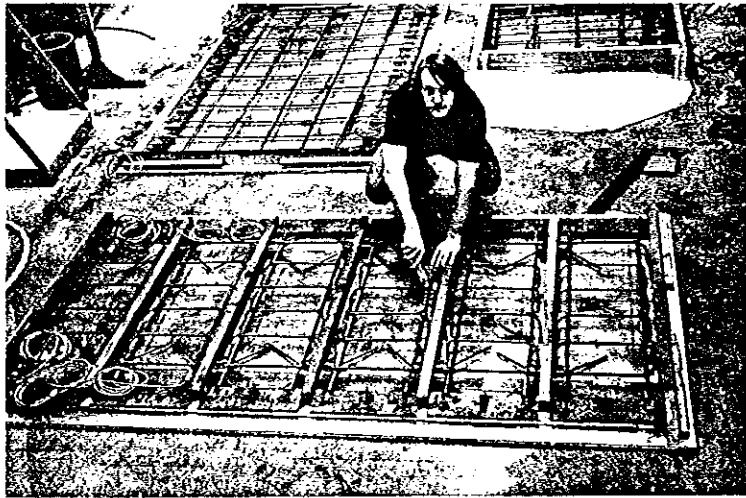


Figure D-28. Formwork and reinforcement layout for the six precast panels of Specimen 5.

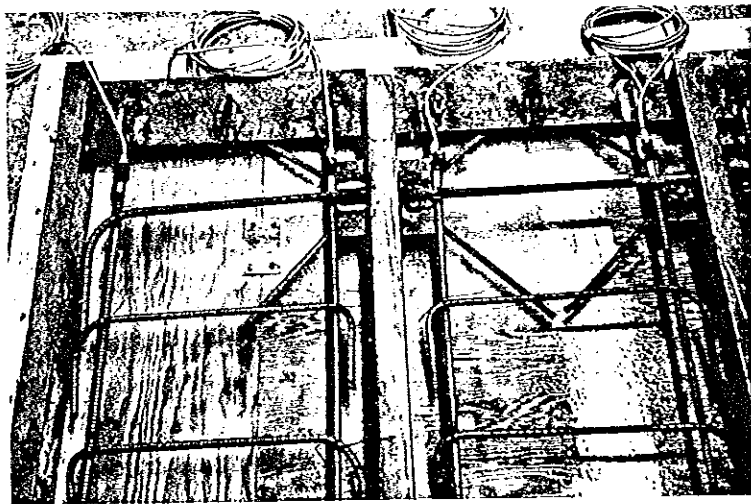


Figure D-29. Backside and top of panels #6, left, and #5, right.

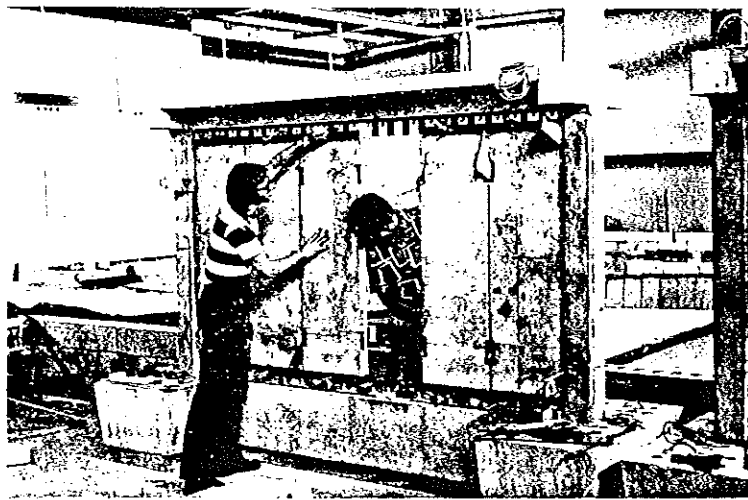


Figure D-30. Positioning of panels in Specimen 5.



Figure D-31. C-clamps used to hold panels prior to welding.

## APPENDIX E

### EPOXY GROUTED REINFORCING BARS - PULLOUT TESTS

#### Introduction

Eleven pullout tests were performed to determine the adequacy of anchorage of #3 reinforcing bars epoxied into holes drilled in existing concrete. The bars were grouted vertically into holes of various diameters and depths. The purpose of the tests was to determine an anchorage which developed the ultimate strength of the #3 dowel bars used in Specimen 3 and which minimized construction effort. The tests were necessary for three reasons: (1) little previous research had been conducted on reinforcing bars epoxied into drilled holes so epoxy anchorage design guidelines were considered too limited; (2) to drill holes of as large a diameter as recommended by the epoxy manufacturer (Sika Chemical Corporation, 53) would have required construction equipment larger than available at the University of Michigan laboratory; and (3) to satisfy development length requirements of the American Concrete Institute (5) would have required holes drilled to depths greater than the column widths and beam depth. Test results showed that the ultimate strength of the dowel bars could be developed eventhough the requirements of the epoxy manufacturer and ACI-318-71 were not satisfied; the results provided evidence for variance with current construction requirements.

A more detailed discussion is given below of the current state-of-the-art of concrete epoxy anchorages and pullout tests, and of the requirements of the epoxy manufacture and ACI-318-71. Thereafter follows the description of the pullout tests and a discussion of the

results.

#### Background

The state-of-the-art of bond and pullout tests were studied to insure that the limited number of pullout tests properly evidenced bond strength and to determine if other anchorage techniques may be superior to epoxy bonding. Little published information is available concerning the strength of reinforcing bars grouted into existing concrete by use of epoxy or other cementing material. One series of tests on epoxy grouted reinforcing bars was performed by Strand (60). He conducted a small series of pullout tests in connection with the rehabilitation of the Kaiser Hospital following the 1971 San Fernando Earthquake. Reinforcing bars were epoxied into holes drilled into an overhead floor slab. A caulking gun was used to fill the holes with epoxy; tape was placed over the holes, and the bars pushed through the tape for embedment. Pullout tests were conducted using two hydraulic jacks and a beam grip. The area immediately surrounding the bar was not confined by the jacking arrangement. The test series is summarized in Table E-1. Hole depths were selected on the basis of code requirements. These tests showed that all bars attained their ultimate capacities; the embedment depths given in Table E1 proved satisfactory.

Conrad (29) and Richard (50) tested the capacity of bolts anchored in holes using portland cement grout. In Conrad's tests holes were drilled into individual concrete blocks. The hex head end of  $1/2$ -in. diameter bolts were placed at the bottom of the holes, and the holes were filled with either a Type 1 portland cement grout, a non-shrink

cement grout or a polymer resin plus portland cement grout. Hole depths were 3 in., and hole diameters were twice the bolt diameters. A universal testing machine was used to pull the bolts; the block was laid flat against one head. Both the regular portland cement and the polymer resin grout showed poor bonding to the existing concrete; all bolts pulled out. The nonshrink grout was superior; it developed over twice the capacity as the portland cement grout. Conrad also tested the bolts in direct shear and found the nonshrink grout best, although the other grouts performed satisfactorily. He reported that in pull-out and shear, Phillips self-drilling mechanical anchors developed loads over 50 percent greater than the nonshrink grout.

Richard (50) reported on tests where 1-in. diameter bolts were anchored into drilled holes using a portland cement grout. Bolts which were grouted into holes 2-1/2 in. diameter and 8-in. deep failed after attaining their ultimate stress of 57,000 psi. Bolts embedded 5-in. and 6-in. failed by pulling out.

Other information concerning the anchorage of reinforcing in concrete has been limited to studies of bars cast in concrete. This information is important in relation to the current study of drilled-in/epoxied anchorages because it provides a reference of comparison both for the anchorage capacity and for the methods of determining that capacity. The state-of-the-art of cast in bars has been documented by the American Concrete Institute (8). Previous research work has concentrated on studying the bonding characteristics of deformed reinforcing bars in concrete beams; both pullout tests and beam flexural tests have been used in these studies (8, 25, 40). The

standard pullout test utilized a bar cast in a concrete block. The block was mounted flat on one head of a universal testing machine while the bar was pulled with the other head. The surface of the block was under uniform compression; only a small area around the protruding reinforcing bar was not loaded. Bar slip data was recorded at both the loaded end of the bar and at the unloaded end which extended slightly through the block. Loaded end displacement was found to be independent of the length of embedment in many pullout tests (40); unloaded end slip generally was used to quantify slip failure criterion.

Simple span and cantilever span beam tests showed that for small bar sizes (#4 bars) the pullout tests gave the same bond stress results as did the beam tests. For larger size bars the beam tests gave lower ultimate bond stress capacities than did the pullout tests (8, 25, 40).

Modified pullout tests have been developed so that the stress in the specimen more closely resembles that in a beam (44). Dynamic, repeated loading tests using this modified pullout specimen have shown that the bond capacity was not adversely affected by repeated loading less than 80 percent of the ultimate capacity (44).

A series of pullout tests, which closely resemble the tests of grouted bars, were conducted to compare the anchorage of straight and hooked reinforcing bars (37). The bars were cast vertically in large concrete slabs measuring about 16 feet square and 5 feet thick. The bars were pulled using a center-hole hydraulic jack which rested on the slab surface. Deformations were recorded at a reference point on

the bars; displacements at the slab surface were calculated based on assuming elastic behavior of the steel bar. A principal conclusion of the study was that anchorage values for Grade 60 reinforcement were greater than the values specified by Section 918 (h) of ACI 318-63 (4) for cases where splitting was prevented. Further, smaller bars developed higher steel stress than larger bars at the same loaded-end displacement and for the same relative embedment; smaller bars showed a higher pullout stiffness.

#### Epoxy Manufacturer Requirements

Sika Chemical Corporation, manufacturer of the epoxy used in this study, recommends epoxy types, hole sizes and construction techniques for reinforcing bars and bolts which are to be anchored into existing concrete (53); yet the corporation did not make available to the author any test data on the strength of bars or bolts epoxy grouted into holds drilled in concrete. Sika recommends using either Colma Dur Gel or Sika Dur Hi-Mod epoxy for reinforcing bar grouting applications where the bars are to be mounted in hole drilled horizontally or vertically overhead. Less viscous epoxies may be used in holes drilled downward. The epoxies may be used neat, or quartz aggregate may be added to extend the amount of grout, to increase its modulus, and to decrease its shrinkage. For holes only slightly larger than the bar diameter, a neat epoxy grout is recommended. Sika recommends an embedment depth of at least 10 bar diameters ( $10 d_b$ ) and a hole diameter 1/2-in. in diameter larger than the reinforcing bar diameter. The epoxy may be placed in the hole before or after the bar is placed; the bar should be rotated slowly to insure wetting of all areas of the

bar.

The tests by Strand (60) noted above satisfied the manufacturer requirements and the results showed that the bar ultimate strengths were developed.

#### ACI Code Requirements

All the above research on cast-in-place anchorage was considered by the American Concrete Institute in developing the Building Code Requirements for Reinforced Concrete, ACI 318-71 (5). The basic development length ( $l_d$ ) for bars in tension is given by the formula in Section 12.5 as

$$l_d = \frac{.04 A_b f_y}{\sqrt{f'_c}}$$

where

$l_d$  = development length (in.)

$A_b$  = area of reinforcing bar ( $\text{in}^2$ )

$f_y$  = yield stress of reinforcing bar ( $\text{in}^2$ )

$f'_c$  = concrete strength (psi)

For bars with yield stress above 60,000 psi,  $l_d$  is required to be multiplied by a factor equal to

$$2 - \frac{60,000}{f_y}$$

But, a further requirement of the section is that  $l_d$  shall not be less than 12 in.

Development length in compression is given in Section 12.6 as

$$l_d = \frac{.02 f_y d_b}{\sqrt{f'_c}}$$

The requirements of ACI 318-71 satisfy the requirements of Section 2612, Uniform Building Code, 1973 Edition (63).

Specimen 3 material properties were used in the above formulas to calculate the development length requirements ( $f_y = 64,000$  psi and  $f'_c = 4,400$  psi). The tension formula gave  $l_d = 4.7$  in.; so the  $l_d = 12$  in. minimum gave the required embedment depth. This minimum satisfied the compression development length.

For construction of Specimen 3 fulfilling the Building Code Requirements would be impossible. Column thickness was 6 in. and top beam depth was 7 in. A straight 12 in. embedment was impossible. Therefore, a variance with Code requirements was necessary; a shorter embedment depth, development length, requirement was needed.

For rehabilitation of structures satisfying the Building Code Requirements would be difficult and costly. In making structural additions, added reinforcing typically has been anchored to the existing structure by drilling in holes and grouting reinforcing bars into the holes. This anchorage requires a straight development length;  $90^\circ$  or  $180^\circ$  hooks cannot be drilled. Costs and difficulty of construction increase for deeper holes and for larger diameter holes. Therefore, it would be desirable to minimize the size of hole, to embed reinforcement only so far as is necessary for developing the bar capacity.

#### Test Setup

Figure E-1 illustrates the test setup of a single specimen. Number 3 reinforcing bars, 24 in. long, were embedded vertically downward in holes drilled into a 12 in. thick reinforced concrete

slab measuring 5 ft by 10 ft. Hole depths and diameters varied. One hole of each size was drilled using termite type drills. Holes were cleaned by blowing with dry air. Depths were 1-1/2, 2-5/8, 3-3/4 and 4-7/8 in., which represented embedment lengths for #3 bars of 4, 7, 10 and 13 bar diameters ( $d_b$ ). Hole diameters were 1/2, 5/8 and 7/8 in. giving holes 1/8, 1/4 or 1/2 in. larger than the nominal bar diameter.

The reinforcing bars used were from the same batch as that used for the construction of the frame specimens. The average stress-strain curve for #3 bars is shown in Appendix C; the average yield stress was 64,100 psi. The concrete slab was constructed several years prior to these pullout tests, and the exact strength of the concrete was unknown. The author estimated the strength to be in excess of 3000 psi and the maximum size aggregate to be 3/4-in. In all cases the epoxy used to cement the bar into the hole was Sika Colma-Dur-Gel epoxy. The epoxy was mixed according to manufacturers instructions and was applied in a neat condition without addition of aggregate.

After the epoxy was mixed, it was placed in a caulking gun. The nozzle of the gun was inserted in a hole, and epoxy injected until the hole was about three-fourths full. Epoxy was spread on the reinforcing bar over the embedment length. This spreading assured that the epoxy surrounded all bar deformation. Next the bar was pushed into the hole and was turned gently and pressed in-and-out several times to assure that no large air pockets existed. The excess epoxy was removed from around the hole, and epoxy was leveled

to the surface of the concrete slab. The vertical bar was braced so that it would not fall, and the specimen was allowed to cure for five days before testing. All pullout specimens were fabricated in this manner.

The specimens were tested as shown in Figure E-1. A hollow-core hydraulic jack was placed over the embedment with the bar extending through the jack and the jack bearing directly on the slab. A load cell was placed between the jack and the prestressing strand grip used to hold the bar.

A dial gage accurate to 0.001 in. was located at the top of the bar to measure the total specimen elongation relative to the slab surface. The end of the grip was 15 in. above the slab; therefore the dial gage measured the elongation of the 15 in. of bar above the slab, the lengthening of the embedded part of the bar and the deformation of the epoxy and concrete within the core area of the jack (about 1-1/4 in. diameter).

#### Test Results

Load and total deflection measurements were taken throughout the pullout tests until the ultimate strength of the bar was achieved or until the bar pulled out of the embedment. Figures E-2 and E-3 show typical load-deflection results. Figure E-2 illustrates the response of bars with embedments of  $4 d_b$ ,  $7 d_b$  and  $10 d_b$  and with holes of 5/8-in. diameter. In Figure E-3 the deflection scale was changed to illustrate more clearly the stiffness of the specimens within the steel's elastic region; Figure E-3 shows results of specimens embedded to  $7 d_b$  but placed in holes of different diameters.

Results from the other tests closely resemble those shown and are not repeated here.

The three bars epoxied in 1-1/2 in. deep holes of 1/2, 5/8 and 7/8 in. diameter all pulled out. The epoxy failed in direct shear at the level of bar deformations. In holes of 1/2 and 5/8 inch diameter the specimens failed at a load below the bars' average yield load, 7.1 kips. For the 7/8-in. diameter hole, the bar sustained its yield load and maintained that load as the bar was slipping; the load then decreased with increasing displacement until the bar was extracted completely.

For all other bars with relative embedments of  $7 d_b$  and greater and with all hole sizes, the specimens failed by the bars reaching their ultimate tensile capacity. Some bars were ruptured to determine if the failure was in the grips or epoxy; the bars broke midway between the grip and epoxy.

After failure the top surface of the epoxy was examined. In cases where the bar pulled out the area around the hole was clipped slightly. Where the bar capacity was attained, the surface of the epoxy was cracked and spalled.

One test was conducted where a #3 bar was embedded 4-7/8 in. ( $13 d_b$ ) in a 5/8-inch diameter hole. The test results were identical to those of the bar embedded  $10 d_b$  in a hole of the same diameter.

#### Discussion

The loaded end deflection of the bar at the joint surface was computed for each test at a bar stress of 32,000 psi (one-half of the average yield stress). The calculated elastic deflection of the

15-in. bar extension was subtracted from the measured total deflection to give the loaded end deflection.

The deflections are listed in Table E-2. Bars embedded  $7 d_b$  and  $10 d_b$  had smaller loaded end deflections than bars embedded  $4 d_b$ . These calculated results would be expected because all bars embedded  $4 d_b$  pulled out; their anchorage at one-half the bar's yield load was not as stiff as that of the bars which did not pull out.

Previous to these tests, the author expected that the greatest loaded-end displacement would be found with the largest diameter holes because of greater shear deformation in the thicker epoxy joint; this behavior could not be established.

Because of the limited number of tests further conclusions relating to loaded end displacements cannot be made.

Holes only  $1/8$  in. diameter larger than the nominal bar diameter were not satisfactory because of difficulties in obtaining a well grouted hole; eventhough, bars embedded in the  $1/2$ -in. diameter holes developed their ultimate capacities. When bars were inserted into the epoxy filled  $1/2$ -in. holes, air bubbles were formed; the holes had to be re-grouted. Special care was required to eliminate air pockets in the epoxy joint. In larger diameter holes air bubbles did not develop, and special construction procedures were not necessary.

The  $7/8$ -in. diameter holes required considerably more effort to drill than the  $5/8$ -in. holes. Because drilling holes overhead would be required for dowelling bars in the top beam, the procedure requiring the least effort was desirable. The  $5/8$ -in. diameter holes were

easier to drill and developed the same anchorage strength as the 7/8-in. diameter holes. Therefore the 5/8-in. diameter hole was considered the optimum diameter.

### Conclusion

The following conclusions were drawn from the eleven pullout tests of #3 reinforcing bars ( $f_y = 64,000$  psi) grouted into holes drilled vertically in a concrete slab:

1. Bars with embedments of 7 bar diameters and greater developed their ultimate strengths.
2. Hole diameter was not found to be a parameter of major significance. A somewhat better connection was provided where the hole was at least 1/4-in. diameter larger than the nominal bar diameter.
3. The epoxy manufacturer's recommendations regarding embedment depth and hole diameter for epoxy grouting were found conservative.

### Application

Based on the above tests the author chose to use a hole depth of 3-3/4 in. ( $10 d_b$ ) and a diameter of 5/8-in. for the embedment of #3 bars into the frame of Specimen 3 for construction of the cast-in-place shear wall.

This embedment depth did not satisfy the  $l_d$  requirements of Sections 12.5 and 12.6 of ACI 318-71. But the test showed that this anchorage developed the ultimate capacity of the reinforcement.

The hole diameter was smaller than suggested by the epoxy manufacturer. But holes of 5/8-in. diameter provided as satisfactory an

anchorage as larger and simplified the construction procedure.

Table E-1

## Pullout Tests by Strand (60)

Bar Size	Embedment Depth (inches)	Relative Embedment $d_b$	Hole Diameter (inches)
#4	6	12.0	7/8
#5	8	12.8	1
#6	14	19.3	1-1/8
#7	17	19.4	1-1/4
#8	23	23.0	1-3/8
#9	28	24.9	1-1/2
#10	36	28.8	1-3/4
#11	44	32.0	1-7/8

Table E-2

## Computed Loaded End Displacement for Pullout Specimens

at Bar Stress of 32,000 psi

Embedment	Embedment Length (in.)	Loaded End Displacement (inch)		
		Hole Diameter		
		1/2-in.	5/8-in.	7/8-in.
4 $d_b$	1-1/2	.023*	.003*	.005*
7 $d_b$	2-5/8	.000	.003	.002
10 $d_b$	3-3/4	.001	.002	.001

\*bars pulled out.

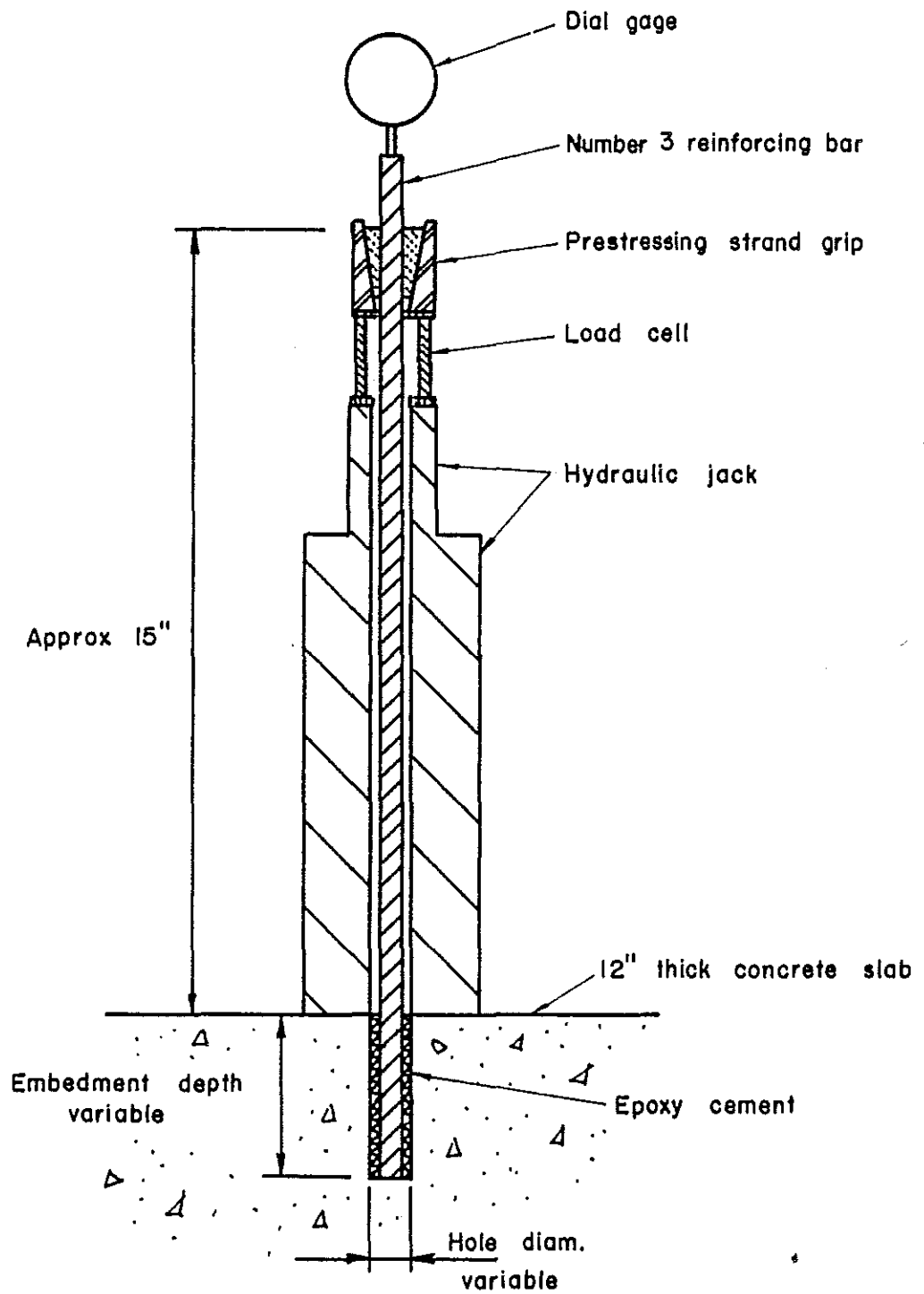


Figure E-1. Schematic diagram of pullout tests.

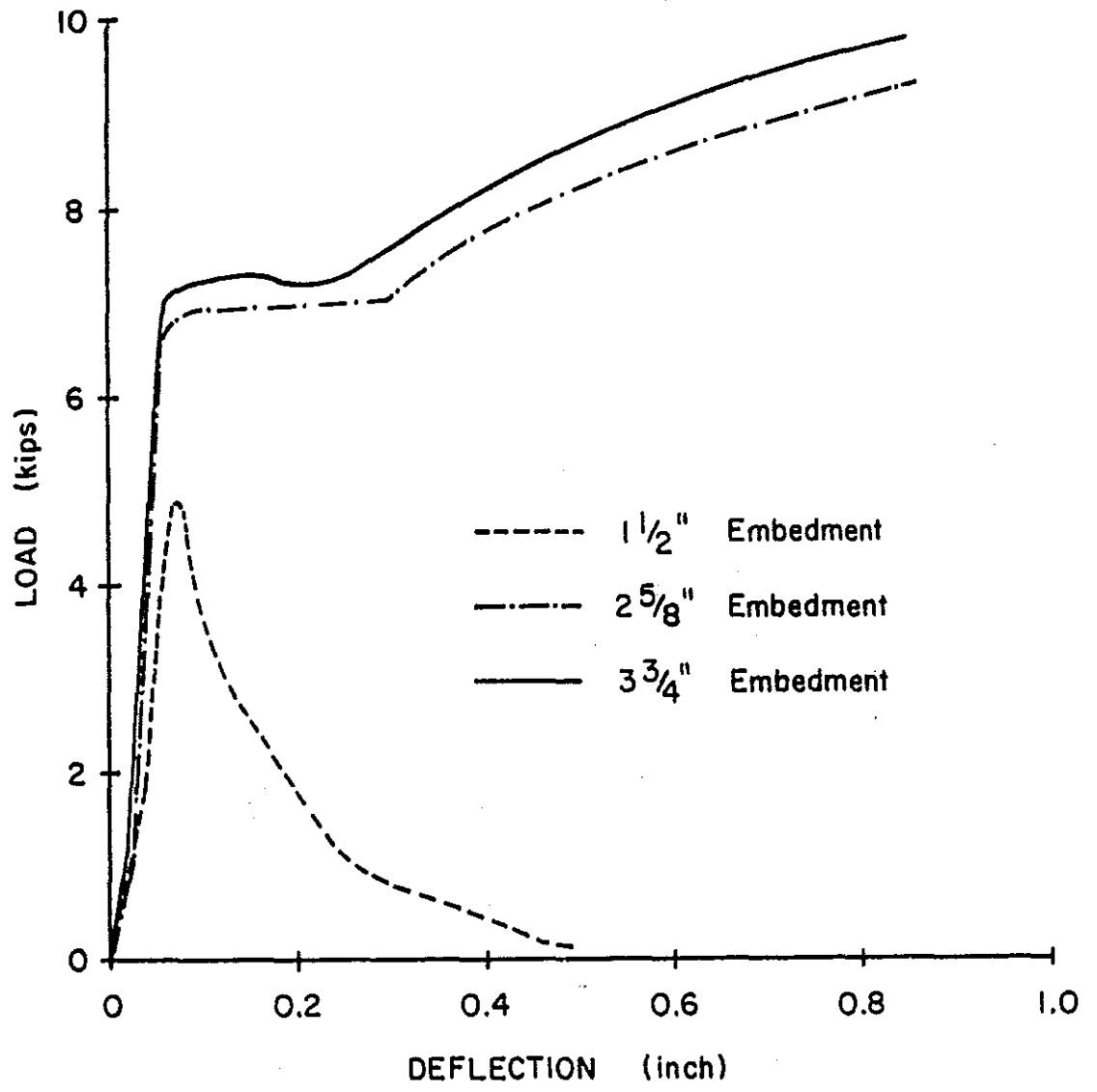


Figure E-2. Load-deflection response for pullout specimens of different embedment lengths epoxied into 5/8-in. diameter holes.

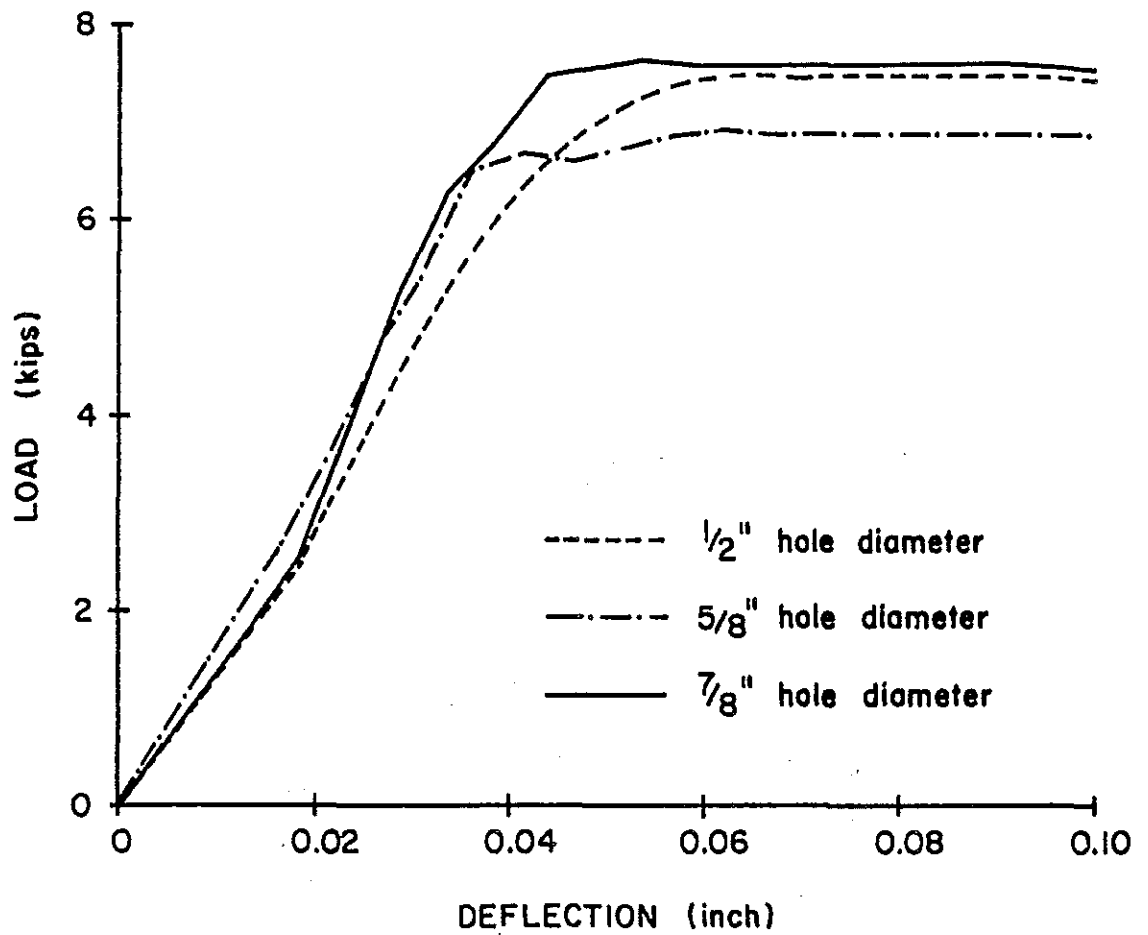


Figure E-3. Load-deflection response for pullout specimens epoxied into holes of various diameters with embedment lengths of 2-5/8 in.

## APPENDIX F

### TEST PROCEDURES AND RESULTS

The following are detailed discussions of the tests of each of the five specimens. Each test was slightly different because of the different structural character of each specimen, but a careful attempt was made for uniformity. The first test performed was of Specimen 1, the monolithic shear wall. This experiment was the first time the hydraulic jacks, test frame and some instrumentation was used; therefore, the test deviated somewhat from the "standard" test procedure described in the main body of this thesis.

Calculated lateral load capacities based on actual material properties are presented and are compared with experimentally determined capacities in Chapter 5 of the main body of this paper.

#### Specimen 1

Testing of Specimen 1 began by determining the compressive strength of the field cured test cylinders. Results of these tests are listed in Appendix C. The strength of the field cured specimens was approximately 13 percent less than that of the 28 day, moist cured cylinders.

The field strength of the wall concrete ( $f'_{cf} = 4990$  psi) and the actual yield stresses of the steel reinforcement were used to calculate the cracking, first yield and ultimate lateral loads. The calculated results are presented in Chapter 5.

### Set-Up

After the specimen was positioned in the test frame (Figure F-1), the tie-down bolts were inserted in the end-block foundations (Figure F-2). With the instrumentation in place, the test was begun using four 50 ton hydraulic jacks to apply the horizontal load (Figure F-3). It was determined after the first four deflection cycles that the four jack set-up was cumbersome and unnecessary (Figure F-4), and a two jack load system was incorporated (Figure F-5).

The four jack load system used two load transfer columns which bore against the edge beam (20 in. between centers of the 5-in. outside diameter columns). A 1/2-in. steel plate between the concrete and the transfer columns served as a bearing plate.

The two jack system incorporated several improvements over the four jack system. Large hinges were placed between the test frame and the 18-in. deep load-beam which held the jacks. These hinges allowed vertical movement of the jacks so that as the specimen deflected, the jack position would remain in about the same position relative to the top beam. A 2-in. thick iron bearing plate distributed the lateral load throughout the top slab and helped to prevent edge beam failure. Two sockets machined into the bearing plate matched with 1-1/4 in. steel balls which were fastened to the load cells. This ball and socket arrangement helped to assure proper location of the load and allowed relative rotation between the specimen and the jack/load cell system. Steel

shims were placed between the load beam and the jacks for correct horizontal positioning of the jacks. A 1/8-in. to 1/2-in. thick piece of plywood was placed between the 2-in. bearing plate and the concrete specimen in order to eliminate stress concentrations caused by an uneven concrete surface.

The centerlines of the two jacks were 16-in. apart. Test results indicated that the two-jack loading system did not induce concrete failure in the slab or in the upper wall or edge beam.

Instrumentation was set-up as discussed in the section "Instrumentation" in Chapter 2.

#### Deflection Sequence

It was planned that the beginning pre-yield loading cycles would be force controlled and based on the calculated yield load, while post-yield cycles would be deflection controlled. Figure F-6 illustrates the approximate deflection-time reversed cycle procedure used for Specimen 1. The planned sequence called for three load cycles to  $\pm 60$  kips, where + represents loading in one direction\* and - represents loading in the opposite direction. The following three cycles were to achieve the yield load,  $\pm 120$  kips. Further deflection cycles were based on the experimentally determined yield deflection.

---

\* In the University of Michigan laboratory the model structures were oriented and deflected in the north (-) and south (+) directions. In following front elevation photographs, the left side of the structure is the north side. Further, a north (-) deflection implies that the north column is under compression while the south column is under tension.

Cycles to  $\pm 0.1$  in.

During testing these planned load level cycles were modified. In the first loading toward the + 60 kip level, small horizontal tension cracks began appearing in the south column under a load of about 20 kips. At a load of 53.4 kips the wall cracked diagonally with a loud report. This "first" cracking load was selected as the maximum cycle load; the following two cycles were to this load. The maximum steel tensile strain reached 940 micro-in./in., about 54 percent of the yield strain. Figure F-7 shows the cracking at this load level.

Cycles to  $\pm 0.5$  in.

The following two and one-half cycles went to double the previous load,  $\pm 107$  kips. It was estimated that this would yield some of the column reinforcement. Maximum tensile strains at the base of the columns ranged between 1700 micro-in./in. and 1920 micro-in./in., or an average 104 percent of the yield strain. The tensile strain on the interior column bar was about 4 percent greater than on the exterior bar, a behavior exactly opposite from the linear strain pattern expected. With succeeding cycles the maximum strain increased slightly, about 50 micro-in./in.

The tensile strains at the base of the reinforcing bars within the wall adjacent to the north and south columns were either about the same as the strain in the column steel or sometimes greater than the column strains. The maximum strain in

these vertical wall bars was about 85 percent of their yield strain. Recall from Appendix C that the #3 wall reinforcement had a higher yield strain than the #5 column bars.

Maximum compressive strains were about half of the yield strains. During the first six load cycles, the neutral axis appeared to remain within the center portions of the wall. Figures F-8 through F-11 present the strain patterns at the bottom and at the top of the wall during the first cycle of load to  $\pm 107$  kips.

The average tensile strain in the south column during the first half load cycle (+ 106.9 kips) was 1750 micro-in./in., nearly the exact yield strain. During the second half cycle (- 106.1 kips) the average tensile column strain was 1860 micro-in./in., 6 percent greater than yield strain. The story deflection determined by LVDT's was + .51 in. and - .47 in. for the first and second half cycles. The deflection difference resulted because the structure slid along the base of the test frame. The average deflection for this 107 kip level was 0.49 in. Because this load produced maximum steel strains very close to the yield strain, the author considers this 107 kips and 0.49 in. deflection as the yield load and yield deflection. Future references are based on these values; deflection levels are relative to this yield deflection; the term DR represents the "Deflection Ratio", of actual deflection to yield deflection.

Figure F-12 illustrates the cracking after the cycles to  $\pm 107$  kips. During these cycles, the entire structure slipped along the test frame base as much as 0.2 in. each direction. This motion showed that the tie-down bolts were not adequately securing the specimen. Furthermore, direct, vertical tension cracks occurred in the base beam of the specimen, and the foundations developed large cracks as shown in Figure F-13. This slipping and foundation break-up was stopped by placing 7-in. thick concrete slabs between the specimen and the test frame. Wood and steel shims between the specimen and slab assured a snug fit with almost no movement.

Cycles to  $\pm 0.8$  in.

The next deflection cycles were originally planned for twice the yield deflection (2 DR, approximately 1.0 in.). The load was first applied in the north direction. Beyond -107 kips, the author noted that the structure's stiffness was decreasing. Suddenly, at approximately -150 kips, the south-east edge beam failed as shown in Figure F-14. The test was stopped.

Observation indicated that the wall, columns and beams were not affected by the edge beam failure. It was decided that the edge beam should be repaired and testing continued.

Broken concrete was removed (Figure F-15), additional vertical shear reinforcement placed, and forms erected. A mortar mix was used for the repair and was made of equal parts sand and Type III cement plus enough water to yield about a 3-in. slump. Three

test cylinders were also cast from this mortar; their average 28 day, moist cured strength was 6750 psi.

The test was continued about six weeks after the edge beam was repaired. Because the last recorded maximum deflection was - 0.8 in., cycles to that deflection were selected for the next three cycle sets. Thus as shown in Figure F-6, two and one-half additional deflection cycles were attempted to about  $\pm 0.8$ -in. (1.6 DR). Actual deflection cycles were to + 0.8 in. and - 0.4 in. The lower column and wall areas cracked significantly during these deflection cycles. At a load of about + 108 kips the south column gave evidence of a compression shear failure. Numerous small cracks occurred and a major diagonal crack extended from the bottom, south corner up through the column and into the wall. The north column showed large tension cracks. Yet the specimen continued to maintain increased load to the end of the deflection cycle, + 125.7 kips. Figures F-16 and F-17 show the cracking in the lower part of the wall at this load, the end of the first cycle to  $\pm 0.8$  in. The tension crack widths were about 0.15 in. for the north column and 0.12 in. for the north edge of the wall. The south compression column was severely damaged.

Figure F-18 shows the load-deflection results of the three cycles to  $\pm 0.8$  in. The additional loading and unloading sequence during the second half-cycle to + 0.8 in. resulted from fitting the concrete restraining slabs into position. Figure F-18 presents several important findings: (1) The maximum load of

the second half cycle (125 kips) was over 16 percent less than that of the first half cycle (approximately -150 kips). (2) The maximum loads continued to decrease with succeeding cycles, a 24 percent decrease in maximum load from the second half cycle to the fourth half cycle and then a further 18% decrease from the fourth to the sixth half cycle. Therefore, over the three cycles the maximum load decreased from 125.7 kips at + 0.8 in. deflection to 87.2 kips at + 0.8 in. deflection, which represents a 37.8 percent reduction.

Another feature illustrated by the curve is the change from a wide, flexure type hysteresis curve to the S shaped, shear type curve after the first cycle. The areas bounded by the curves of the second half cycle and the fourth half cycle were compared to determine the relative energy dissipated during each succeeding half cycle. The fourth half cycle dissipated 22 percent of the energy compared to the second half cycle. Besides the deterioration of maximum load and energy dissipation, the stiffness of the structure greatly decreased near the zero deflection point. Such softening is typical of shear sensitive structures.

The maximum compressive strain on the steel column bars was -1050 micro-in./in. during the first half cycle. Using a linear strain approximation, the maximum concrete compressive strain was -1280 micro-in./in.

Some cracking along the column bars under compression at the column base was noted after a column had been yielded in tension

during a previous cycle. Such cracking was evidence of bond failure along the column bars. Reduction in bond, the diagonal crack through the columns, and some concrete crushing apparently caused the deterioration in load deformation response.

After the first half cycle to  $-0.8$  in., most of the bottom strain gages became inactive; therefore, strain results were limited. Figures F-19 and F-20 show the strains for the lower and upper gages during the first half cycle to  $-0.8$  in. From Figure F-19 it is evident that a south column bar and a wall bar have yielded at the  $-142$  kip load level. That the strain in the other column bar decreased may have resulted because of crack spacing above or below the gage location. The compression strains vary little. The point where the interpolated strain lines cross the zero strain axis is at  $93.5$  inches from the tension face, or  $14.5$  inches from the compression face. This point did not vary with increasing load; that is, the approximate "c" distance remained constant at  $14.5$  inches. Figure F-20 illustrates that one of the wall bars was yielding in tension near the point of load application.

#### Cycles to $\pm 1.3$ inches

Figure F-21 shows the load deflection results for the three cycles to  $\pm 1.3$  in. and the final cycle to  $-2.6$  in. and  $+2.1$  in.

At loads greater than  $-88$  kips, significant cracking occurred along the reinforcement at the base of the north, compression column. No obvious concrete spalling or crushing was observed at the maximum  $-103$  kip load.

In the next half cycle, the maximum load at + 1.3 in. deflection was 76 kips. This maximum load was 26 percent less than that in the first half cycle. As the specimen was being loaded toward the south, further compression failure in the column was noted. The base of the wall was crushing between vertical bars about 38 in. from the north side. At the maximum load, the base of the wall had crushed to a distance 22 in. from the south, compression side. Figures F-22 and F-23 show the lower column segments under compression and tension at the maximum deflection of +1.3 in. during the second half cycle. The north column had not indicated any concrete crushing during the first half cycle; but when it was subjected to tension, concrete spalled.

With the next half cycle, the maximum northward load was -43.7 kips, which was 58 percent less than the preceding northward maximum. The maximum southward load during the fourth half cycle was +33.6 kips, which was 56 percent less than the preceding southward maximum.

During the third complete cycle, the maximum northward load was -22.4 kips. This was 49 percent less than the preceding maximum, and it represented a total 78 percent deterioration from the first cycle northward maximum. The maximum southward load was 22.5 kips. The latter was 33 percent less than the preceding southward maximum, and it represented a total 71 percent deterioration from the first cycle southward maximum and 78 percent deterioration from the maximum northward load. Thus, over

three cycles to  $\pm 1.3$  in. deflection, the structure lost more than three-fourths of its load capacity.

Figures F-24 and F-25 show the base of the north and south columns respectively after the 3 cycles to  $\pm 1.3$  in. The exposed column hoops were expanded. The  $90^\circ$  hooks of the lowest horizontal wall bar were retaining the broken concrete within the north and south column.

Much of the lateral movement during the last two cycles was limited within the lower 3 to 6 in. of the wall and columns. The column bars flexed as though they were beams fixed at the footing base and in the column, about 6 in. above the base. Crushing occurred around some of the vertical wall reinforcement below the lowest horizontal bar. The spalling allowed observation of some of these vertical bars. These bars flexed as did the column bars except the length was about 3 in.

The total energy dissipated in the second cycle was 38 percent of that dissipated in the first cycle, while that in the third cycle was 25 percent of the first.

Cycles to -2.6 in, +2.1 in.

Figure F-21 shows the single maximum deflection cycle to -2.6 in. and +2.1 in. As the wall was deflected northward, much of the base of the wall crushed, although the concrete did not spall. The compressive force retained the broken material, yet broken material at the south end fell out. The maximum load at -2.6 in. (5.3 DR) was -57.8 kips.

With reversal of loading, most of the broken material fell out of the north column and wall. Because of the gaps at the south end of the structure, most of the compression was carried by inner portions of the wall. The column bars flexed, and column concrete spalled up to 12 in. above the base. At a southward deflection of about 2.0 in., the southwest base of the wall completely crushed and spalled as shown in Figure F-26; the specimen tilted westward approximately 1.2 in. Further southward deflection caused increased tilting. Loading was reversed, and the test was terminated when the structure was returned to the zero deflection position.

Figures F-27 and F-28 show details of the north and south portions of the structure after the test. Figure F-29 shows the entire specimen. Toward the end of the test the deflection principally resulted from the wall slipping along the base. The lateral resistance gradually increased with deflection, but at the zero deflection position the average lateral resistance ranged between +4.9 kips and -6.7 kips for the last three cycles.

Specimen 2

The strengths of the field cured concrete cylinders were determined first and are listed in Appendix C. The column and top beam  $f'_{cf}$  were 4510 psi and 2940 psi respectively. The yield and ultimate loads were calculated based on  $f'_{cf}$  and were 6.7 kips and 8.6 kips respectively. The anticipated yield deflection was 0.35 in.

Specimen 2 was placed in the test frame as was the previous Specimen 1 (Figure F-30); deflection and load instrumentation were identical. Eight strain gages were used to measure effects in the column 3 in. from the base and from the top beam; the VIDAR unit recorded all strain output.

## Deflection Sequence

The deflection sequence of Specimen 2 is shown in Figure F-31 and was similar to that of Specimen 1 in order to facilitate comparisons. The first three cycles were to 0.25 in. rather than 0.10 in. as for Specimen 1 so that the deflection would be about two-thirds the frame's calculated yield deflection. Two deflection cycles at an amplitude of 2.6 inches were conducted rather than one because Specimen 2 was in good condition and so deterioration could be studied further.

Cycles to  $\pm 0.25$  in.

The specimen remained elastic, and no cracks were observed in the cycles to  $\pm 0.25$  in. Maximum column reinforcement strain was 36 percent of yield.

Cycles to  $\pm 0.50$  in.

Figure F-32 shows the load deflection response of the three cycles to  $\pm 0.50$  in. First cracking occurred at a deflection of  $-0.4$  in. under a load of  $-4.2$  kips. On the second half cycle cracking started at  $+0.35$  in. at  $+3.8$  kips. After, the three cycles cracks were in the lower two feet and upper one foot of the column and in the beam near the column as shown in Figure F-30.

While these cycles were nearly elastic, the load deflection curve was ogee shaped and showed a deflection hardening response. These characteristics probably resulted from shear slip in the cracks.

Maximum load dropped only slightly between cycles although the stiffness near zero deflection position decreased significantly after the first cycle. Furthermore the hysteretic energy dissipation was less in the second and third cycles than in the first because little new cracking occurred after the first cycle.

Cycles to  $\pm 0.8$  in.

Figure F-33 shows the load-deflection response for the three cycles to  $\pm 0.8$  in. First steel yielding occurred at the base of the south column at a deflection of  $-0.70$  in. under  $-6.4$  kips during the first half cycle. This yielding was accompanied by additional cracking in the column and the top beam. Reduction to zero load showed a residual deformation of  $-0.10$  in. During the second half cycle, reinforcement yielded at the base of the north column at a deflection of  $+0.70$  in. under a load of

+6.4 kips. The author notes that while such symmetry of yield loads and deflection should occur, it is unusual in experimental research.

The calculated yield load was 6.7 kips which was 5 percent greater than that observed. The calculated yield deflection was 0.35 in. which was one-half of that observed. This difference is discussed in Chapter 5.

Again, the load-deflection curves were ogee shaped with energy dissipation in the second cycle equal to 62 percent of that in the first and in the third cycle equal to 48 percent of that in the first.

Cycles to  $\pm 1.3$  in.

Figure F-34 shows the load deflection curves for the three cycles to  $\pm 1.3$  in. Cracking in the top beam and top of the columns increased during these cycles. The outer surfaces of the column-beam connection cracked extensively as shown in Figure F-35.

Residual deformations averaged 0.35 in. during these cycles. This plastic deformation was evidenced by the larger hysteretic energy dissipation shown in the load deflection curves.

As in the previous deflection cycles, the curves were ogee shaped, and the maximum load decreased only slightly with increasing cycles.

Cycles to  $\pm 2.6$  in.

Figure F-36 shows the load-deflection curves for the two cycles to  $\pm 2.6$  in. During the first half cycle the steel at the top of the north column yielded for the first time at a deflection of about -1.7 in. under -8.6 kips. During the second half cycle, the top of the south column first yielded about +1.7 under +7.1 kips.

At -2.0 in. under -8.8 kips during the first half cycle, the column at the beam-column intersection crushed as shown in Figure F-37. During the second half cycle, diagonal cracking became obvious at the base of the north column as shown in Figure F-38.

The load deflection curves show significant hysteretic energy dissipation nearly four times greater than in the first  $\pm 1.3$  in. cycle. Residual plastic deformations averaged 1.3 in. The curves of these high deflection cycles (3.7 DR) did not show an ogee shape but rather a more oval shape similar to the Ramberg-Osgood shapes assumed by many analysts. Of significance was the very small loss in maximum load between the two cycles, no loss for the positive loads and only 11 percent loss for the negative loads. The energy dissipated in the second cycle was 88 percent of that dissipated in the first. Even at these large deflection cycles the hysteresis curves were stable.

## Specimen 3

Field cured concrete cylinders were first tested to determine their strengths; results are recorded in Appendix C. The main cast section of the wall had an  $f'_{cf} = 2820$  psi (19 percent less than  $f'_c$ ) while the drypack section had an  $f'_{cf} = 7500$  psi (9 percent greater than  $f'_c$ ).

Specimen 3 was instrumented and set-up in the test frame as Specimen 1. The deflection sequence was nearly identical to that of Specimen 2 except only one  $\pm 2.6$  in. deflection cycle was conducted.

Cycles  $\pm 0.2$  in.

Figure F-39 shows the load-deflection response for the three cycles between +0.25 in. and -0.17 in. deflections, 84.4 kips and -47.9 kips respectively. Maximum load degraded less than 5 percent between cycles.

The approximate 0.3 in. offset resulted by the specimen sliding along the test frame. Further sliding was restrained by placing more slims between the specimen and the southern-end restraining block.

During the first half cycle, cracks first occurred in the top of the south column (-33.5 kips) and then between the top beam and drypack section (-43.2 kips). The joint crack extended from the south column about 48 inches to the mid-section of the wall. During the second half cycle, the top of the cast-in-

place (CIP) wall cracked extensively; cracks extended from the drypack - CIP joint downward as shown in Figure F-40. At a load of +58.9 kips the remaining beam-drypack joint cracked. Such cracking during this first cycle was not noticeable in the hysteresis curve where the first cycle appeared quite linear and elastic (Figure F-39).

Few new cracks appeared during the next two cycles at this deflection level. Yet, the load-deflection curve shows an ogee shape which indicates that shear slipping occurred near the zero deflection region.

Maximum strain in the column reinforcement occurred at the maximum load (74.4 kips) and was 1410 micro-in./in., about 80 percent of yield. The strains indicated little flexure in the columns; strain pattern appeared as in Specimen 1.

Cycles  $\pm$  0.5 in.

Figure F-41 shows the load-deflection response for the three cycles between -0.41 in. and +0.56 in. The hysteresis curve shows a distinct ogee shape implying definite shear-slip, and it shows load degradation and decreased energy dissipation with increasing cycles.

During the first half cycle, yielding of south column reinforcement occurred at the column base at -95.7 kips load and -0.36 in. deflection. During the second half cycle, yielding of the north column reinforcement occurred at the column base

at 85.0 kips and 0.33 in. deflection. The average yield load and deflections were 90.4 kips and 0.34 in.

Also during the second half cycle, the vertical wall reinforcing bar near the base of the north column first yielded at 105.1 kips and 0.43 in. deflection. At this same load-deflection point, a diagonal crack was noted which passed through the base of the north column and into the base beam as shown in Figure F-42.

In succeeding cycles the strains at the base of the specimen were less than the maximum strains recorded during the first cycle.

Tension yielding occurred at the top of the south column at the maximum load during the first half cycle and at the top of the north column at the maximum load during the second half cycle. Yielding at the upper level gages did not occur in Specimen 1.

Strain patterns for this first cycle are shown in Figures F-43 through F-46. At the base of the compression column the strains indicated flexural column behavior (Figures F-43 and F-45); one side of the column was in compression while the other was in tension. Such flexural response is not typical shear wall response as exemplified by Specimen 1. The strain pattern in the wall and tension column was more typical of a shear wall, for it illustrated column-wall bending continuity. Apparently this CIP wall and surrounding frame were beginning to have separate structural action at this yield deflection level. The top

gages showed tension strains about 50 percent greater in the "tension" column of Specimen 3 than similar strains recorded in Specimen 1 at the same deflection. Yet, the maximum strain magnitudes at the base were about the same for the two specimens.

During the third half cycle to  $-0.41$  in. deflection, a vertical crack was noted between the wall and the north, compression column extending 18 in. above the base beam. This crack verified the indication of the strain readings that the frame and wall were separating.

The three cycles to the nominal  $\pm 0.5$  in. produced extensive diagonal cracking in the wall as shown in Figure F-47.

After three cycles the maximum loads decreased 20 percent for negative loads and 14 percent for positive loads. For the same deflection cycles Specimen 1 showed no load degradation.

Cycles  $\pm 0.8$  in.

Figure F-48 shows the load-deflection response for the three deflection cycles between  $-0.76$  in. and  $+0.83$  in. The hysteresis curve shows significant load degradation over cycles and increased shear-slip behavior for the second and third cycles. The curve also illustrates a typical yielding behavior during the first cycle. The initially stiff structure became plastic above approximately 90 kips and the stiffness greatly decreased. The negative and positive loads at which this yielding began were nearly the same as the first yield loads determined in the previous deflection sequence; yet the yield deflections averaged 70 percent greater.

During the first half cycle at a load of -100.3 kips and -0.52 in. deflection, the top south corner of the wall began to crush at the drypack-beam joint as shown in Figure F-49.

At the maximum load and deflection (-105.5 kips, -0.75 in.) a large diagonal crack was noticed at the top of the north column, Figure F-50. This crack indicated a large, direct shear load and resulting shear failure of the column. Inspection showed extensive slip between the CIP wall and drypack on the north half of the wall and between the drypack and the beam on the south half. Figure F-51 shows the 1/4-in. wide vertical crack through the drypack which joins the two halves of the slipping joints. Slip on the north (left) side of the structure is clearly indicated by the offset of the vertical striping. The drypack vertically cracked at or next to most of the vertical dowel bars. Spalling began at two locations in the CIP wall at the joint below the drypack (Figure F-51); yet, the drypack did not show any sign of crushing.

While considerable cracking and slip were occurring at the top of the wall, the base of the structure showed no sign of deterioration. Cracks in the compression column and base beam did not close at the maximum load, which indicated that all compression was carried by the reinforcement.

As the specimen was loaded in the second half cycle, the vertical crack in the drypack closed as did the north column diagonal crack at the deflection of +0.45 in. At 69 kips the CIP wall below the drypack crushed in the top south corner

(Figure F-52). As load was increased, the top of the south column cracked diagonally; crack width was about  $5/32$  in. The drypack and CIP wall crushed at the top north corner (Figure F-53). Further, the middle three feet of the CIP wall below the drypack began to crush on the eastern (back) face. Thus, during this first cycle of nominal  $\pm 0.8$  in. deflection, the infilled structure was failing at the joints between the drypack to CIP wall and drypack to beam. The joint failure apparently resulted in shear load transfer to the columns which caused diagonal shear failures of columns.

Strain data during the first cycle indicate a typical shear wall type response at the bottom of the wall, maximum tension on one side which decreases to maximum compression on the other. Increased tension yielding did occur. The top gages showed a more erratic behavior. The upper columns showed distinct flexural behavior; the vertical wall bars yielded in tension to various amounts. Recall that dowel bars were strain gaged  $2-1/2$  in. below the beam. At the maximum positive and negative loads, the upper frame and wall showed no strain continuity.

As the specimen was loaded in the third half cycle, small chunks of concrete fell from the crushed areas. At the maximum deflection, areas in the drypack next to vertical dowels appeared crushed. The diagonal crack in the north column was  $9/16$  in. wide (Figure F-54).

In the fourth half cycle, more concrete spalled. The slip between the drypack and CIP wall was measured using the vertical stripes as references. At 20 in. from the north column, the movement was  $25/32$  in.; at the middle,  $5/32$  in.; and at 20 in. from the south column,  $2/32$  in. That the slip was not uniform showed that shear load was being transferred into the CIP wall gradually.

In the fifth and sixth half cycles, the crushed areas continued to deteriorate as shown in Figures F-55 and F-56.

Between the first and second cycle the maximum loads decreased an average 38.9 percent, and between the first and third cycle they decreased an average 55.5 percent. For similar cycles in Specimen 1, the three cycle load deterioration was 37.8 percent. Deterioration of Specimen 3 resulted primarily because of joint slip.

Such slip was evident in the load deflection curve, Figure F-48. The author believed that slip occurred until vertical cracks in the drypack closed and the drypack bore against the vertical bars extending from the CIP wall.

Cycles  $\pm$  1.3 in.

Figure F-57 shows the load-deflection response for the three cycles between  $-1.31$  in. and  $+1.31$  in. During the first half cycle the load was reduced to zero then reapplied so that a shim could be placed between the loading plate and the specimen. This load-unload sequence showed the non-linear, non-elastic

behavior at this -1.00 in. deflection level, without any cycle reversal.

Considerable crushing and joint deterioration occurred during the second half cycle. Once positive load was applied, large pieces of drypack fell out. Inspection of the broken drypack concrete showed that the concrete was not bonded well to the dowel or wall reinforcing bars. No bar deformation grooves or powdering of concrete in the bar location was present. Very loose pieces of drypack were removed by hand so that the pieces would not fall on LVDT instrumentation.

Figures F-58 and F-59 show the north and south sides of the specimen at the maximum positive load during the second half cycle. The drypack and the CIP wall just below the drypack had spalled considerably. A hole through the CIP wall at the north corner is noticeable in Figure F-58. The beam was not cracked even though its concrete strength was about the same as that of the CIP wall. The concrete confinement provided by the 1/8-in. stirrups and the #4 bars was sufficient to keep the beam intact.

During the next two cycles, drypack concrete continued to fall out until at the end of the three cycles little drypack remained. Figure F-60 shows the north, rear face of the specimen at the maximum negative load of the fifth half cycle. The north half of the north column had split away from the rest of the structure; most of the drypack was gone.

The load capacity decreased an average 72.4 percent between the first and second cycles and an average 79.8 percent between the first and third cycles. Specimen 1 load capacity decreased an average 74.2 percent over these three cycles. But the load capacity for the last cycle of Specimen 1 was an average 22.5 kips while that of Specimen 3 was an average 8.7 kips, 39 percent of Specimen 1 capacity. The capacity of Specimen 3 was about the same as that of Specimen 2, the plain frame.

Strain gage readings during these cycles indicated that the base of the structure was behaving as a shear wall with a neutral axis within the column and that it was not yielding. The top strains were erratic and yielded in tension.

Cycle  $\pm$  2.6 in.

The load-deflection curve for the single cycle to -2.58 in. and to +2.63 in. is shown in Figure F-57. During this cycle the CIP wall around the upper dowel bars crushed further, and the upper horizontal dowel bars fell out as did the loose concrete in the column-wall joints. Figures F-61 and F-62 clearly show the deteriorated structure at the maximum positive load.

The structure was returned to the zero deflection level after these extreme cycles. Figure F-63 shows the specimen after the complete test. All drypack concrete and about 5 in. of CIP wall near each column had fallen away. Column hoops were

bowed considerably and nearly were untied. The author believed that the structure had lost all vertical load carrying capability. The floor above would have fallen 3 in. until it rested upon the remaining CIP wall.

Figure F-64 shows the bottom surface of the top beam which was hand chiseled before the infilled wall was cast. Most of the ragged, chisel marking remained; peaks appeared as if they had been worn off and were slightly rounded. This joint condition implied that the drypack did not bond to, nor significantly bore against the beam. Load had been transferred from the beam to the drypack and CIP wall by direct bearing of the dowels and of the embedded vertical bars.

Figure F-65 shows a close-up of a dowel bar with accompanying vertical wall bar (second bar from north column). The wall bar was bent away from the dowel bar. Apparently, no tensile load was transferred between bars in the area of drypack or upper CIP wall. Lack of vertical cracking in the remaining CIP wall showed bond remained good there. The reader will recall that the lap splice was designed longer than required. Such design conservatism proved beneficial here because of the inadequate bond in the drypack.

Bottom strain gages remained elastic during this last cycle, and again they illustrated a shear wall type behavior.

## Specimen 4

Tests of the concrete control cylinders gave  $f'_{cf}$  for the single precast wall panel and the columns of 2940 psi and 3030 psi, respectively, which were 35 percent and 31 percent less than their  $f'_c$  values.

Instrumentation and set-up of Specimen 4 was nearly identical to that of Specimen 3. Two dial gages were mounted between the base beam and wall panel as illustrated in Figure F-66. The gages, oriented horizontally, were located 16-1/2 in. from the inside face of the north and south column; each dial gage support was epoxied to the base beam while the reference block was epoxied to the wall panel. The dial gage measured the relative movement (slip) between the panel and the base beam. As the data showed, the two gages gave nearly identical slip measurements; so, the average of the two gages was used as the measure of "base slip". Similarly an additional two dial gages were epoxied horizontally to the top beam and measured the slip between the top beam and the panel. These top dial gages were mounted after the specimen was cycled three times at the  $\pm 0.2$  in. level.

The sum of the average slip between the top beam and panel and the average slip between the bottom beam and panel was termed the "total slip". This total slip was the overall relative movement between the frame and infilled wall. The deflection of the frame-wall system is given by the following:

$$D = S + W$$

where

D = total lateral deflection measured by the LVDT's  
or dial gage

S = total slip measurement

W = shear distortion of the wall

With the lateral deflection of the specimen and the total slip measurements, the wall distortion, W, was calculated.

As a preview to the following step-by-step discussion of test results, the reader should note that two distinct failure modes were determined in this test, one in the northward direction (- deflection) and one in the southward direction (+ deflection). Ear plate weld failure and anchor bolt pullout dominated the northward response while localized concrete crushing in the panel determined the failure in the southward direction.

Cycles  $\pm$  0.2 in.

Figure F-67 shows the specimen after three cycles to -0.20 in. and +0.20 in., and Figure F-68 gives the load-deflection response for these cycles. Unlike Specimens 1 and 3, the load-deflection curve shows significant energy dissipation during these small deflection cycles. The specimen was not elastic but had plastic deflections of 0.22 in. Total slip accounted for about one-third of the lateral deflection.

Before the specimen was loaded, all anchor bolts were checked to assure that the nuts were tight. After one loading cycle, all bottom nuts and four of the top nuts were loose. Again, the top nuts were fully tightened by wrenching  $1/4$  to  $1/2$  turn. At the base four bolts near both the north and south columns were quite loose and required one full turn to tighten. The central bolts required  $1/2$  turn to tighten. A full turn tightening meant that the bolts had been extracted from the drilled holes or had yielded 0.09 in. (based on 11 threads per inch for  $5/8$  in. anchor bolts). The tightening of the nuts did not change any slip or deflection readings and altered strain readings by less than 75 micro-in./in. With the following two deflection cycles, the bolts were extracted again. For example, in northward deflections the south edge of the bottom connector plate lifted off the base beam approximately  $3/32$  in.

The maximum load capability did not degrade over these three cycles, even though considerable residual deformation was observed. Approximately half of the residual deformation resulted from slip. As shown in Figure F-67, the frame and panel cracked little during these cycles.

Cycles  $\pm$  0.5 in.

Figure F-69 shows the load deflection response for the three cycles to  $-0.50$  in. and  $+0.49$  in. While the maximum load degraded slightly over the three cycles, the energy dissipated in each cycle decreased as much as 76 percent between first and third cycle.

The structural behavior of Specimen 4 was a combination of frame and shear-wall action as determined by cracking, slip deformation and strain gage data. Figures F-70 and F-71 are photographs of the north column during the second half cycle. The column cracks did not penetrate the entire column; thus the column was shown to be subjected to flexural behavior as Specimen 2. In shear wall behavior (Specimen 1), cracks penetrated the entire column and continued into the wall. Slip measurements indicated that wall distortion equaled about one-half of the total lateral deflection, and the other half was slip. In pure shear wall behavior, the wall distortion approximately would equal the total lateral deflection. Slip deformation was frame deformation alone. Finally, Figures F-72 and F-73 present the bottom and top strain gage data, respectively, for the first half cycle. Strain data showed that both columns were in flexure with the south column carrying a superimposed tensile force. At the base the wall was under tension on the south side and compression at the north side; this wall behavior was identical to that of Specimen 1. Tension and compression were reversed at the top of the wall, as would be anticipated because of maximum diagonal compression stress. The partial slip permitted some independent frame response as shown by cracking and strain data while the connector restraint forced the wall and frame into shear wall behavior.

Strain gages at the top of the north and south columns indicated that the steel yielded in tension at the inside face of

each column under the respective + and - maximum loads in these cycles. In plain frame response (Specimen 2) the top of the columns did not begin yielding until a deflection of + 1.7 in., about three times the yield deflection as for Specimen 4. The imposed column tensile force caused by shear wall action produced the high tensile strains.

The maximum loads also caused diagonal cracks at both ends of the top beam about 5 in. from each column. These cracks resulted from high shear condition produced by the tension load in the column and compression load in the adjacent wall; these tension and compression loads were indicated by the top strain gages. The beam acted to maintain continuity between column and wall. The resulting shear stress was sufficient to cause cracking as shown in Figure F-70.

Diagonal cracking also occurred in the base beam as shown in Figure F-74. Base beam cracking was emphasized further by pullout action of the wedge anchor bolts. Figure F-71 shows that at the north side of the base cracks radiated from the anchors. Similar but more pronounced cracking occurred near the south column. Pullout of the south side anchors was indicated by vertical cracks in the base beam at the anchor locations and by the horizontal crack in the base beam (Figure F-74). This horizontal crack was about 4 in. below the top of the base beam; this was at the level of the bottom of the anchor bolt holes. Bolt pullout was estimated to be 1/8 in.

Cycles  $\pm$  0.9 in.

First cycle. Figure F-75 presents the load deflection response for the three cycles to -0.88 in. and +0.89 in. As the specimen was loaded in the first half cycle, the top, inside reinforcing bar in the south column began to yield extensively at -80.9 kips, 0.54 in. deflection; final strain at -0.88 in. was 11,800 micro-in./in. The bottom, outside bar in the south column began yielding at -84.8 kips, -0.60 in. deflection; final strain at -0.88 in. was 10,300 micro-in./in.

At a load -95.5 kips, -0.78 in. deflection, the top beam failed in diagonal shear as shown in Figure F-76. The load immediately dropped to -55.6 kips as the deflection jumped to -0.89 in. The load was gradually removed and the specimen inspected.

The welds failed which connected the two top, southern ear plates to the embedded connector plate; the ear plate connector was securely attached to the top beam and panel plate at all other locations. The ear plate connector was bent down to conform to the fractured shape of the beam.

Near the south column the base connector plate was lifted off the base beam over 1/2 in., and a 3/16 in. gap existed between the anchor nut and the connector plate as shown in Figure F-77. The anchor had been extracted about 11/16 in. during the cycle.

Strain patterns during this first half cycle are presented in Figures F-78 and F-79 for the bottom and top gages, respectively.

Strain response was similar to that observed in the previous deflection sequence. The top gages at the south side showed column flexure with extensive tensile yielding; compressive strain in the wall next to the south column averaged -785 micro-in./in.

The average compressive stress in the wall was computed as 2420 psi using a modulus

$$E = 57000 \sqrt{f'_{cf}}$$

By assuming a length of compression between the column and second wall bar of 11 in., the compression force was calculated to be 85 kips. If this load were carried by the three ear plates in that location, the force on each weld would have been 9.5 kips/in. This load would far exceed the 2.6 kips/in. allowable. Similarly high weld loads occurred at the north-end ear plates during the second half cycle, and those welds did not fail. The author believes that the southern most weld between the column and the ear plate was weak because the location of the weld made welding difficult.

The author concludes that the failure sequence was as follows:

- (1) Pullout of bottom, south end anchor bolts caused the imposed lateral load to be carried through the wall in a direct diagonal compression rather than in a more uniform shear. This diagonal placed a greater concentrated compression at the upper south corner

of the ear plate connector than if a more uniform shear were present.

- (2) Weld failure resulted from the concentrated force and from a weak weld.
- (3) The weld failure separated the wall from the beam and left a long, unsupported length of beam to carry the direct compression and the shear between the south column and wall.
- (4) The beam failed in diagonal shear-compression.

With investigation of the beam failure completed, Specimen 4 was loaded in the positive direction and deflected to position equivalent to the previous maximum negative deflection. Failure did not occur.

During the second half cycle, the steel at the top of the north column began yielding extensively at 83.2 kips, 0.69 in. deflection; a base column yielding began at 86.6 kips, 0.77 in. deflection. Near the north column the gap between the base connector and the base beam was less than  $1/4$  in. This gap was about one-third that which occurred at the south end during the previous half cycle. Apparently the shear connection between the north column and wall was maintained at the base as well as at the top beam.

The wall did not contact either column during this first deflection cycle; although the gap between them was reduced to as little as  $1/32$  in.

101

Repair. After the first cycle was completed, the loading system was modified so that reversed cycle deflections could be continued. The objective of the repair was to build a structure which would transfer the jacking load to the slab while bypassing the fractured zone of the beam. Steel angle 3-1/2 x 3-1/2 x 3/8 in. and 60 in. long were epoxied<sup>\*</sup> to the edges of the top slab as shown in Figure F-80. Epoxy was omitted in the area of the south column so that the angle would not bond together the upper and lower parts of the failure zone. The loaded end of the angles were joined by welding a 1/2 x 3 in. steel plate to each angle. Angles 1-1/2 x 1-1/2 x 1/8 in. were epoxied to the top of the main angles to prevent the angles from spreading. Before epoxy was applied the top and side edges of the slab were chiseled until they were rough. The angles were sandblasted.

Testing continued. After the epoxy had cured for three days, testing was resumed to deflection cycles of -0.88 in. and +0.89 in. As shown in Figure F-75, the load capacity degraded significantly over the second and third cycles with maximum negative load decreasing as much as 60 percent and positive load 41 percent. Energy dissipation was reduced over 80 percent between first and third cycles.

---

\*

Sika brand Colma-dur-gel was the epoxy used.

Over the last two cycles, slip amounted to more than one-half of the total deflection. During the fourth and fifth half cycles the wall began bearing on the columns. The bottom, south corner of the wall bore against a 6 in. length of the south column in the sixth half cycle.

Cycles  $\pm$  1.3 in.

Figure F-81 gives the load-deflection response for the three cycles to -1.32 in. and +1.28 in. and for the one cycle to -1.68 in. and +2.58 in. During the first half cycle the top beam failure zone deteriorated further as shown in Figure F-82. The top slab of the beam had separated from the column; the diagonal crack was approximately 1/2 in. wide. The ear plates with the broken welds bore directly on the top edge of the wall. Such vertical deflection was permitted by pullout of the south-end base anchors as shown in Figure F-83. Extensive cracking around the anchor bolts allowed the bolts to tilt laterally. The maximum load during the first half cycle (-55.9 kips) was about 59 percent of the maximum load in the previous deflection sequence.

The maximum load in the second half cycle (88.4 kips) was about 98 percent of the maximum load in the previous deflection sequence. The southward deflection behavior showed far less load degradation than the northward behavior. During the second half cycle at a deflection of 0.82 in. (30.0 kips), the bottom, south corner of the wall began bearing against the south column. At

1.12 in. (73.2 kips) the base of the south column cracked in diagonal shear (Figure F-84); yet the structure continued to maintain increased loads.

Base anchor bolts at the north end were extracted about  $3/8$  in.

Strain data showed that the wall continued to remain elastic with tensile and compressive strain patterns like those presented before. Column strains indicated flexure; reinforcement yielded in both tension and compression. Compression yielding occurred after a bar was yielded in tension in the previous half cycle. As an example, at the base of the north column one bar had a plastic residual strain of 5190 micro-in./in. at the beginning of this deflection sequence. At -1.32 in. the strain was 350 micro-in./in., a compressive strain of 4840 micro-in./in.; yet, the concrete crack remained open so that little compression was carried by the concrete. Continuing cycles showed maximum negative loads decreased by 54 percent while positive loads decreased only 32 percent. The base beam continued cracking horizontally at the level of the bottom of the anchor bolt holes. The failure zone in the top beam deteriorated considerably; the beam stirrups were rounded out and the concrete was fractured extensively.

With southward deflections the wall did come into bearing against the lower part of the south column; but with northward deflections the wall did not bear on the columns.

Cycle -1.68 in., +2.58 in.

The load deflection response of the final cycle is shown in Figure F-81. The specimen was not deflected to the full -2.6 in. because of the large angle deflection of the wall. The loading system could not be adjusted to the large vertical deflection of the south end of the specimen. The top of the slab deflected up about 2 in.; most of that deflection occurred at the crack separating the slab and the column. As shown in Figure F-85, the top, south corner of the wall was crushed because of the bearing of the ear plate on the wall. Figure F-86 shows the base connector at the -1.68 in. deflection. Nearly all anchor bolts were extracted. The maximum load carried was about twice that of the plain frame, Specimen 2.

The second half cycle demonstrated completely different behavior. At a deflection of 1.42 in. (63.8 kips) as the wall was bearing on the base of the south column, new diagonal cracks developed in the column. As load was increased to 80.9 kips, the concrete at the base of the south column began spalling. At the same load the top, north corner of the wall cracked; the wall was not bearing against the north column. As deflection increased and as load gradually decreased, the wall did contact the top of the north column. Beyond 2.3 in. the top north corner of the wall was crushing as shown in Figure F-87. Apparently, the compression applied to the wall through the embedded connector plate caused crushing at a level just below the base of the

embedded plate. The ear plates bent so that the compressive load was no longer concentric. The torsion on the embedded plate caused by the bent ear plates may have initiated the crushing in the wall. The failure mode in this southward direction was a combination of diagonal shear failure at the base of the south column and compression failure in the wall initiated by the embedded connector plate.

After the test was completed the connectors were inspected. All base anchor bolts were extracted more than 1/4 in. The center, top anchor bolts were extracted only slightly, although all nuts were loose. Except for the weld failures of the top, south side ear plates mentioned previously, all welds appeared uncracked.

## Specimen 5

As discussed in Appendix D, Specimen 5 was constructed using six precast panels to infill the standard frame. The panels were designated numbers #1 through #6, with #1 located next to the north column, #2 next to #1, and so forth with #6 next to the south column. Gaps of about 3/8 in. were left between the columns and the panels; gaps of about 1/4 in. were between panels.

Compression tests of field cured cylinders gave  $f'_{cf}$  of the panels as 2910 psi and of the columns as 3520 psi. These values were 36 percent less than and 5 percent greater than their respective  $f'_c$  values.

Strain gage instrumentation was altered for Specimen 5; load and deflection instrumentation was the same as for other specimens. Column reinforcing bars were gaged as in the other four frames. Location of gages in the wall was changed so that panel-to-panel behavior could be observed and so that both a panel next to a column and an interior panel could be studied. Strain gages were epoxied to the vertical #3 bars in panels #5 and #6 as shown in the drawing, Figure F-88. In the following figures which present the strain magnitudes related to gage location, the straight lines joining the data values serve to clarify the data and are not intended to represent the strain between positions where the data was taken. It should be noted that the strain gages were placed between the panel-to-panel connectors and the

embedded panel plate connector. The assumed (and experimentally evidenced) panel response was that of a fixed-end beam with points of fixity between the panel-to-panel connectors and panel-to-frame connector. Therefore, the gage position was within a few inches of the fixed position. As the reinforcing bars yielded, the yielding probably spread from the maximum moment position (fixed position) to the gage position. Therefore, the load and deflection level at panel yielding were determined approximately. Crack location and width were also used to determine yield conditions.

Dial gages were epoxied to the base and top beam to measure the slip of panels #1 and #6. The reference block was located at the centerline of each panel, 8-3/4 in. from the inside face of each column. The dial gage readings resulted from relative slip between panel and frame and from the relative rotation of the panel and beam. The two effects could not be separated, so the dial gage measurements were termed "apparent slip". The maximum apparent slip deformations at the base were somewhat greater than at the top beam, 0.12 in. versus 0.10 in. during cycles to  $\pm 1.3$  in. At times during a deflection cycle, the top slip was often much greater than the base slip. Most interesting was the difference in apparent slip between the end of the wall at which the load was applied (loaded end) and the unloaded end. The total apparent slip at the loaded end was between 50 percent and 100 percent greater than the slip at the unloaded end. Panels deflected relative to each other and not as a single wall unit.

Average apparent total slip was about  $\pm 0.07$  in. at the  $\pm 0.2$  in. deflection cycles and as much as  $\pm 0.26$  in. at the  $\pm 1.3$  in. cycles.

Cycles  $\pm 0.2$  in.

The load-deflection response for the first three cycles to  $-0.22$  in. and  $+0.22$  in. is given in Figure F-89. Response showed little load degradation and stable hysteresis loops. Some flexural cracking was evidenced in the columns. Interior panels #2, #3, #4 and #5 cracked along and across the  $45^\circ$  diagonal auxiliary reinforcement as shown in Figure F-90.

Both the cracking and strain behavior illustrated that the structure responded as a series of fixed-end flexural elements.

As stated above, total apparent slip was  $0.07$  in. Nuts on the anchor bolts remained tight through these three cycles.

Cycles  $\pm 0.5$  in.

Figure F-91 presents the load deflection response for the three cycles to  $-0.53$  in. and  $+0.50$  in. Over the three cycles the maximum load degraded an average of 10 percent while the energy dissipated decreased about 46 percent. The hysteresis loop did change to the shear slip, ogee type curve.

Diagonal shear cracks propagated from the panel-to-panel connectors during the first cycle as shown in Figure F-92. The cracking was the same as would be anticipated in a fixed-end deep beam. Width of flexural cracks near the panel-to-panel connectors indicated that vertical reinforcement under tension

in the interior panels was yielding. Strain gages in #5 did show tension yielding beginning at a deflection of +0.41 in. (44.1 kips). Strain magnitudes in panel #6 were about 20 percent of those in #5, and maximum column strains were 85 percent of yield strain values.

Cracking and strain data indicated the frame and panels were behaving as a series of flexural elements. Figures F-93 and F-94 present bottom and top strain patterns for the first half cycle, and Figures F-95 and F-96 present bottom and top strain patterns for the second half cycle. The two sets of figures show that moments existed in each column and panel and that the moments were of opposite sense at the top and bottom of each structural segment. Further, the moments indicated correspond to fixed-end moments resisting the imposed lateral loads.

The strain data also indicate that the loaded end of the structure was under a uniform tensile strain superimposed on the flexural strain. A definite area of diagonal compression across the shear wall was not indicated by strain data and cracking of Specimen 5 as such areas were delineated by strain data and cracking of Specimens 1 and 3, and to some degree of Specimen 4. What was shown was that the curvature and end moment were different at the top and bottom of individual segments. This behavior means that moments were distributed between panels by their interaction.

By the end of the three cycles, nuts on base anchors near each column were loose about one turn or less; only two nuts were loose on top anchor bolts.

Cycles  $\pm$  0.8 in.

Load deformation response for the three cycles to -0.85 in. and +0.74 in. is given in Figure F-97. Maximum loads decreased over the three cycles about 9 percent, while energy dissipation decreased by 43 percent.

During the first half cycle the inner reinforcing bar at the top of the south column began yielding at a deflection of -0.60 in. (-46.5 kips); at -0.76 in. (-51.9 kips) the outer bar at the column base yielded in tension. The column moment was greater at the top than at the base; this behavior was opposite that of the plain frame. Figures F-98 and F-99 present the bottom and top strain patterns for this first half cycle. The strain data show that the vertical bars in the panels were near yield in tension and compression; flexural response again was illustrated.

Diagonal cracking increased; where cracks crossed, concrete began crushing and spalling. Such increased diagonal cracking and cracking parallel to the horizontal #3 reinforcing bar near the panel-to-panel connectors lead to larger horizontal shear deformations in the panels. In the first half cycle these shear deformations resulted in panel-to-panel contact between #2 and #3 at a point above the lower panel-to-panel connector.

During the second half cycle, several other panels contacted their neighbors at locations below the upper panel-to-panel connectors or above the lower panel-to-panel connectors; these locations were where the greatest shear deformation was occurring.

Figure F-100 shows the upper panel-to-panel connector between #1 and #2; Figure F-101 shows the upper part of panel #3 which contacts #2; and Figure F-102 shows the entire specimen at this +0.74 in. deflection level. Even though some panels came together on one side of the connector, the construction gap remained on the other side as shown in Figure F-102. In no case did the panel-to-panel connection welds fracture.

The remaining two cycles enlarged some of the panel cracks. More panels began to come into contact with each other. As the panels bore against each other it is believed that the lateral compression load was transferred diagonally through the center of the panel from contact point to contact point.

The panel-to-frame connectors demonstrated a different behavior than in Specimen 4. The connector plate pulled off the beam (either top or bottom) about 0.05 in. on the tension side of each panel, and the plate was flattened against the beam on the compression side. This behavior made the connector plate take six "waves" on the beam as tension and compression alternated. No anchor bolt appeared pulled out more than 1/16 in.

Strain data indicated that the panel next to a column under tension (loaded side column) was under a high compression stress. It is recalled that in Specimen 4 the loaded side of the single panel was in compression while the loaded side column was in tension. Apparently a similar flexure-shear wall behavior occurred in Specimen 5 and Specimen 4.

Cycles  $\pm$  1.3 in.

The load-deflection response for the three cycles to -1.26 in. and +1.32 in. plus the one cycle to -2.59 in. and +2.68 in. is given in Figure F-103. Over the three cycles the maximum load degraded 35 percent and 55 percent in the negative and positive directions, respectively; energy dissipation decreased an average 56 percent.

Slip measurements indicated that the average maximum apparent slip at the top and at the base was about 0.12 in.; total apparent slip was about 1/4 in. The maximum slip was attained during each positive half cycle at +0.4 in. deflection and during each negative half cycle at -0.4 in.; slipping stopped as deflections increased.

During the first half cycle, cracks widened. Concrete spalled from the panels at the #3 horizontal bar locations near the panel-to-panel connectors; most spalling occurred in panels nearest the point of load application. The southern most bar in panel #6 was yielding extensively in tension at the base; yet at the top, the same bar apparently was buckling. Concrete broke away from that bar at the upper corner of #6. Tension yielding occurred at the top of the north side bars in #6 and #5 as well as at the top, inside bar of the south column.

The reverse cycle saw further cracking and spalling as shown in Figure F-104.

During the fifth half cycle, the south column began bearing on the remaining portion of #6 about 12 in. below the beam as shown in Figure F-105. Areas of panel-to-panel bearing were deteriorating over the three cycles as illustrated in Figure F-106 (the area at the top of #3 and #4). The shear deflection of panel #3 is evidenced in Figure F-106 by observing the exposed vertical reinforcement.

During the sixth half cycle, the north column bore against panel #1 at the maximum deflection level as shown in Figure F-107. Bearing was between 12 in. and 18 in. below the beam. By this sixth half cycle the maximum load had decreased to one-half the maximum load of the first cycle. The large shear deformation at the upper and lower levels of the panels was visually evident as shown in Figure F-107. The interesting curved crack in #1 and #6 resulted because the end panels were not connected to the columns.

Cycle  $\pm$  2.6 in.

Figure F-103 shows the load deformation response for the final cycle to -2.59 in. and +2.68 in. The following actions occurred during the first half cycle: (1) at -1.57 in. (-29.8 kips) a  $45^{\circ}$  diagonal shear crack at the top of the north column, (2) at -1.80 in. (-30.5 kips) a  $60^{\circ}$  diagonal shear crack at the top of the south column (Figure F-108), (3) at -2.58 in. (-29.0 kips) a  $45^{\circ}$  shear crack at the base of the north column (Figure F-109). Figure F-110 shows the large shear deformations at the top of panels #2, #3, #4 and #5. Panel #1 bore against the

north column about 18 in. under the beam, and panel #6 bore against the south column about 20 in. under the beam. This bearing caused the upper portions of the column to behave as short columns and to fail in shear.

During the second half cycle at a deflection of  $-0.08$  in. ( $+8.1$  kips), a crossing diagonal shear crack developed at the top of the north column; at  $+1.84$  in. ( $+20.9$  kips) this crack opened widely and the load fell (Figure F-111). As deflections increased spalling accelerated in the panels. Most lateral deflection occurred at the top shear area of the panels as shown in Figure F-112. The top connector between #2 and #3 is shown in Figure F-113.

As the specimen was returned to the zero deflection position, the stiffness and load capacity were less than those of the plain frame Specimen 2 after the same cyclic history. After the test, all fractured concrete was picked off the model. The remaining structure clearly showed that the area of high shear and the shear capacity of the structure were deteriorated completely (Figure F-114).

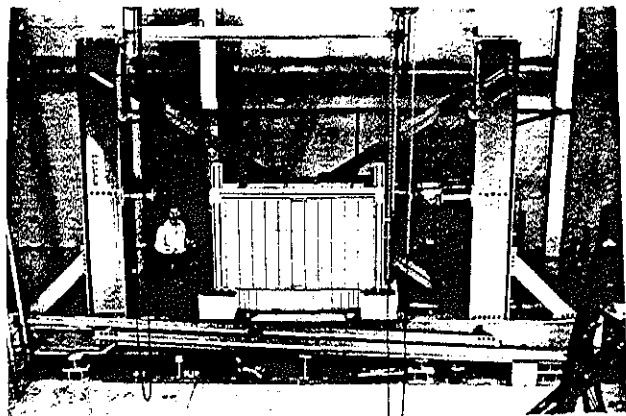


Figure F-1. Specimen 1 in test frame.



Figure F-2. Specimen 1, tie down bolts in end-block foundation.

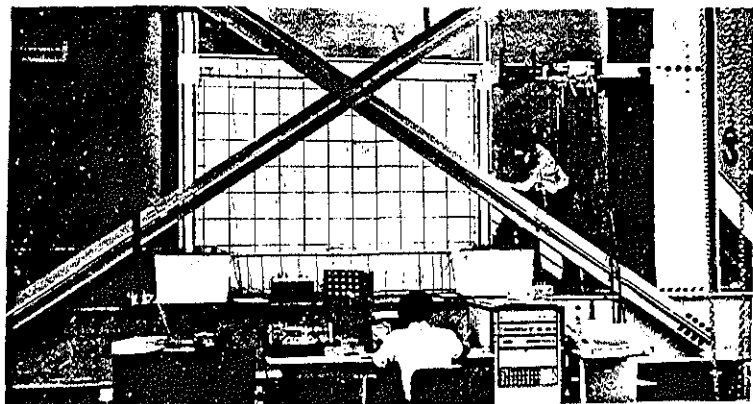


Figure F-3. Specimen 1 under first load, strain and load recording equipment in foreground.

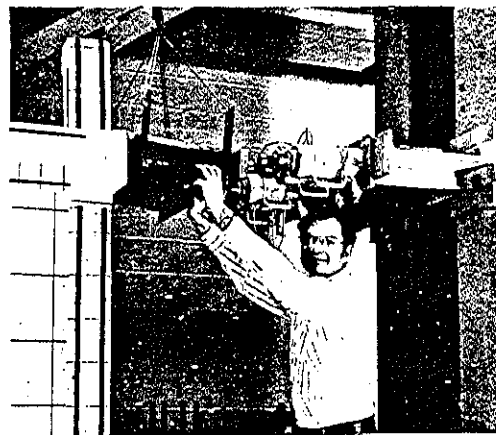


Figure F-4. Specimen 1, four jack load system.

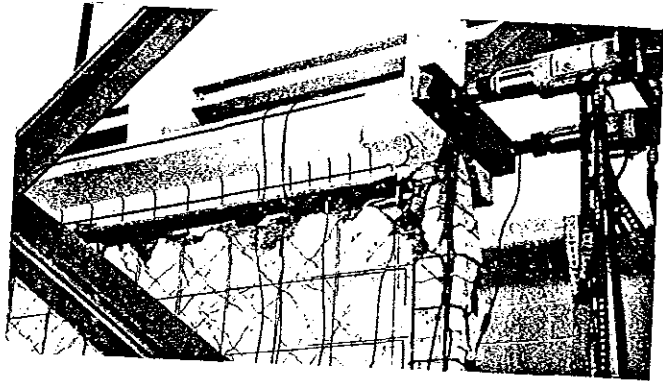


Figure F-5. Specimen 1, two jack load system

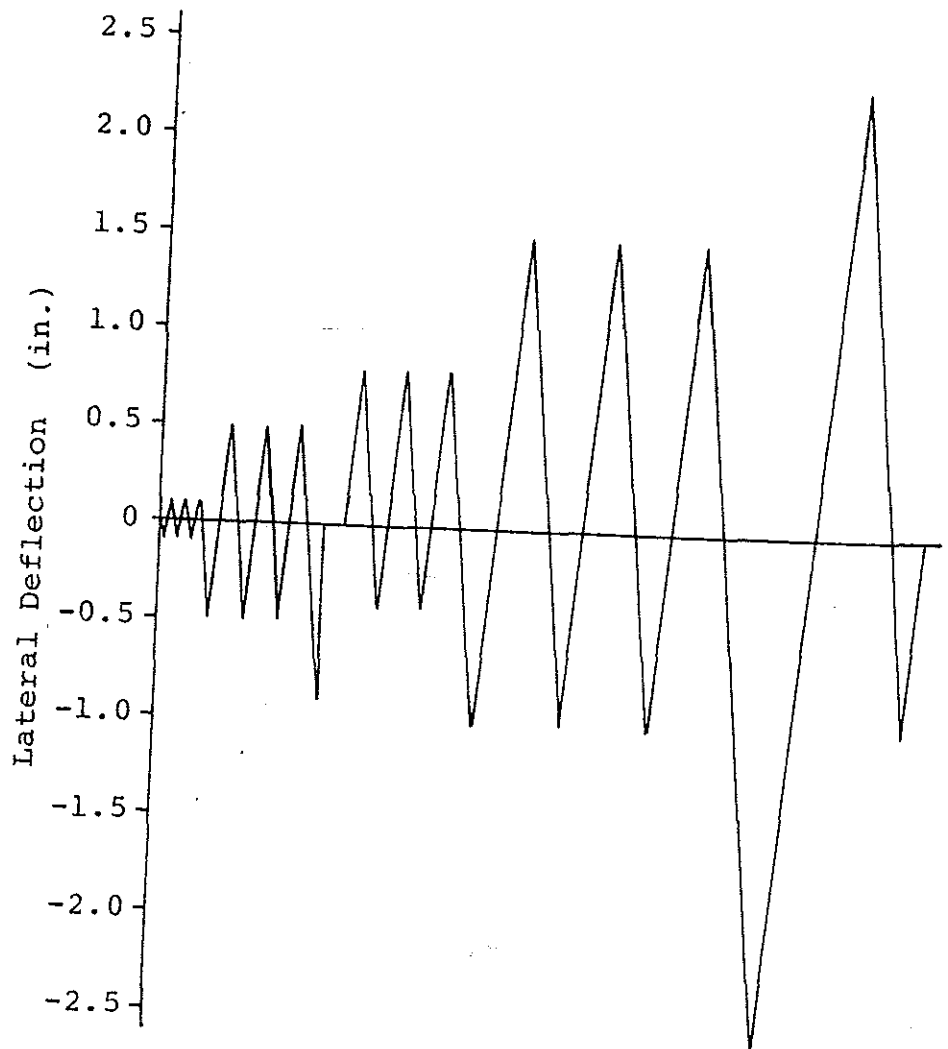


Figure F-6. Specimen 1, diagram illustrating deflection-time reversed cycle procedure.

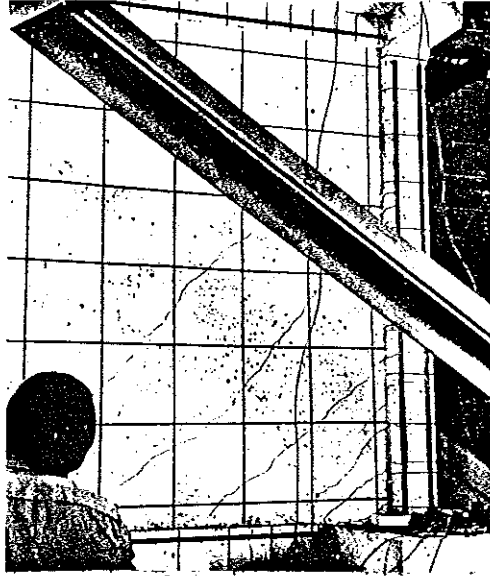


Figure F-7. Specimen 1, cracking at +53.4 kips load level.

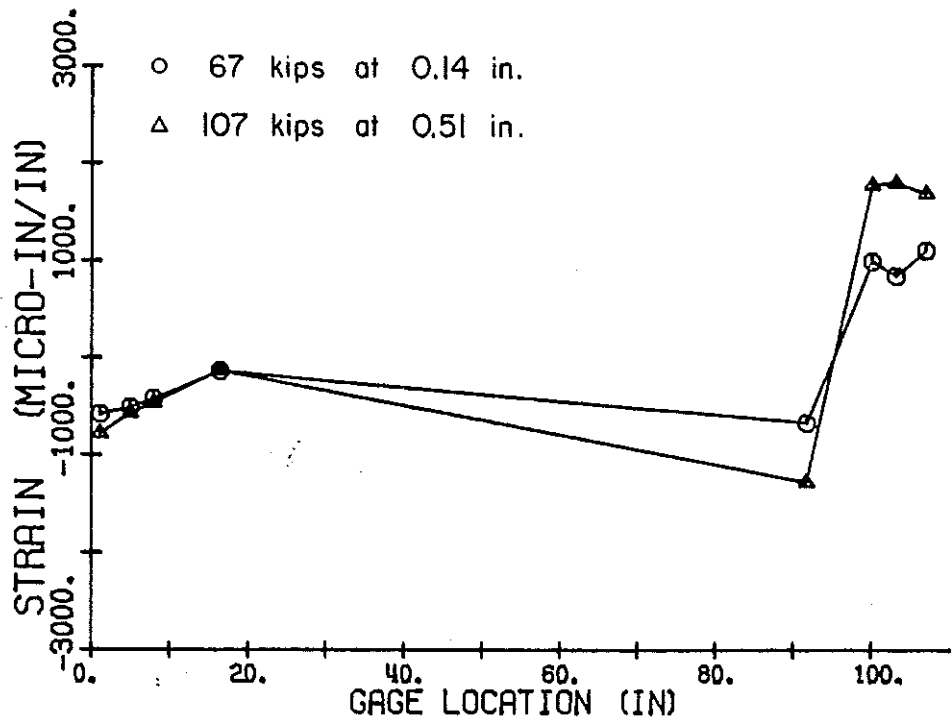


Figure F-8. Specimen 1, strain pattern at bottom of wall during first load cycled to +107 kips.

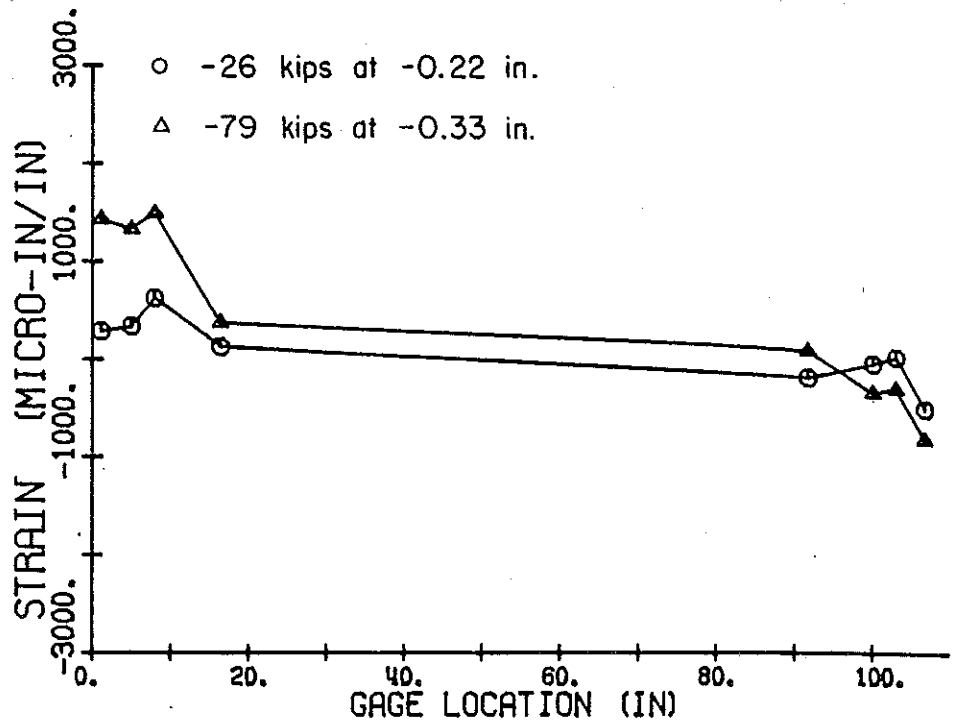


Figure F-9. Specimen 1, strain pattern at top of wall during first load cycle to +107 kips.

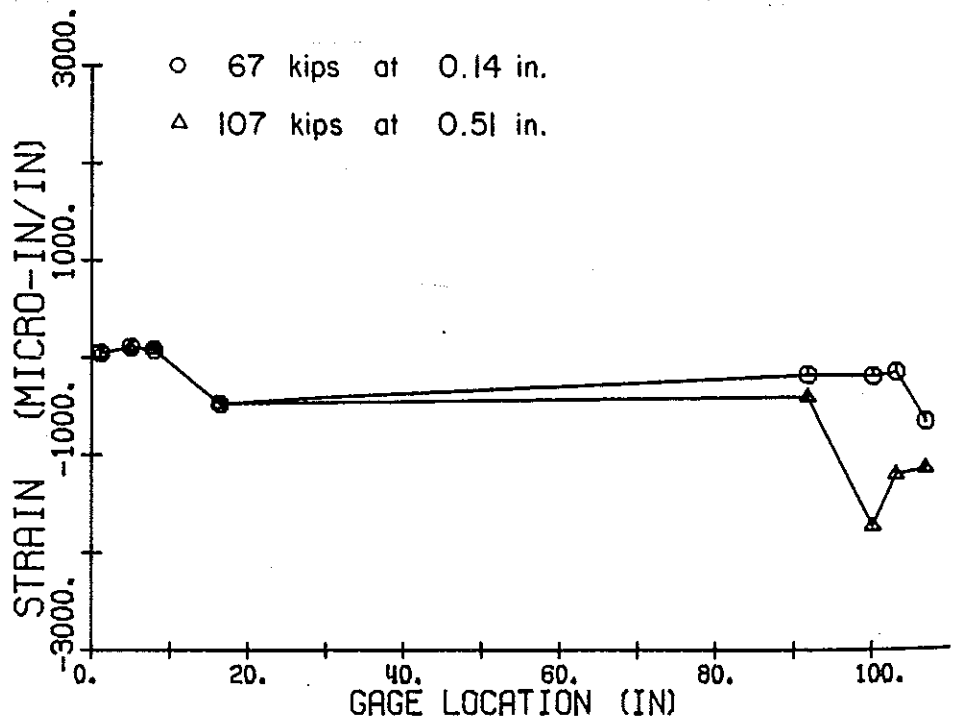


Figure F-10. Specimen 1, strain pattern at bottom of wall during first load cycle to -107 kips.

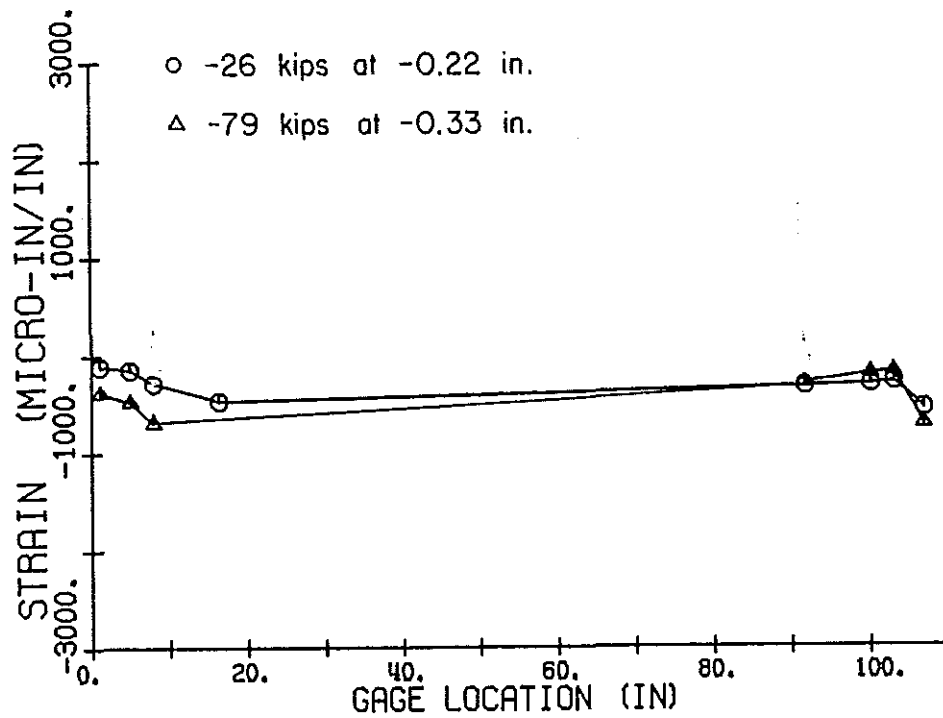


Figure F-11. Specimen 1, strain pattern at top of wall during first load cycle to -107 kips.

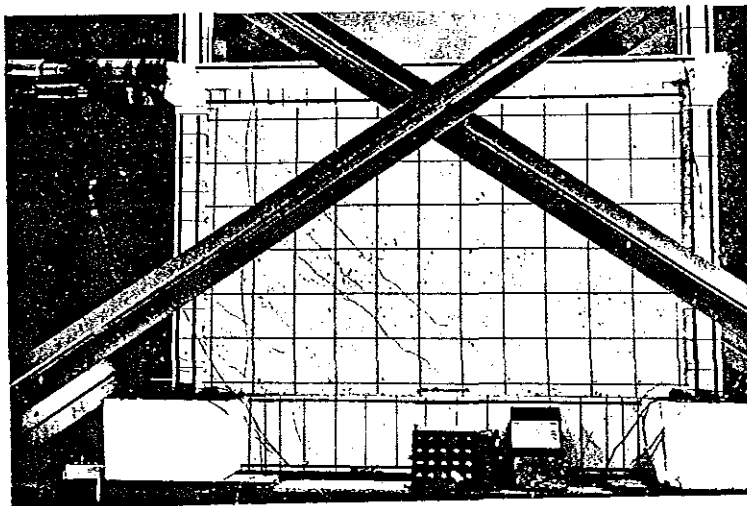


Figure F-12. Specimen 1, crack pattern after cycles to +107 kips.

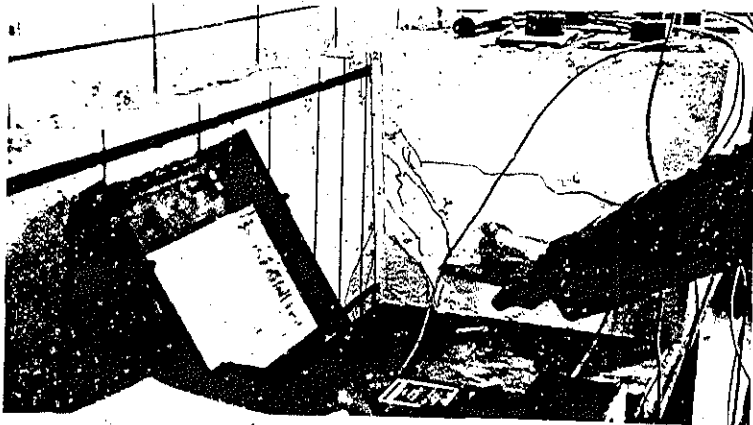


Figure F-13. Specimen 1, cracking of foundation.

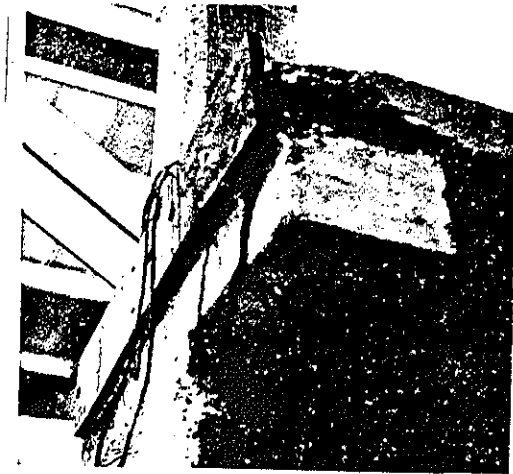


Figure F-14. Specimen 1, edge beam failure at -150 kips.



Figure F-15. Specimen 1, repair of edge beam.

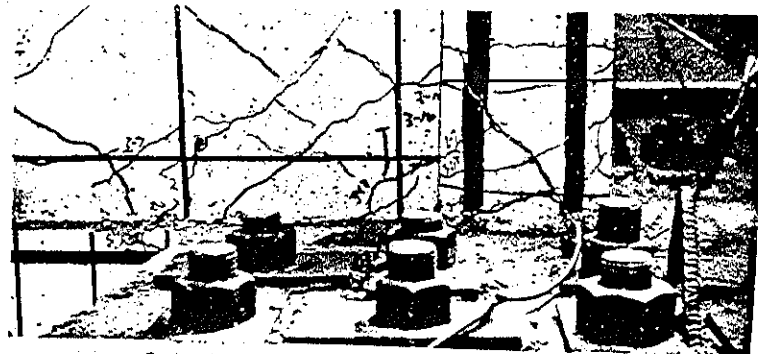


Figure F-16. Specimen 1, compression column at load of +125.7 kips.

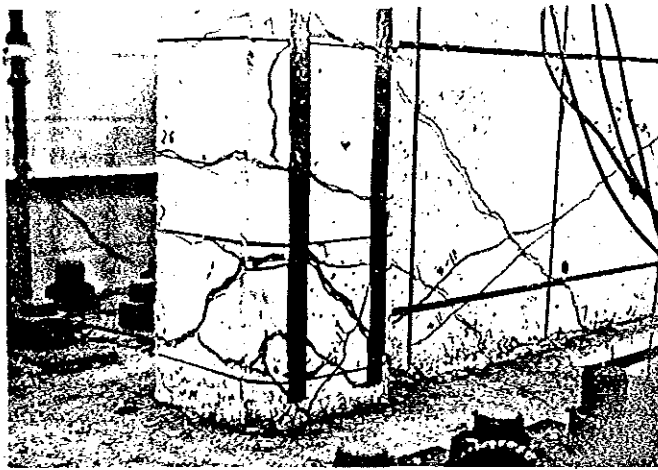


Figure F-17. Specimen 1, tension column at load of +125.7 kips.

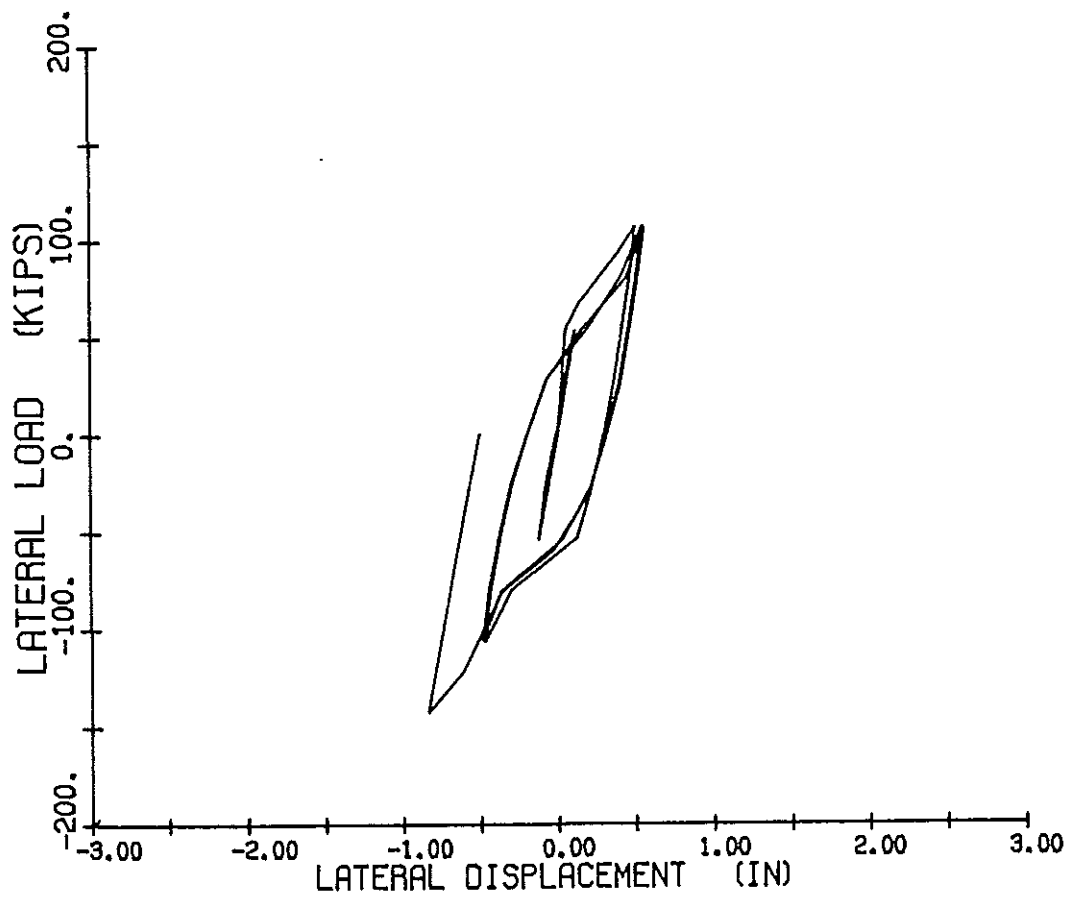


Figure F-18. Specimen 1, load deflection response for three cycles to  $\pm 0.8$  in.

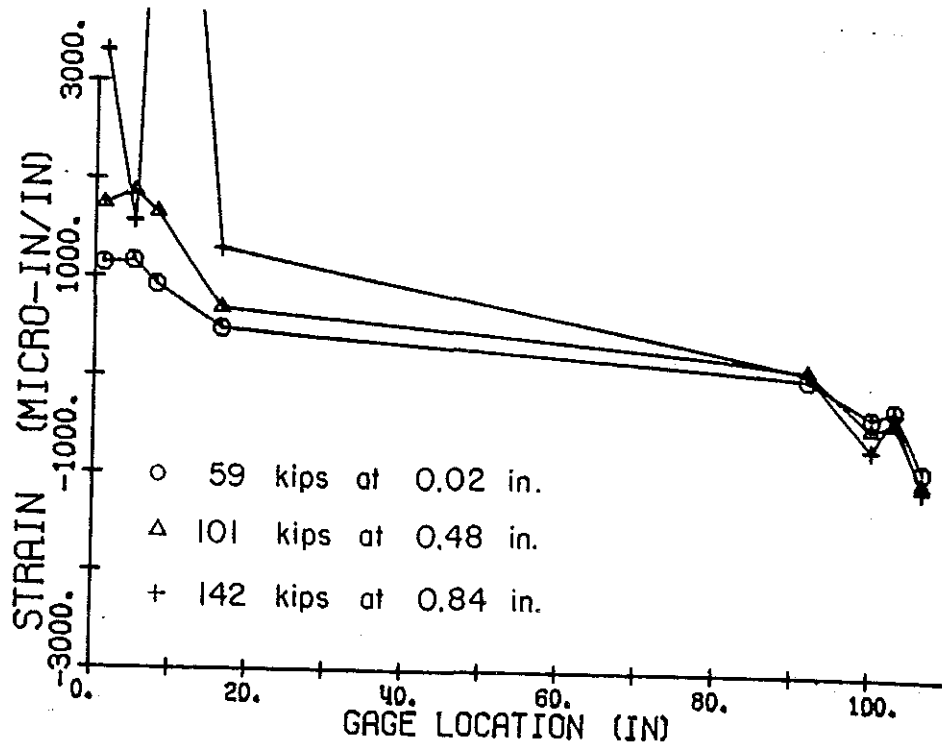


Figure F-19. Specimen 1, bottom strain gage at first half cycle to -0.8 in.

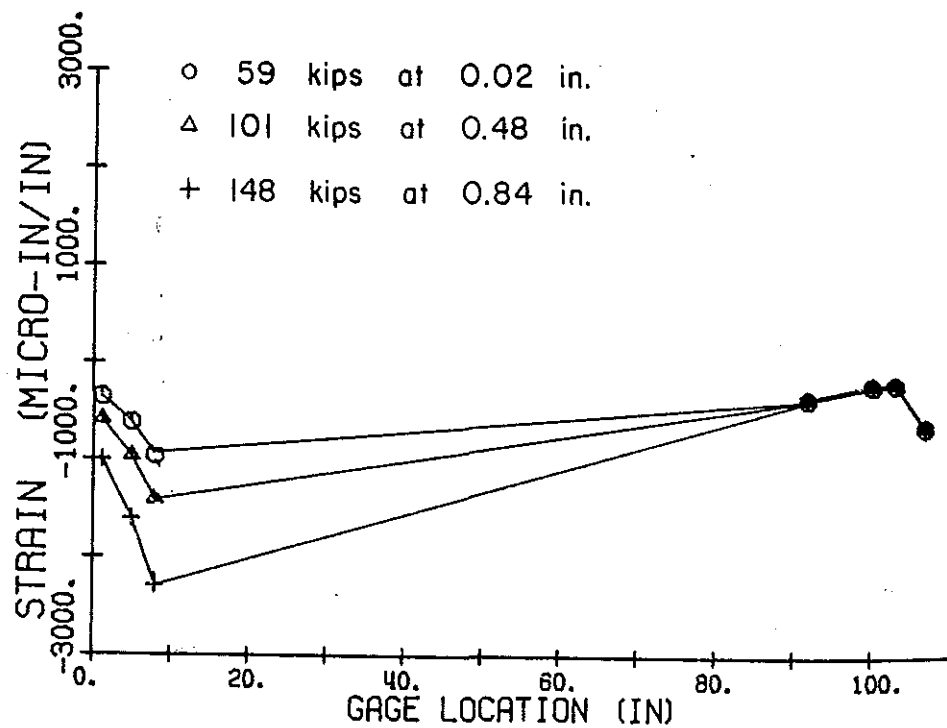


Figure F-20. Specimen 1, top strain gage at first half cycle to -0.8 in.

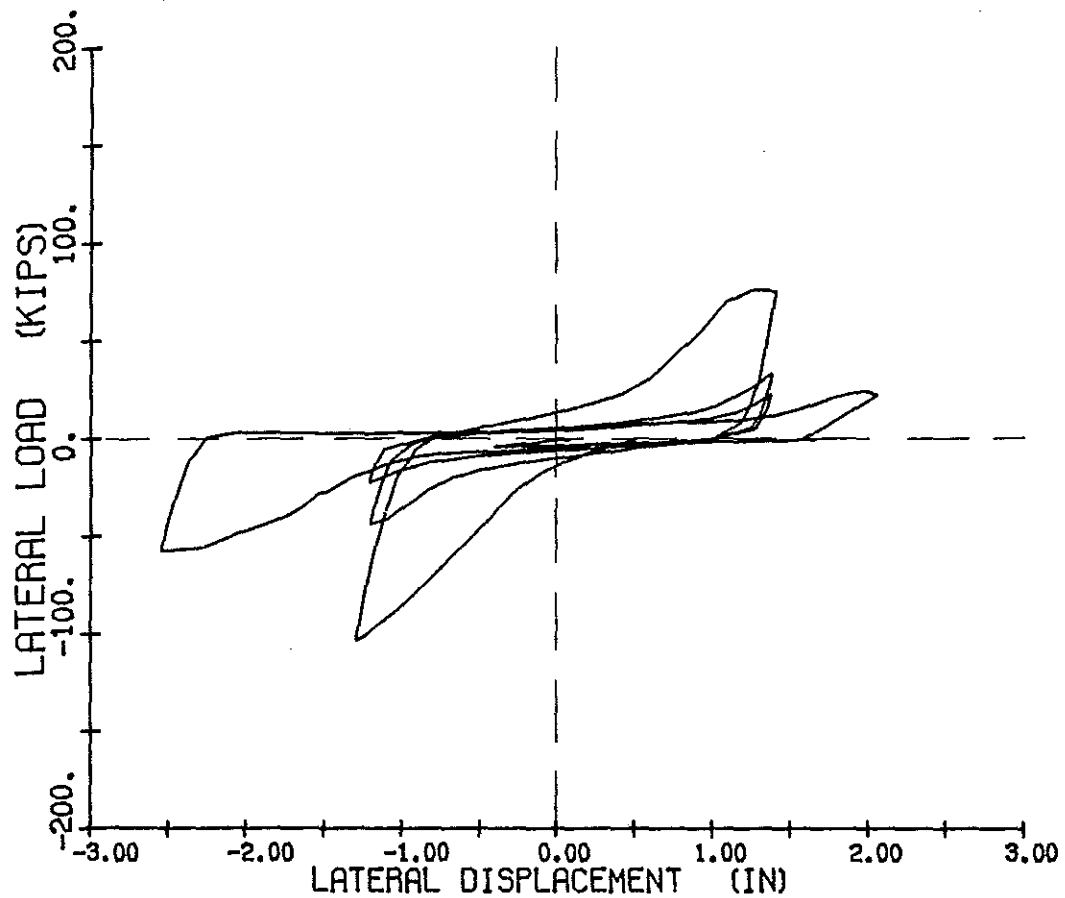


Figure F-21. Specimen 1, load-deflection curve to  $\pm 1.3$  and  $-2.7$  and  $+2.1$  in.



Figure F-22. Specimen 1, compression side at second half cycle to  $+1.3$  in.

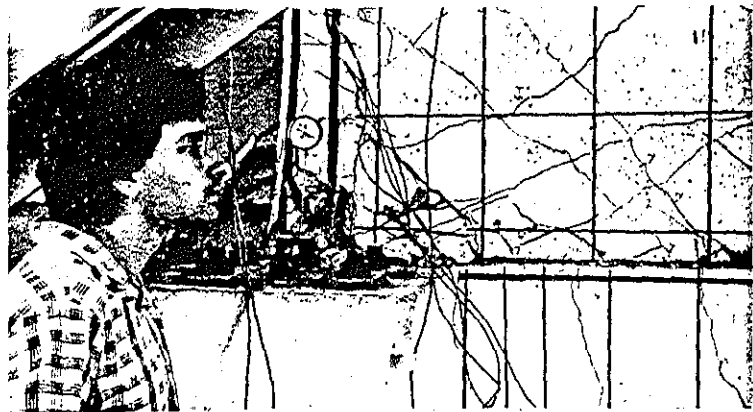


Figure F-23. Specimen 1, tension side at second half cycle to  $+1.3$  in.

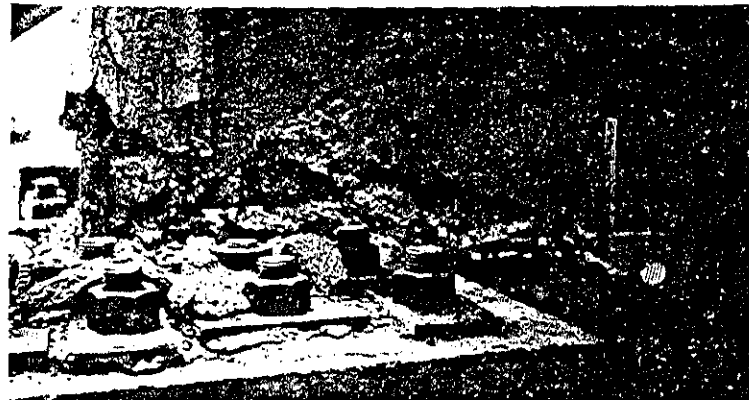


Figure F-24. Specimen 1, south column after three cycles to  $+1.3$  in.

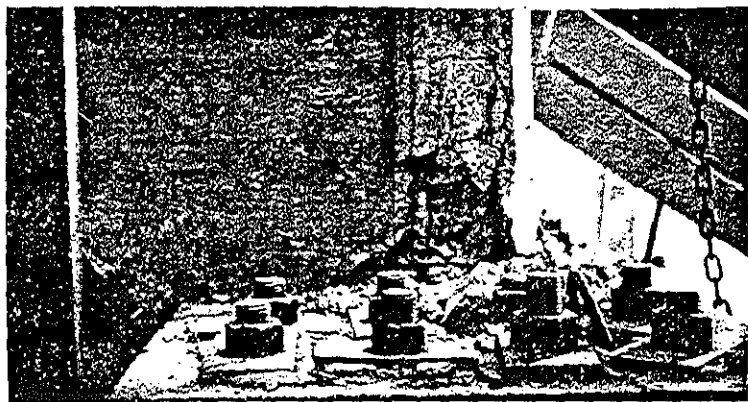


Figure F-25. Specimen 1, north column after three cycles to  $+1.3$  in.

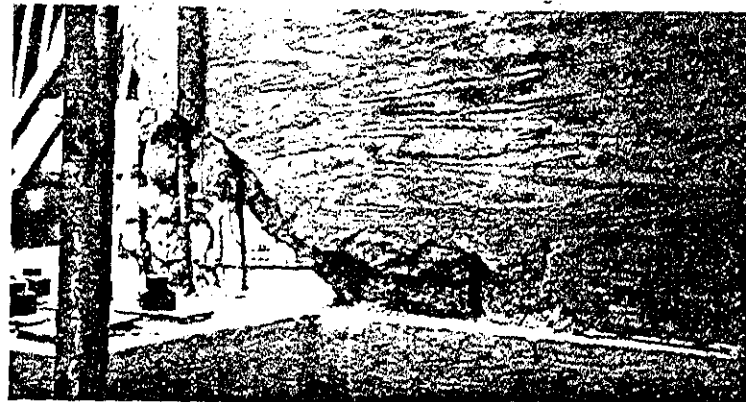


Figure F-26. Specimen 1, southwest portion collapse.

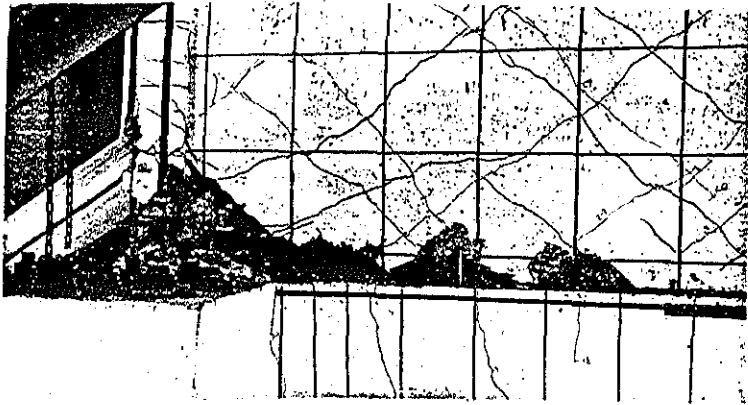


Figure F-27. Specimen 1, north portion after test.



Figure F-28. Specimen 1, south portion after test.

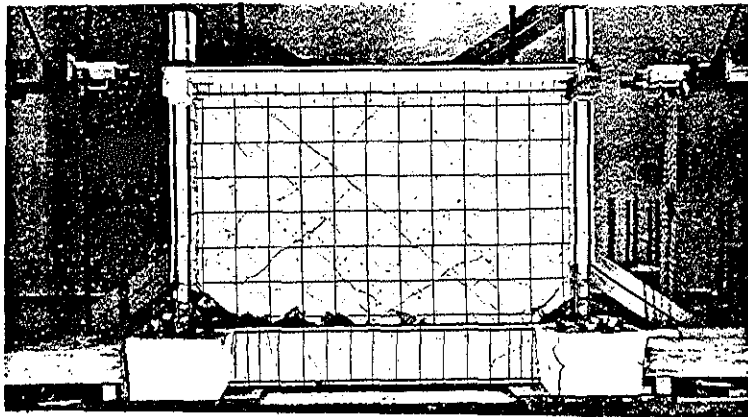


Figure F-29. Specimen 1, entire specimen after test.

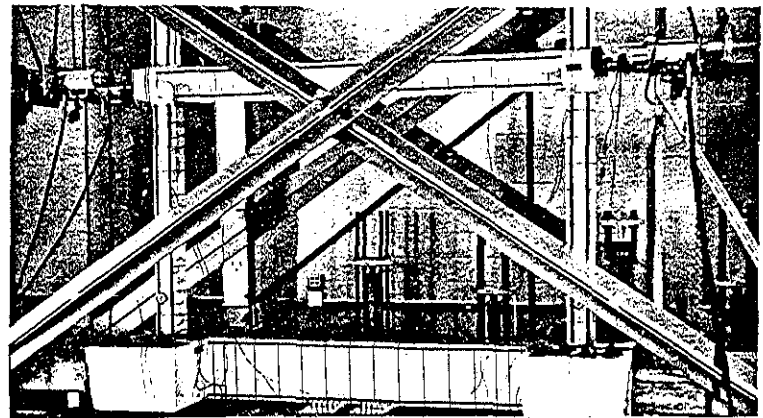


Figure F-30. Specimen 2, after three cycles to  $\pm 0.5$  in.

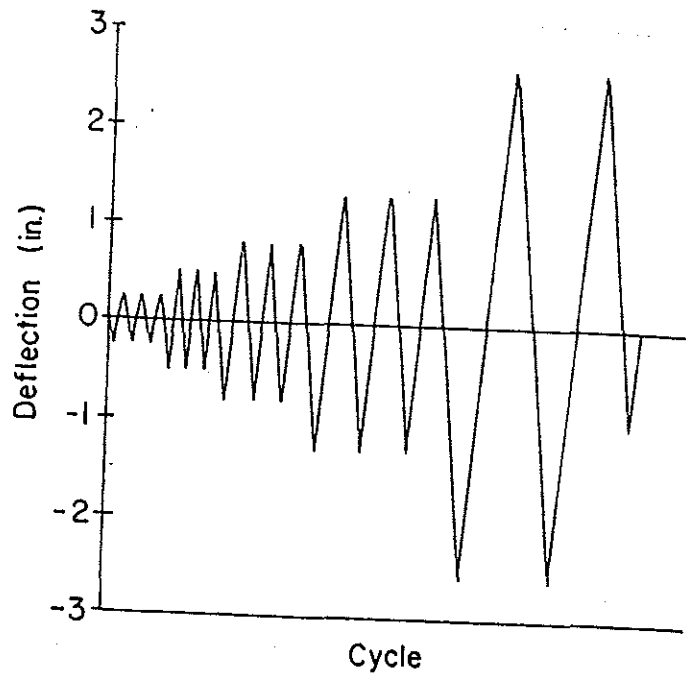


Figure F-31. Specimen 2, deflection sequence.

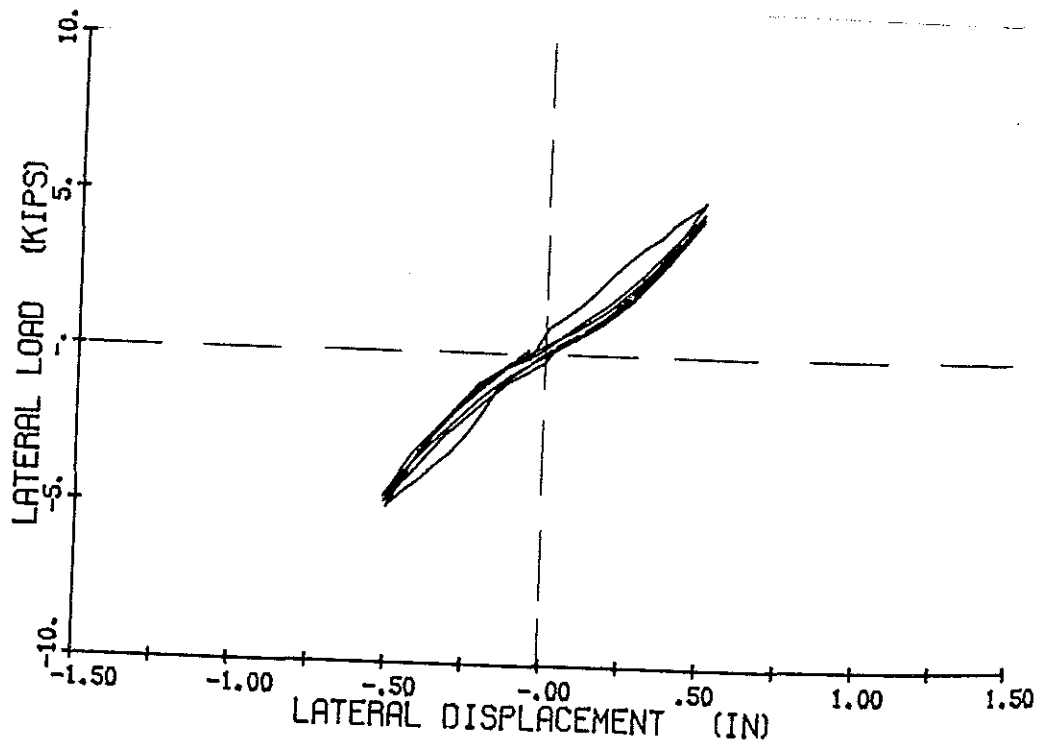


Figure F-32. Specimen 2, load-deflection curve for three cycles to +0.5 in.

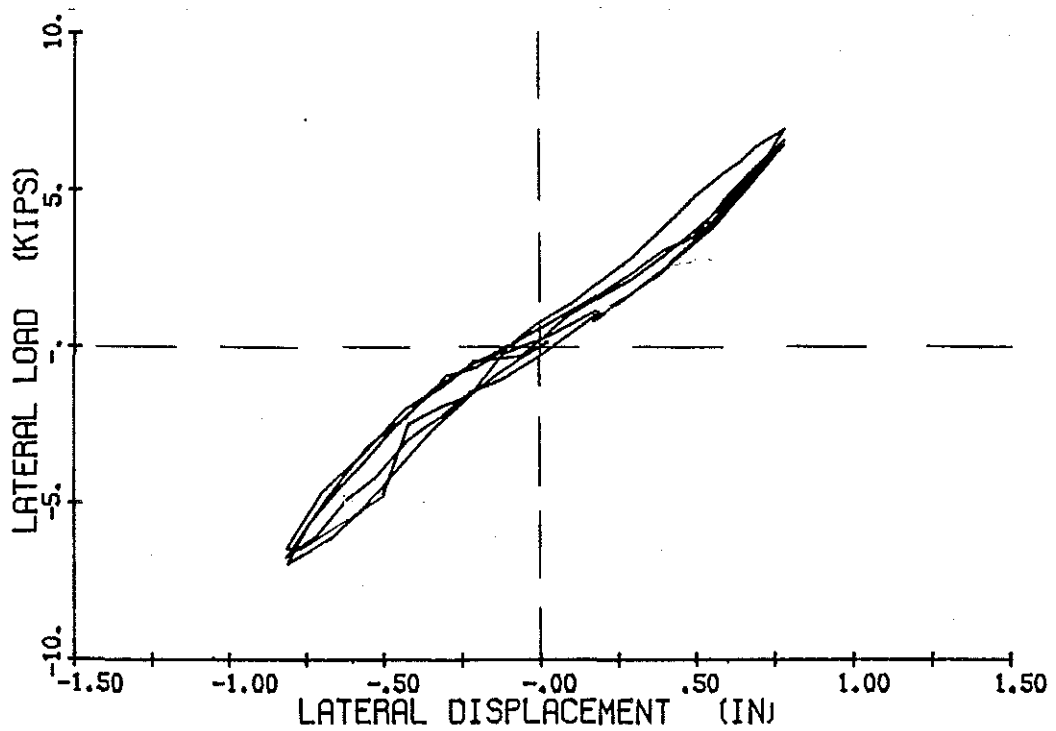


Figure F-33. Specimen 2, load-deflection curve for three cycles to  $\pm 0.8$  in.

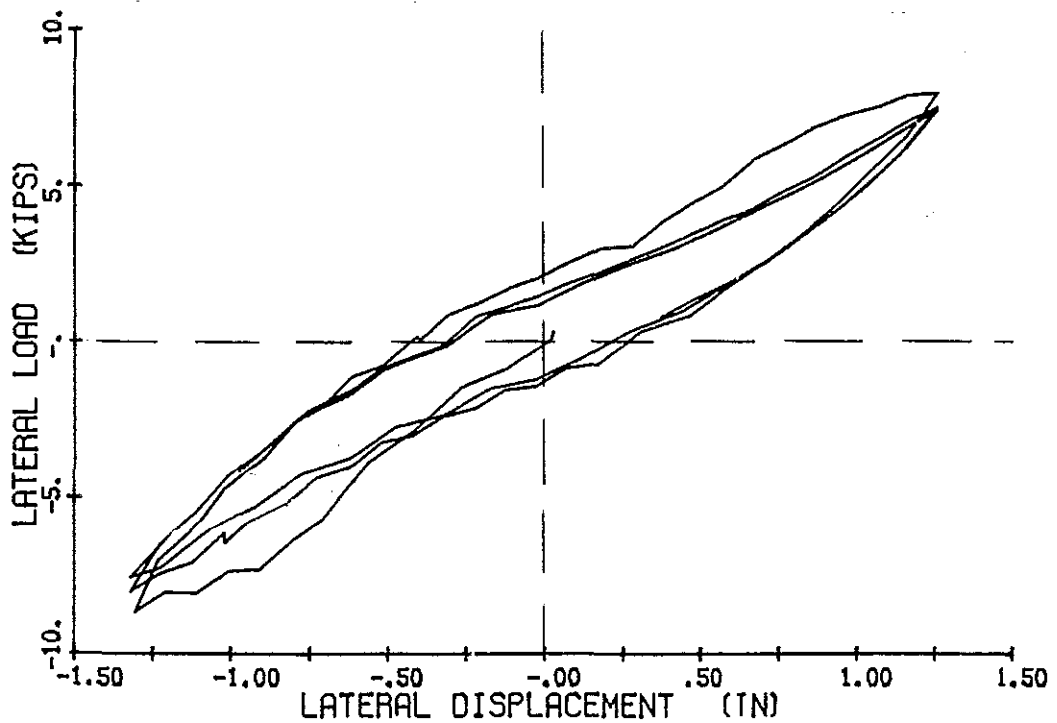


Figure F-34. Specimen 2, load-deflection curve for three cycles to  $\pm 1.3$  in.

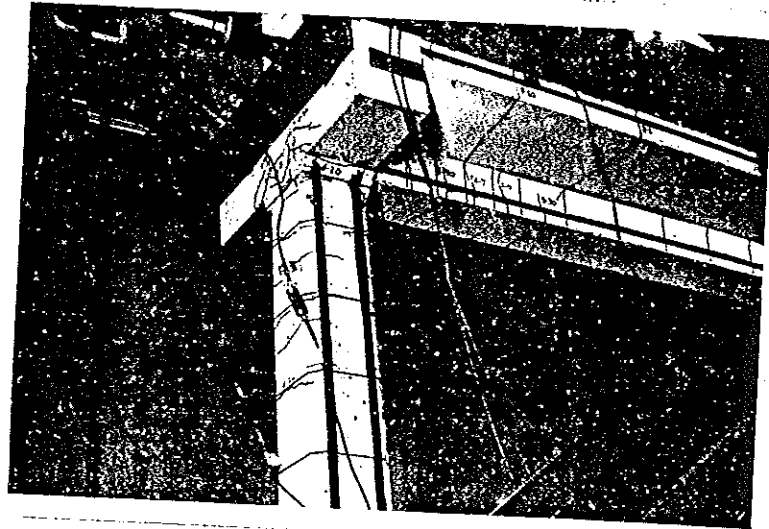


Figure F-35. Specimen 2, beam-column cracking at +1.3 in. deflection.

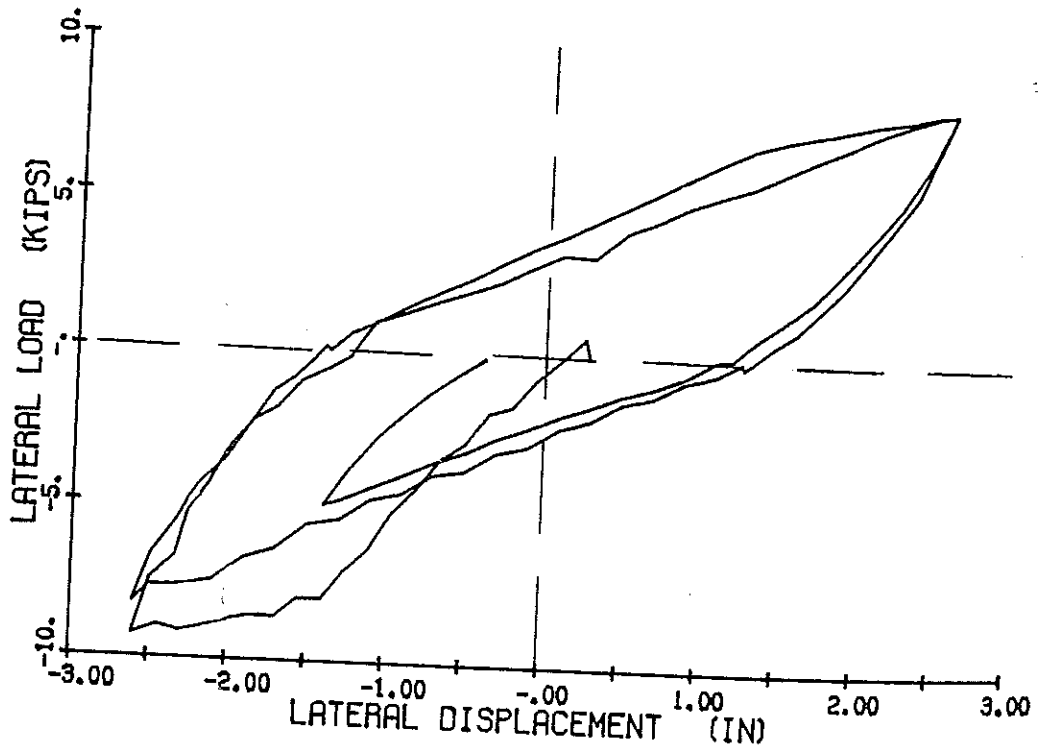


Figure F-36. Specimen 2, load-deflection curve for two cycles to +2.6 in.

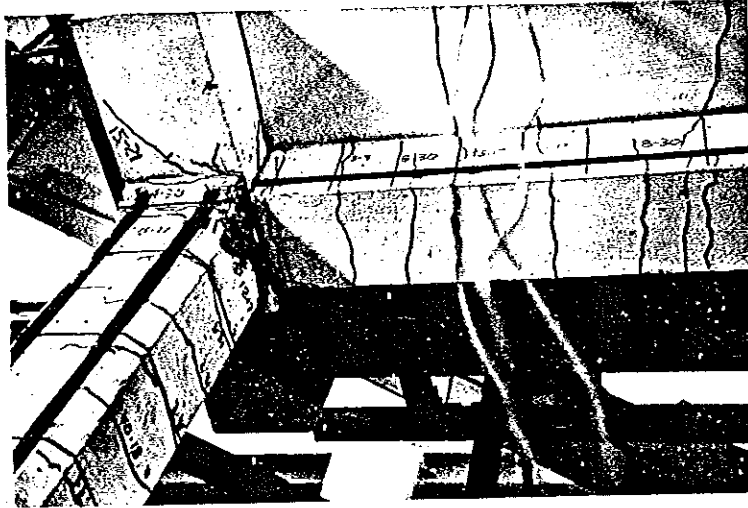


Figure F-37. Specimen 2, crushing at beam-column connection.

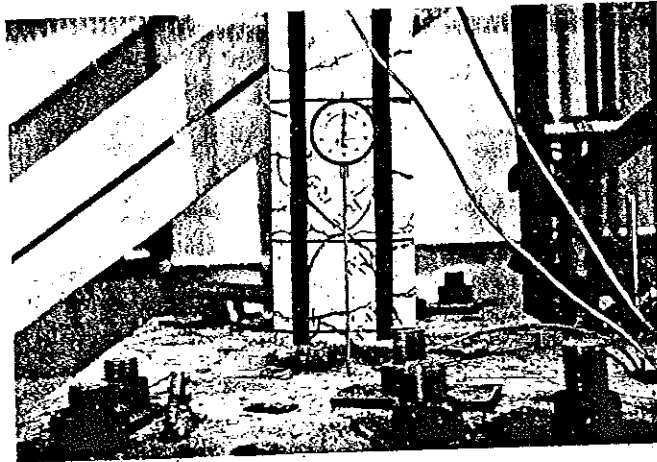


Figure F-38. Specimen 2, diagonal cracking in north column.

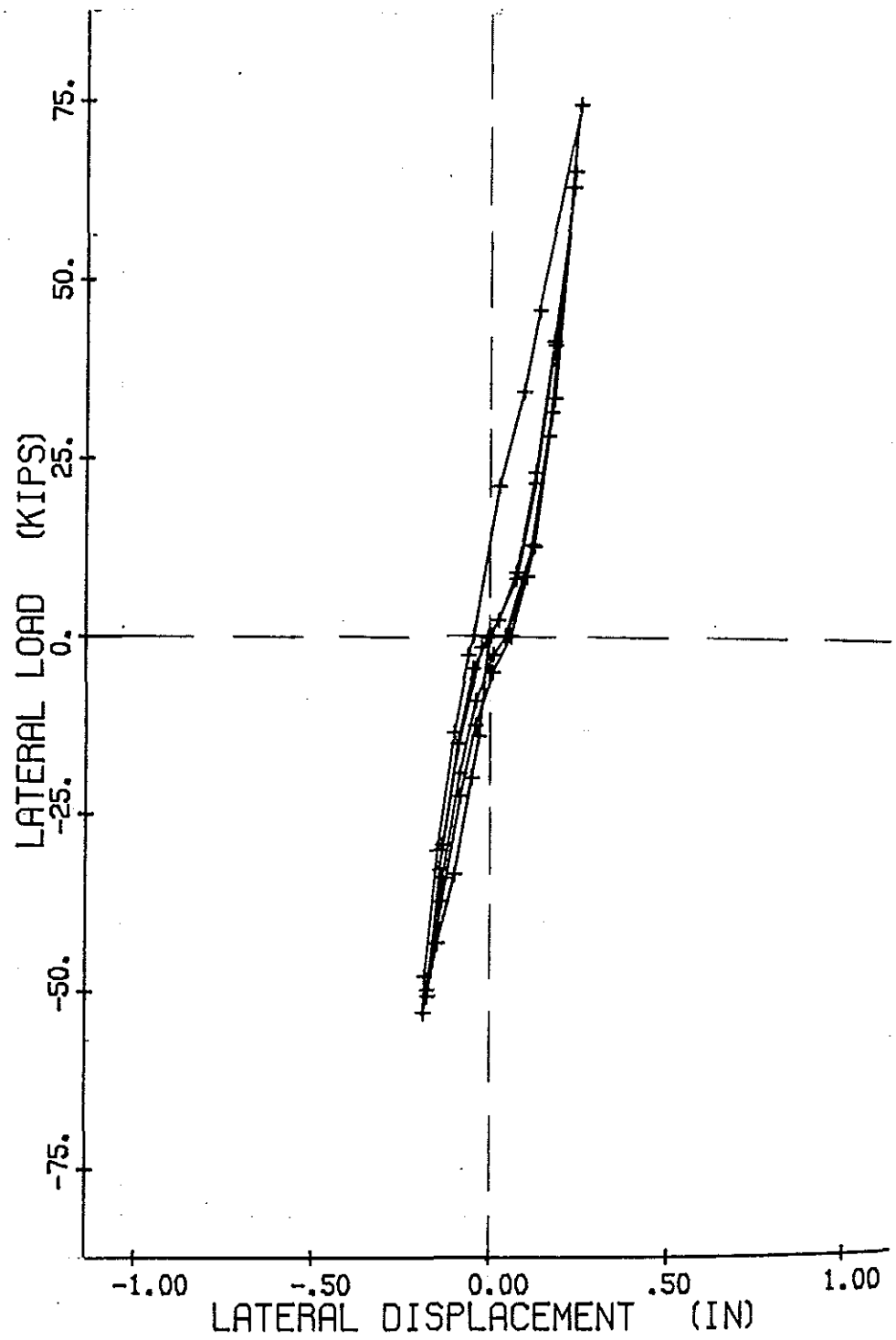


Figure F-39. Specimen 3, load-deflection curve for +0.1 in. cycles.

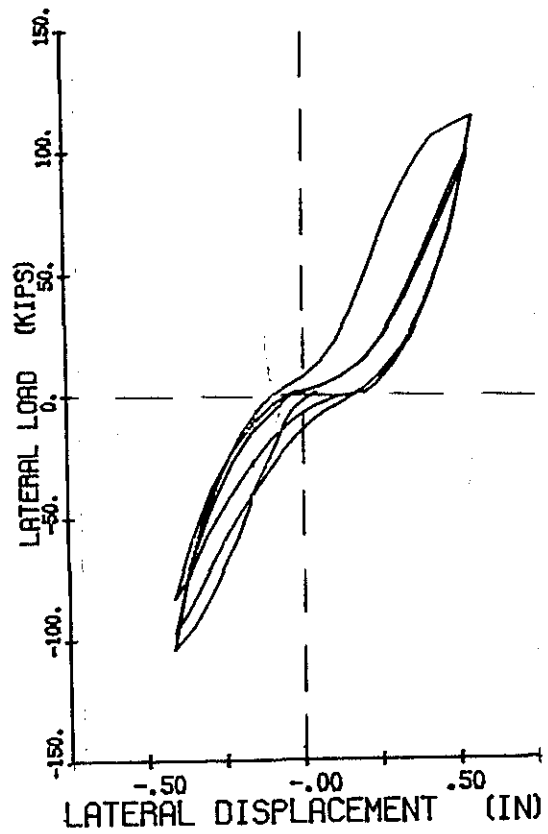


Figure F-41. Specimen 3, load deflection curve of  $\pm 0.5$  in. cycles.

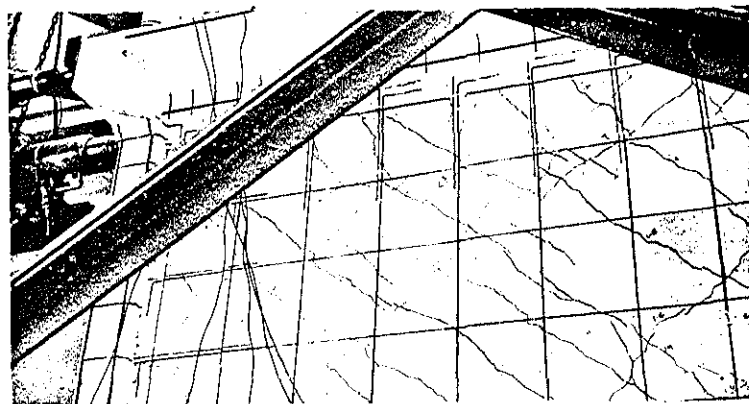


Figure F-40. Specimen 3, second half cycle to  $+0.2$  in.,  $+74.4$  kips.

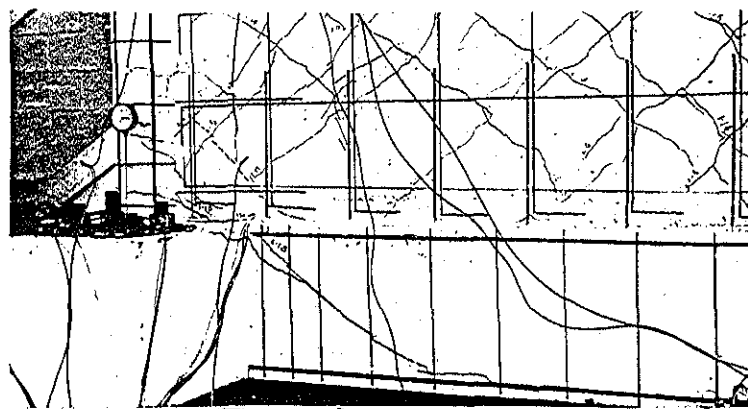


Figure F-42. Specimen 3, diagonal crack through north column and base beam during second half cycle to  $+0.56$  in.

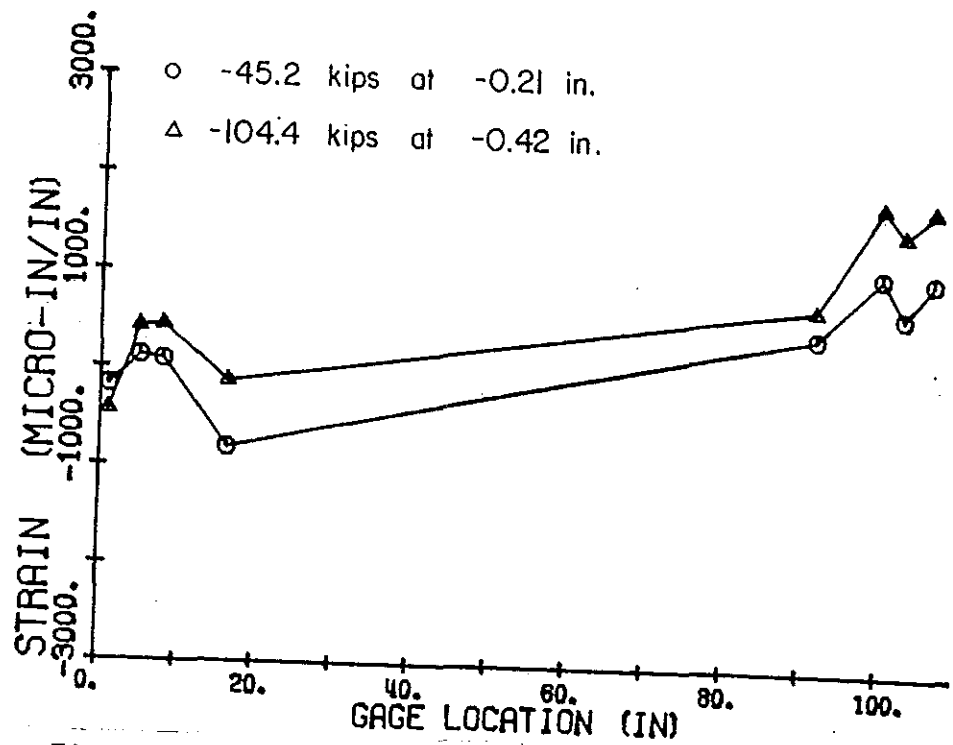


Figure F-43. Specimen 3, strain pattern, bottom gages first half cycle to -0.5 in.

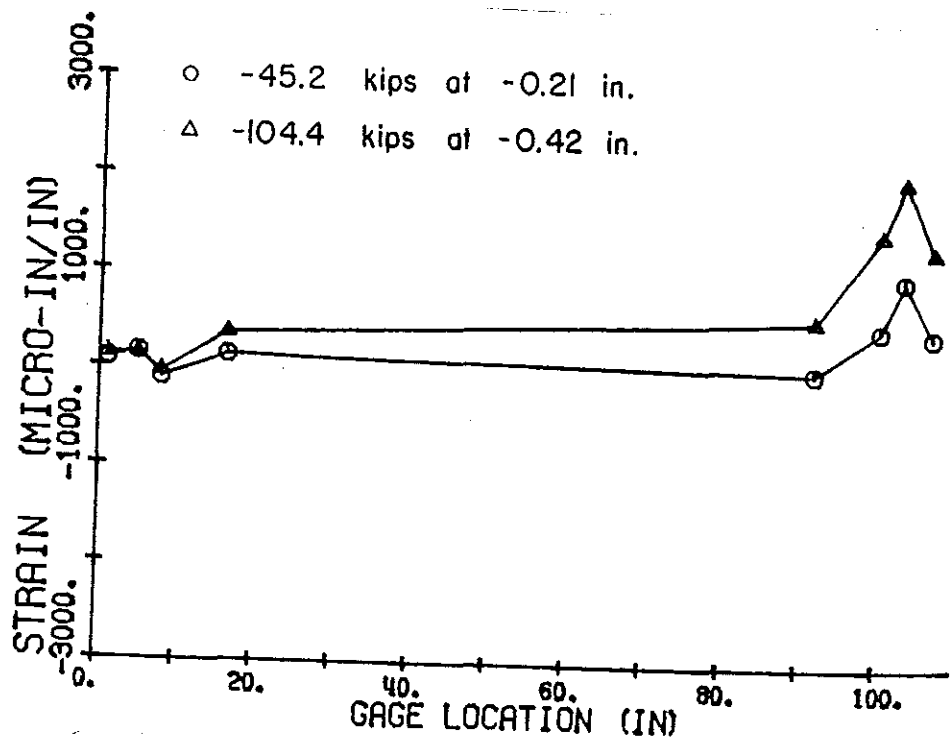


Figure F-44. Specimen 3, strain pattern, top gages first half cycle to -0.5 in.

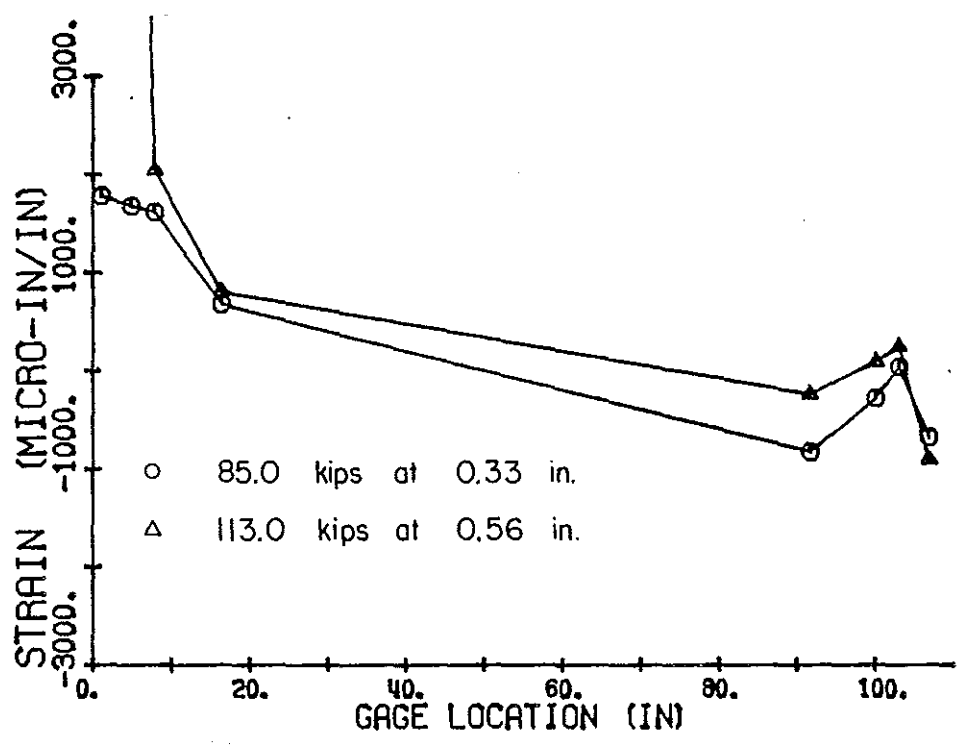


Figure F-45. Specimen 3, strain pattern, bottom gages second half cycle to +0.5 in.

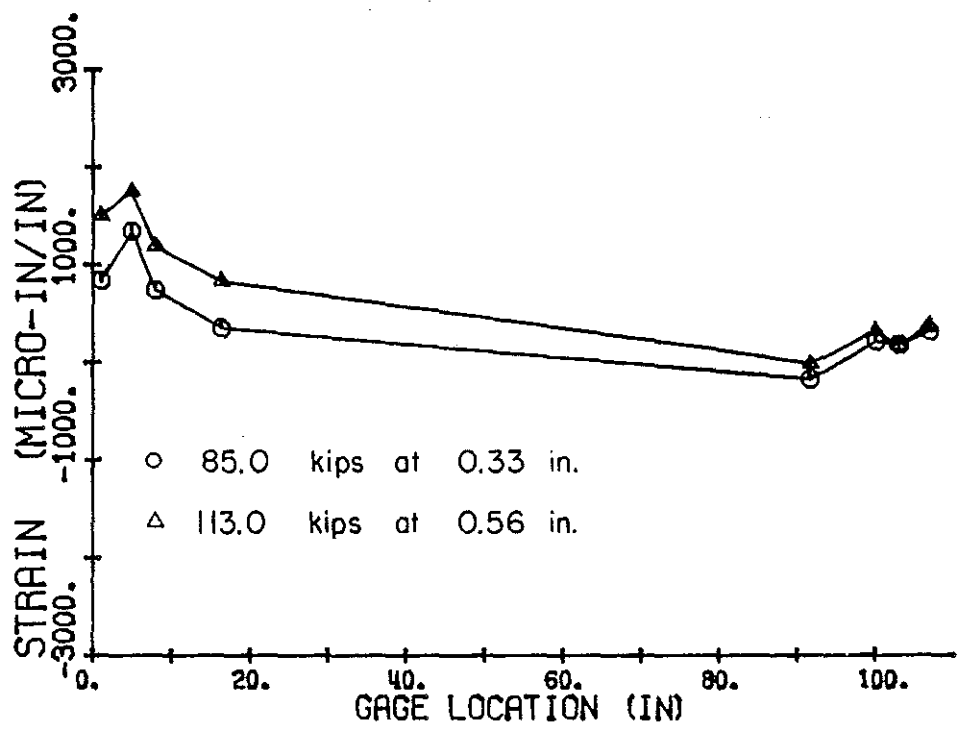


Figure F-46. Specimen 3, strain pattern, top gages second half cycle to +0.5 in.

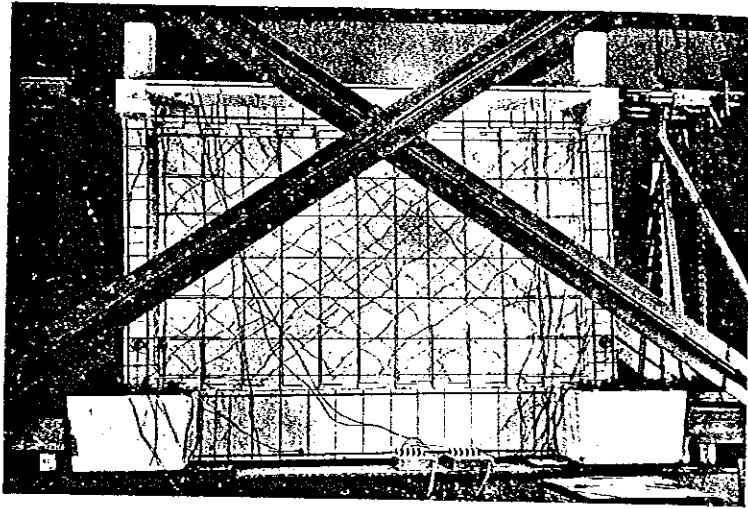


Figure F-47. Specimen 3, extensive diagonal cracking after  $\pm 0.5$  in cycle.

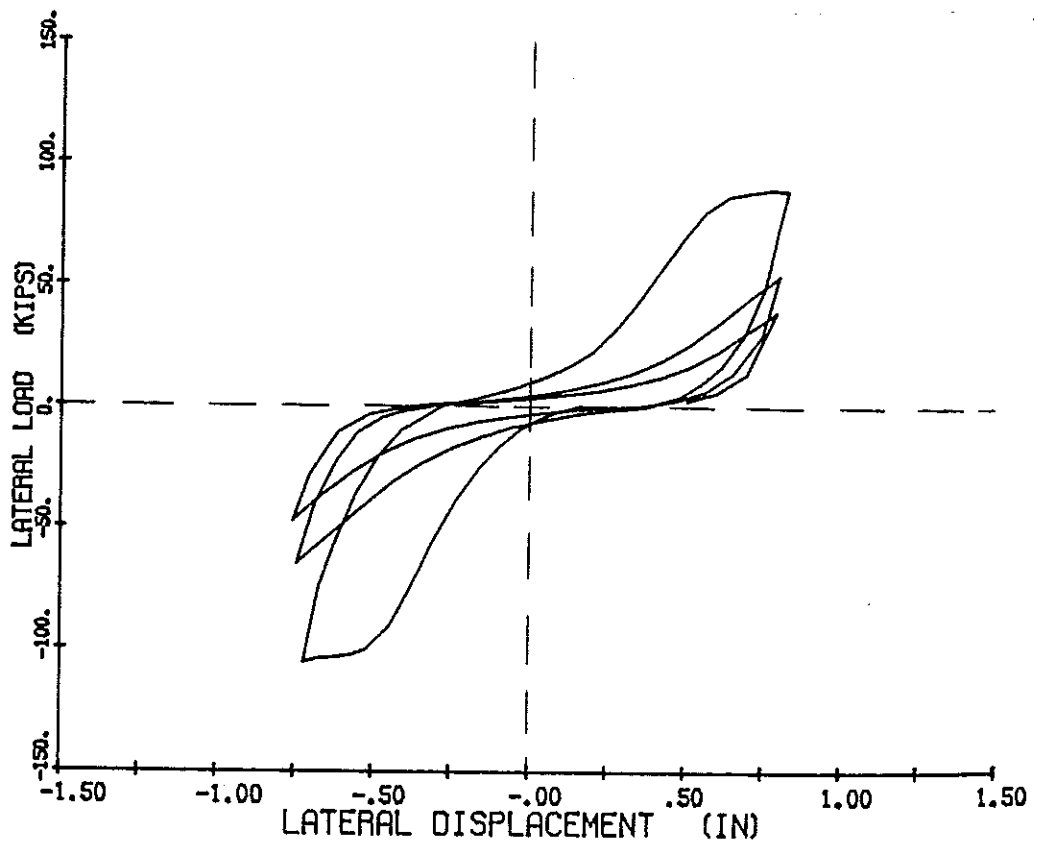


Figure F-48. Specimen 3, load-deflection curve  $\pm 0.8$  in. deflection.

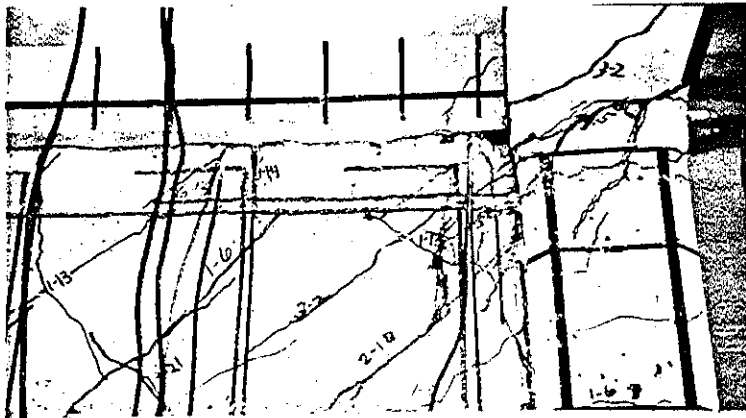


Figure F-49. Specimen 3, beginning of corner crushing, -0.72 in. deflection.



Figure F-51. Specimen 3, joint slip and drypack crack, -0.72 in. deflection.

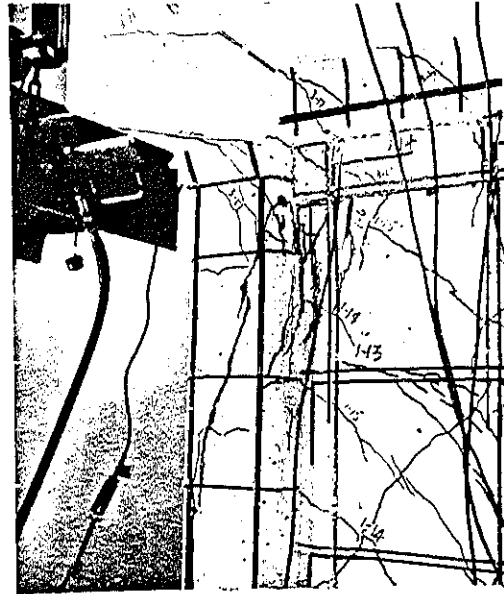


Figure F-50. Specimen 3, diagonal crack in north column, -0.72 in. deflection.

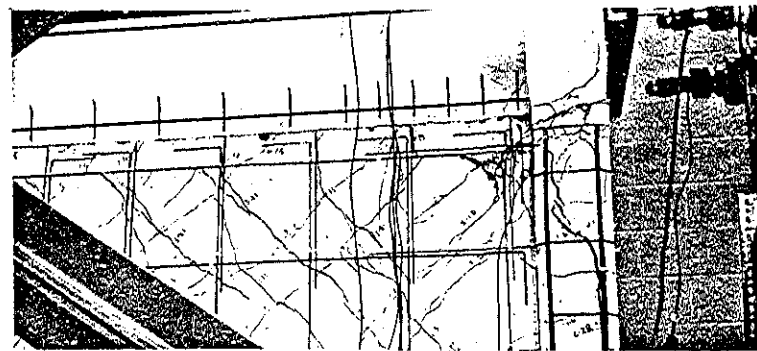


Figure F-52. Specimen 3, crushing in CIP wall and south column diagonal crack, +0.83 in.

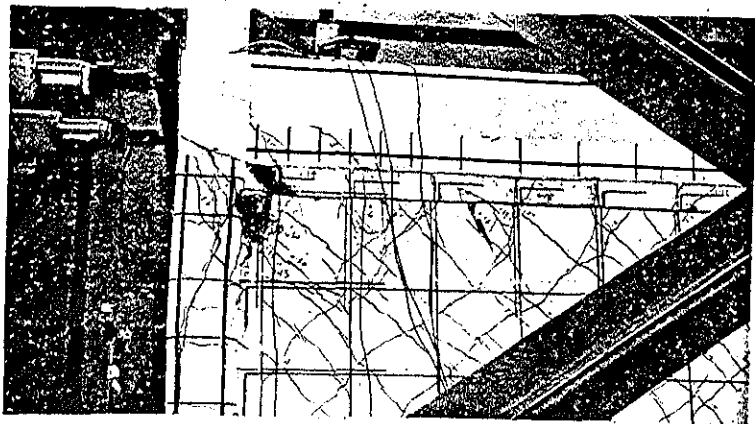


Figure F-53. Specimen 3, crushing in drypack and CIP top north corner, +0.83 in.

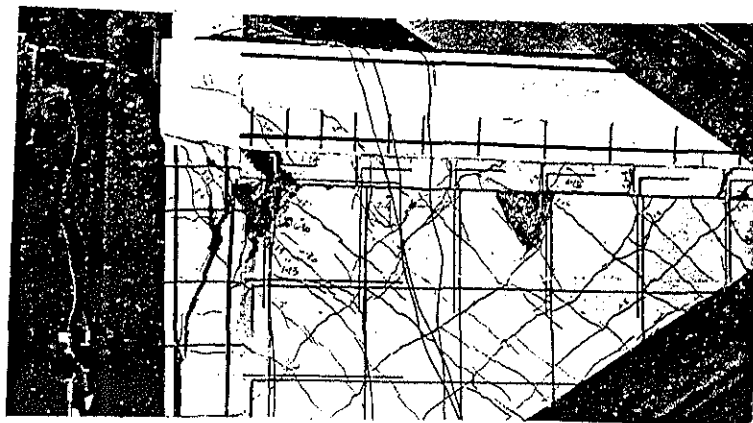


Figure F-54. Specimen 3, third half-cycle to -0.72 in. deflection.

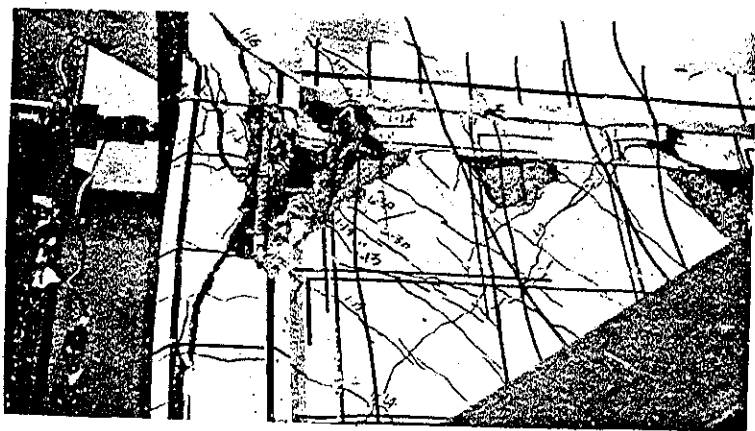


Figure F-55. Specimen 3, north column and wall at third cycle to +0.83 in.

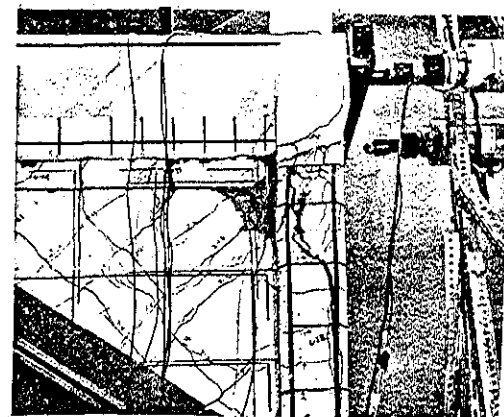


Figure F-56. Specimen 3, south column and wall after third cycle to +0.83 in.

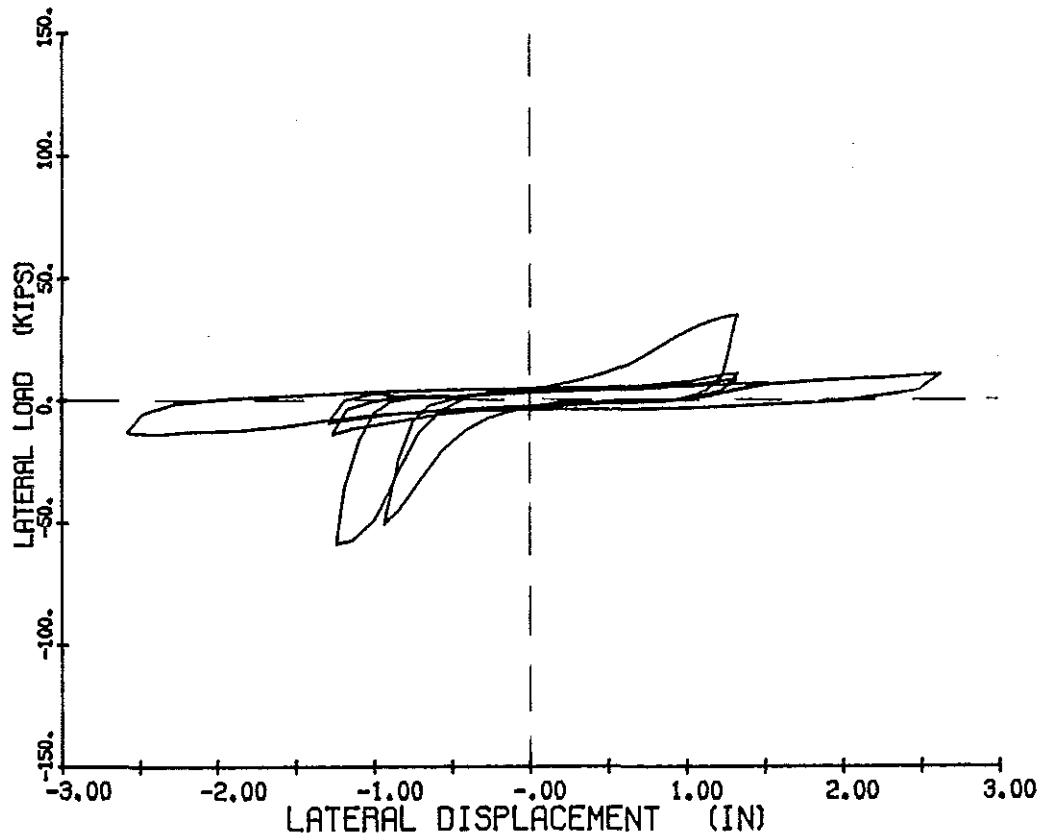


Figure F-57. Specimen 3, load-deflection curve for three cycles to  $\pm 1.3$  in and one cycle to  $\pm 2.6$  in.

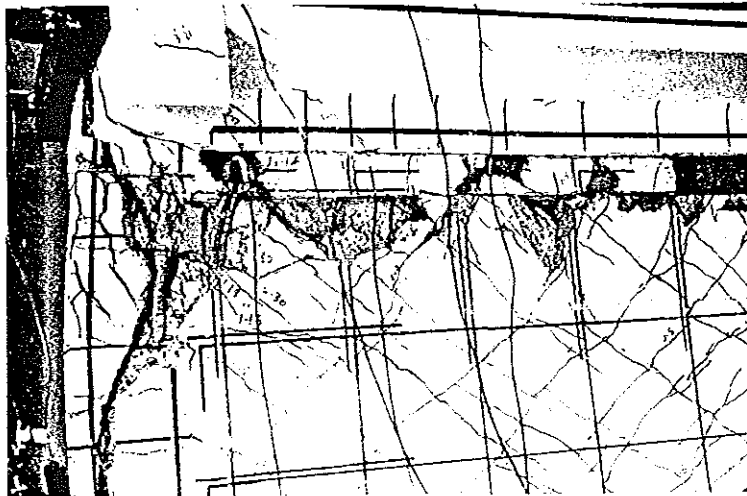


Figure F-58. Specimen 3, north side at deflection of  $\pm 1.3$  in.

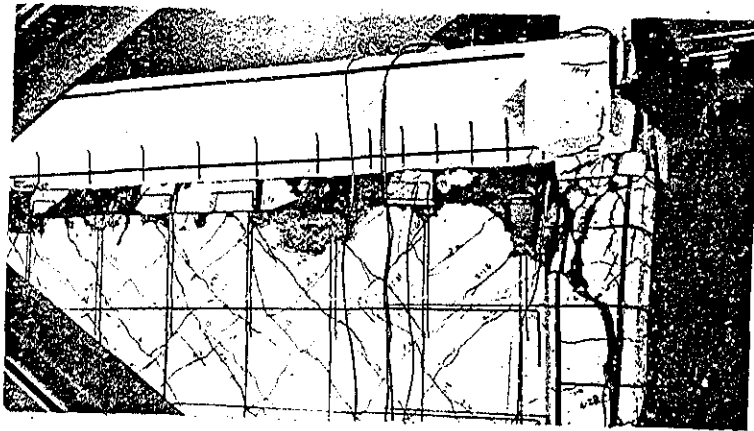


Figure F-59. Specimen 3, south side at deflection of +1.3 in.



Figure F-60. Specimen 3, north side after 2-1/2 cycles to -1.3 in.

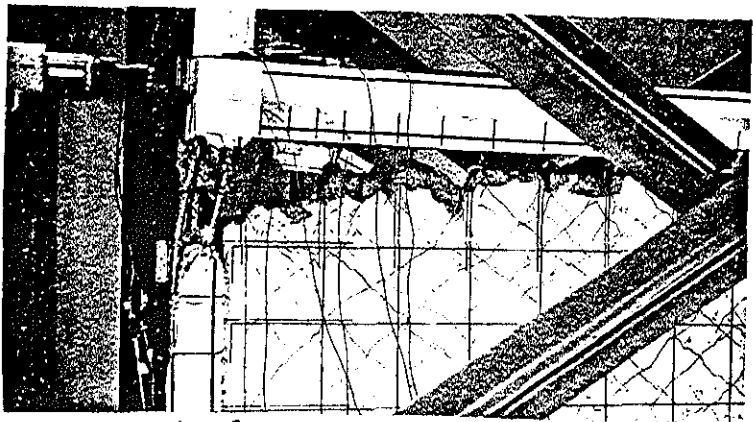


Figure F-61. Specimen 3, north column at +2.63 in.

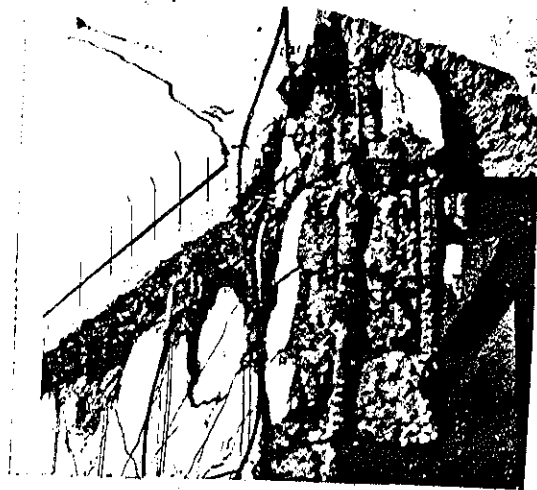


Figure F-62. Specimen 3, south column at +2.63 in.

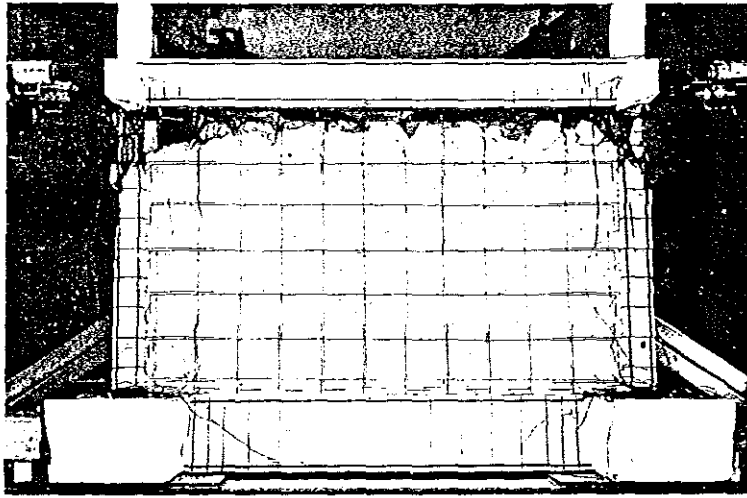


Figure F-63. Specimen 3 at completion of test.

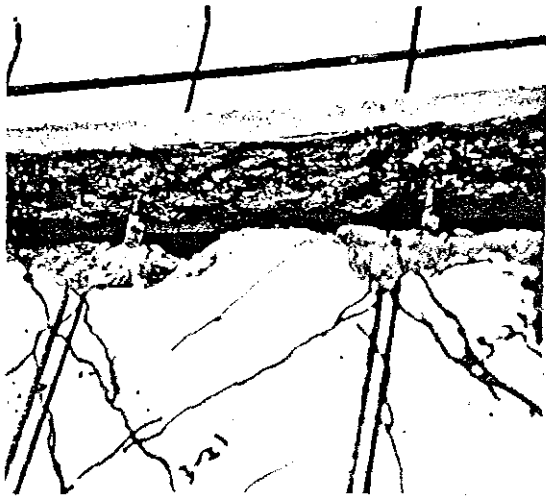


Figure F-64. Specimen 3, bottom surface of beam after test completed.



Figure F-65. Specimen 3, close-up of vertical dowel bar after test.

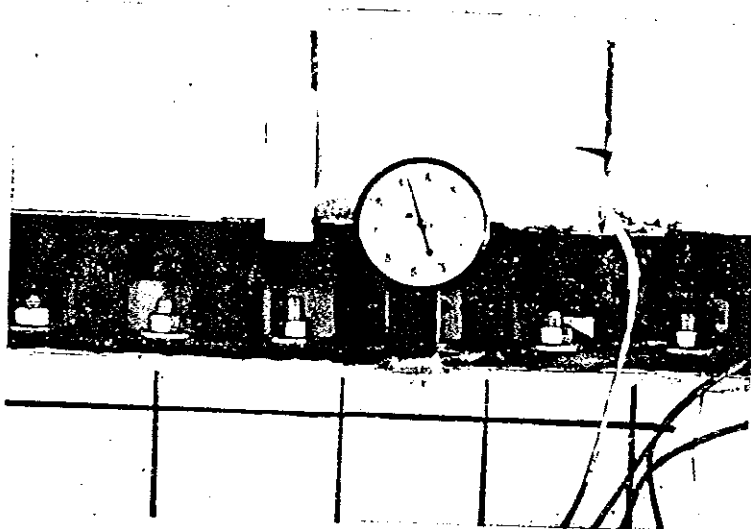


Figure F-66. Specimen 4, dial gage used for slip measurement.

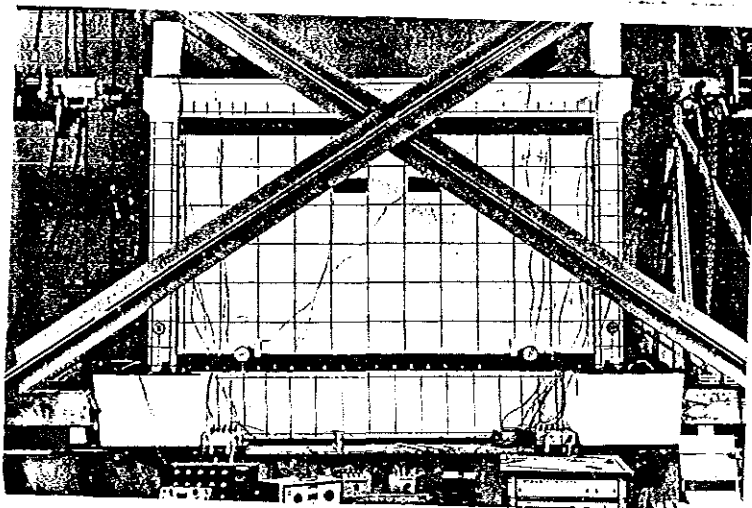


Figure F-67. Specimen 4, after three cycles to +0.20 in.

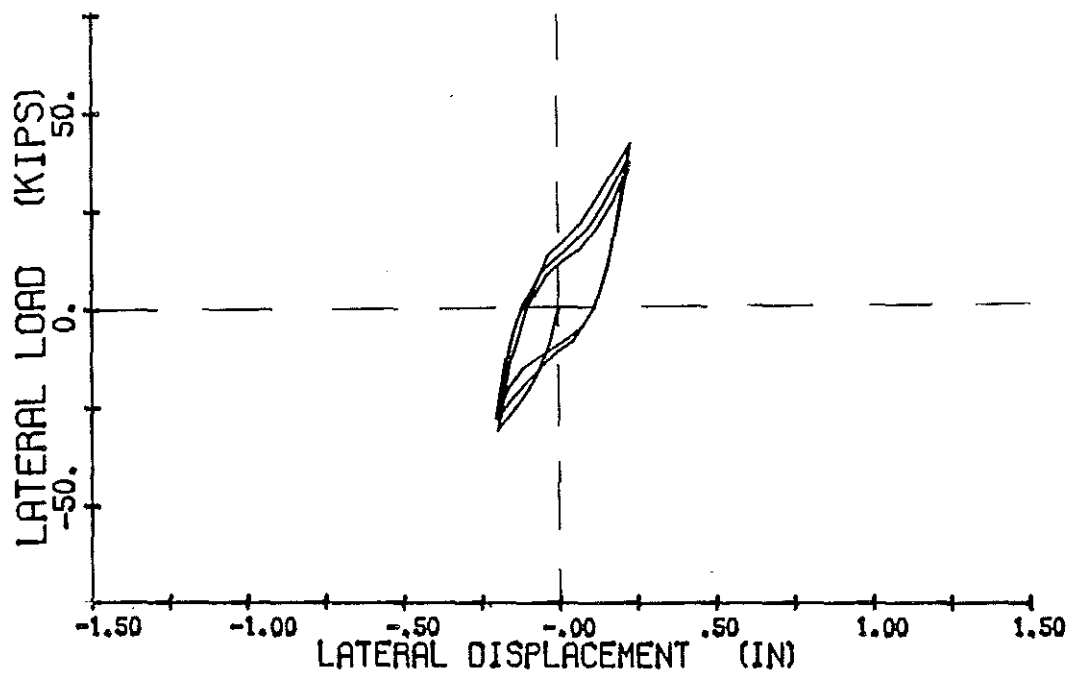


Figure F-68. Specimen 4, load-deflection curve for +0.2 in cycles.

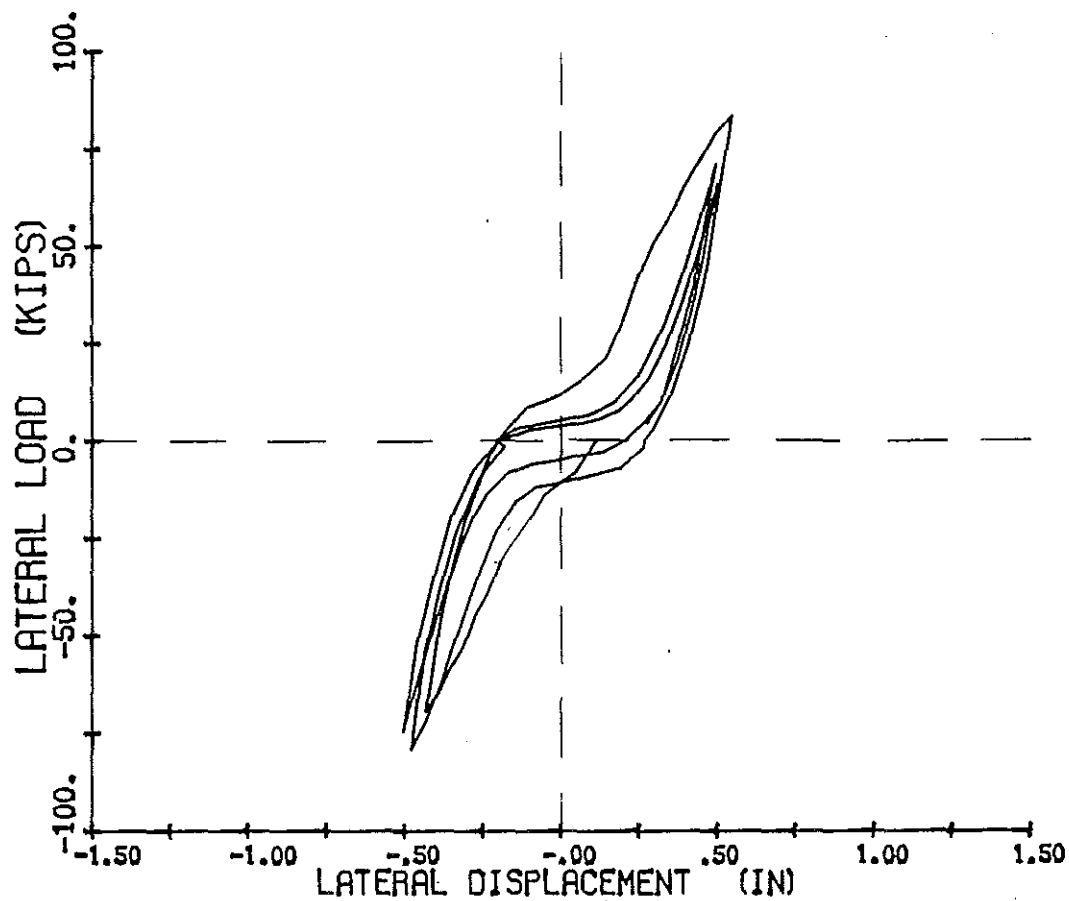


Figure F-69. Specimen 4, load-deflection curve for +0.5 in. cycles.

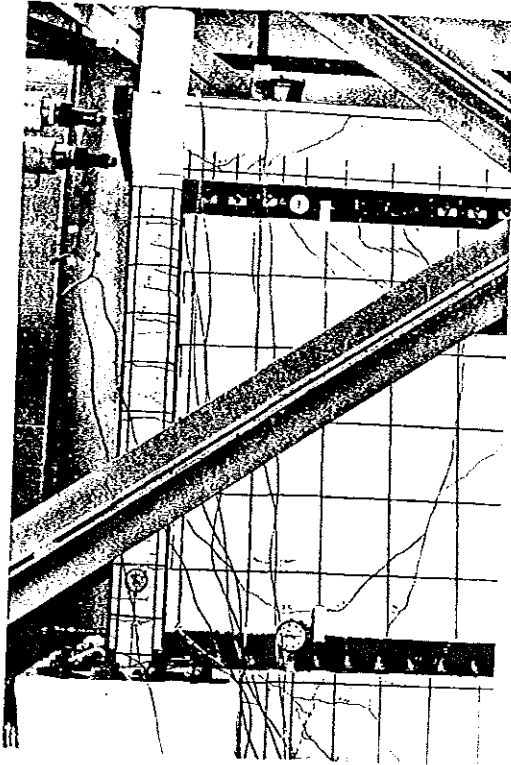


Figure F-70. Specimen 4, north column at +0.5 in., second half cycle.

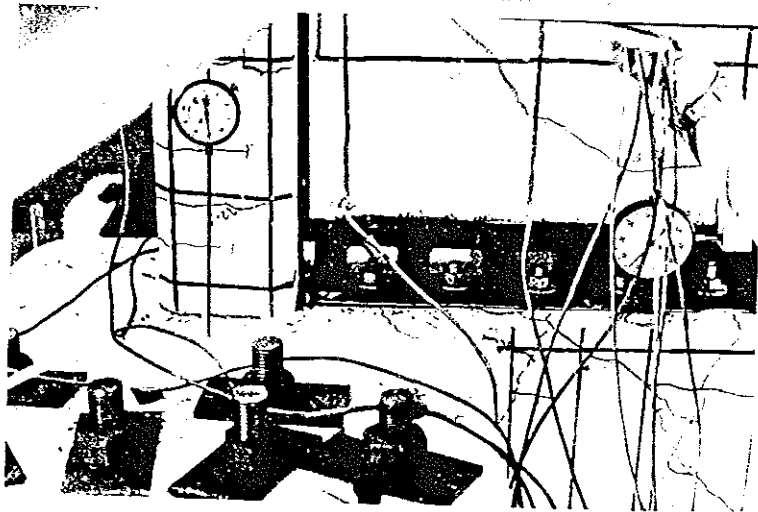


Figure F-71. Specimen 4, base of north column at +0.5 in., second half cycle.

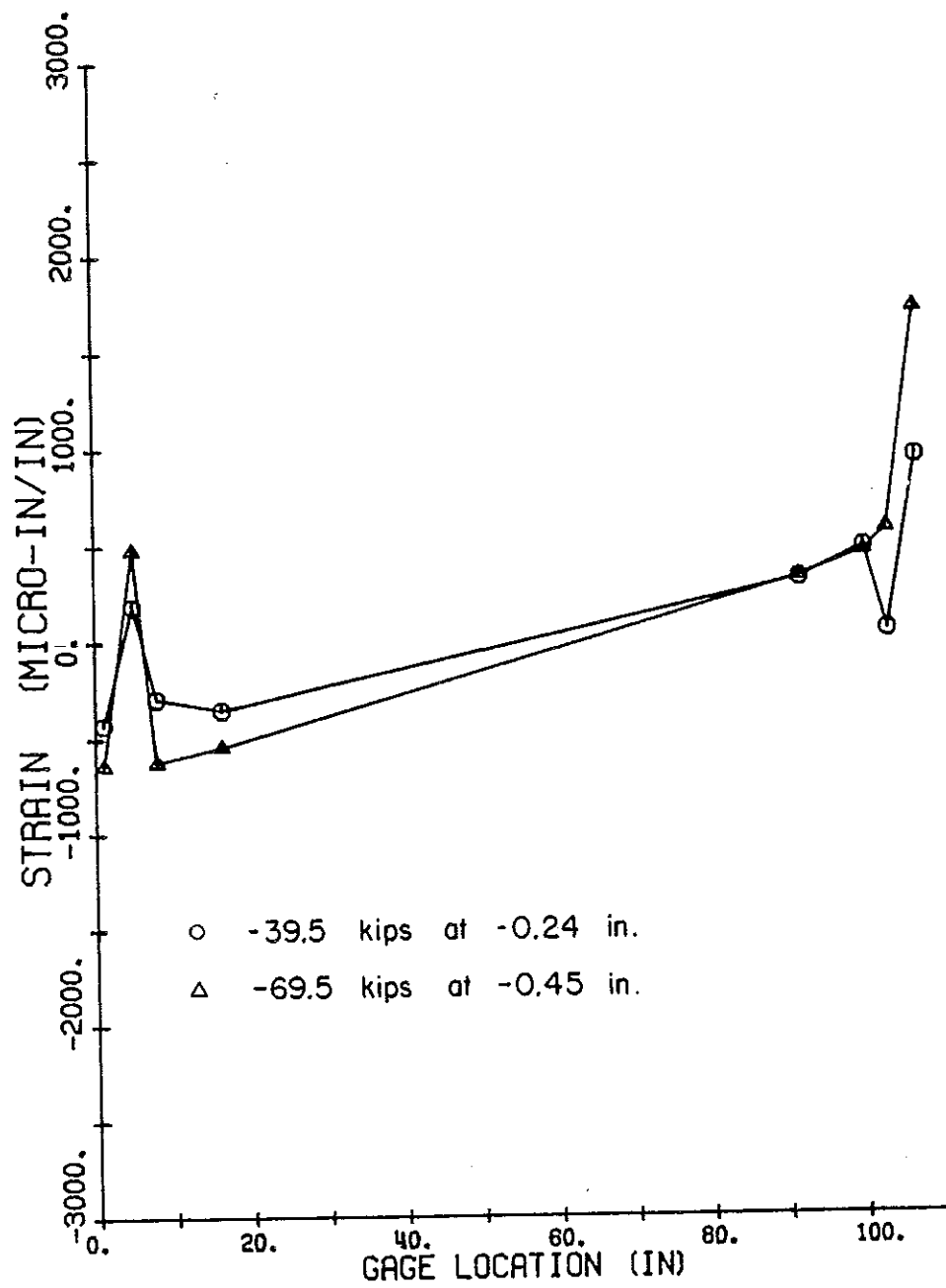


Figure F-72. Specimen 4, bottom strain for first half cycle to -0.45 in.

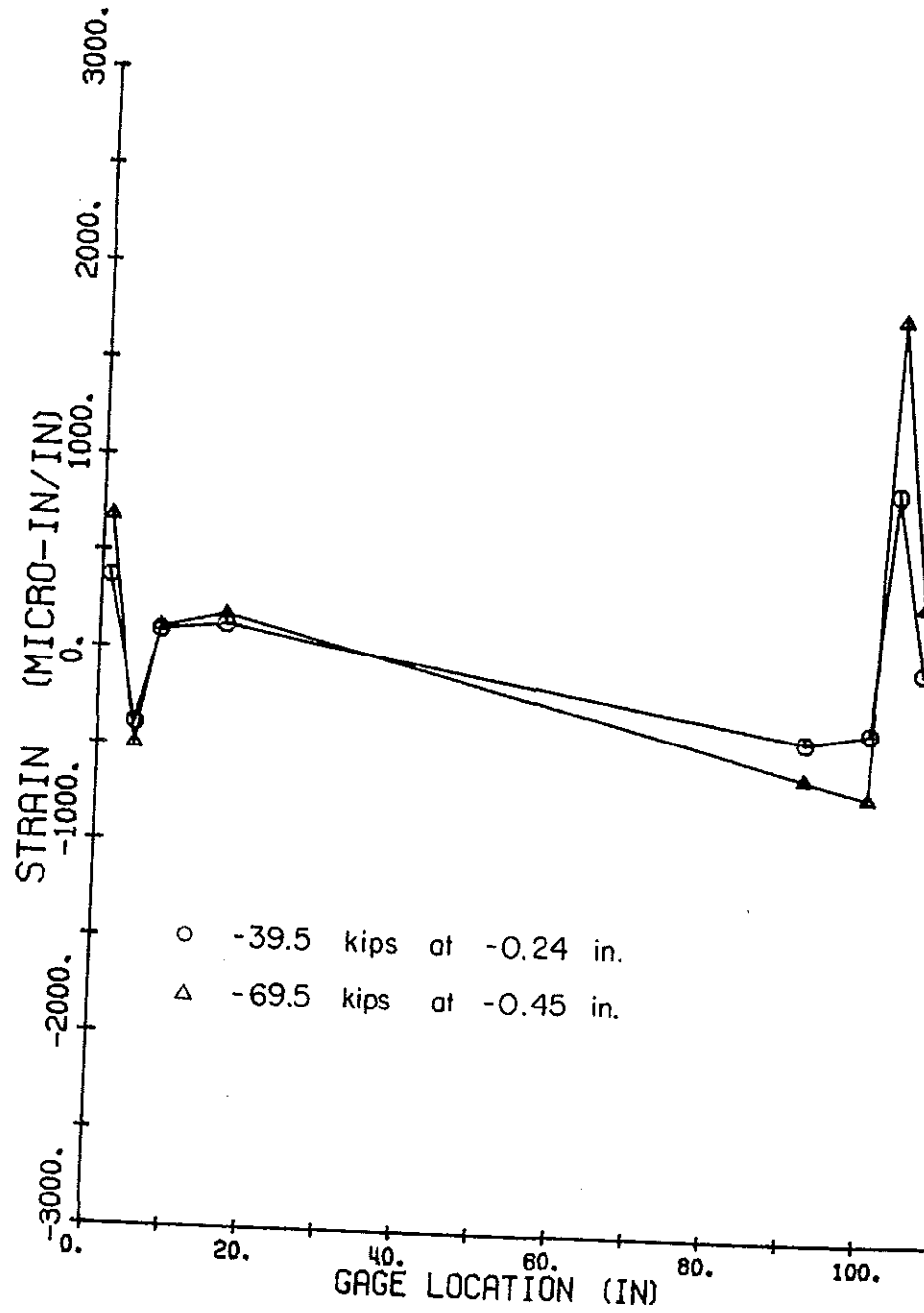


Figure F-73. Specimen 4, top strain for first half cycle to -0.45 in.

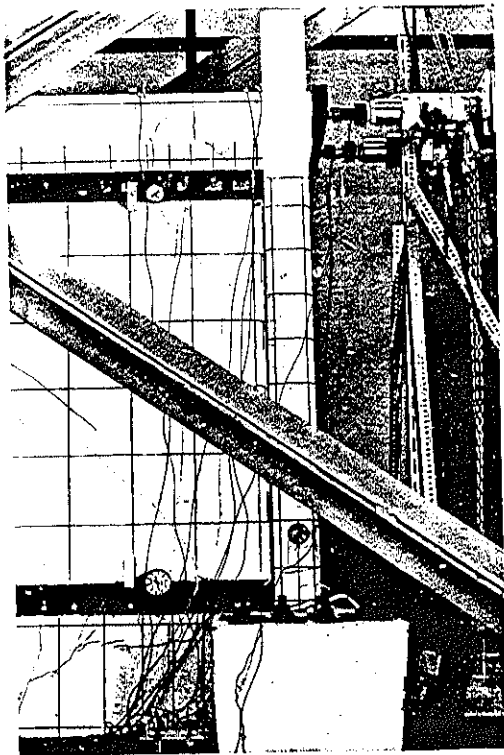


Figure F-74: Specimen 4, south side of base beam after fifth cycle to -0.5 in.

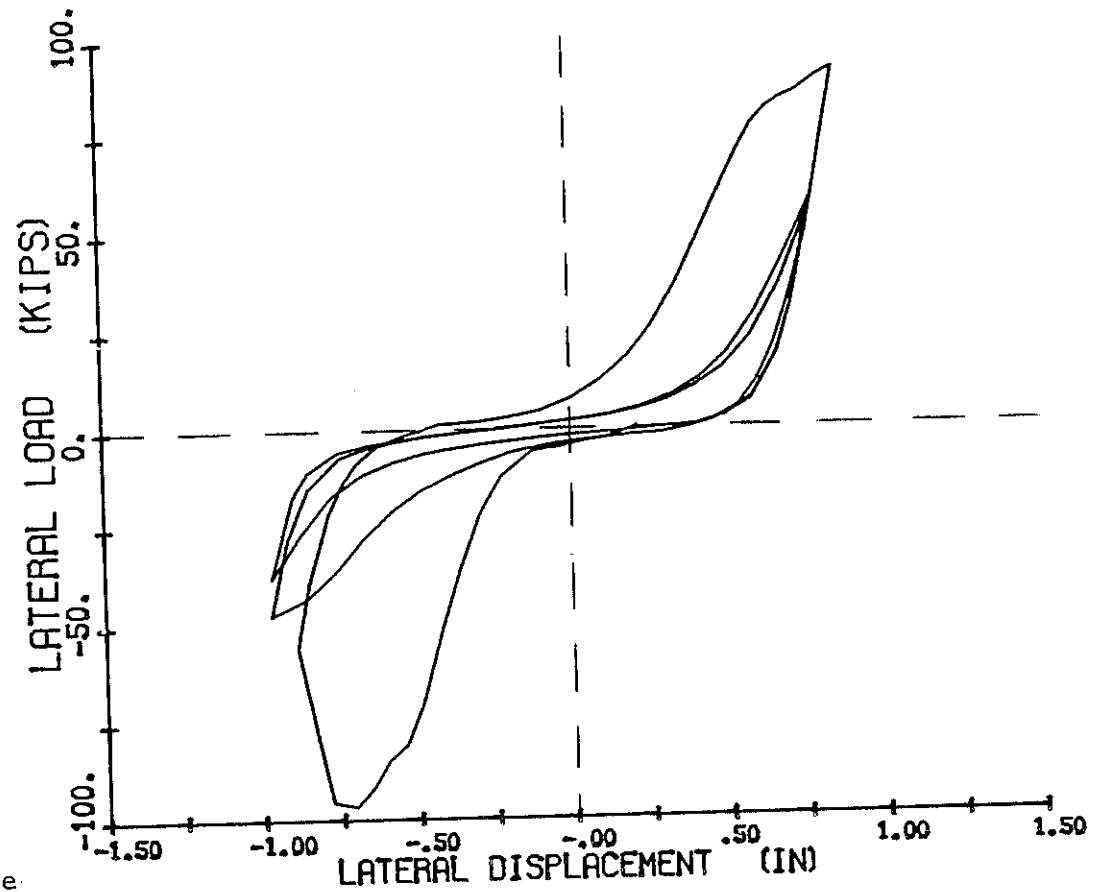


Figure F-75. Specimen 4, load-deflection curve for three cycles to  $\pm 0.9$  in.

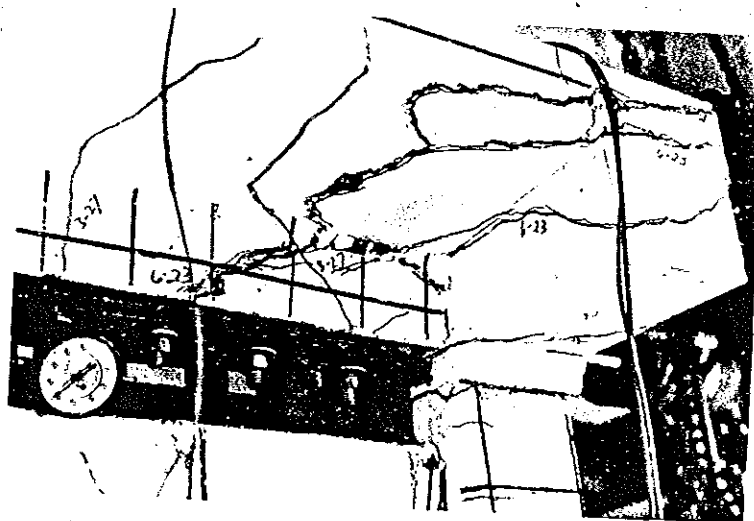


Figure F-76. Specimen 4, diagonal shear failure to top beam, -95.5 kips.

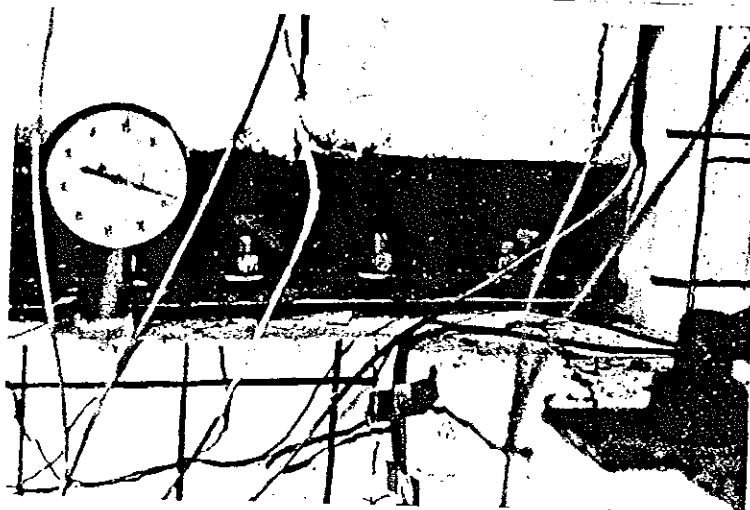


Figure F-77. Specimen 4, pullout of anchors after first half cycle to -0.89 in.

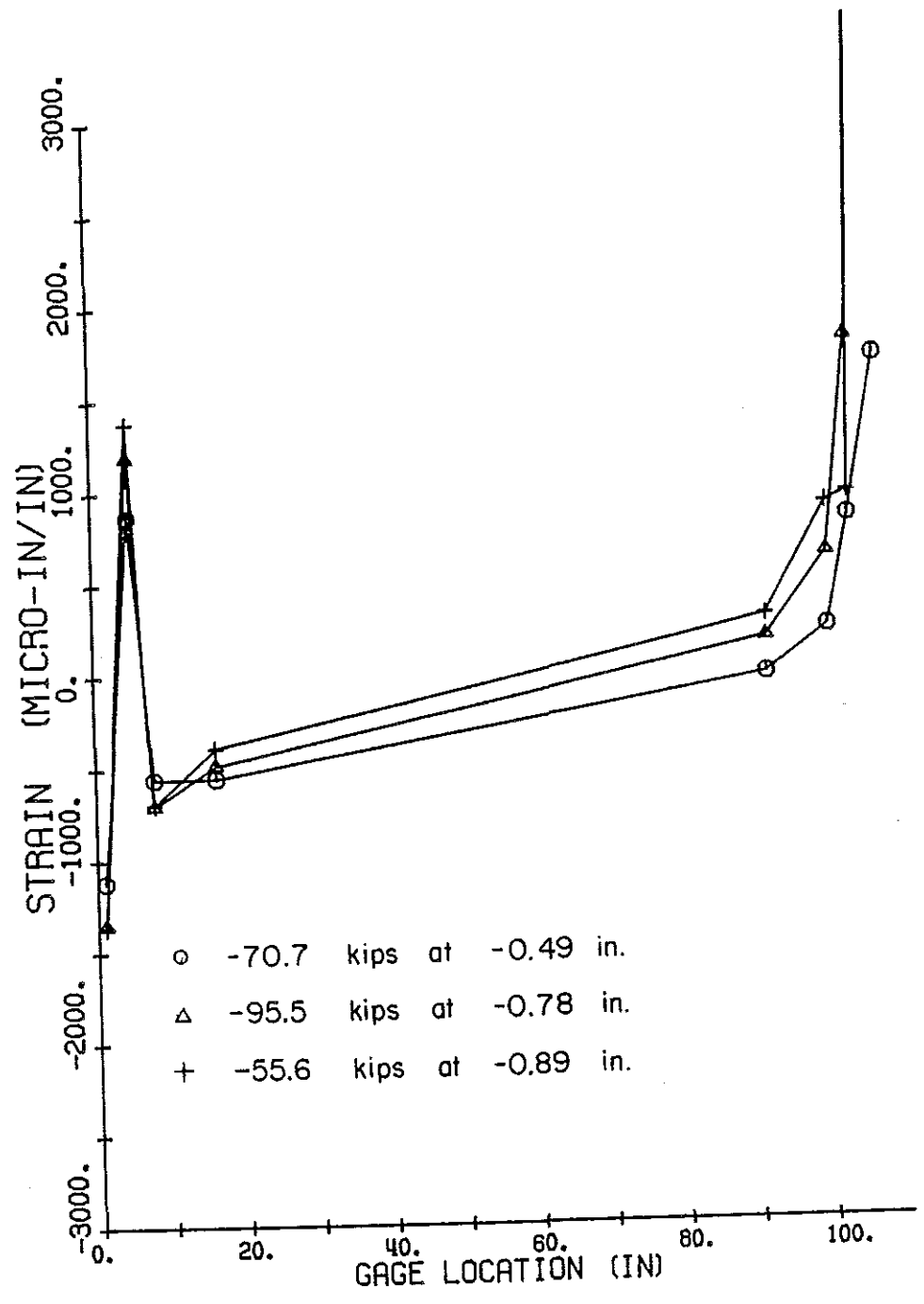


Figure F-78. Specimen 4, bottom strain pattern for first half cycle to -0.89 in.

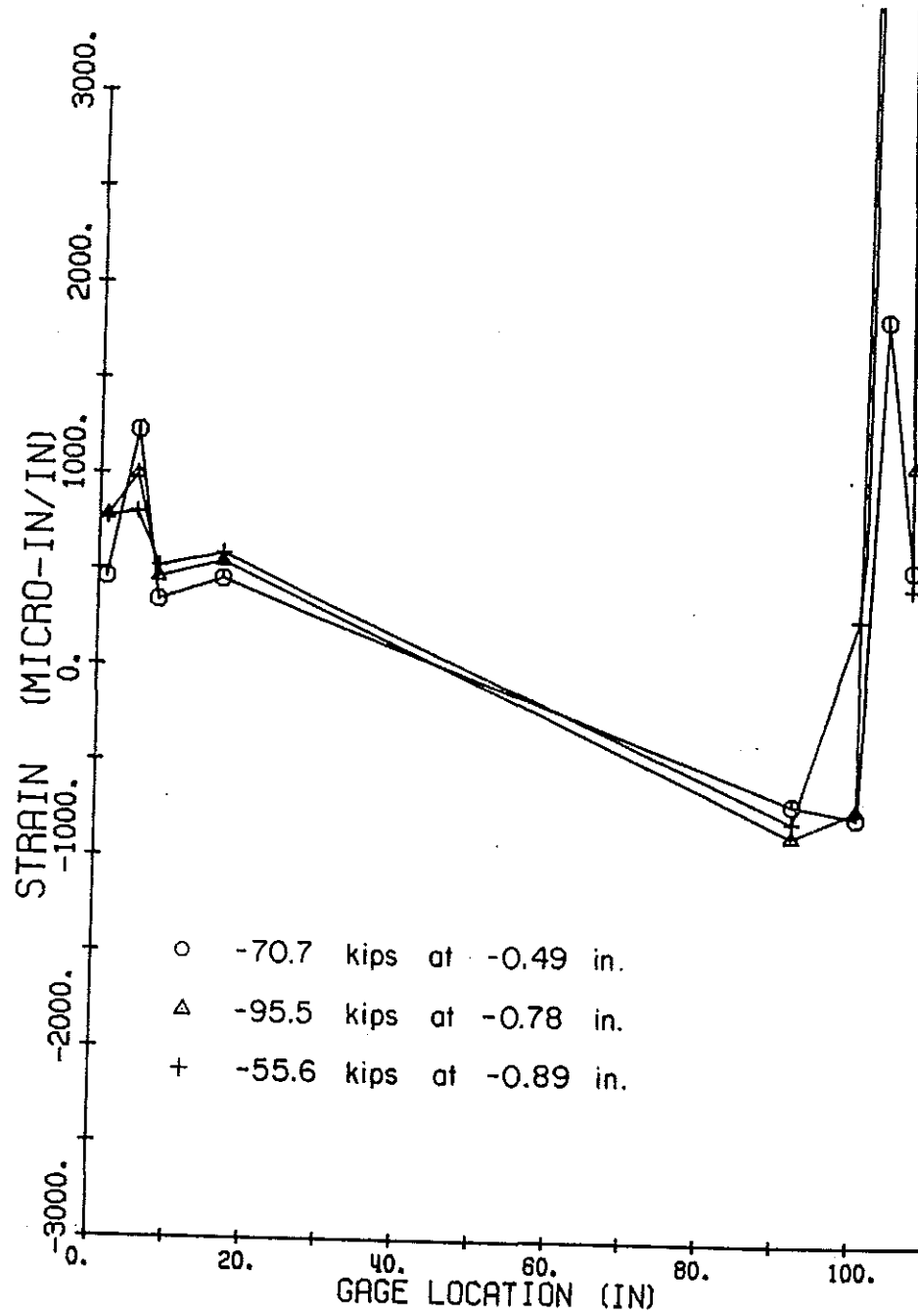


Figure F-79. Specimen 4, top strain pattern for first half cycle to -0.89 in.

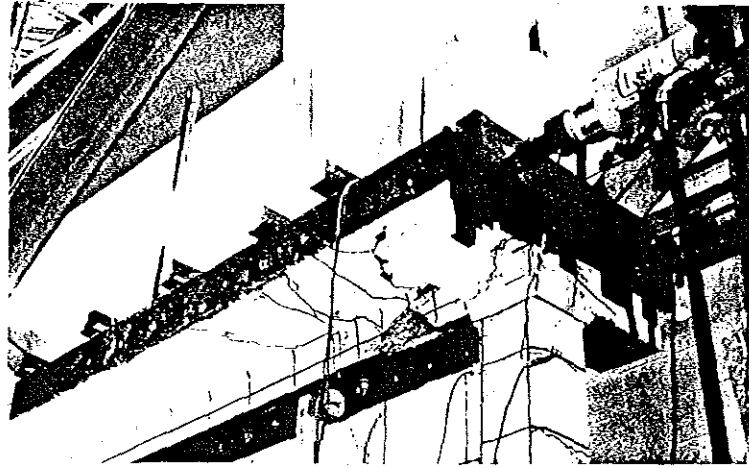


Figure F-80. Specimen 4, top beam showing repair using steel angles.

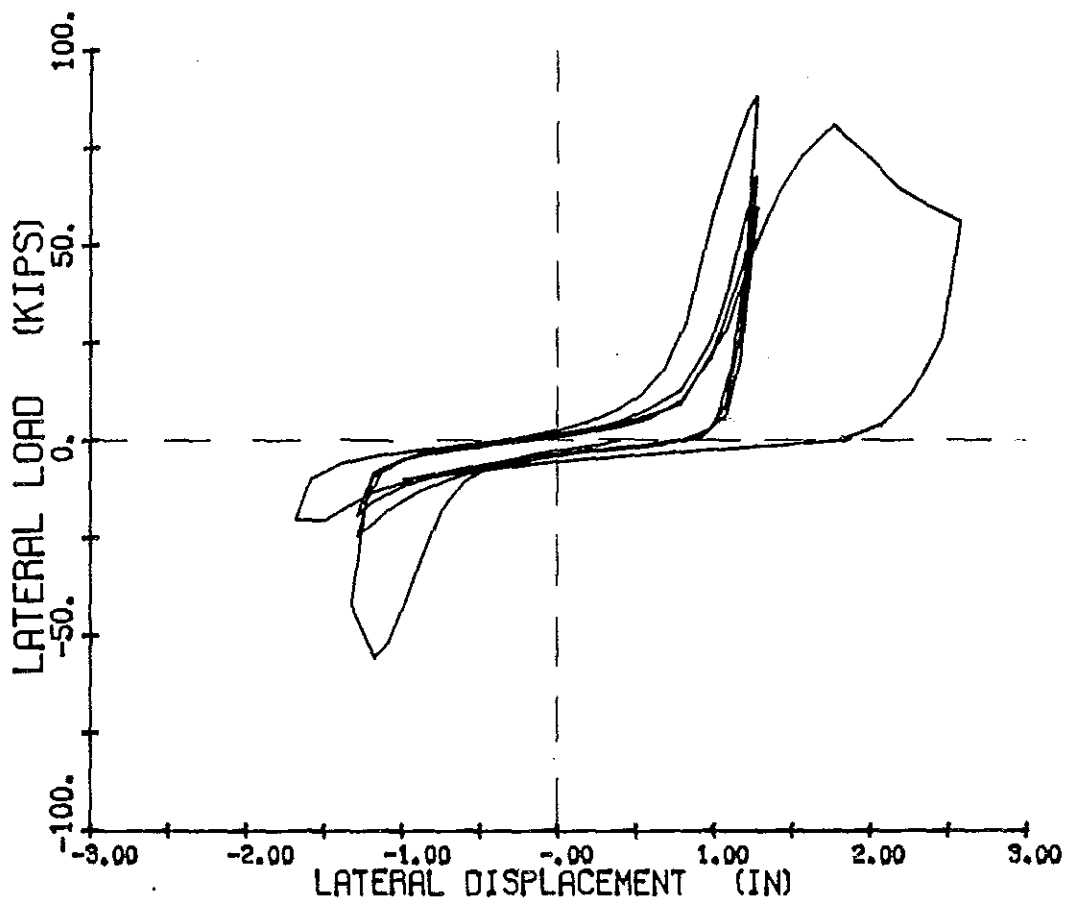


Figure F-81. Specimen 4, load-deflection curve for three cycles +1.3 in. and one cycle -1.7 in., +2.6 in.

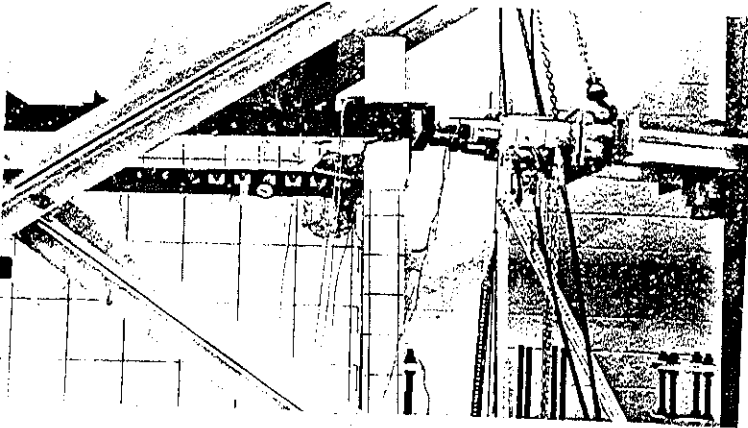


Figure F-82. Specimen 4, top beam at first half cycle to -1.32 in.

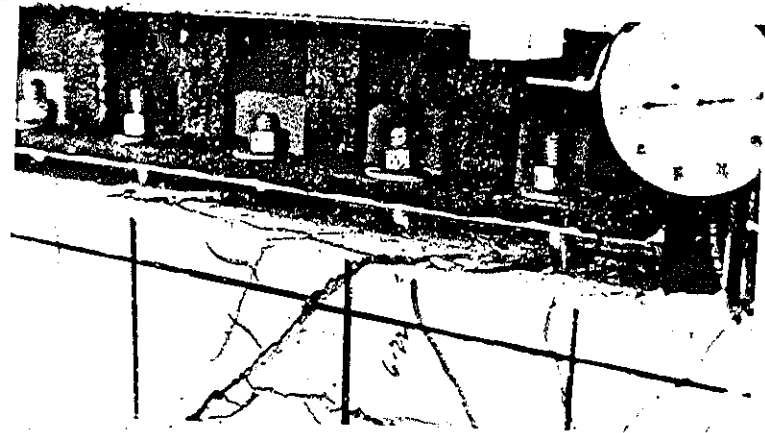


Figure F-83. Specimen 4, ear plate connector at south end of base beam, deflection of -1.32 in.

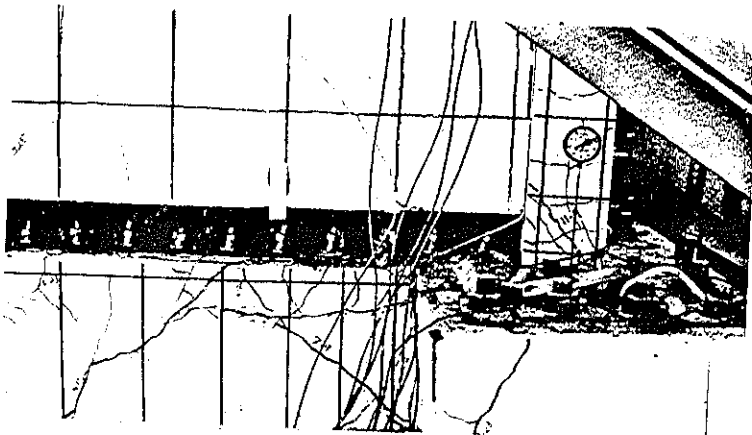


Figure F-84. Specimen 4, diagonal shear crack in column resulting from wall bearing on column.

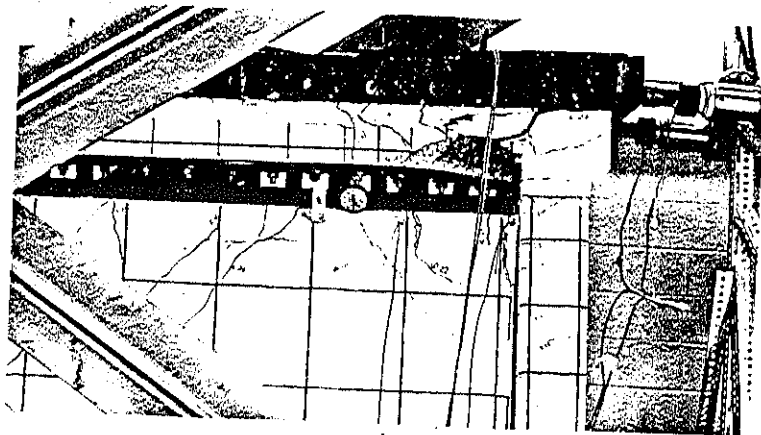


Figure F-85. Specimen 4, maximum negative deflection -1.68 in.

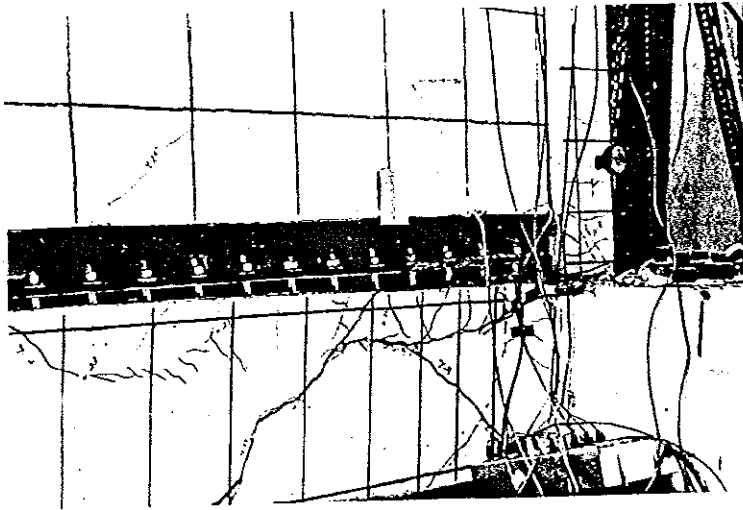


Figure F-86. Specimen 4, pullout of anchors at -1.68 in.

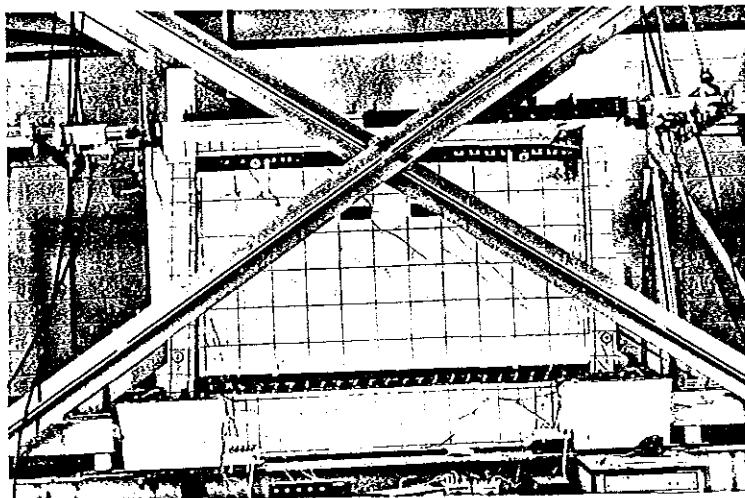
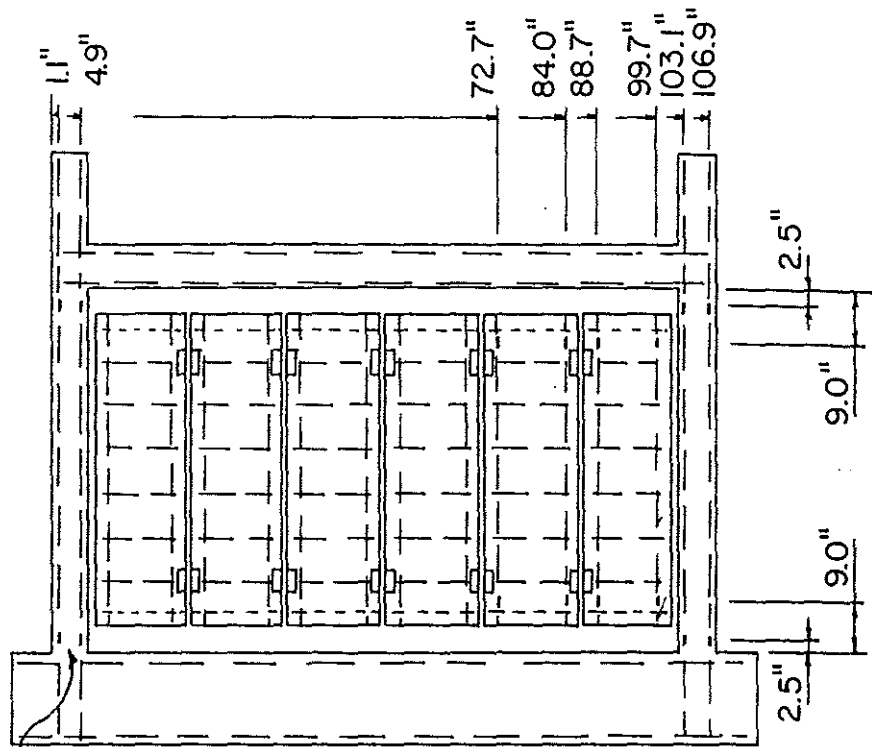


Figure F-87. Specimen 4, maximum positive deflection +2.58 in.



1/4" electrical resistance strain gages, typical

Figure F-88. Strain gage location in Specimen 5.

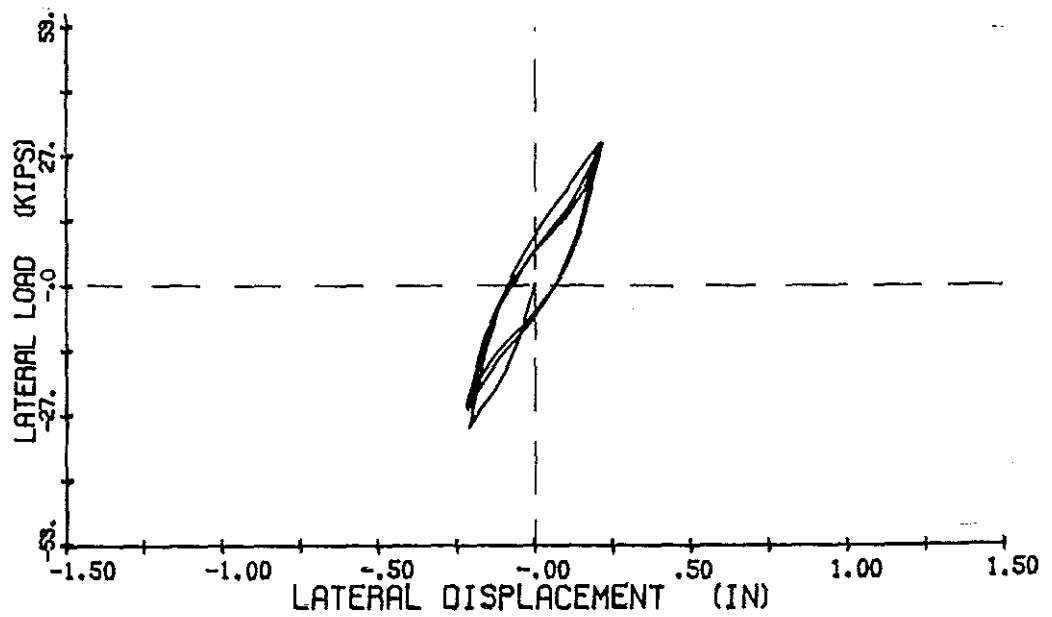


Figure F-89. Specimen 5, load-deflection curve for three cycles to  $\pm 0.22$  in.

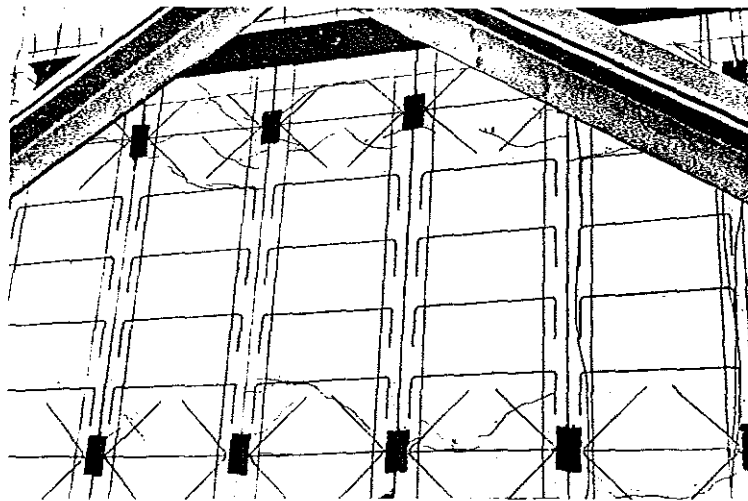


Figure F-90. Specimen 5, panels #1 through #5, left to right, after three cycles  $\pm 0.22$  in.

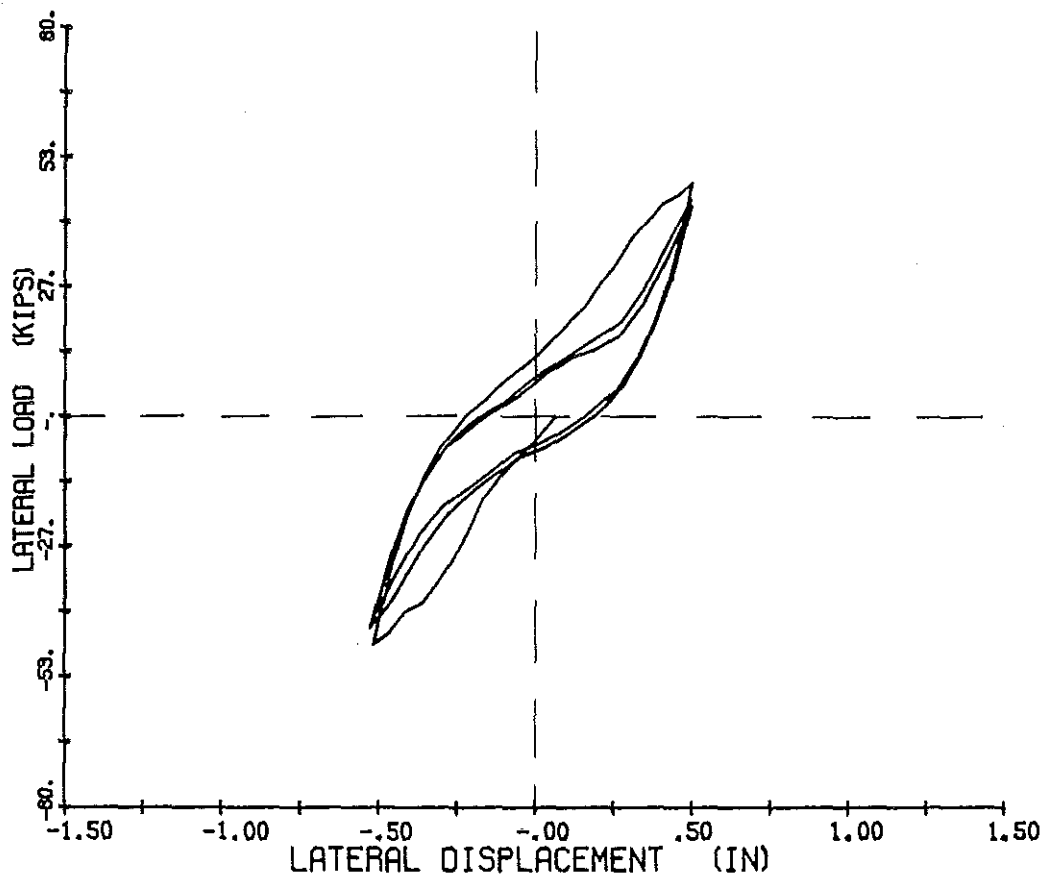


Figure F-91. Specimen 5, load-deflection curve for three cycles to  $\pm 0.5$  in.

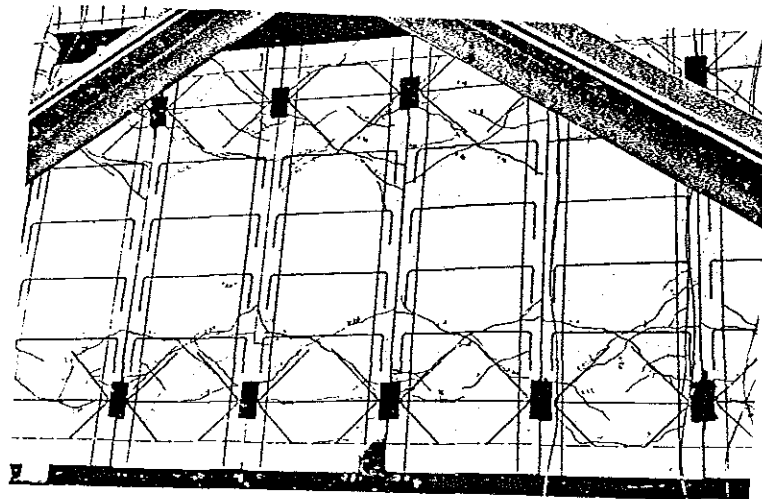


Figure F-92. Specimen 5, panels after first cycle  $+0.5$  in. showing diagonal shear cracks.

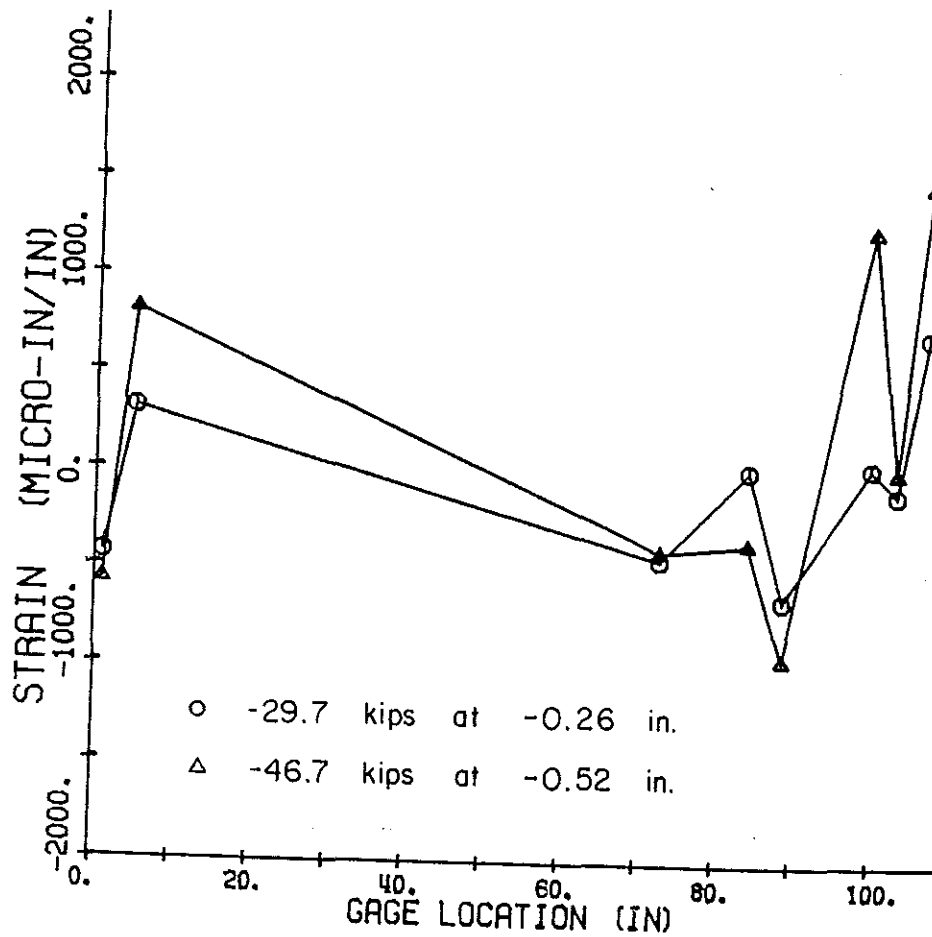


Figure F-93. Specimen 5, bottom strain pattern for first half cycle to  $-0.52$  in.

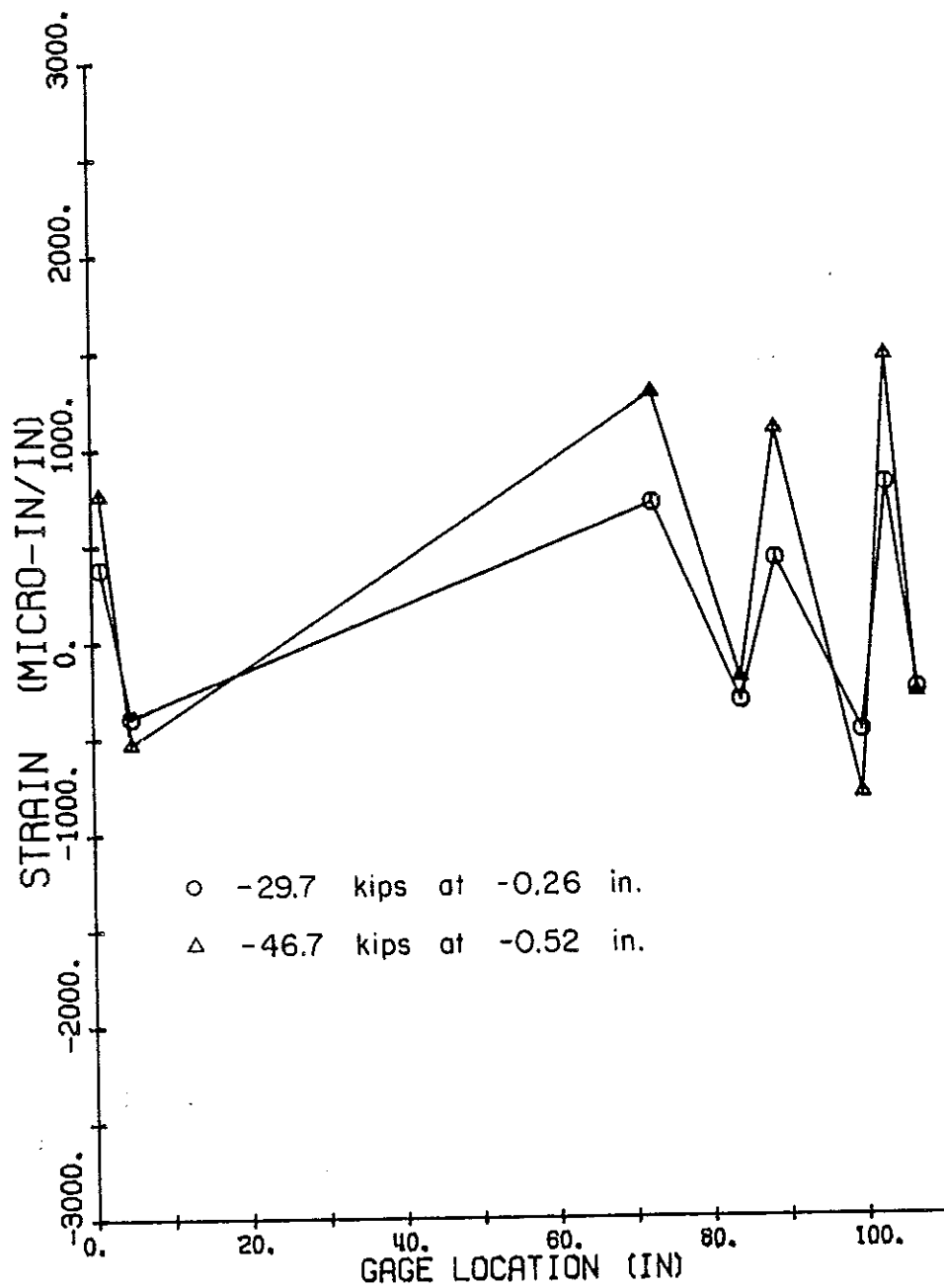


Figure F-94. Specimen 5, top strain pattern for first half cycle to -0.52 in.

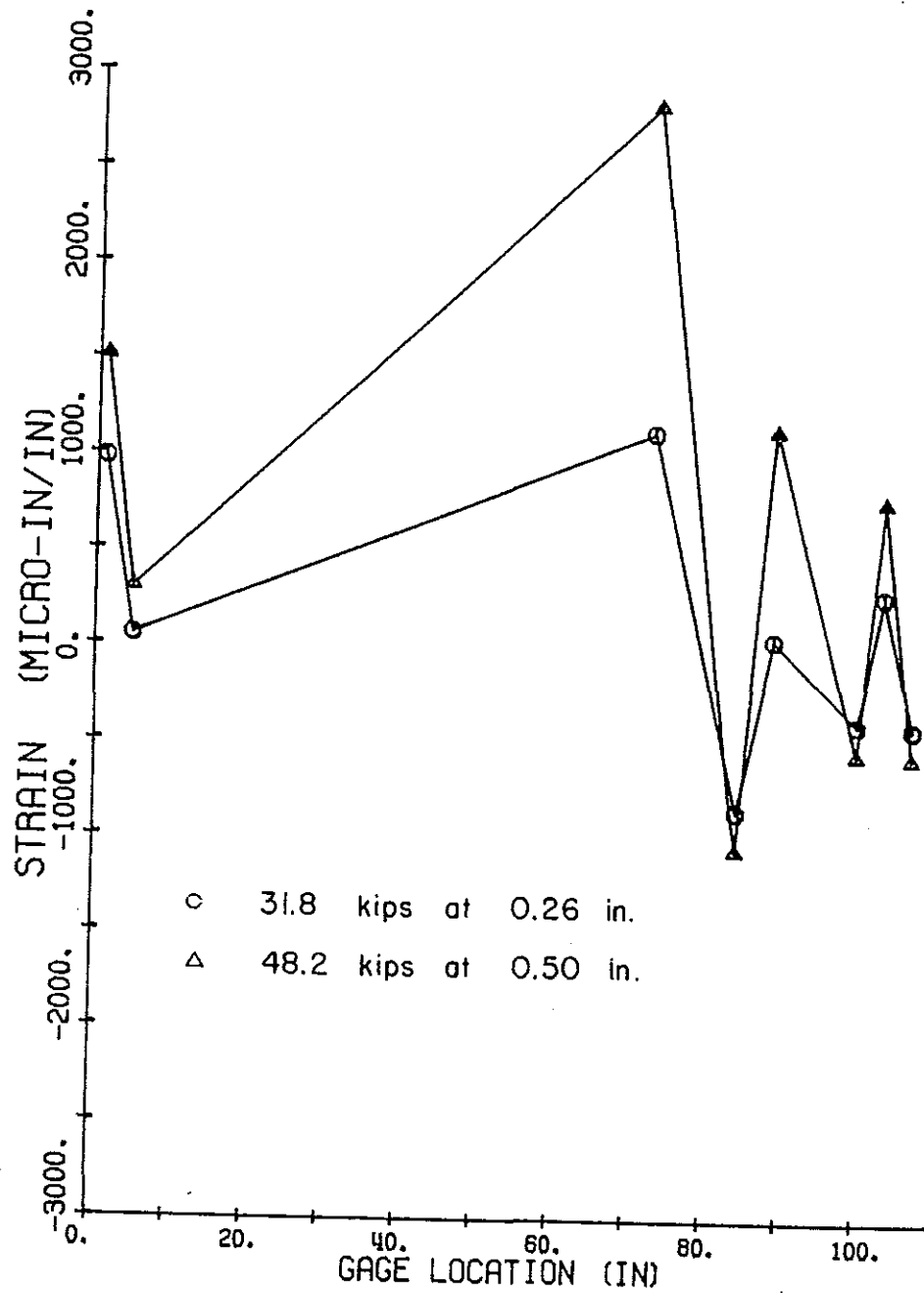


Figure F-95. Specimen 5, bottom strain pattern for second half cycle to +0.50 in.

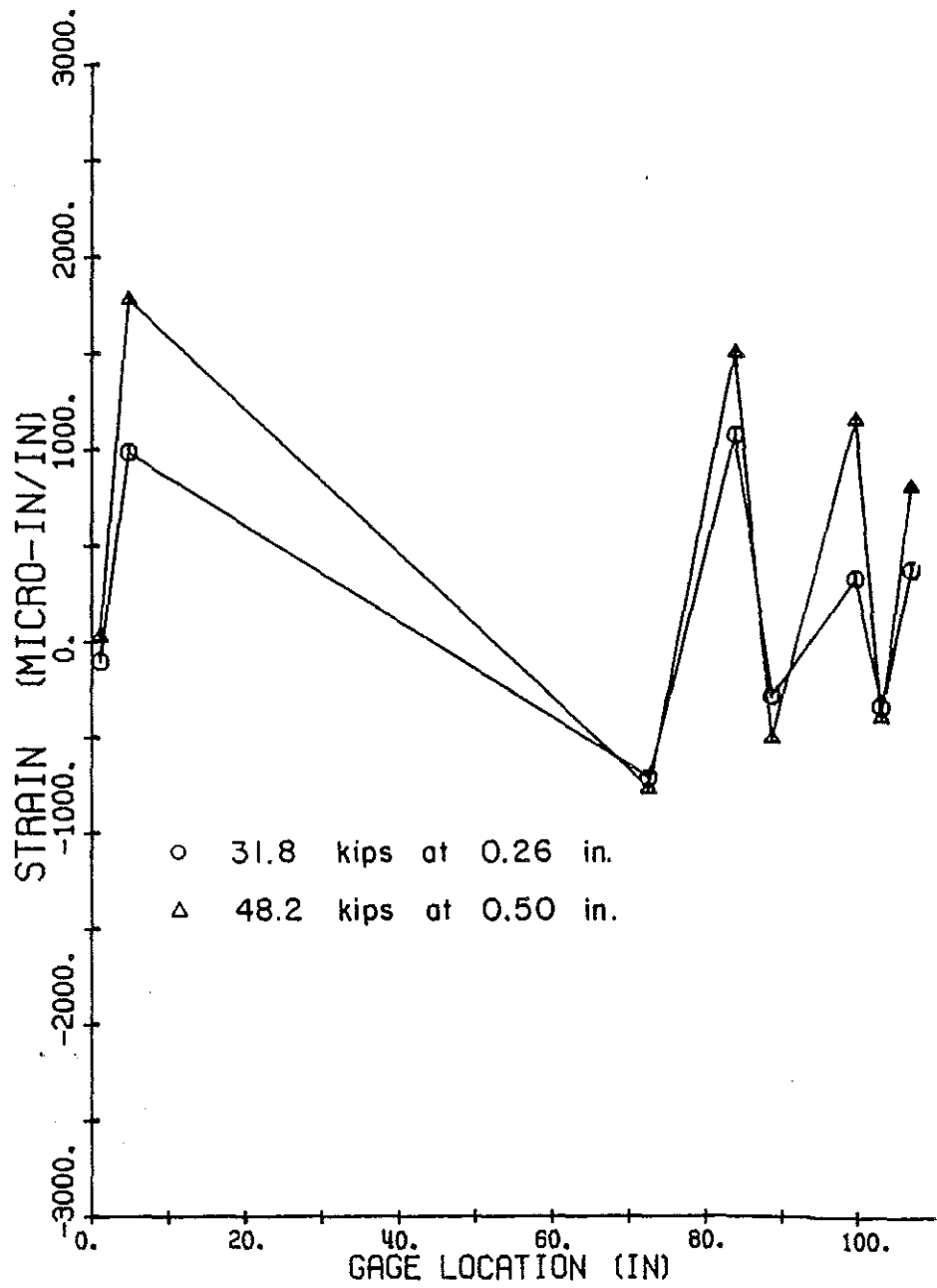


Figure F-96. Specimen 5, top strain pattern for second half cycle to +0.50 in.

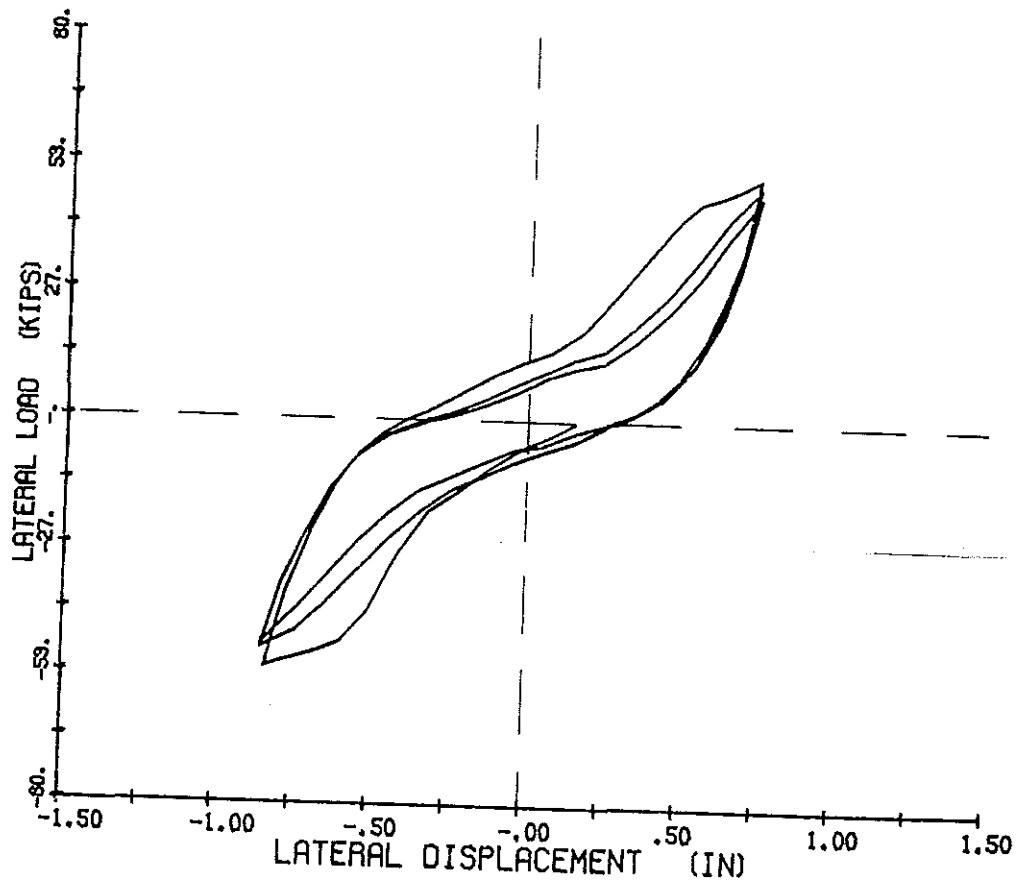


Figure F-97. Specimen 5, load-deflection curve for three cycles to +0.8 in.

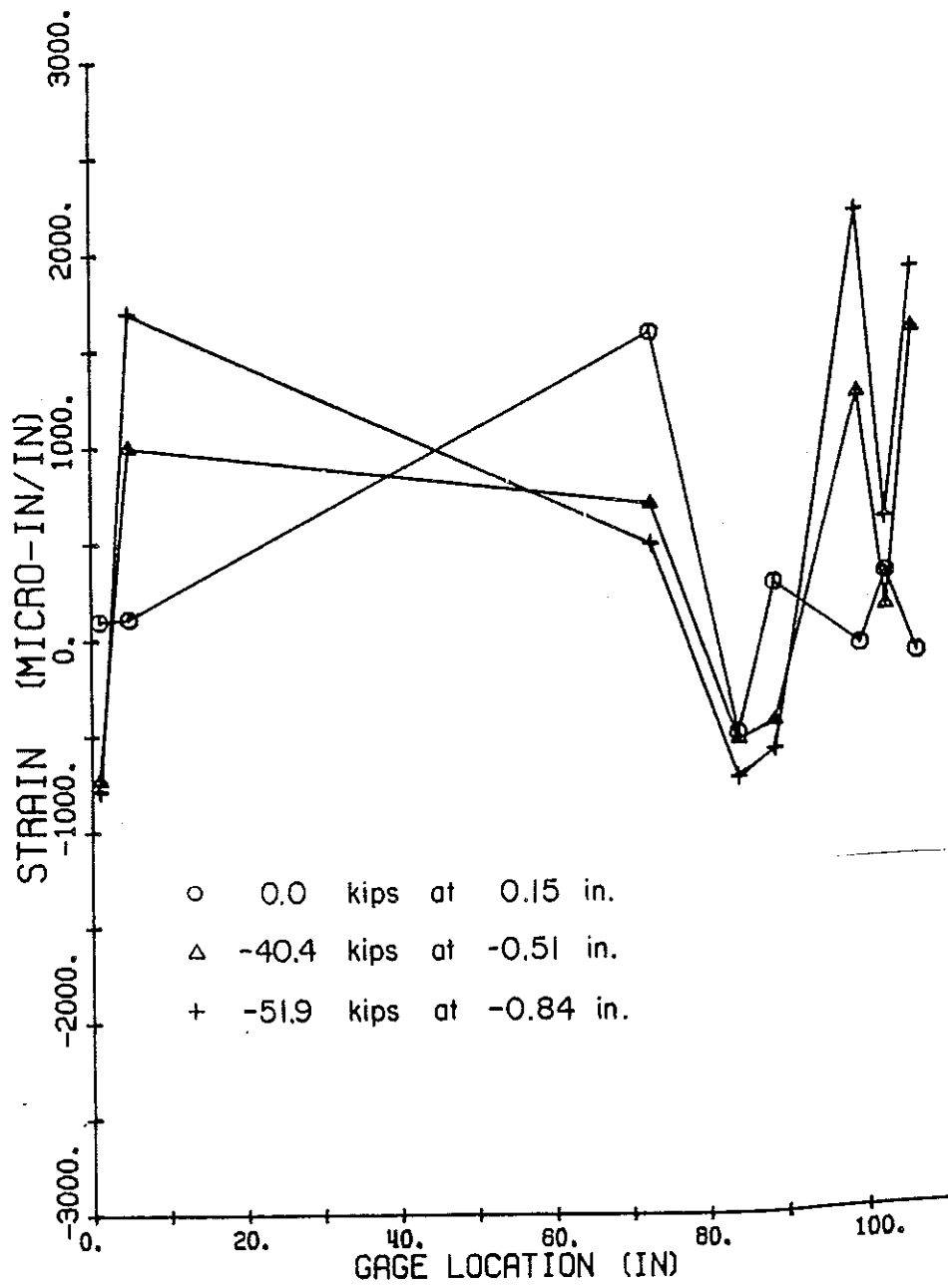


Figure F-98. Specimen 5, bottom strain pattern for first half cycle to -0.84 in.

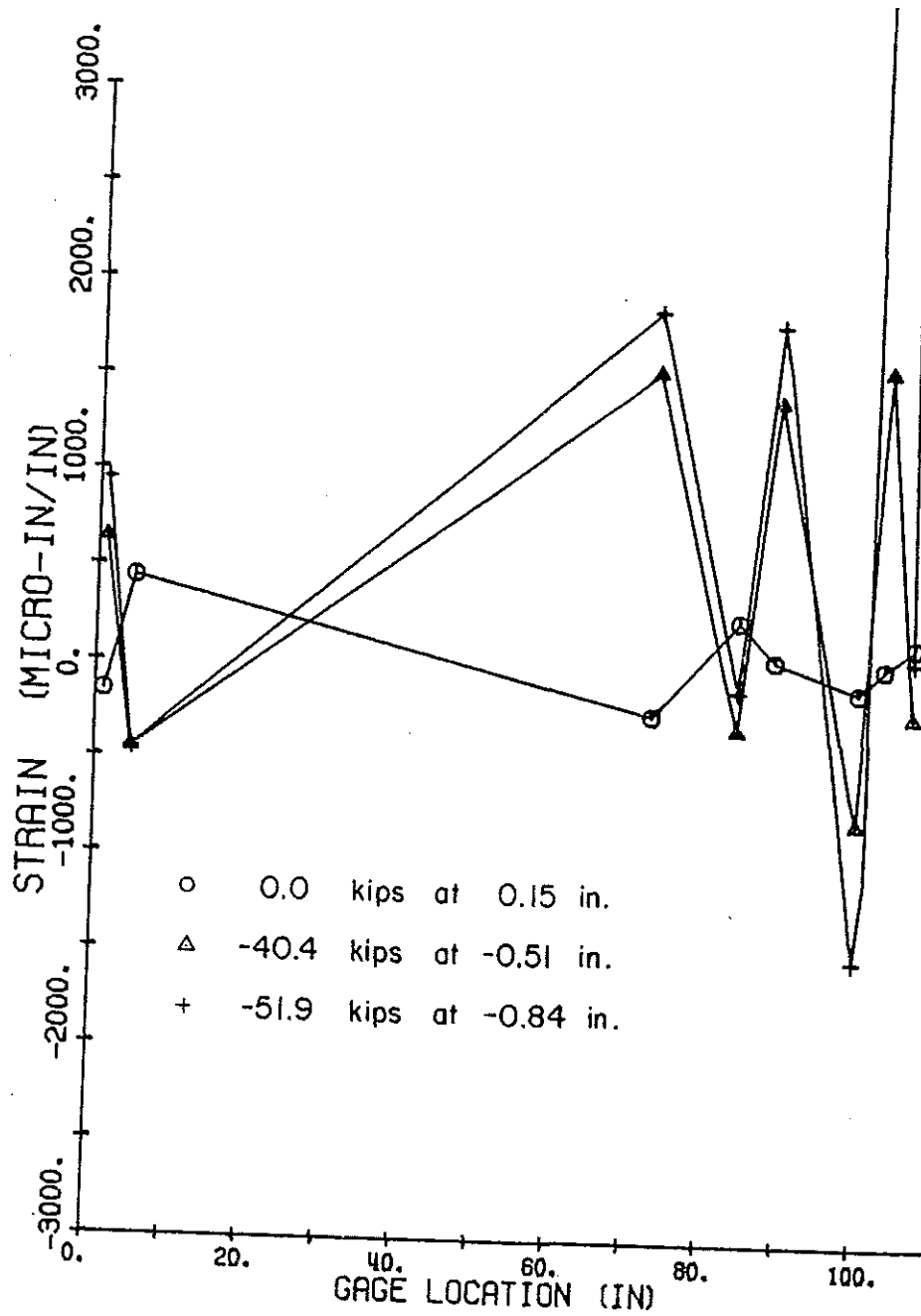


Figure F-99. Specimen 5, top strain pattern for second half cycle to -0.84 in.

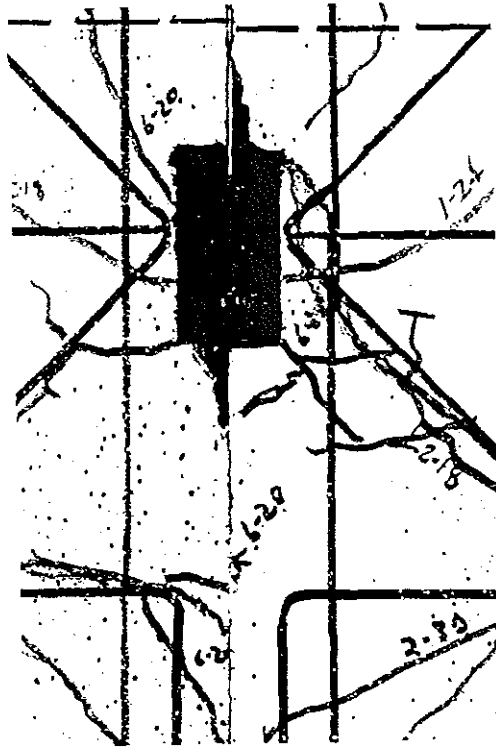


Figure F-100. Specimen 5, top connector between #1 and #3 at +0.74 in.

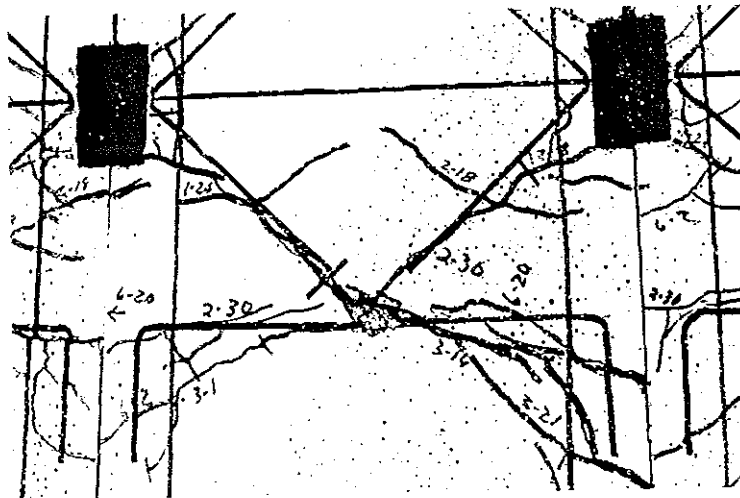


Figure F-101. Specimen 5, top of panel #3 at +0.74 in., second half cycle.

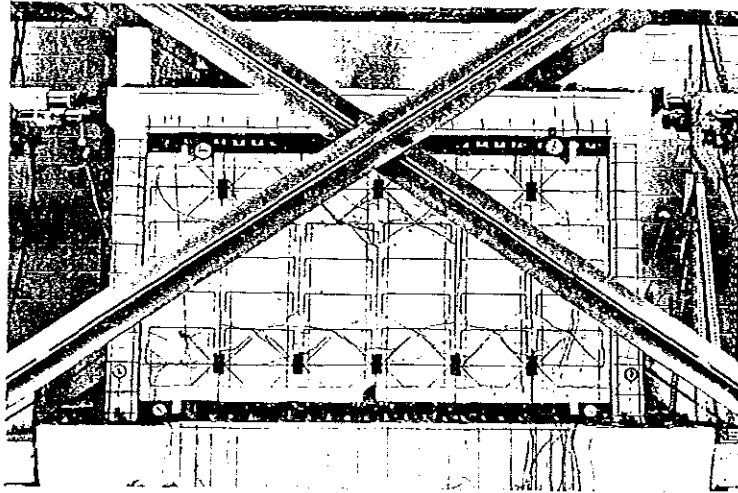


Figure F-102. Specimen 5, second half cycle to +0.74 in.

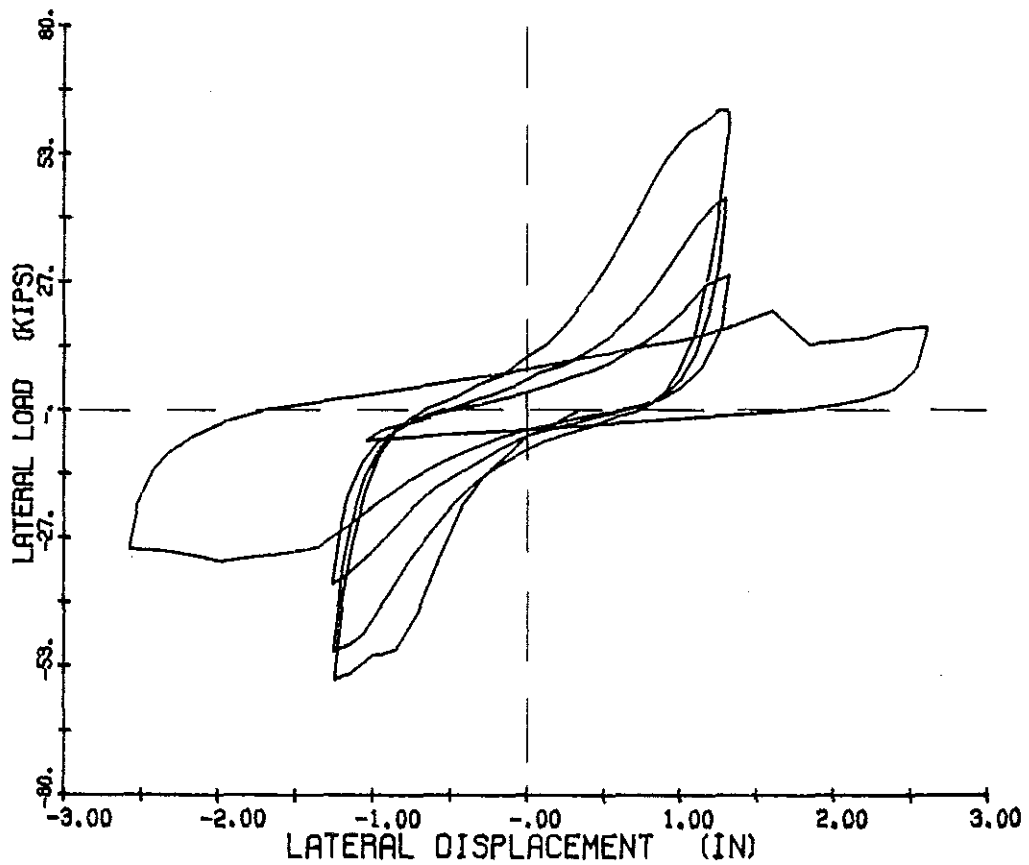


Figure F-103. Specimen 5, load deflection for three cycles  $\pm 1.3$  in. and one cycle  $\pm 2.6$  in.

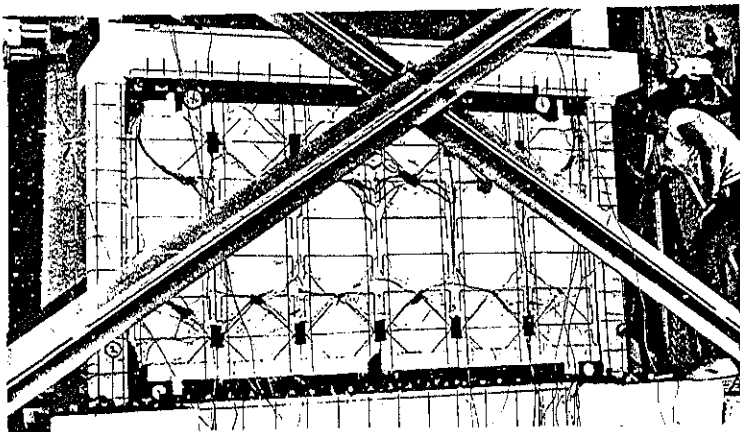


Figure F-104. Specimen 5, first cycle at +1.32 in.

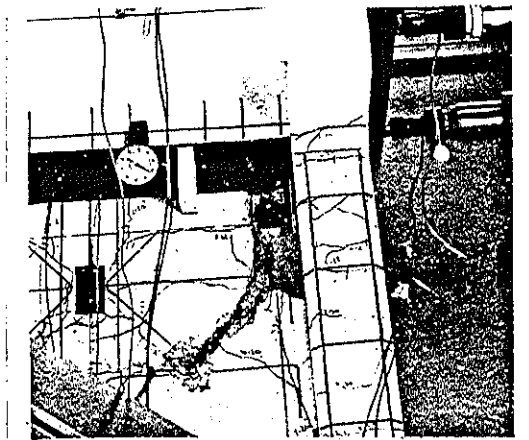


Figure F-105. Specimen 5, fifth cycle at -1.26 in.

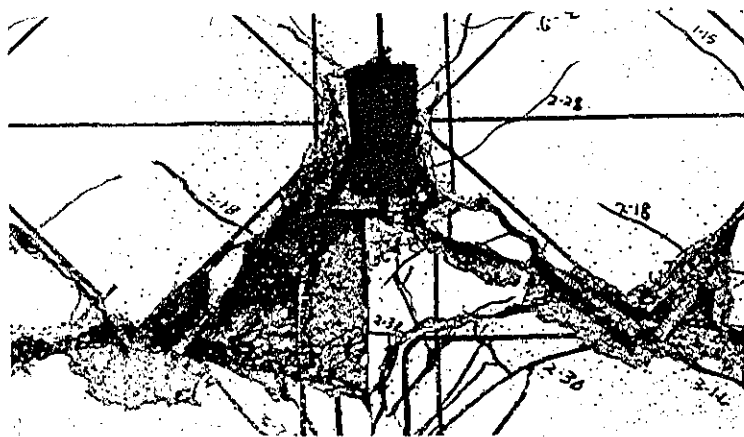


Figure F-106. Specimen 5, during sixth half cycle at +1.32 in., top panel-to-panel connector between #3 and #4.

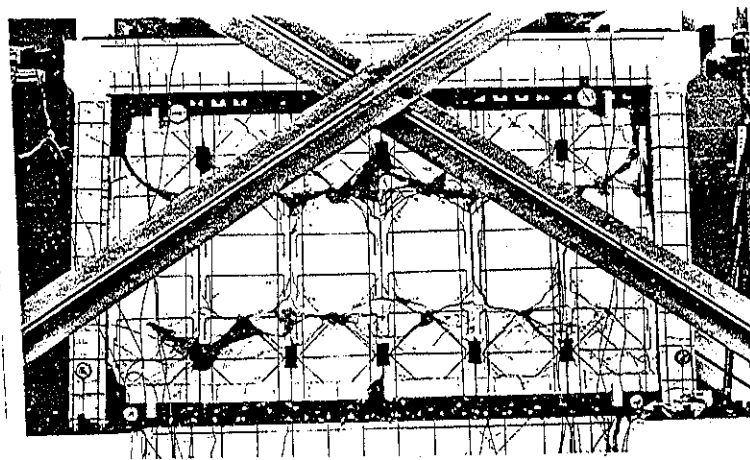


Figure F-107. Specimen 5, sixth half cycle at +1.32 in.

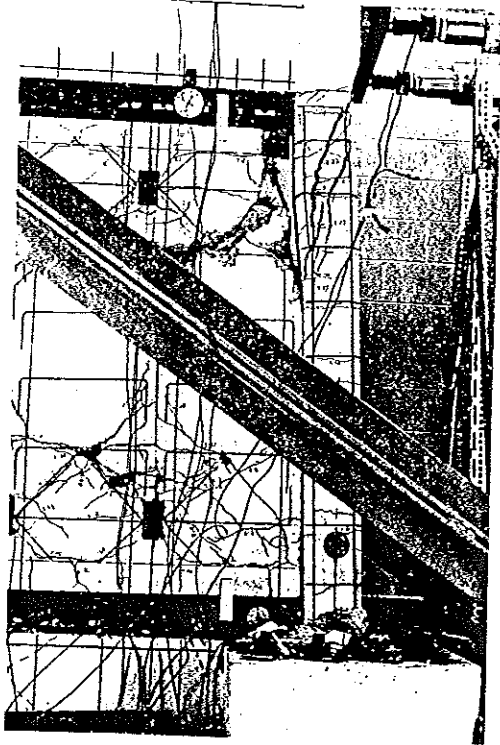


Figure F-108. Specimen 5, shear failure at south column at -2.59 in.

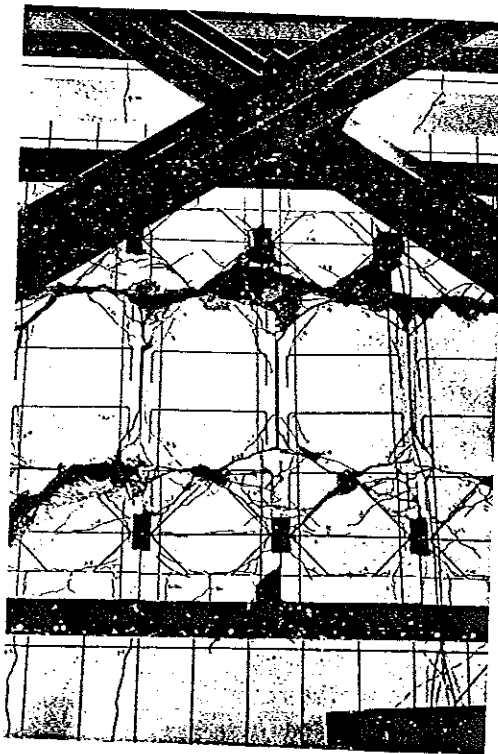


Figure F-110. Specimen 5, from left to right, panels #2 through #5 at -2.59 in.

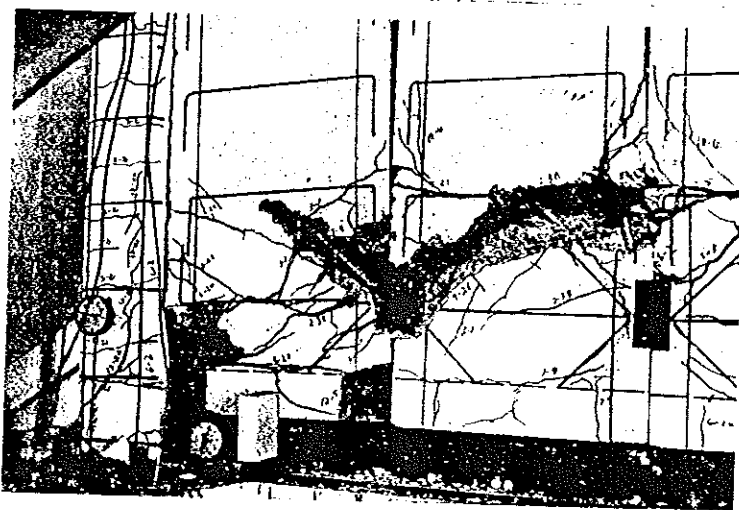


Figure F-109. Specimen 5, shear failure at base of north column at -2.59 in.

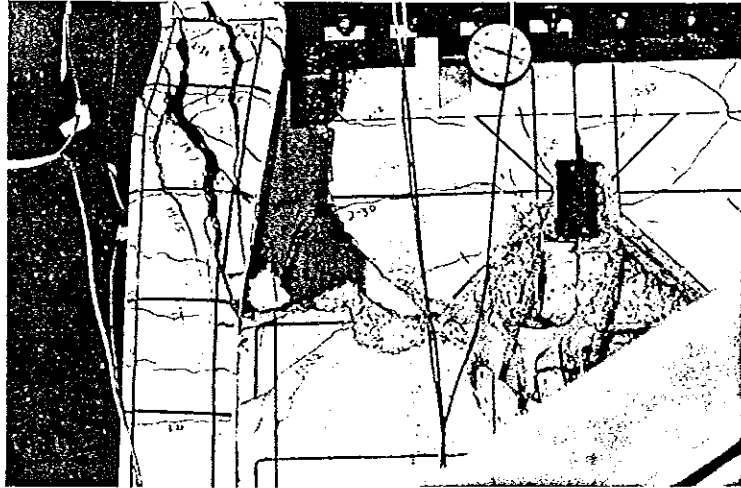


Figure F-111. Specimen 5, shear failure at top of north column at +2.68 in.

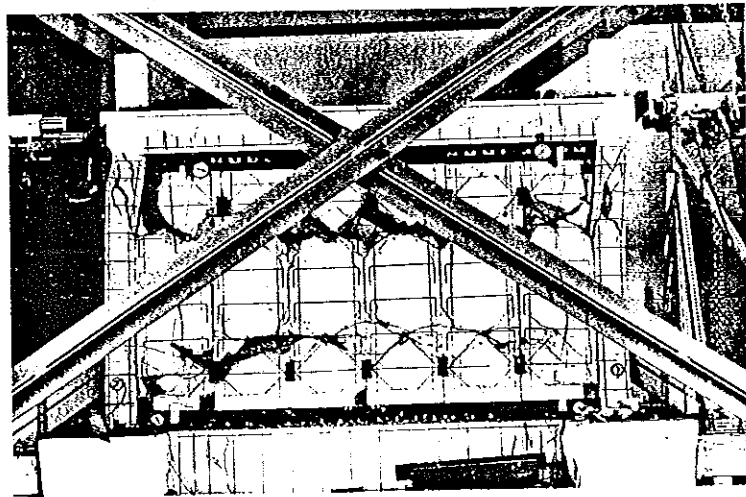


Figure F-112. Specimen 5, shear deflection at top of panels at +2.68 in.

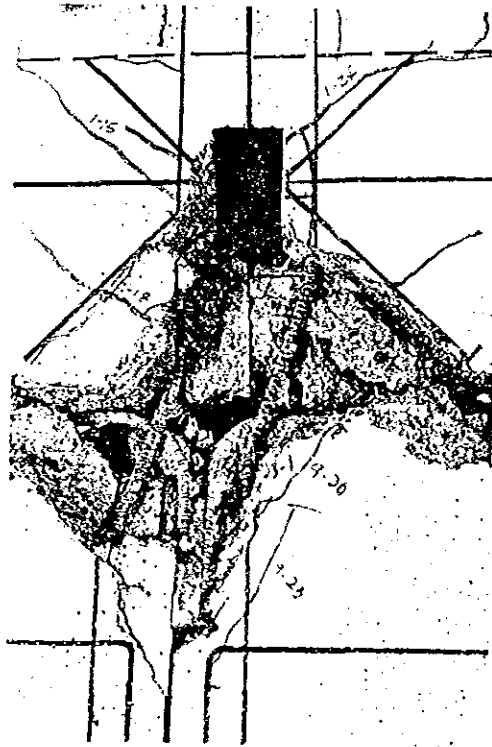


Figure F-113. Specimen 5, top panel-to-panel connector between #2 and #3 at +2.68 in.

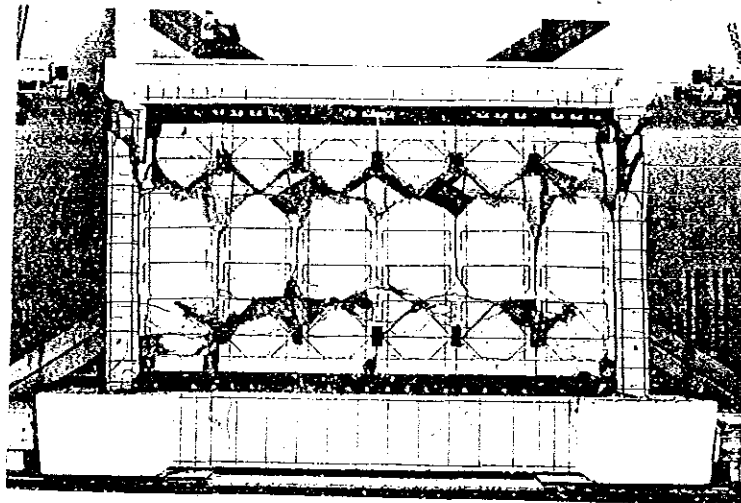


Figure F-114. Specimen 5, test completed, zero deflection.

## REFERENCES

1. Adams, R. F., "Some Factors Which Influence the Strength of Bolt Anchors in Concrete," Journal of the American Concrete Institute, Vol. 52, No. 2, October 1955, pp. 131-138.
2. Alexander, C. M., Heidebrecht, A. C., and Tso, W. K., "Cyclic Load Tests on Shear Wall Panels," Proceedings of the Fifth World Conference on Earthquake Engineering, Paper 135, Rome, 1973.
3. American Concrete Institute, Committee 318, Building Code Requirements for Reinforced Concrete (ACI 318-56), American Concrete Institute, Detroit, Michigan, 1956.
4. \_\_\_\_\_, Building Code Requirements for Reinforced Concrete (ACI 318-63), American Concrete Institute, Detroit, Michigan, 1963.
5. \_\_\_\_\_, Building Code Requirements for Reinforced Concrete (ACI 318-71), American Concrete Institute, Detroit, Michigan, 1971.
6. \_\_\_\_\_, Commentary on Building Code Requirements for Reinforced Concrete (ACI 318-71), American Concrete Institute, Detroit, Michigan, 1971.
7. American Concrete Institute, Committee 315, "Seismic Details for Special Ductile Frames," Journal of the American Concrete Institute, Vol. 67, No. 5, May 1970, pp. 374-379.
8. American Concrete Institute, Committee 408, "Bond Stress - The State of the Art," Journal of the American Concrete Institute, Vol. 63, No. 11, November 1966, pp. 1161-1190.
9. American Concrete Institute, Committee 442, "Response of Buildings to Lateral Forces," Journal of the American Concrete Institute, Vol. 68, No. 2, February 1971, pp. 81-106.
10. American Concrete Institute, Committee 512, "Suggested Design of Joints and Connections in Precast Structural Concrete," Journal of the American Concrete Institute, Vol. 61, No. 8, August 1964, pp. 921-937.

11. American Concrete Institute, Precast Concrete Wall Panels, Publication SP-11, American Concrete Institute, Detroit, Michigan, March 1964.
12. Barda, F., "Shear Strength of Low-Rise Walls with Boundary Elements," thesis presented to Lehigh University, Bethlehem, Pennsylvania, in partial fulfillment of the requirements for the degree of Doctor of Philosophy, 1972.
13. Barda, F., Hanson, J. M., and Corley, W. G., "An Investigation of the Design and Repair of Low Rise Shear Walls," Proceedings of the Fifth World Conference of Earthquake Engineering, Vol. 1, Rome, 1974, pp. 872-881.
14. Basic Building Code, 1960 Edition, Building Officials Conference of America, Owl Printing Company, Chicago, Illinois, 1961.
15. Bechtel Power Corporation, "FFTF Report, Drilled-in Expansion Bolts under Static and Alternation Load," Report BR-5853-C-4 prepared for the Hanford Engineering Development Laboratory, Richland, Washington, by Bechtel Power Corporation, 50 Beale Street, San Francisco, California, January 1975.
16. Benjamin, J. R., and Williams, H. A., "The Behavior of One-Story Reinforced Concrete Shear Walls," Journal of the Structural Division, ASCE, Vol.83, No. ST3, May 1957, pp.1254-1 through 1254-49.
17. \_\_\_\_\_, "Reinforced Concrete Shear Wall Assemblies," Journal of the Structural Division, ASCE, Vol. 86, No. ST8, August 1960, pp. 1-32.
18. Bertero, V. V., Popov, E. P., and Wang, T-Y, "Seismic Design Implications of Hysteretic Behavior of Reinforced Concrete Elements under High Stress," Proceedings of the U. S. - Japan Cooperative Research Program in Earthquake Engineering With Emphasis on Safety of School Buildings, Honolulu, Hawaii, August 1975.
19. Birkeland, P. W., and Birkeland, H. W., "Connections in Precast Concrete Construction," Journal of the American Concrete Institute, Vol. 63, No. 3, March 1966, pp. 345-368.
20. Blume, J. A., Newmark, N. M., and Corning, L. H., Design of Multistory Reinforced Concrete Buildings for Earthquake Motion, Portland Cement Association, Chicago, Illinois, 1961.
21. Burton, K. T., Corley, W. G., and Hognestad, E., "Connections in Precast Concrete Structures - Effects of Restrained Creep and Shrinkage," Journal of the Prestressed Concrete Institute, Vol. 12, No. 2, April 1967, pp. 18-37.

22. Cardenas, A. E., Hanson, J. M., Corley, W. G., and Hognestad, E., "Design Provisions for Shear Walls," Journal of the American Concrete Institute, Vol. 70, No. 3, March 1973, pp. 331-230.
23. Cardenas, A. E., and Magura, D., "Strength of High-Rise Shear Walls - Rectangular Cross Section," Response of Multistory Concrete Structures to Lateral Forces, Publication SP-36, American Concrete Institute, Detroit, Michigan, 1973, pp 119-131.
24. Cervenka, V., "Inelastic Finite Element Analysis of Reinforced Concrete Panels Under In-plane Loads," thesis presented to the University of Colorado, Boulder, Colorado, in partial fulfillment of the requirements for the degree of Doctor of Philosophy, 1970.
25. Clark, A. P., "Bond of Concrete Reinforcing Bars," Journal of the American Concrete Institute, Vol. 46, No. 3, November 1949, pp. 161-184.
26. Collins, F. T., "Prestressed Tilt-up Walls for Earthquake Resistance," Western Construction, Vol. 27, No. 12, December 1953, pp. 66-68.
27. Concrete Reinforcing Steel Institute Design Handbook, 1952 Edition, Concrete Reinforcing Steel Institute, Chicago, Illinois, 1952
28. Concrete Reinforcing Steel Institute Design Handbook, 1972 Edition, Concrete Reinforcing Steel Institute, Chicago, Illinois, 1972.
29. Conrad, R. F., "Tests of Grouted Anchor Bolts in Tension and Shear," Journal of the American Concrete Institute, Vol. 66, No. 9, September 1969, pp. 725-728.
30. Dawson, R. V., and Ward, M. A., "Dynamic Response of Framed Structures with Infill Walls," Proceedings of the Fifth World Conference on Earthquake Engineering, Vol. 2, Rome, 1974, pp. 1507-1516.
31. Delisle, D., and Heidebrecht, A. C., "Comparison of the Behavior of Load Bearing Shear Wall Panels Subjected to Repeated Cyclic Lateral Loading," Proceedings of the First Canadian Conference on Earthquake Engineering, University of British Columbia, Vancouver, B. C., May 1971, pp. 270-285.
32. Diamant, R. M. E., Industrialized Building, Volume 1, 2, and 3, Iliffe Book Ltd., London, 1965, 1966 and 1968.
33. Farrell, J., Representative of Sika Chemical Corporation, personal communications, 1974.

34. Fratt, J. M., "Structural Repair of Earthquake Damaged Buildings," ASCE National Structural Engineering Meeting, Preprint 1973, San Francisco, California, April, 1973.
35. Higashi, Y., and Kokusho, S., "The Strengthening Methods of Existing Reinforced Concrete Buildings," Proceedings of the U. S. - Japan Cooperative Research Program in Earthquake Engineering with Emphasis on the Safety of School Buildings, Honolulu, Hawaii, August 1975.
36. Holmes, M., and Posner, C. D., "Factors Affecting the Strength of Steel Plate Connections Between Precast Concrete Elements," Structural Engineer, Vol. 48, No. 10, October 1970, pp. 399-406.
37. Hribar, J. A., and Basko, R. C., "End Anchorage of High Strength Steel Reinforcing Bars," Journal of the American Concrete Institute, Vol. 66, No. 11, November 1969, pp. 875-883.
38. ITT Phillips Drill Company, "Anchoring Systems," Catalog F-500, Michigan City, Indiana, 1973.
39. \_\_\_\_\_, Red Head Engineering Bulletin Numbers 101, 102, 103, 106 and 111, Michigan City, Indiana, 1973.
40. Mathey, R. G., and Watstein, D., "Investigation of Bond in Beam and Pullout Specimens with High-Yield Strength Deformed Bars," Journal of the American Concrete Institute, Vol. 57, No. 9, March 1961, pp. 1071-1090.
41. Muto, K., Ohmori, N., and Takahashi, T., "A Study on Reinforced Concrete Slitted Shear Walls for High-Rise Buildings," Proceedings of the Fifth World Conference on Earthquake Engineering, Vol. 1, Rome, 1974, pp. 1135-1138.
42. Nishikawa, T., Hanson, R. D., and Streeter, V. L., "Characteristics Method Applied in Structural Dynamics," ASCE Structural Engineering Conference, Preprint 2464, New Orleans, Louisiana, April, 1974.
43. Otani, S., and Sozen, M. A., "Behavior of Multistory Reinforced Concrete Frames During Earthquakes," Civil Engineering Studies, Structural Research Series No. 392, University of Illinois, Urbana, Illinois, November 1972.
44. Perry, E. S., and Jundi, N., "Pullout Bond Stress Distribution Under Static and Dynamic Repeated Loadings," Journal of the American Concrete Institute, Vol. 66, No. 5, May 1969, pp. 377-380.

45. Portland Cement Association, Analysis of Small Reinforced Concrete Buildings for Earthquake Forces, Portland Cement Association, Chicago, Illinois, 1955.
46. \_\_\_\_\_, "Design and Control of Concrete Mixtures, Eleventh Edition," Portland Cement Association, Skokie, Illinois, July, 1968.
47. Prestressed Concrete Institute, Connection Details for Precast, Prestressed Concrete Buildings, Publication MNL-119-63, Prestressed Concrete Institute, Chicago, Illinois, 1963.
48. \_\_\_\_\_, "Summary of Basic Information on Precast Concrete Connections," Journal of the Prestressed Concrete Institute, Vol. 14, No.6, December 1969, pp. 14-58.
49. \_\_\_\_\_, Design Handbook, Prestressed Concrete Institute, Chicago, Illinois, 1971.
50. Richard, E. L., "Anchor Bolts Set in Drilled Holes," Journal of the American Concrete Institute, Vol. 44, No. 1, September, 1947, pp. 81-83.
51. Schutz, R. J., "Design of Joints in Precast Concrete Wall Panels," Journal of the Prestressed Concrete Institute, Vol. 11, No. 5, October 1966, pp. 60-67.
52. Shiga, T., Shibata, A., and Takahashi, J., "Experimental Study on Dynamic Properties of Reinforced Concrete Shear Walls," Proceedings of the Fifth World Conference on Earthquake Engineering, Vol. 1, Rome, 1974, pp. 1157-1166.
53. Sika Chemical Corporation, "Anchor-Bolt Grouting," Technical Bulletin TB-71-1, Sika Chemical Corporation, Lyndhurst, New Jersey.
54. \_\_\_\_\_, "How to Use Colma-Dur Gel," Sika Data Sheet CDG-871, Sika Chemical Corporation, Lyndhurst, New Jersey.
55. \_\_\_\_\_, "Grouting Under Base Plates with Colma-Dur," Technical Bulletin TB-69-10, Sika Chemical Corporation, Lyndhurst, New Jersey.
56. \_\_\_\_\_, "Sikastix 370, Sikadur Hi-Mod," Technical Bulletin TB:74/04, Sika Chemical Corporation, Lyndhurst, New Jersey.
57. \_\_\_\_\_, "Sikadur Epoxy Adhesives," Sika Chemical Corporation, Lyndhurst, New Jersey.

58. Smith, B. S., and Carter, C., "A Method of Analysis of Infilled Frames", Proceedings Institution of Civil Engineers, Vol. 44, September 1969, pp. 31.
59. Spracklen, R. W., "Repair of Earthquake Damage at Holy Cross Hospital," ASCE National Structural Engineering Conference, Preprint 1941, San Francisco, California, April 1973.
60. Strand, D. R., "Earthquake Repairs, Kaiser Hospital, Panorama City, California," ASCE National Structural Engineering Conference, Preprint 1996, San Francisco, California, April 1973.
61. Tamura, R., Murakami, M., Osawa, Y., Miyajima, N., Tanaka, Y., "A Vibration Test of a Large Model Steel Frame with Precast Concrete Panel Until Failure," Proceedings of the Fourth World Conference on Earthquake Engineering, Vol. 1, Santiago, Chile, 1969, p. B2-15.
62. Uniform Building Code, 1946 Edition, International Association of Building Officials, Pasadena, California, 1956.
63. Uniform Building Code, 1973 Edition, International Association of Building Officials, Pasadena, California, 1973.
64. Viest, I. M., "Review of Research on Composite Steel-Concrete Beams," Journal of the Structural Division, ASCE, Vol. 84, No. ST6, June 1960.